Computation and Physics in Algebraic Geometry

Von der Fakultät für Mathematik und Informatik
der Universität Leipzig
angenommene

D I S S E R T A T I O N

zur Erlangung des akademischen Grades

DOCTOR RERUM NATURALIUM
(Dr.rer.nat.)

im Fachgebiet

Mathematik

vorgelegt

von M.Sc. Claudia Fevola
geboren am 13.07.1995 in Atripalda (Italien)

Die Annahme der Dissertation wurde empfohlen von:

1. Professor Dr. Bernd Sturmfels (Max Planck Institute for Mathematics in the Sciences)
2. Professor Dr. Daniele Agostini (Eberhard Karls Universität Tübingen)
3. Professor Dr. Fatemeh Mohammadi (Katholieke Universiteit Leuven)

Die Verleihung des akademischen Grades erfolgt mit Bestehen der Verteidigung am 21.06.2023 mit dem Gesamtprädikat summa cum laude.

Abstract

Physics provides new, tantalizing problems that we solve by developing and implementing innovative and effective geometric tools in nonlinear algebra. The techniques we employ also rely on numerical and symbolic computations performed with computer algebra.

First, we study solutions to the Kadomtsev-Petviashvili equation that arise from singular curves. The Kadomtsev-Petviashvili equation is a partial differential equation describing nonlinear wave motion whose solutions can be built from an algebraic curve. Such a surprising connection established by Krichever and Shiota also led to an entirely new point of view on a classical problem in algebraic geometry known as the Schottky problem. To explore the connection with curves with at worst nodal singularities, we define the Hirota variety, which parameterizes KP solutions arising from such curves. Studying the geometry of the Hirota variety provides a new approach to the Schottky problem. We investigate it for irreducible rational nodal curves, giving a partial solution to the weak Schottky problem in this case.

Second, we formulate questions from scattering amplitudes in a broader context using very affine varieties and D-module theory. The interplay between geometry and combinatorics in particle physics indeed suggests an underlying, coherent mathematical structure behind the study of particle interactions. In this thesis, we gain a better understanding of mathematical objects, such as moduli spaces of point configurations and generalized Euler integrals, for which particle physics provides concrete, non-trivial examples, and we prove some conjectures stated in the physics literature.

Finally, we study linear spaces of symmetric matrices, addressing questions motivated by algebraic statistics, optimization, and enumerative geometry. This includes giving explicit formulas for the maximum likelihood degree and studying tangency problems for quadric surfaces in projective space from the point of view of real algebraic geometry.

Authorship

The results presented in this thesis are based on six works of my mine joint with co-authors. Parts of this thesis are prepublished.

Chapter 1 is written by myself.

Chapter 2 is based on two works. The first section relies on the joint article [AFMS23] with Daniele Agostini, Yelena Mandelshtam, and Bernd Sturmfels. All coauthors equally contributed to all aspects of the publication. I made major contributions to developing Theorem 2.1.2, Examples 2.1.1 and 2.1.19, and implementing the algorithm discussed in Subsection 2.1.3. The article appeared in the *Journal of Symbolic Computation*. The second section is devoted to the joint article [FM22] with Yelena Mandelshtam. My coauthor and I contributed equally to all mathematical exposition and results. The article was submitted to *Journal of Symbolic Computation* and is under revision.

Chapter 3 is also divided in two sections. Section 3.1 is based on the joint article [ABF$^+$23] together with Daniele Agostini, Taylor Brysiewicz, Lukas Kühne, Bernd Sturmfels, and Simon Telen. The article was motivated by a problem arising in particle physics. An ample spectrum of tools from nonlinear algebra were required to tackle the problem. The six authors were all equally involved in all aspects of the publication with a major focus on some aspects: Agostini and myself on algebraic geometry (Subsections 3.1.1 and 3.1.4), Kühne on combinatorics (Subsection 3.1.2 and 3.1.4), Brysiewicz and Telen on numerical nonlinear algebra (Subsections 3.1.3, 3.1.5, 3.1.7), Sturmfels on tropical geometry (Subsection 3.1.6). The article is published in the journal *Advances in Mathematics*. Section 3.2 in based on the joint article [AFST22] with Daniele Agostini, Anna-Laura Sattelberger, and Simon Telen. My coauthors and I contributed equally to all mathematical exposition and results. I made major contributions to developing Subsections 3.2.1 and 3.2.2. The article was submitted to *Communications in Number Theory and Physics* and is under revision.

Chapter 4 is also divided in two sections. The first section is based on the article [FMS21] with Yelena Mandelshtam and Bernd Sturmfels. The second section is based on the article [BFS21] with Taylor Brysiewicz and Bernd Sturmfels. Both articles are published in *Le Matematiche* and came out of the project "Linear Spaces of Symmetric Matrices" (LSSM) held at the MPI MiS in Leipzig with the purpose of advancing the understanding of such matrix spaces. All coauthors equally contributed to all aspects of both publications.

Appendix A is written by myself.

Acknowledgements

Contents

List of Figures

List of Tables

Introduction

In recent years, modern algebraic geometry has been employed to solve problems in engineering, physics, and other sciences. Furthermore, this interplay has inspired new developments in classical and applied algebraic geometry thanks to the insights and intuitions emerging in the natural sciences. The occurrence of nonlinear equations in applied mathematics and the advancement of computational methods in computer algebra have promoted the development of nonlinear algebra [BÇD+21, MS21b]. This is a diverse and emerging field of mathematics combining techniques mainly from modern algebraic geometry, combinatorics, differential algebra, and commutative algebra.

In this thesis, we use methods from algebraic geometry and nonlinear algebra to explore open questions arising in the study of two distinct branches of physics: integrable systems and scattering amplitudes. In addition, we study classical problems in algebraic geometry by addressing new questions motivated by algebraic statistics, optimization, and enumerative geometry. The new findings are presented in the three major chapters (Chapters 2–4), each of which begins with an introduction to the problems under consideration and a summary of our main results. Symbolic and numerical computations play an essential role in proving our results and working out many of the examples in this thesis. The mathematical software programs we mainly use are `Macaulay2`, `Maple`, `Julia`, and `SageMath`. The supplementary codes and research data supporting our findings are guaranteed to be freely accessible and suitable for reuse by interested users at the website `https://mathrepo.mis.mpg.de`. This is an online repository for mathematical research data MathRepo which we describe in [FG22].

We now describe the results of the thesis in more detail. In the interplay between algebraic geometry and integrable systems, the study of complex algebraic curves is connected to the Kadomtsev–Petviashvili (KP) equation. This is a nonlinear partial differential equation whose solution function represents the amplitude of shallow water waves. Krichever provided an algebro-geometric procedure to construct KP solutions from a point on a complex algebraic curve [Kri77]. Chapter 2 in this thesis studies KP solutions whose underlying algebraic curves undergo tropical degenerations. The curve in the limit becomes singular with possibly many irreducible components. The limiting object can be described entirely combinatorially, and we use such combinatorial data to perform a degeneration also at the level of the KP solution. We show that this procedure can give rise to solitons. These are a subset of KP solutions that have been proven to have a fascinating connection with the theory of total positivity for the Grassmannian [KW14].

Our interest in KP solutions is also driven by how they relate to the Schottky problem [Gru12]. This is a classical problem in algebraic geometry concerning characterizing Jacobian varieties among abelian varieties. There is currently no complete algebro-geometric solution to the Schottky problem. The only known solution [Shi86] employs analytical tools as well as

the connection to KP theory. We study the Schottky problem when restricting to irreducible rational nodal curves and provide a solution for curves up to genus nine. The proof relies on symbolic computations. Our novel approach provides a way of formulating the Schottky problem via the variety that parametererizes degenerate KP solutions.

In Chapter 3, we transition from water waves to elementary particles. We present a line of research built around problems arising in particle physics. This field of study explores the interactions of elementary particles that constitute matter and radiation. Scattering amplitudes compute the probabilities of particular outcomes of interactions taking place in particle accelerators. In the recent past, the increase in interactions among theoretical physicists working in scattering amplitudes and mathematicians has led to significant advances in both disciplines. New interesting mathematical problems and brand-new geometric objects were developed in works by, among others, Arkani-Hamed, Cachazo, Sturmfels, and Williams, [AHT14, BCFW05, ST21, Wil21].

In both sections of Chapter 3, we reduce a physics problem to studying properties and geometry of a very affine variety, that is, a closed subvariety of an algebraic torus. In Section 3.1 the very affine varieties of interest are moduli spaces of point configurations. They appear when counting the number of critical points of the potential function, or equivalently, the number of solutions to the scattering equations [CEGM19, ST21]. We connect the study of such solutions to computing the maximum likelihood degree of the likelihood function in algebraic statistics. We introduce the likelihood degeneration, which is a type of degeneration providing effective ways to compute the numbers of interest. Using the likelihood degeneration, we are able to confirm the computations appearing in the physics literature as well as give new results using numerical computations.

In Section 3.2, the very affine varieties of interest are complements in an algebraic torus of a finite set of hypersurfaces. In this case, the motivation comes from the study of Feynman integrals. These are mathematical expressions used to calculate the probabilities of some elementary particle interactions, as we explain in Appendix A. We study the more general setting of vector spaces associated to a family of generalized Euler integrals, to which Feynman integrals provide non-trivial examples. Using tools from homological algebra and D-module theory, we prove that the dimension of such vector spaces coincides with the Euler characteristic of very affine varieties given by hypersurfaces complements. A common theme to both sections is the connection to the maximum likelihood degree. In particular, the essential tool is the equality between the maximum likelihood degree and the Euler characteristic proved by Huh [Huh13] for smooth varieties.

Finally, Chapter 4 is concerned with classical themes in algebraic geometry. We study linear spaces of symmetric matrices with the goal of broadening the understanding of these matrix spaces by approaching them from various perspectives. Although these objects appear to be simple, they have a significant impact and are encountered in a broad range of mathematics. In Section 4.1, we study pencil of quadrics, i.e. two-dimensional linear subspaces in the space of (real or complex) symmetric matrices, according to the classification by Segre symbols [HP52]. We address questions motivated by algebraic statistics and optimization. In our main result in this section, we provide explicit formulas for the number of critical points of the log-likelihood function, when restricting to a pencil of quadrics, in terms of Segre symbols. Section 4.2 examines quadratic surfaces in the projective space that are tangent to nine given figures. These figures can be points, lines, planes or quadrics. The numbers of tangent quadrics were determined by Hermann Schubert in 1879. We study the associated systems of polynomial equations, also in the space of complete quadrics, and

we solve them using certified numerical methods. We present explicit instances where all tangent quadrics are real. Our results represent a first step toward the problem of deciding whether there exist nine real quadrics such that all complex solutions are real.

For the sake of readability, we briefly discuss the outline of the thesis. Every chapter is divided into two sections. Chapter 1 presents the notions required to state the Schottky problem, which will be central in Chapter 2, along with the basic concepts from D-module theory that will help in understanding Chapter 3. Furthermore, most of the contents of this thesis have appeared in slightly altered form in several papers. In particular, the two sections of Chapter 2 are based on [AFMS23] and [FM22], respectively. Analogously, Chapter 3 presents our research results from [ABF$^+$23] and [AFST22]. Finally, [FMS21] and [BFS21] serve as the basis for Chapter 4.

A fundamental requirement for reading this thesis is being versatile. To tackle mathematical problems that arise in the natural sciences, it is in fact very helpful to be equipped with a large toolbox of diverse mathematical languages from which to choose the one that best fits the problem. It is a sort of adaptation, as required by nature. Just as an organism must evolve and develop traits that are best suited to their environment in order to survive and thrive, in this thesis we choose the most appropriate mathematical tools and methods at our disposal to solve a problem arising in physics.

Chapter 1

Background

This chapter describes the key ingredients in developing Chapters 2 and 3. Section 1.1 discusses Jacobian varieties of algebraic curves, Abel's theorem, and the Schottky problem. In particular, the last will be central in Chapter 2, where we will study such a classical problem in algebraic geometry in relation to degeneration of curves. For extended discussions and proofs, we refer to [ACGH85, Gru12, Mir95]. Section 1.2 reviews relevant definitions and results regarding D-module theory, based mainly on [SST00, SS19]. These notions will be helpful to understand Section 3.2.

1.1. Jacobian varieties of algebraic curves

Let X be a smooth projective curve of genus g over $\mathbb{C}$. Then X can be thought of as a compact Riemann surface and, in what follows we will use the two terms interchangeably.

Recall that the first homology group $H_1(X, \mathbb{Z})$ of X is a free abelian group of rank $2g$. It is an elementary fact that one can always fix a symplectic basis $\alpha_1, \beta_1, \alpha_2, \beta_2, \ldots, \alpha_g, \beta_g$ for $H_1(X, \mathbb{Z})$. This is just a basis such that $\alpha_i \cdot \beta_j = \delta_{ij}$, where δ_{ij} denotes the Kronecker-Delta.

For any choice of a symplectic basis, Riemann proved that one can construct a basis of holomorphic differentials $\omega_1, \ldots, \omega_g$ such that the matrix B whose j-th column is given as

$$B_j = \left(\int_{\beta_j} \omega_1, \ldots, \int_{\beta_j} \omega_g \right)^T$$

is a complex, symmetric $g \times g$ matrix with positive definite imaginary part. We call it the *Riemann matrix* associated to the curve X. Furthermore, in this setting, we have

$$A_i = \left(\int_{\alpha_i} \omega_1, \ldots, \int_{\alpha_i} \omega_g \right)^T = e_i,$$

where e_i denotes the i-th vector in the standard basis of $\mathbb{Z}^g$. It is a well-known fact that the $2g$ vectors A_i, B_j are $\mathbb{R}$-linearly independent in $\mathbb{C}^g$ and therefore generate a g-dimensional lattice $\Lambda = \mathbb{Z}^g + B \cdot \mathbb{Z}^g$ in $\mathbb{C}^g$. The *Jacobian* of the Riemann surface X is defined as the quotient

$$\mathrm{Jac}(X) := \mathbb{C}^g / \Lambda = \mathbb{C}^g / (\mathbb{Z}^g + B \cdot \mathbb{Z}^g). \tag{1.1.1}$$

Notice that $\mathrm{Jac}(X)$ is also an abelian group. Moreover, the Jacobian variety of an algebraic curve X can also be introduced via a definition that does not rely on any basis choice.

Consider the map that integrates holomorphic 1-forms along 1-cycles, i.e.,

$$\phi : H_1(X, \mathbb{Z}) \longrightarrow H^0(X, \omega_X)^{\vee}$$

$$\gamma \longmapsto \left(\omega \mapsto \int_{\gamma} \omega \right),$$

where the $V^{\vee}$ stands for the dual space of V. The image of the map ϕ is a discrete lattice of maximal rank inside $H^0(X, \omega_X)^{\vee}$. Therefore, the Jacobian can also be defined as the quotient by this lattice, namely

$$\mathrm{Jac}(X) \coloneqq H^0(X, \omega_X)^{\vee}/H_1(X, \mathbb{Z}).$$

The definition in (1.1.1) thus gives a description in coordinates of the Jacobian of an algebraic curve. The map taking a curve X into its Riemann matrix provides an explicit description of the map taking the curve X into its Jacobian $\mathrm{Jac}(X)$.

Evaluating Riemann matrices is a rich and active research topic, implementations of algorithms to numerically evaluate Riemann matrices are available in `Maple` [DHB+04] and `SageMath` [BSZ19]. Here we illustrate in an example how to compute the Riemann matrix of a hyperelliptic curve using `SageMath` [The22].

Example 1.1.1. Consider a genus two curve $y^2 = f(x)$ where $f(x)$ is a polynomial of degree six given by

$$f(x) = (x-1)(x-2)(x-3)(x-4)(x-5)(x-6).$$

The Riemann matrix of such a curve is generated in `SageMath` as follows

```
from sage.schemes.riemann_surfaces.riemann_surface import RiemannSurface
R.<x,y> = QQ[]
f = y^2-(x-1)*(x-2)*(x-3)*(x-4)*(x-5)*(x-6)
S = RiemannSurface(f,prec=100)
M = S.riemann_matrix()
```

One can check that the output is a 2×2 symmetric complex matrix with positive definite imaginary part. The class `RiemannSurface` is used to model the Riemann surface determined by a plane algebraic curve over a subfield of the complex numbers. The Riemann matrix is then determined numerically with 100 bits of precision, using certified homotopy continuation methods.

1.1.1. Abel-Jacobi map and the theta function

To fully exploit the construction of the Jacobian of an algebraic curve X, we must explicitly relate the Jacobian to the curve itself. This connection is provided by the *Abel-Jacobi map*.

Choose a base point $p_0 \in X$. For each point $p \in X$, we denote γ_p the path on X from p_0 to p. The map sending a point $p \in X$ to the element of $H_0(X, \omega_X)^{\vee}$ defined by integration along γ_p is not well-defined since the integral depends on the path. Such a map is indeed well-defined modulo the subgroup Λ defined above. Hence, one considers the *Abel-Jacobi* map

$$\mu : X \longrightarrow \mathrm{Jac}(X)$$

$$p \longmapsto \mu(p) \coloneqq \left(\int_{\gamma_p} \omega_i \right)_{i=1,\ldots,g} \mod \Lambda.$$

Changing the base point p_0 changes the map by a translation of the torus. Furthermore, the Abel-Jacobi map μ extends to divisors on X by linearity, i.e., $\mu(\sum n_i p_i) = \sum n_i \mu(p_i)$, and hence we can speak of the value of the map μ on divisors. The following result assures the invariance of the Abel-Jacobi map under the linear equivalence between divisors on X.

Theorem 1.1.2 (Abel's Theorem). *Let D and D' be effective divisors of degree d on a smooth algebraic curve X. Then D is linearly equivalent to D' if and only if $\mu(D) = \mu(D')$.*

There exist several interpretations and fundamental consequences of Abel's theorem. For instance, it implies that the Abel-Jacobi map induces an injection of abelian groups from the space of degree 0 divisor classes to the Jacobian. Later Jacobi proved that this map is also surjective. This result is known as *Jacobi inversion theorem*. A more geometric interpretation is the following. Recall that the divisor $\mathrm{div}(f)$ associated to a meromorphic function on a compact Riemann surface X has degree 0. However, this is not a sufficient condition. Abel's theorem gives a precise criterion to check if a degree 0 divisor comes from a meromorphic function of X. For more discussions and proofs we refer to [ACGH85, Mir95].

Another consequence of Abel's theorem, combined with Riemann-Roch, is that the Zariski closure of the image of the map $\mu^{(g-1)} : X^{g-1} \to \mathrm{Jac}(X)$ is an irreducible divisor in $\mathrm{Jac}(X)$, called the *theta divisor*

$$\Theta \subset \mathrm{Jac}(X).$$

It corresponds to an analytic hypersurface in $H^0(X, \omega_X)^\vee$ defined as the zero locus $\{\mathbf{z} \in \mathbb{C}^g \,|\, \theta(\mathbf{z}, B) = 0\}$, where $\theta(\mathbf{z}, B)$ is the *theta function*, and B denotes the Riemann matrix of the curve X. The importance of the theta divisor on the Jacobian of a curve X stems for the fact that it closely reflects the geometric properties of the curve itself. The next paragraph describes the theta function explicitly.

For any integer $g \geq 1$, let $\mathcal{H}_g$ denote the *Siegel upper half space* which consists of all complex symmetric $g \times g$ with positive definite imaginary part. There is an explicit way of embedding the Jacobian variety of an algebraic curve X into a projective space by using the so called *(universal) theta function*. This is the holomorphic function

$$\theta : \mathbb{C}^g \times \mathcal{H}^g \longrightarrow \mathbb{C} \quad (\mathbf{z}, B) \longmapsto \sum_{\mathbf{c} \in \mathbb{Z}^g} \exp[\pi i \mathbf{c}^T B \mathbf{c} + 2\pi i \mathbf{c}^T z]. \tag{1.1.2}$$

The restriction on the choice of the matrices ensures that it is an absolutely convergent series. For fixed B, it has the following easily verified property in $\mathbf{z}$:

$$\theta(\mathbf{z} + B\mathbf{c} + \mathbf{d}, B) = \exp[-\pi i \mathbf{c}^T B \mathbf{c} - 2\pi i \mathbf{c}^T \mathbf{z}] \cdot \theta(\mathbf{z}, B), \quad \text{for all } \mathbf{c}, \mathbf{d} \in \mathbb{Z}^g.$$

As a consequence, the zero locus of $\theta(\mathbf{z}, B)$ is invariant under the shifts by the lattice $\mathbb{Z}^g + B \cdot \mathbb{Z}^g$, and thus the theta divisor is well defined.

Starting from the theta function $\theta(\mathbf{z}, B)$ we can define a modification of it, namely the *theta function with characteristic $m, m' \in \{0, 1\}^g$*. This is the complex analytic function

$$\theta \begin{bmatrix} m \\ m' \end{bmatrix} (\mathbf{z} | B) = \sum_{\mathbf{c} \in \mathbb{Z}^g} \exp \left[\pi i \left(\mathbf{c} + \frac{m}{2} \right)^T \tau \left(\mathbf{c} + \frac{m}{2} \right) + 2\pi i \left(\mathbf{c} + \frac{m}{2} \right)^T \left(\mathbf{z} + \frac{m'}{2} \right) \right]. \tag{1.1.3}$$

Evaluating theta functions with characteristic at the point $\mathbf{z} = (0, \dots, 0)$ gives the so called *theta constants*. The importance of such variants of the theta function is due to the fact that they provide explicit embeddings of the Jacobian of an algebraic curve inside some projective space. The survey [Gru12] by Grushevsky provides a modern overview of the possible embeddings.

Mathematical software packages are available to compute also with theta functions [AC21, FJK19, SD16]. We illustrate this with an example.

Example 1.1.3 (Example 1.1.1 continued)**.** Given the Riemann matrix B for the hyperelliptic genus 2 curve computed in Example 1.1.1, the following lines provide an instance of how to evaluate the theta function at a point:

```
Pkg.add("Theta")
B = [0.59213731583710508241952598139 + 0.52072406882870882285671333256*im
      -0.59213731583710508241952598138 - 0.34855310487952156451686559943*im]
     [-0.59213731583710508241952598140 - 0.34855310487952156451686559942*im
      1.00000000000000000000000000000 + 0.69710620975904312903373119884*im]
R = RiemannMatrix(B, siegel=true, epsilon=1.0e-12, nderivs=4);
z = [1.041+0.996*im; 1.254+0.669*im];
theta(z, R)
```

This is using the `Julia` package `Theta` developed by Agostini and Chua, see [AC21].

1.1.2. The Schottky problem

The Jacobian variety of an algebraic curve X is a principally polarized abelian variety. This means that it is a projective variety which is also an abelian group. We write $\mathcal{A}_g$ for the set of isomorphism classes of principally polarized abelian varieties of dimension g. In general, this space can be identified as

$$\mathcal{A}_g \simeq \mathcal{H}_g/\mathrm{Sp}(2g, \mathbb{Z}),$$

where $\mathrm{Sp}(2g, \mathbb{Z})$ denotes the symplectic group with action defined by

$$\begin{pmatrix} E & F \\ G & H \end{pmatrix} \cdot B = (GB + H)^{-1}(EB + F).$$

At this point, we have the main tools required to introduce the Schottky problem. Let $\mathcal{M}_g$ denote the moduli space of smooth algebraic curves of genus g. The map that associates to each curve its Jacobian is a map of moduli spaces called the *Torelli map*

$$J : \mathcal{M}_g \to \mathcal{A}_g \quad X \mapsto \mathrm{Jac}(X).$$

Torelli proved the injectivity of the map J, in other words a curve is identified up to isomorphism by its Jacobian. This result is known as Torelli's theorem. The Schottky problem is a classical problem in algebraic geometry asking to characterize Jacobian varieties amongst all abelian varieties. To be precise, the Schottky problem asks to find the defining equations for the locus of Jacobians, defined as the Zariski closure of $J(\mathcal{M}_g)$ in $\mathcal{A}_g$, which is referred to as the *Schottky locus* in the literature. In other words, this is the locus of Riemann matrices in the Siegel upper half space that are of algebraic curves. The *weak Schottky problem* is to find an ideal whose zero locus contains the locus of Jacobians as an irreducible component.

Recall that $\dim \mathcal{M}_g = 3g - 3$, while $\dim \mathcal{A}_g = \binom{g+1}{2}$. These numbers coincide when $g \leq 3$, thus in genus $g \leq 3$ the Schottky problem is trivial, in the sense that every polarized abelian variety is the Jacobian of a curve. Instead, for genus $g \geq 4$, the inclusion of the Schottky locus inside $\mathcal{A}_g$ is proper. In particular, Igusa [Igu82] proved that in genus 4 the locus of Jacobian varieties is an analytic irreducible hypersurface in the space of abelian varieties.

For genus larger than 5 the Schottky problem has proven to be difficult, with only partial results for genus 5 and weak solutions for higher genus. Many approaches to the Schottky problem have been developed (e.g., [ADC84, Igu82]) and an explicit solution to the weak

Schottky problem was provided in [FGSM21] and investigated numerically for genus 5 in [AC21]. However, a complete algebro-geometric solution is still missing, and the only known solution was given by Shiota [Shi86] through the connection to the KP equation. This will be discussed in the next chapter. Finally, the proof of Theorem 2.2.3 in this thesis gives a solution to the weak Schottky problem for irreducible rational nodal curves, which we provide for $g \leq 9$.

1.2. D-modules

This section introduces the fundamental concepts of D-module theory that are required to comprehend Section 3.2. We review the Fundamental Theorem of Algebraic Analysis, introduce holonomic D-ideals, and discuss their holonomic rank. We state the CKK theorem, which will play a key role in proving the main theorem in Subsection 3.2.3. We conclude by defining Bernstein–Sato polynomial and ideals. The major interest of such D-modules is the algebraic approach they provide to the theory of linear partial differential equations. However, D-modules provide a useful tool also for concrete problems in applied algebraic geometry [BÇD$^+$21]. In Section 3.2, D-modules will be shown to be powerful tools for studying generalized Euler integrals and problems in particle physics. The presentation we give follows closely the ones in [HTT08, SST00, SS19].

For any integer $n \geq 1$, the *n-th Weyl algebra*, denoted

$$D_n := \mathbb{C}[x_1, \ldots, x_n]\langle \partial_1, \ldots, \partial_n \rangle,$$

or just D if the number of variables is clear from the context, is the non-commutative ring gathering linear differential operators with polynomial coefficients. Formally, it is the free associative $\mathbb{C}$-algebra generated by $x_1, \ldots, x_n$ and $\partial_1, \ldots, \partial_n$ modulo the following relations: all generators are assumed to commute, except ∂_i and x_i. Their commutator is

$$[\partial_i, x_i] := \partial_i x_i - x_i \partial_i = 1 \neq 0, \quad \text{for } i = 1, \ldots, n. \tag{1.2.1}$$

This is in accordance with Leibniz' rule for determining the derivative of a product of functions. One can generalize the Weyl algebra by considering a ring of differential operator in which the coefficients are allowed to be rational functions in n variables. Such a generalization gives rise to the *rational Weyl algebra*

$$R_n = \mathbb{C}(x_1 \ldots, x_n)\langle \partial_1, \ldots, \partial_n \rangle,$$

where $\mathbb{C}(x_1, \ldots, x_n)$ denotes the field of rational functions over the complex numbers. Notice that D_n is a subalgebra of R_n. Furthermore, the multiplication in R_n is defined by extending the product rule (1.2.1) from polynomials to rational functions, i.e.,

$$\partial_i r(x) = r(x)\partial_i + \frac{\partial_r}{\partial x_i}(x), \quad \text{for all } r \in \mathbb{C}(x_1, \ldots, x_n).$$

We are interested in studying left modules M over the Weyl algebra D or the rational Weyl algebra R. The action of a differential operator to a function will be denoted by the symbol $\bullet$., i.e.,

$$\bullet : D \times M \to M \quad (\text{resp. } \bullet : R \times M \to M).$$

For instance, the natural action of the Weyl algebra on polynomials $p \in M = \mathbb{C}[x_1, \ldots, x_n]$ is as follows

$$\partial_i \bullet p = \frac{\partial p}{\partial x_i}, \qquad x_i \bullet p = x_i p, \quad \text{for } i = 1, \ldots, n. \tag{1.2.2}$$

In this notation, $\partial_i \cdot x_i = x_i \cdot \partial_i + 1 \in D_n$, whereas $\partial_i \bullet x_i = 1 \in \mathbb{C}[x_1, \ldots, x_n]$.

We use the notation $\theta_i \coloneqq x_i\partial_i$ for the *i-th Euler operator* and θ for the vector $(\theta_1, \ldots, \theta_n)^\top \in D^n$. We will later also need the ring of global linear differential operators

$$D_{\mathbb{G}_m^n} \coloneqq \mathbb{C}[x_1^{\pm 1}, \ldots, x_n^{\pm 1}]\langle \partial_1, \ldots, \partial_n \rangle = \mathbb{C}[x_1^{\pm 1}, \ldots, x_n^{\pm 1}]\langle \theta_1, \ldots, \theta_n \rangle \tag{1.2.3}$$

on the algebraic n-torus $\mathbb{G}_m^n = \mathrm{Spec}(\mathbb{C}[x_1^{\pm 1}, \ldots, x_n^{\pm 1}])$. In the rest of this work, we will be less strict about notation and used $(\mathbb{C}^*)^n$ both for the algebraic n-torus $\mathbb{G}_m^n$ and its analytification $(\mathbb{C}^*)^n$, since it is clear from the context which one is meant. Here and in Subsection 3.2.2, we stick to the more careful distinction, which is also the standard in D-module theory.

In what follows, we study *left D-modules* of the form D/I for some left ideal I in the Weyl algebra D, and *left D-ideals*, unless stated otherwise. We will refer to them simply as D-modules and D-ideals. Those ideals encode systems of linear partial differential equations with polynomial coefficients in algebraic terms. Likewise, rational coefficients lead to modules over the rational Weyl algebra R_n.

Example 1.2.1. The Weyl algebra D has a natural action on many function spaces. This turns many function spaces into D-modules. For instance, if F is the space of holomorphic functions on a domain $\mathbb{C}^n$, such that F is closed under taking partial derivatives, the action of the Weyl algebra D on F is defined as in (1.2.2) where the polynomial p is replaced by a function $f \in F$.

Definition 1.2.2. Let $Mod(D)$ denote the category of D-modules. Consider a D-ideal I and $M \in Mod(D)$. We call the *solution space* of I in M the $\mathbb{C}$-vector space

$$Sol_M(I) \coloneqq \{m \in M \mid P \bullet m = 0\}.$$

1.2.1. Holonomicity

Any element P of D has a unique normally ordered expression

$$P = \sum_{(a,b) \in C} c_{ab} \cdot x^a \partial^b, \tag{1.2.4}$$

where C is a finite subset of $\mathbb{Z}^{2n}$, $c_{ab} \in \mathbb{C} \setminus \{0\}$, $x^a = x_1^{a_1}\cdots x_n^{a_n}$, and $\partial^b = \partial_1^{b_1}\cdots\partial_n^{b_n}$. This fact gives us a natural $\mathbb{C}$-vector space isomorphism between the commutative ring of polynomials in $2n$ variables $\mathbb{C}[x, \xi] \coloneqq \mathbb{C}[x_1, \ldots, x_n, \xi_1, \ldots, \xi_n]$ and the Weyl algebra:

$$\phi : \mathbb{C}[x, \xi] \to D, \quad x^a \xi^b \mapsto x^a \partial^b.$$

Example 1.2.3. Consider $n = 2$, and $P = \partial_1\partial_2^2 x_1 x_2^2 - \partial_2 x_2$. Using a built-in command in Macaulay2 [LT]

```
D = QQ[x1,x2,d1,d2, WeylAlgebra => {x1=>d1,x2=>d2}];
d1*d2^2*x1*x2^2-d2*x2
```

we find its normal expression as $x_1 x_2^2 \partial_1 \partial_2^2 + 4 x_1 x_2 \partial_1 \partial_2 + x_2^2 \partial_2^2 + 2 x_1 \partial_1 + 3 x_2 \partial_2 + 1$.

Given a real vector $(u_1, \ldots, u_n, v_1, \ldots, v_n) \in \mathbb{R}^{2n}$, this is a *weight vector* for the Weyl algebra if

$$u_i + v_i \geq 0 \quad \text{for } i = 1, \ldots, n.$$

The *associated graded ring* $\mathrm{gr}_{(u,v)}(D)$ of the Weyl algebra D with respect to the weight vector (u,v) is the $\mathbb{C}$-algebra generated by

$$\{x_1,\ldots,x_n\} \cup \{\partial_i : u_i + v_i = 0\} \cup \{\xi_i : u_i + v_i > 0\},$$

where all the variables are assumed to commute except for x_i and ∂_i, consistently with (1.2.1). In fact, when $u,v \in \mathbb{Z}^{2n}$, $\mathrm{gr}_{(u,v)}(D)$ is the associated graded ring under the filtration of D by the weights (u,v):

$$\mathrm{gr}_{(u,v)}(D) = \begin{cases} D & \text{if } u + v = 0 \\ \mathbb{C}[x,\xi] & \text{if } u + v > 0 \\ \text{a mixture of the above} & \text{otherwise} \end{cases}$$

Set $m = \max_{(a,b)\in C}(a \cdot u + b \cdot v)$. The *initial form* of $P \in D$ is defined as

$$\mathrm{in}_{(u,v)}(P) = \sum_{\substack{(a,b)\in C \\ a\cdot u + b\cdot v = m}} c_{ab} \prod_{k:u_k+v_k>0} x_k^{a_k}\xi_k^{b_k} \prod_{k:u_k+v_k} x_k^{a_k}\partial_k^{b_k} \in \mathrm{gr}_{(u,v)}(D),$$

and $\mathrm{in}_{(u,v)}(0) = 0$. In words, one selects the terms of maximum weight m in the normally ordered expression (1.2.4), and then replace ∂_i by ξ_i for all i such that $u_i + v_i > 0$.

Given a real weight vector, for a D-ideal I, the vector space $\mathrm{in}_{(u,v)}(I) = \mathbb{C}\{\mathrm{in}_{(u,v)}(P)\,|\,P \in I\}$ is the *initial ideal* of I. In particular, this is a left ideal in the associated graded algebra $\mathrm{gr}_{(u,v)}(D)$, [SST00, Corollary 1.1.2]. Computing initial ideals $\mathrm{in}_{(u,v)}(I)$ and their associated Gröbner bases via the *Buchberger algorithm* in D is a key step towards many practical applications of D-modules, e.g., [ALSS20].

A significant case is when u is the zero vector and v is the all-one vector $e = (1,\ldots,1)$.

Definition 1.2.4. Fix $e = (1,\ldots,1)$ and $0 = (0,\ldots,0) \in \mathbb{R}^n$. Given any D-ideal I, the *characteristic variety* $\mathrm{Char}(I)$ is the vanishing set of the characteristic ideal $\mathrm{ch}(I) := \mathrm{in}_{(0,e)}(I)$ in $\mathbb{C}^{2n} = \mathbb{C}_x^n \times \mathbb{C}_\xi^n$. The characteristic ideal is the ideal in the commutative polynomial ring $\mathbb{C}[x,\xi]$ which is generated by the symbols $\mathrm{in}_{(0,e)}(P)$ of all differential operators $P \in I$.

In the theory of D-modules, one refers to $\mathrm{Char}(I)$ as the characteristic variety of the D-module D/I. The characteristic variety is the object of the following theorem, established by Sato, Kawai, and Kashiwara in [SKK73]:

Theorem 1.2.5 (Fundamental Thorem of Algebraic Analysis)**.** *Let I be a proper D-ideal. Every irreducible component of its characteristic variety $\mathrm{Char}(I)$ has dimension at least n.*

Definition 1.2.6. A D-ideal I is *holonomic* if $\dim(\mathrm{ch}(I)) = n$, i.e., if the dimension of its characteristic variety in $\mathbb{C}^{2n}$ is minimal. Fix the field $\mathbb{C}(x) = \mathbb{C}(x_1,\ldots,x_n)$ and $\mathbb{C}(x)[\xi] = \mathbb{C}(x)[\xi_1,\ldots,\xi_n]$. The *holonomic rank* of I is

$$\mathrm{rank}(I) := \dim_{\mathbb{C}(x)}(\mathbb{C}(x)[\xi]/\mathbb{C}(x)[\xi]\mathrm{ch}(I)) = \dim_{\mathbb{C}(x)}(R/RI).$$

Both dimensions count the standard monomials for a Gröbner basis of RI in R with respect to e.

Example 1.2.7. Let $n = 1$ and consider the D-ideal generated by the operator

$$P = p_m(x)\partial^m + p_{m-1}(x)\partial^{m-1} + \cdots + p_0(x), \quad \text{with } p_m \neq 0.$$

This operator also defines a linear ordinary differential equation of order m. We have $\mathrm{in}_{(0,e)}(I) = \langle a_m(x)\xi^m\rangle$, hence I is holonomic or rank m. Here is how to compute the using the initial ideal and the holonomic rank in `Macaulay2` using the package `Dmodules` [LT]:

```
needsPackage "Dmodules"
makeWA(QQ[x])
J = ideal((x^2+2*x+1)*dx^2+(x^3-1)*dx+(x-1))
inw(J,{0,1})
holonomicRank J
```

As expected the initial ideal is principally generated by $(x^2 + 2x + 1)\xi^2$ and the holonomic rank equals 2.

Furthermore, if a D-ideal I is holonomic, then $\mathrm{rank}(I)$ is finite. But, the converse is not true. There exists holonomic ideals with infinite holonomic rank. For some examples and a proof of this fact we refer to [SST00, Proposition 1.4.9].

We finally conclude with the last definition required to state the famous CKK theorem.

Definition 1.2.8. The *singular locus* $\mathrm{Sing}(I)$ of I is the variety in $\mathbb{C}^n$ defined by

$$\mathrm{Sing}(I) \coloneqq (\mathrm{ch}(I) : \langle \xi_1, \ldots, \xi_n \rangle^\infty) \cap \mathbb{C}[x_1, \ldots, x_n].$$

Geometrically, the singular locus is the closure of the projection of $\mathrm{Char}(I) \smallsetminus (\mathbb{C}^n \times \{0\})$ onto the first n coordinates of $\mathbb{C}^{2n}$. If I is holonomic, then $\mathrm{Sing}(I)$ is a proper subvariety of $\mathbb{C}^n$.

Theorem 1.2.9 (Cauchy–Kowalevskaya–Kashiwara). *Let I be a holonomic D-ideal and let U be an open subset of $\mathbb{C}^n \smallsetminus Sing(I)$ that is simply connected. Then the space of holomorphic functions on U that are solutions to I has dimension equal to rank(I). In symbols, $\dim(Sol(I)) = rank(I)$.*

The application of this theorem to determine the dimension of the solution space of a D-ideal and its holonomic rank in relation to the theory of GKZ systems will be crucial in Subsection 3.2.3. and we also refer to this subsection for some fascinating explicit examples.

1.2.2. Bernstein–Sato polynomial

We now recall Bernstein–Sato polynomials and ideals. These will be of main importance in Section 3.2. Let $f \in \mathbb{C}[x_1, \ldots, x_n]$ be a polynomial and assume s is a new formal variable that we adjoin to the Weyl algebra D_n such that s commutes with all x_i and ∂_i. Consider the $D_n[s]$-module $\mathbb{C}[x_1, \ldots, x_n, f^s, f^{-1}, s]$. The natural action of $D_n[s]$ on this module is given by

$$\partial_i \bullet f^s = s \cdot \frac{\partial f}{\partial x_i} \cdot f^{s-1}.$$

The *s-parametric annihilator of f^s* is the $D_n[s]$-ideal

$$\mathrm{Ann}_{D_n[s]}(f^s) \coloneqq \{P \in D_n[s] \mid P \bullet f^s = 0\}. \tag{1.2.5}$$

The next example shows how to compute it using `Singular` [DGPS22].

Example 1.2.10. Let $f = (x - 1)(x - 2) \in \mathbb{C}[x]$. The *s*-parametric annihilator of f^s can be computed running the following code in the computer algebra system `Singular` using the library `dmod_lib` [ABL+10]:

```
LIB "dmod.lib";
ring r = 0,x,dp; poly f = (x-1)*(x-2);
def A = operatorBM(f); setring A;
LD; // s-parametric annihilator of f^s
```

In this case, the $D_n[s]$-ideal $\mathrm{Ann}_{D_n[s]}(f^s)$ is generated by the operator $P = f\partial_x - s\partial_x \bullet f$.

Definition 1.2.11. The *Bernstein–Sato polynomial* $b_f \in \mathbb{C}[s]$ of a polynomial $f \in \mathbb{C}[x_1,\ldots,x_n]$ is the unique monic polynomial of smallest degree for which there exists $P_f \in D_n[s]$ such that

$$P_f(s) \bullet f^{s+1} = b_f(s) \cdot f^s. \tag{1.2.6}$$

If f is smooth, $b_f = s+1$. Moreover, the converse is also true [BM96]. Observe that while the Bernstein polynomial is unique, the Bernstein–Sato operator P_f is unique only modulo $\mathrm{Ann}_{D_n[s]}(f^{s+1})$. It is known that b_f is non-trivial and that its roots are negative rational numbers. Bernstein–Sato polynomials were originally studied to construct a meromorphic continuation of the distribution-valued function $s \mapsto f^s$, which is a priori defined only for complex numbers $s \in \mathbb{C}$ with positive real part. Nowadays, it is an important object of study in singularity theory, among others in work on the monodromy conjecture such as [BvdVVW21, BvdVWZ21].

For $\ell > 1$ polynomials $f_1,\ldots,f_\ell$, one needs to study Bernstein–Sato *ideals* instead. The *Bernstein–Sato ideal* of $(f_1,\ldots,f_\ell)$ is the ideal $B_{(f_1,\ldots,f_\ell)}$ in $\mathbb{C}[s_1,\ldots,s_\ell]$ consisting of all polynomials $p \in \mathbb{C}[s_1,\ldots,s_\ell]$ for which there exists $P \in D_n[s_1,\ldots,s_\ell]$ s.t.

$$P \bullet \left(f_1^{s_1+1} \cdots f_\ell^{s_\ell+1} \right) = p \cdot f_1^{s_1} \cdots f_\ell^{s_\ell}. \tag{1.2.7}$$

Sabbah [Sab87] proved that $B_{(f_1,\ldots,f_\ell)}$ is non-trivial and moreover that the irreducible components of $V(B_{(f_1,\ldots,f_\ell)})$ of codimension one are affine-linear hyperplanes defined by polynomials with nonnegative rational coefficients. This is analogous to the fact that the zeroes of the Bernstein–Sato polynomial are negative rational numbers. A generalization of the Bernstein–Sato ideal to any integer shift will be discussed in Section 3.2.

Chapter 2

Integrable systems and algebraic curves

The *Korteweg-de Vries (KdV) equation* is the nonlinear partial differential equation

$$4p_t - 6pp_x - p_{xxx} = 0,$$

providing a mathematical model for wave propagation in one dimension, such as beach waves moving parallel to the coastline or waves in a narrow canal.

In 1973, Kadomtsev and Petviashvili [KP70] proposed a $(2+1)$-dimensional dispersive wave equation to investigate the stability of KdV equation solutions under the impact of weak transversal perturbations. This equation is known as the *Kadomtsev–Petviashvili (KP) equation* and is given by

$$\partial_x(4p_t - 6pp_x - p_{xxx}) = 3p_{yy}, \tag{2.0.1}$$

where ∂_x denotes the usual partial derivative with respect to the variable x. The solution function $p = p(x, y, t)$ represents the amplitude of a shallow water wave at the point (x, y) in the xy-plane for fixed time t. The KP equation can be interpreted as a 2-dimensional generalization of the KdV equation, and it turns out to have a much richer structure than the KdV. Furthermore, it belongs to the most fundamental integrable system in the sense that many known integrable systems can be derived as special reductions of the *KP hierarchy* [AC91]. The KP equation has been recognized to be related to various areas of mathematics and physics, such as algebraic and enumerative geometry, combinatorics, quantum field theory, representation theory, and random matrix theory [Kod04, KS13, Wit88, ACvM12]. In this thesis, we are interested in the interplay between algebraic geometry and integrable systems, connecting the study of complex algebraic curves to the KP equation. There is a substantial body of literature on this topic: see for example [AG18, AÇS21, Dub81, KX21, Kri77, Nak18, Nak19].

A fundamental contribution to building the connection to algebraic geometry is due to Krichever, [Kri77] who provided an algebro-geometric procedure to construct KP solutions starting from a smooth point on a genus g complex algebraic curve. Given a smooth complex algebraic curve, we write B for its Riemann matrix. One considers the associated Riemann theta function

$$\theta = \theta(\mathbf{z} \mid B) = \sum_{\mathbf{c} \in \mathbb{Z}^g} \exp\left[\frac{1}{2}\mathbf{c}^T B \mathbf{c} + \mathbf{c}^T \mathbf{z}\right]. \tag{2.0.2}$$

This formulation of the Riemann theta function differs slightly from the one presented (1.1.2) because we use the Riemann matrix B normalized to have a negative definite real part to emphasize the real numbers. Krichever [Kri77] constructed g-phase solutions to the KP equation as follows. Let $\tau(x, y, t)$ be obtained from (2.0.2) by setting $\mathbf{z} = \mathbf{u}x + \mathbf{v}y + \mathbf{w}t$. Here,

$\mathbf{u} = (u_1, \ldots, u_g)$, $\mathbf{v} = (v_1, \ldots, v_g)$, $\mathbf{w} = (w_1, \ldots, w_g)$ are coordinates on the weighted projective space $\mathbb{WP}^{3g-1}$ that is defined by

$$\deg(u_i) = 1, \quad \deg(v_i) = 2, \quad \deg(w_i) = 3 \quad \text{for} \quad i = 1, 2, \ldots, g. \qquad (2.0.3)$$

We require that the trivariate tau function $\tau(x, y, t)$ satisfies Hirota's differential equation

$$\tau\tau_{xxxx} - 4\tau_{xxx}\tau_x + 3\tau_{xx}^2 \; + \; 4\tau_x\tau_t - 4\tau\tau_{xt} + 3\tau\tau_{yy} - 3\tau_y^2 \; = \; 0. \qquad (2.0.4)$$

Under this hypothesis, the following function satisfies (2.0.1), and we call it the *KP solution*:

$$p(x, y, t) \; = \; 2\partial_x^2 \log \tau(x, y, t). \qquad (2.0.5)$$

The *Dubrovin threefold* studied in [AÇS21] comprises all points $(\mathbf{u}, \mathbf{v}, \mathbf{w})$ in $\mathbb{WP}^{3g-1}$ for which (2.0.4) holds. We refer to [AÇS21, §2] for a detailed explanation of Krichever's parameterization of KP solutions.

This chapter concerns the study of the aforementioned objects when the smooth curve is defined over a non-archimedean field $\mathbb{K}$ such as $\mathbb{Q}(\epsilon)$ or the Puiseux series $\mathbb{C}\{\{\epsilon\}\}$. The Riemann matrix B_ϵ depends analytically on the parameter ϵ, and hence so do the tau function and KP solution. In the limit $\epsilon \to 0$, the curve degenerates to a curve with only rational components with at worst nodal singularities, and the theta function becomes a finite sum of exponentials. We aim to study the behavior of the KP solution in this context and connect it to the so-called *soliton solutions*.

This chapter is organized as follows. In Subsection 2.1 we review the derivation of tropical Riemann matrices. Theorem 2.1.2 characterizes degenerations of theta functions from algebraic curves over $\mathbb{K}$. Proposition 2.1.3 shows that $\mathcal{C}$ is the vertex set of a Delaunay polytope in $\mathbb{Z}^g$. In Subsection 2.1.1 we study the *Hirota variety* $\mathcal{H}_\mathcal{C}$, which parameterizes soliton solutions and lives in $(\mathbb{K}^*)^m \times \mathbb{WP}^{3g-1}$. Theorem 2.1.8 characterizes the Hirota variety of the g-simplex.

A key idea in this chapter is to never compute a Riemann matrix or the theta function (2.0.2). Instead we follow the approach in [KX21, Nak18, Nak19] that rests on the Sato Grassmannian (Theorem 2.1.11). This setting is entirely algebraic and hence amenable to symbolic computation over $\mathbb{K}$. Subsection 2.1.2 explains the computation of tau functions from points on the Sato Grassmannian.

In Subsection 2.1.3 we start from an algebraic curve X over $\mathbb{K}$. Certain Riemann-Roch spaces on X are encoded as points on the Sato Grassmannian. Following [Nak19], we present an algorithm and its `Maple` implementation for computing these points and the resulting tau functions, for X hyperelliptic. Proposition 2.1.20 addresses the case when X is reducible. This is followed up in Subsection 2.1.4, where we present Algorithm 2.1.24 for attaining KP solitons from nodal rational curves.

Section 2.2 focuses on X being an irreducible rational nodal curve of genus g. In this case, the Riemann theta function, in the limit $\epsilon \to 0$, is supported on the g-dimensional cube $\mathcal{C} = \{0, 1\}^g$. We study in detail the Hirota variety $\mathcal{H}_\mathcal{C}$ associated to X. Of particular interest is the irreducible subvariety defined as the image of a parameterization map, we call this the *main component*. Proving that this is an irreducible component of the Hirota variety corresponds to solving a classical problem in algebraic geometry, namely the *weak Schottky problem* for rational nodal curves. Theorem 2.2.3 solves this problem up to genus nine using computational tools. Finally, Subsection 2.2.3 studies the equations of the *main component* of the variety $\mathcal{H}_\mathcal{C}$ and how this relates to the combinatorics of the cube. We conclude the section with a more explicit discussion on the Schottky problem for irreducible rational nodal curves. Finally, in Section 2.3, we propose some open problems and conjectures.

Soliton solutions

One of the main breakthroughs in KP theory was given by Sato [Sat81], who realized that solutions of the KP equation could be written in terms of points of an infinite-dimensional Grassmannian. Multiline soliton solutions are a special class of KP solutions that may be characterized with a finite-dimensional version of Sato theory. These are solutions of type (2.0.5) where the τ function is defined as follows. Fix positive integers $k < n$ and a vector of parameters $\kappa = (\kappa_1, \kappa_2, \ldots, \kappa_n)$. For each k-element index set $I \in \binom{[n]}{k}$, we introduce an unknown p_I that serves as a Plücker coordinate. Then the function τ is defined as a linear combination of exponential functions

$$\tau(x, y, t) = \sum_{I \in \binom{[n]}{k}} p_I \cdot \prod_{\substack{i,j \in I \\ i < j}} (\kappa_j - \kappa_i) \cdot \exp\left[x \cdot \sum_{i \in I} \kappa_i + y \cdot \sum_{i \in I} \kappa_i^2 + t \cdot \sum_{i \in I} \kappa_i^3 \right]. \qquad (2.0.6)$$

The following result establishes the connection between finite Grassmannians and solitons:

Proposition 2.0.1. *The function τ is a solution to Hirota's equation (2.0.4) if and only if the point $p = (p_I)_{I \in \binom{[n]}{k}}$ lies in the Grassmannian $\mathrm{Gr}(k, n)$, i.e. there is a $k \times n$ matrix $A = (a_{ij})$ such that, for all $I \in \binom{[n]}{k}$, the coefficient p_I is the $k \times k$-minor of A with column indices I.*

Proof. This follows from [Kod17, Theorem 1.3]. ∎

We define a (k, n)-*soliton* to be any function $\tau(x, y, t)$ where $\kappa \in \mathbb{R}^n$ and $p \in \mathrm{Gr}(k, n)$. The pair (κ, A) is often referred to as *soliton data*.

Furthermore, Kodama and Williams [KW14] enlarged the interdisciplinarity of KP theory to combinatorics by building a surprising connection between positive finite-dimensional Grassmannians and the structure of real regular soliton solutions.

In this chapter, our aim is to compute the KP solutions associated to algebraic curves admitting at worst nodal singularities to recover KP solitons explicitly using computer algebra. The underlying idea is to study the behavior of the curve and the corresponding Riemann theta function. Theorem 2.1.2 proves that, in the limit, the Riemann theta function reduces to a finite sum

$$\theta_{\mathcal{C}}(\mathbf{z}) = a_1 \exp\left[\mathbf{c}_1^T \mathbf{z} \right] + a_2 \exp\left[\mathbf{c}_2^T \mathbf{z} \right] + \cdots + a_m \exp\left[\mathbf{c}_m^T \mathbf{z} \right], \qquad (2.0.7)$$

where $\mathcal{C} = \{\mathbf{c}_1, \mathbf{c}_2, \ldots, \mathbf{c}_m\}$ is a certain subset of the integer lattice $\mathbb{Z}^g$. Each lattice point $\mathbf{c}_i = (c_{i1}, \ldots, c_{ig})$ specifies a linear form $\mathbf{c}_i^T \mathbf{z} = \sum_{j=1}^g c_{ij} z_j$, just like in (2.0.2). The coefficients $\mathbf{a} = (a_1, a_2, \ldots, a_m)$ are unknowns that serve as coordinates on the algebraic torus $(\mathbb{K}^*)^m$. We refer to (2.0.7) as the *degenerate theta function*.

2.1. Nodal curves

We work over a field $\mathbb{K}$ of characteristic zero with a non-archimedean valuation. Let X be a *Mumford curve* of genus g, that is, X is a smooth curve over $\mathbb{K}$ whose Berkovich analytification is a graph with g cycles, see [Bra20]. This metric graph is the tropicalization $\mathrm{Trop}(X)$ of a faithful embedding of X. In spite of the recent advances in [Jel20], computing $\mathrm{Trop}(X)$ from X remains a nontrivial task, with no known algorithm. All our examples were derived with the methods in [Bra20, Chapter 4].

If the curve X is hyperelliptic, given by an equation $y^2 = f(x)$, then $\mathrm{Trop}(X)$ is a metric graph with a harmonic two-to-one map onto the phylogenetic tree encoding the roots of $f(x)$. The combinatorics of harmonic maps is subtle. We refer to [BBC17, Definition 2.2] for a detailed explanation.

Example 2.1.1 ($g = 2$). Consider a genus two curve $y^2 = f_i(x)$ where $f_i(x)$ is a polynomial of degree six with coefficients in $\mathbb{Q}(\epsilon)$. Two instances are given by the polynomials:

$$\begin{aligned} f_1(x) &= (x-1)(x-2\epsilon)(x-3\epsilon^2)(x-4\epsilon^3)(x-5\epsilon^4)(x-6\epsilon^5), \\ f_2(x) &= (x-1)(x-1-\epsilon)(x-2)(x-2-\epsilon)(x-3)(x-3-\epsilon). \end{aligned} \tag{2.1.1}$$

Note that f_2 is an example of a degeneration as in [Nak19, §7]. The six roots determine a subtree with six leaves in the Berkovich line. The edge lengths are invariants of the semistable model [Bra20] over the valuation ring of $\mathbb{K}$. There are two combinatorial types of trivalent trees with six leaves, the *caterpillar* and the *snowflake*. These are realized by the polynomials in (2.1.1):
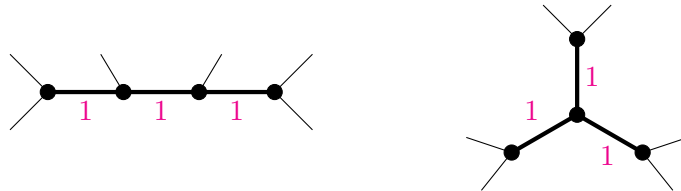
Figure 2.1. The metric trees for the polynomials f_1 (left) and f_2 (right) in (2.1.1)

Each trivalent metric tree with $2g + 2$ leaves has a unique hyperelliptic covering by a metric graph of genus g. This is the content of [BBC17, Lemma 2.4]. The edge lengths of the genus g graph are obtained from those of the tree by stretching or shrinking with a factor of 2. Figure 2.2 shows the graphs that give a two-to-one map to the trees in Figure 2.1.
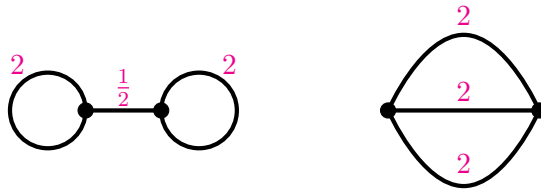
Figure 2.2. The metric graphs $\mathrm{Trop}(X)$ for the curves X in (2.1.1) and Figure 2.1.

For any fixed $\epsilon \in \mathbb{C}^*$, we can compute the Dubrovin threefold in $\mathbb{WP}^5$, using [AÇS21, Theorem 3.7], and derive KP solutions from its points. The difficulty is to maintain ϵ as a parameter and to understand what happens for $\epsilon \to 0$. The use of the tropical Riemann matrix together with the degeneration techniques we introduce in what follows provide an alternative method to deal with the parameter ϵ.

From the tropical curve $\mathrm{Trop}(X)$ we can read off the tropical Riemann matrix Q. This is a positive definite real symmetric $g \times g$ matrix. Fix a basis of cycles in $\mathrm{Trop}(X)$ and write them as the g rows of a matrix Λ whose columns are labeled by the edges. Let Δ be the diagonal matrix whose entries are the edge lengths of $\mathrm{Trop}(X)$. Then we have $Q = \Lambda \Delta \Lambda^T$.

The genus two graphs in Figure 2.2 have three edges. Their Riemann matrices are

$$Q_1 = \begin{bmatrix} 1 & 0 & 0 \\ 0 & 0 & 1 \end{bmatrix} \begin{bmatrix} 2 & 0 & 0 \\ 0 & \frac{1}{2} & 0 \\ 0 & 0 & 2 \end{bmatrix} \begin{bmatrix} 1 & 0 \\ 0 & 0 \\ 0 & 1 \end{bmatrix} = \begin{bmatrix} 2 & 0 \\ 0 & 2 \end{bmatrix} \quad \text{and} \quad Q_2 = \begin{bmatrix} 1 & -1 & 0 \\ 0 & 1 & -1 \end{bmatrix} \begin{bmatrix} 2 & 0 & 0 \\ 0 & 2 & 0 \\ 0 & 0 & 2 \end{bmatrix} \begin{bmatrix} 1 & 0 \\ -1 & 1 \\ 0 & -1 \end{bmatrix} = \begin{bmatrix} 4 & -2 \\ -2 & 4 \end{bmatrix}.$$

We now consider the degeneration of our curve X over $\mathbb{K} = \mathbb{C}\{\{\epsilon\}\}$ to its tropical limit. The Riemann matrix can be written in the form $B_\epsilon = -\frac{1}{\epsilon}Q + R_\epsilon$, where R_ϵ is a symmetric $g \times g$ matrix whose entries are complex analytic functions in ϵ that converge as $\epsilon \to 0$.

Fix a point $\mathbf{a} \in \mathbb{R}^g$. Replacing $\mathbf{z}$ by $\mathbf{z} + \frac{1}{\epsilon}Q\mathbf{a}$ in the Riemann theta function (2.0.2), we obtain

$$\theta\left(\mathbf{z} + \frac{1}{\epsilon}Q\mathbf{a} \,\middle|\, B_\epsilon\right) \;=\; \sum_{\mathbf{c}\in\mathbb{Z}^g} \exp\left[-\frac{1}{2\epsilon}\mathbf{c}^T Q\mathbf{c} + \frac{1}{\epsilon}\mathbf{c}^T Q\mathbf{a}\right] \cdot \exp\left[\frac{1}{2}\mathbf{c}^T R_\epsilon \mathbf{c} + \mathbf{c}^T \mathbf{z}\right]. \qquad (2.1.2)$$

This expression converges for $\epsilon \to 0$ provided $\mathbf{c}^T Q\mathbf{c} - 2\mathbf{c}^T Q\mathbf{a} \geq 0$ for all $\mathbf{c} \in \mathbb{Z}^g$. Equivalently,

$$\mathbf{a}^T Q\mathbf{a} \leq (\mathbf{a} - \mathbf{c})^T Q(\mathbf{a} - \mathbf{c}) \quad \text{for all } \mathbf{c} \in \mathbb{Z}^g. \qquad (2.1.3)$$

This means that the distance from $\mathbf{a}$ to the origin, in the metric given by Q, is at most the distance to any other lattice point $\mathbf{c} \in \mathbb{Z}^g$. In other words, (2.1.3) means that $\mathbf{a}$ belongs to the *Voronoi cell* for Q. Under this hypothesis, we now consider the associated *Delaunay set*

$$\mathcal{D}_{\mathbf{a},Q} \;=\; \left\{ \mathbf{c} \in \mathbb{Z}^g \,:\, \mathbf{a}^T Q\mathbf{a} = (\mathbf{a} - \mathbf{c})^T Q(\mathbf{a} - \mathbf{c}) \right\}. \qquad (2.1.4)$$

This is the set of vertices of a polytope in the Delaunay subdivision of $\mathbb{Z}^g$ induced by Q. If $\mathbf{a}$ is a vertex of the Voronoi cell then the Delaunay polytope $\mathrm{conv}(\mathcal{D}_{\mathbf{a},Q})$ is g-dimensional. Figure 2.3 shows an example of a Delaunay polytope and the corresponding Voronoi cells for $g = 3$.
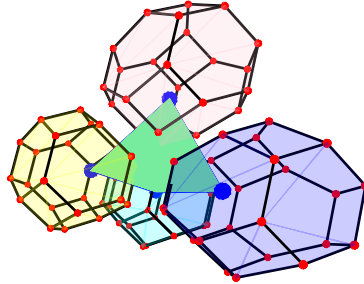
Figure 2.3. The Delaunay polytope in the figure is given by the green tetrahedron. The four coloured permutohedra need to be thought as glued together, they are Voronoi cells with the tetrahedron as corresponding Delaunay set. The polytopes were computed using `Maple` [MGH+12] and the figures were created using `polymake` [GJ20].

As in [AÇSS21, §4], we observe that $\exp\left[-\frac{1}{2\epsilon}\mathbf{c}^T Q\mathbf{c} + \frac{1}{\epsilon}\mathbf{c}^T Q\mathbf{a}\right]$ converges to 1 for $\mathbf{c} \in \mathcal{D}_{\mathbf{a},Q}$ and to 0 for $\mathbf{c} \in \mathbb{Z}^g \backslash \mathcal{D}_{\mathbf{a},Q}$. We have thus derived the following generalization of [AÇSS21, Theorem 4]:

Theorem 2.1.2. *Fix $\mathbf{a}$ in the Voronoi cell of the tropical Riemann matrix Q. For $\epsilon \to 0$, the series (2.1.2) converges to a theta function (2.0.7) supported on the Delaunay set $\mathcal{C} = \mathcal{D}_{\mathbf{a},Q}$, namely*

$$\theta_{\mathcal{C}}(\mathbf{z}) \;=\; \sum_{\mathbf{c}\in\mathcal{C}} a_{\mathbf{c}} \exp\left[\mathbf{c}^T \mathbf{z}\right], \quad \text{where} \quad a_{\mathbf{c}} = \exp\left[\frac{1}{2}\mathbf{c}^T R_0 \mathbf{c}\right]. \qquad (2.1.5)$$

The Delaunay polytope $\mathrm{conv}(\mathcal{C})$ can have any dimension between 0 and g, depending on the location of $\mathbf{a}$ in the Voronoi cell (2.1.3). If $\mathbf{a}$ lies in the interior then $\mathcal{C} = \{\mathbf{0}\}$ is just the origin. We are most interested in the case when $\mathbf{a}$ is a vertex of the Voronoi cell, and we now assume this to be the case. This ensures that $\mathcal{C}$ is the vertex set of a g-dimensional

Delaunay polytope. For fixed g, there is only a finite list of Delaunay polytopes, up to lattice isomorphism. Thanks to [Dut04] and its references, that list is known for $g \leq 6$. However, not every Delaunay polytope arises from a curve X and its tropical Riemann matrix $Q = \Lambda \Delta \Lambda^T$. To illustrate these points, we present the list of all relevant Delaunay polytopes for $g \leq 4$.

Proposition 2.1.3. *The complete list of Delaunay polytopes $\mathcal{C}$ arising from metric graphs for $g \leq 4$ is as follows. For $g = 2$ there are two types: triangle and square. For $g = 3$ there are five types: tetrahedron, square-based pyramid, octahedron, triangular prism and cube. For $g = 4$ there are 17 types. These $\mathcal{C}$ have between 5 and 16 vertices. They are listed in Table 2.1.*

Proof. For any edge e of the graph, let $\lambda_e \in \mathbb{Z}^g$ be the associated column of Λ. The Voronoi cell is a zonotope, obtained by summing line segments parallel to λ_e for all e. It has $\mathbf{a}$ as a vertex. After reorienting edges, in the corresponding expression of $\mathbf{a}$ as a linear combination of the vectors λ_e, all coefficients are positive. This means that the Delaunay polytope equals

$$\text{conv}(\mathcal{C}) = \left\{ \mathbf{c} \in \mathbb{R}^g \,:\, 0 \leq \lambda_e^T \mathbf{c} \leq 1 \ \text{ for all edges } e \right\}. \tag{2.1.6}$$

Our task is to classify the polytopes (2.1.6) for all graphs of genus g and all their orientations. For $g = 2$ this is easy, and for $g = 3$ it was done in [AÇSS21, Theorem 4]. We see from [AÇSS21, Figure 2] that every Delaunay polytope can be realized by a curve over $\mathbb{K}$. For $g = 4$ we started from the classification of 19 Delaunay polytopes in [ER87, Theorem 6.2], labeled $1, 2, \ldots, 16$ in [ER87, Table V] and labeled A,B,C in [ER87, Table VI]. Two types do not arise from graphs, namely the pyramid over the octahedron (#B) and the cross polytope (#C). The other 17 Delaunay polytopes all arise from graphs. They are listed in Table 2.1. The second row gives the number of vertices. The third row gives the number of facets. These two numbers uniquely identify the isomorphism type of $\mathcal{C}$. The last row indicates which graphs give rise to that Delaunay polytope. We refer to the 16 graphs of genus 4 by the labeling used in [CKS19, Table 1]. Table 2.1 was constructed by a direct computation. It establishes the $g = 4$ case in Proposition 2.1.3. ∎

polytopes	1	2	3	4	5	6	7	8	9	10	11	12	13	14	15	16	A
vertices	5	6	7	7	8	8	8	9	9	9	10	10	10	12	12	16	6
facets	5	6	6	8	7	9	6	7	9	6	7	12	10	7	10	8	9
graphs	1,2,3,4 5,7,10,13	1,3,4 5,6,9	3,7,10	4	7	5	8,11,15	6	10	12	11	9	13	12	15	16	2

Table 2.1. The 17 Delaunay polytopes that arise from the 16 graphs of genus 4. Polytopes are labeled as in [ER87, Tables V and VI] and graphs are labeled as in [CKS19, Table 1]. For instance, the complete bipartite graph $K_{3,3}$ is #2, and it has two Delaunay polytopes, namely the simplex (#1) and the cyclic 4-polytope with 6 vertices (#A). The polytope #3 has 7 vertices and 6 facets. It is the pyramid over the triangular prism, and it arises from three graphs (#3,7,10).

2.1.1. Hirota varieties

As aforementioned, the solutions to the KP equation arising from a fixed complex algebraic curve of genus g are parametrized by a threefold in a weighted projective space $\mathbb{WP}^{3g-1}$, which was named after Boris Dubrovin by Agostini, Çelik, and Sturmfels in [AÇS21]. Furthermore, using current methods from nonlinear algebra, they also study parameterizations

and defining ideals of Dubrovin threefolds. In this subsection we introduce the Hirota variety as the analogue to the Dubrovin threefold [AÇS21] for the degenerate Riemann theta function (2.0.7) of a nodal curve.

Starting from the configuration $\mathcal{C}$ and its theta function in (2.0.7), we consider the tau function

$$\tau(x,y,t) \;=\; \theta_{\mathcal{C}}(\mathbf{u}x + \mathbf{v}y + \mathbf{w}t) \;=\; \sum_{i=1}^{m} a_i \exp\!\left[\left(\sum_{j=1}^{g} c_{ij}u_j\right)x + \left(\sum_{j=1}^{g} c_{ij}v_j\right)y + \left(\sum_{j=1}^{g} c_{ij}w_j\right)t\right].$$

The *Hirota variety* $\mathcal{H}_{\mathcal{C}}$ consists of all points $\big(\mathbf{a},(\mathbf{u},\mathbf{v},\mathbf{w})\big)$ in the parameter space $(\mathbb{K}^{*})^{m} \times \mathbb{WP}^{3g-1}$ for which $\tau(x,y,t)$ satisfies Hirota's differential equation (2.0.4). Here, the grading for the weighted projective space $\mathbb{WP}^{3g-1}$ is the same as in (2.0.3).

We recall from [Kod17, equation (2.25)] that (2.0.4) can be written via the Hirota differential operators as $P(D_x, D_y, D_t)\tau \bullet \tau = 0$, for the special polynomial $P(x,y,t) = x^4 - 4xt + 3y^2$. For any fixed index j, the equation $P(u_j, v_j, w_j) = 0$ defines a curve in the weighted projective plane $\mathbb{WP}^2$. More generally, for any two indices k, ℓ in $\{1, \dots, m\}$, we consider the hypersurface in $\mathbb{WP}^{3g-1}$ defined by

$$P_{k\ell}(\mathbf{u}, \mathbf{v}, \mathbf{w}) \;:=\; P\big((\mathbf{c}_k - \mathbf{c}_\ell)\cdot\mathbf{u},\, (\mathbf{c}_k - \mathbf{c}_\ell)\cdot\mathbf{v},\, (\mathbf{c}_k - \mathbf{c}_\ell)\cdot\mathbf{w}\big).$$

This expression is unchanged if we switch k and ℓ. The defining equations of the Hirota variety $\mathcal{H}_{\mathcal{C}}$ can be obtained from the following lemma, which is proved by direct computation.

Lemma 2.1.4. *The result of applying the differential operator (2.0.4) to the function $\tau(x,y,t)$ equals*

$$\sum_{1 \le k < \ell \le m} a_k a_\ell\, P_{k\ell}(\mathbf{u}, \mathbf{v}, \mathbf{w}) \exp\!\big[\,((\mathbf{c}_k+\mathbf{c}_\ell)\cdot\mathbf{u})\, x + ((\mathbf{c}_k+\mathbf{c}_\ell)\cdot\mathbf{v})\, y + ((\mathbf{c}_k+\mathbf{c}_\ell)\cdot\mathbf{w})\, t\,\big]. \quad (2.1.7)$$

The polynomials defining the Hirota variety of $\mathcal{C}$ are the coefficients we obtain by writing (2.1.7) as linear combination of distinct exponentials. These correspond to points in the set

$$\mathcal{C}^{[2]} \;=\; \big\{\, \mathbf{c}_k + \mathbf{c}_\ell \;:\; 1 \le k < \ell \le m \,\big\} \quad \subset \quad \mathbb{Z}^g. \qquad (2.1.8)$$

A point $\mathbf{d}$ in $\mathcal{C}^{[2]}$ is *uniquely attained* if there exists precisely one index pair (k,ℓ) such that $\mathbf{c}_k + \mathbf{c}_\ell = \mathbf{d}$. In that case, (k,ℓ) is a *unique pair*, and this contributes the quartic $P_{k\ell}(\mathbf{u}, \mathbf{v}, \mathbf{w})$ to our defining equations. If $\mathbf{d} \in \mathcal{C}^{[2]}$ is not uniquely attained, then we seek the polynomial

$$\sum_{\substack{1 \le k < \ell \le m \\ \mathbf{c}_k + \mathbf{c}_\ell = \mathbf{d}}} P_{k\ell}(\mathbf{u}, \mathbf{v}, \mathbf{w})\, a_k a_\ell. \qquad (2.1.9)$$

Corollary 2.1.5. *The Hirota variety $\mathcal{H}_{\mathcal{C}}$ is defined by the quartics $P_{k\ell}$ for all unique pairs (k,ℓ) and by the polynomials (2.2.19) for all non-uniquely attained points $\mathbf{d} \in \mathcal{C}^{[2]}$. If all points in $\mathcal{C}^{[2]}$ are uniquely attained then $\mathcal{H}_{\mathcal{C}}$ is defined by the $\binom{m}{2}$ quartics $P_{k\ell}(\mathbf{u}, \mathbf{v}, \mathbf{w})$, so its equations do not involve the coefficients $a_1, \dots, a_m$. This is the case when $\mathcal{C}$ is the vertex set of a simplex.*

Proof. To obtain the defining equation of the Hirota variety we ask for the vanishing of the polynomials in the ring $\mathbb{C}[\mathbf{a}, \mathbf{u}, \mathbf{v}, \mathbf{w}]$ which provide coefficients for the exponentials appearing in (2.1.7). Notice that such exponential terms depend exclusively on the sums $\mathbf{c}_k + \mathbf{c}_\ell$. Denote e_i the i-th unitary vector in $\mathbb{Z}^g$. When $\mathcal{C} = \{\mathbf{0}, e_1, \dots, e_g\}$, the set $\mathcal{C}^{[2]} = \{e_i, e_{i+j}, : i, j \in [g], i < j\}$, where e_i is uniquely attained as $e_i + \mathbf{0}$ and e_{i+j}, can only be attained as $e_i + e_j$. ∎

Example 2.1.6 (The Square)**.** The configuration in $\mathbb{Z}^2$ that arises from the polynomial f_1 in (2.1.1), where the genus $g = 2$, is the square $\mathcal{C} = \{(0,0),(1,0),(0,1),(1,1)\}$. Here,

$$\mathcal{C}^{[2]} = \{(0,1),(1,0),(1,1),(1,2),(2,1)\}.$$

The Hirota variety $\mathcal{H}_\mathcal{C}$ is a complete intersection of codimension three in $(\mathbb{K}^*)^4 \times \mathbb{WP}^5$. There are four unique pairs (k,ℓ) and these contribute the two quartics $P_{13} = P_{24} = u_1^4 - 4u_1w_1 + 3v_1^2$ and $P_{12} = P_{34} = u_2^4 - 4u_2w_2 + 3v_2^2$. The point $\mathbf{d} = (1,1)$ is not uniquely attained in $\mathcal{C}^{[2]}$. The polynomial (2.2.19) contributed by this $\mathbf{d}$ equals

$$P(u_1 + u_2, v_1 + v_2, w_1 + w_2)\, a_{00}a_{11} \; + \; P(u_1 - u_2, v_1 - v_2, w_1 - w_2)\, a_{01}a_{10}. \qquad (2.1.10)$$

For any point in $\mathcal{H}_\mathcal{C}$, we can write $\tau(x,y,t)$ as a $(2,4)$-soliton, as shown in [Kod17, § 2.5]. Therefore, in order for the associated theta function $\theta_\mathcal{C} = a_{00} + a_{10}\exp[z_1] + a_{01}\exp[z_2] + a_{11}\exp[z_1 + z_2]$ to yield a KP solution, the following three polynomial identities are necessary and sufficient:

$$\begin{array}{ll} u_1^4 - 4u_1w_1 + 3v_1^2 = 0, & \big((u_1+u_2)^4 - 4(u_1+u_2)(w_1+w_2) + 3(v_1+v_2)^2\big)\, a_{00}a_{11} \\ u_2^4 - 4u_2w_2 + 3v_2^2 = 0, & +\big((u_1-u_2)^4 - 4(u_1-u_2)(w_1-w_2) + 3(v_1-v_2)^2\big)\, a_{01}a_{10} = 0. \end{array}$$

If these conditions hold then $p(x,y,t)$ can be written as a $(2,4)$-soliton by [Kod17, §2.5].

We now consider the simplex $\mathcal{C} = \{\mathbf{0}, e_1, \ldots, e_g\}$. This arises from plane quartics ($g = 3$) that degenerate to four lines or to a conic plus two lines [AÇSS21, Example 5]. For higher genus, it is not obvious understanding the degeneration that would lead to the simplex. The tau function is

$$\tau(x,y,t) = a_0 + a_1\exp[u_1x + v_1y + w_1t] + a_2\exp[u_2x + v_2y + w_2t] + \cdots + a_g\exp[u_gx + v_gy + w_gt].$$

We know from Corollary 2.1.5 that the conditions imposed by Hirota's differential equation (2.0.4) do not depend on $\mathbf{a}$ but only on $\mathbf{u}, \mathbf{v}, \mathbf{w}$. We thus consider the Hirota variety $\mathcal{H}_\mathcal{C}$ in $\mathbb{WP}^{3g-1}$.

Lemma 2.1.7. *The Hirota variety $\mathcal{H}_\mathcal{C}$ of the simplex $\mathcal{C}$ is the union of two irreducible components of dimension g in $\mathbb{WP}^{3g-1}$. One of the two components has the following parametric representation:*

$$u_j \mapsto \kappa_j - \kappa_0\,, \;\; v_j \mapsto \kappa_j^2 - \kappa_0^2\,, \;\; w_j \mapsto \kappa_j^3 - \kappa_0^3 \quad \text{for } j = 1, 2, \ldots, g. \qquad (2.1.11)$$

The other component is obtained from (2.1.11) by the sign change $v_j \mapsto -v_j$ for $j = 1, \ldots, g$.

Proof. By Corollary 2.1.5, the variety $\mathcal{H}_\mathcal{C}$ is defined by the quartics $P(u_i, v_i, w_i)$ and $P(u_i - u_j, v_i - v_j, w_i - w_j)$. The first g quartics imply $u_j = \kappa_j - \kappa_{j+g}$, $v_j = \kappa_j^2 - \kappa_{j+g}^2$, $w_j = \kappa_j^3 - \kappa_{j+g}^3$ for $j = 1, \ldots, g$. Under these substitutions, the remaining $\binom{g}{2}$ quartics factor into products of expressions $\kappa_i - \kappa_j$. Analyzing all cases up to symmetry reveals the two components. $\blacksquare$

Setting $t = \kappa_0$ and $\kappa_j = u_j + t$, the parameterization (2.1.11) of $\mathcal{H}_\mathcal{C}$ can be written as follows:

$$u_j \mapsto u_j\,, \;\; v_j \mapsto 2u_jt + u_j^2\,, \;\; w_j \mapsto 3u_jt^2 + 3u_j^2t + u_j^3 \quad \text{for } j = 1, 2, \ldots, g. \qquad (2.1.12)$$

Theorem 2.1.8. *The prime ideal of the Hirota variety in (2.1.11) is minimally generated by*

(a) the $\binom{g}{2}$ cubics $\underline{v_iu_j - v_ju_i} - u_iu_j(u_i - u_j)$ for $1 \leq i < j \leq g$,

(b) the g quartics $4\underline{w_i u_i} - 3v_i^2 - u_i^4$ for $i = 1, \ldots, g$,

(c) the $g(g-1)$ quartics $4\underline{w_j u_i} - 3v_i v_j + 3u_i(u_i - u_j)v_j - u_i u_j^3$ for $i \neq j$, and

(d) the $\binom{g}{2}$ quintics $4\underline{w_i v_j} - 4w_j v_i + 3u_i v_j(v_j - v_i) + u_i v_j(u_j - u_i)(u_i - 2u_j) + u_i u_j^3(u_i - u_j)$.

These $2g^2 - g$ ideal generators are a minimal Gröbner basis with the underlined leading terms.

Proof. We consider the subalgebra of $\mathbb{K}[t, u_1, \ldots, u_g]$ that is generated by the $3g$ polynomials in the parametrization (2.1.12). We sort terms by t-degree. We claim that this is a *Khovanskii basis*, or *basis*, as defined in [KM19] or [Stu96, Chapter 11]. The parametrization given by the leading monomials $u_j \mapsto u_j$, $v_j \mapsto 2u_j t$, $w_j \mapsto 3u_j t^2$ defines a toric variety, namely the embedding of $\mathbb{P}^1 \times \mathbb{P}^{g-1}$ into $\mathbb{P}^{3g-1}$ by the very ample line bundle $\mathcal{O}(2, 1)$. Its toric ideal is generated by the leading binomials $v_i u_j - v_j u_i$, $4w_i u_i - 3v_i^2$, $4w_j u_i - 3v_i v_j$, $w_i v_j - w_j v_i$ seen in (a)-(d). In fact, by [Stu96, §14.A], these $2g^2 - g$ quadrics form a square-free Gröbner basis with underlined leading monomials. Under the correspondence in [Stu96, Theorem 8.3], this initial ideal corresponds to a unimodular triangulation of the associated polytope $(2\Delta_1) \times \Delta_{g-1}$.

One checks directly that the polynomials (a), (b), (c), (d) vanish for (2.1.12). Since only two indices i and j appear, by symmetry, it suffices to do this check for $g = 2$. Hence the generators of the toric ideal are the leading binomials of certain polynomials that vanish on the Hirota variety. By [KM19, Theorem 2.17] or [Stu96, Corollary 11.5], this proves the Khovanskii basis property. Geometrically speaking, we have constructed a toric degeneration from the Hirota variety to a toric variety in $\mathbb{WP}^{3g-1}$. Furthermore, using [KM19, Proposition 5.2] or [Stu96, Corollary 11.6 (1)] we conclude that the polynomials in (a)-(d) are a Gröbner basis for the prime ideal of (2.1.12), where the term order is chosen to select the underlined leading terms. ∎

Using the methods described above, we can compute the Hirota variety $\mathcal{H}_\mathcal{C}$ for each of the known Delaunay polytopes $\mathcal{C}$, starting with those in Proposition 2.1.3. We did this above for the triangle, the square, and the tetrahedron. Here is one more example.

Example 2.1.9 (Triangular prism). Let $g = 3$ and take $\theta_\mathcal{C}$ to be the six-term theta function

$$a_{000} + a_{100} \exp[z_1] + a_{001} \exp[z_3] + a_{101} \exp[z_1 + z_3] + a_{011} \exp[z_2 + z_3] + a_{111} \exp[z_1 + z_2 + z_3].$$

The prism $\mathcal{C}$ arises in the degeneration as in Theorem 2.1.2 from a smooth plane quartic to a cubic plus a line. This is the second diagram in Figures 1 and 2 in [AÇS21, page 11]. The Hirota variety is cut out by four quartics in u_i, v_i, w_i, one for each edge direction, plus three relations involving the a_{ijk}, one for each of the three quadrangle facets. The edges from the two triangle facets define a reducible variety of codimension 3. One irreducible component is given by

$$\langle u_1^4 + 3v_1^2 - 4u_1 w_1, \ u_2^4 + 3v_2^2 - 4u_2 w_2, \ u_1^2 u_2 + u_1 u_2^2 - u_2 v_1 + u_1 v_2 \rangle.$$

Together with the four other relations, this defines an irreducible variety of codimension 4 inside $(\mathbb{K}^*)^6 \times \mathbb{WP}^8$. That irreducible Hirota variety has the parametric representation

$$
\begin{aligned}
u_1 &= \kappa_1 - \kappa_2, & v_1 &= \kappa_1^2 - \kappa_2^2, & w_1 &= \kappa_1^3 - \kappa_2^3, \\
u_2 &= \kappa_2 - \kappa_3, & v_2 &= \kappa_2^2 - \kappa_3^2, & w_2 &= \kappa_2^3 - \kappa_3^3, \\
u_3 &= \kappa_4 - \kappa_5, & v_3 &= \kappa_4^2 - \kappa_5^2, & w_3 &= \kappa_4^3 - \kappa_5^3,
\end{aligned}
$$
$$
a_{000} = (\kappa_1 - \kappa_4)\lambda_0, \quad a_{100} = (\kappa_2 - \kappa_4)\lambda_0 \lambda_1, \quad a_{110} = (\kappa_3 - \kappa_4)\lambda_0 \lambda_1 \lambda_2,
$$
$$
a_{001} = (\kappa_1 - \kappa_5)\lambda_0 \lambda_3, \quad a_{101} = (\kappa_2 - \kappa_5)\lambda_0 \lambda_1 \lambda_3, \quad a_{111} = (\kappa_3 - \kappa_5)\lambda_0 \lambda_1 \lambda_2 \lambda_3.
$$

This allows us to write the τ-function as a $(2,5)$-soliton, with $A = \begin{pmatrix} 1 & 1 & 1 & 0 & 0 \\ 0 & 0 & 0 & 1 & 1 \end{pmatrix}$. The six bases of the matrix A correspond to the six terms in $\theta_{\mathcal{C}}$.

2.1.2. Sato Grassmannian

The Sato Grassmannian is a device for encoding all solutions to the KP equation. Recall that the classical Grassmannian $\mathrm{Gr}(k,n)$ parameterizes k-dimensional subspaces of $\mathbb{K}^n$. It is a projective variety in $\mathbb{P}^{\binom{n}{k}-1}$, cut out by quadratic relations known as *Plücker relations*. Following [MS21b, Chapter 5], the Plücker coordinates p_I are indexed by k-element subsets I of $\{1,2,\ldots,n\}$. As is customary in Schubert calculus [MS21b, §5.3], we identify these $\binom{n}{k}$ subsets with partitions λ that fit into a $k \times (n-k)$ rectangle. Such a partition λ is a sequence $(\lambda_1, \lambda_2, \ldots, \lambda_k)$ of integers that satisfy $n - k \geq \lambda_1 \geq \lambda_2 \geq \cdots \geq \lambda_k \geq 0$. The corresponding Plücker coordinate $c_\lambda = p_I$ is the maximal minor of a $k \times n$ matrix M of unknowns, as in [MS21b, §5.1], where the columns are indexed by $I = \{\lambda_k + 1, \lambda_{k-1} + 2, \ldots, \lambda_2 + k-1, \lambda_1 + k\}$. With this notation, the Plücker relations for $\mathrm{Gr}(k,n)$ are quadrics in the unknowns c_λ.

Example 2.1.10. We revisit [MS21b, Example 5.9] with Plücker coordinates indexed by partitions. The Grassmannian $\mathrm{Gr}(3,6)$ is a 9-dimensional subvariety in $\mathbb{P}^{19}$. Its prime ideal is generated by 35 Plücker quadrics. These are found easily by the following lines in Macaulay2 [GS]:

```
R = QQ[c,c1,c11,c111,c2,c21,c211,c22,c221,c222,c3,c31,c311,
c32,c321,c322,c33,c331,c332,c333];
I = Grassmannian(2,5,R)
```

The output consists of 30 three-term relations, like $\underline{c_{211}c_{22}} - c_{21}c_{221} + c_2 c_{222}$ and five four-term relations, like $\underline{c_{221}c_{31}} - c_{21}c_{321} + c_{11}c_{331} + c\, c_{333}$. These quadrics form a minimal Gröbner basis.

The *Sato Grassmannian* SGM is the zero set of the Plücker relations in the unknowns c_λ, where we now drop the constraint that λ fits into a $k \times (n-k)$-rectangle. Instead, we allow arbitrary partitions λ. What follows is the description of a minimal Gröbner basis for SGM.

Partitions are order ideals in the poset $\mathbb{N}^2$. The set of all order ideals, ordered by inclusion, is a distributive lattice, known as *Young's lattice*. Consider any two partitions λ and μ that are incomparable in Young's lattice. They fit into a common $k \times (n-k)$-rectangle, for some k and n. There is a canonical Plücker relation for $\mathrm{Gr}(k,n)$ that has leading monomial $c_\lambda c_\mu$. It is known that these *straightening relations* form a minimal Gröbner basis for fixed k and n. This property persists as k and $n-k$ increase, hence yielding a Gröbner basis for SGM.

The previous paragraph rephrases the definition in [DE18, Sat81] of the Sato Grassmannian as an inverse limit of projective varieties. This comes from the diagram of maps $\mathrm{Gr}(k,n{+}1) \dashrightarrow \mathrm{Gr}(k,n)$ and $\mathrm{Gr}(k{+}1,n{+}1) \dashrightarrow \mathrm{Gr}(k,n)$, where these rational maps are given by dropping the last index. This corresponds to *deletion* and *contraction* in matroid theory [MS21b, Chapter 13]. One checks that the simultaneous inverse limit for $k \to \infty$ and $n-k \to \infty$ is well-defined. The straightening relations in our equational description above are those in [DE18, Example 4.1]. That they form a Gröbner basis is best seen using Khovanskii bases [KM19, Example 7.3].

We next present the parametric representation of SGM that is commonly used in KP theory. Let $V = \mathbb{K}((z))$ be the field of formal Laurent series with coefficients in our ground field $\mathbb{K}$. Consider the natural projection map $\pi \colon V \to \mathbb{K}[z^{-1}]$ onto the polynomial ring in z^{-1}. We regard V and $\mathbb{K}[z^{-1}]$ as $\mathbb{K}$-vector spaces, with Laurent monomials z^i serving as bases.

Points in the Sato Grassmannian SGM correspond to $\mathbb{K}$-subspaces $U \subset V$ such that

$$\dim \operatorname{Ker} \pi_{|U} \ = \ \dim \operatorname{Coker} \pi_{|U}, \tag{2.1.13}$$

and this common dimension is finite. We can represent $U \in \mathrm{SGM}$ via a doubly infinite matrix as follows. For any basis $(f_1, f_2, f_3, \dots)$ of U, the jth basis vector is a Laurent series,

$$f_j(z) \ = \ \sum_{i=-\infty}^{+\infty} \xi_{i,j} z^{i+1}.$$

Then U is the column span of the infinite matrix $\xi = (\xi_{i,j})$ whose rows are indexed from top to bottom by $\mathbb{Z}$ and whose columns are indexed from right to left by $\mathbb{N}$. The ith row of ξ corresponds to the coefficients of z^{i+1}. Sato proved that a subspace U of V satisfies (2.1.13) if and only if there is a basis, called a *frame* of U, whose corresponding matrix has the shape

$$\xi \ = \ \begin{pmatrix}
\ddots & \vdots & \vdots & \vdots & \vdots & \cdots & \vdots \\
\cdots & \mathbf{1} & 0 & 0 & 0 & \cdots & 0 \\
\cdots & * & \mathbf{1} & 0 & 0 & \cdots & 0 \\
\cdots & * & * & \xi_{-\ell,\ell} & \xi_{-\ell,\ell-1} & \cdots & \xi_{-\ell,1} \\
\cdots & * & * & \xi_{-\ell+1,\ell} & \xi_{-\ell+1,\ell-1} & \cdots & \xi_{-\ell+1,1} \\
\vdots & \vdots & \vdots & \vdots & \vdots & \cdots & \vdots \\
\cdots & * & * & \xi_{-1,\ell} & \xi_{-1,\ell-1} & \cdots & \xi_{-1,1} \\
\cdots & * & * & \xi_{0,\ell} & \xi_{0,\ell-1} & \cdots & \xi_{0,1} \\
\cdots & * & * & \xi_{1,\ell} & \xi_{1,\ell-1} & \cdots & \xi_{1,1} \\
& \vdots & \vdots & \vdots & \vdots & \cdots & \vdots
\end{pmatrix}. \tag{2.1.14}$$

This matrix is infinite vertically, infinite on the left and, most importantly, it is eventually lower triangular with 1 on the diagonal, at the $(-n, n)$ positions. The space U is described by the positive integer ℓ and the submatrix with ℓ linearly independent columns whose upper left entry is $\xi_{-\ell,\ell}$. This description implies that a subspace U of V satisfies (2.1.13) if and only if

$$\text{there exists } \ell \in \mathbb{N} \text{ such that} \quad \dim U \cap V_n \ = \ n+1 \quad \text{for all } n \geq \ell, \tag{2.1.15}$$

where $V_n = z^{-n} \mathbb{K}[\![z]\!]$ denotes the space of Laurent series with a pole of order at most n.

The Plücker coordinates on SGM are computed as minors ξ_λ of the matrix ξ. Think of a partition λ as a weakly decreasing sequence of nonnegative integers that are eventually zero. Setting $m_i = \lambda_i - i$ for $i \in \mathbb{N}$, we obtain the associated *Maya diagram* $(m_1, m_2, m_3, \dots)$. This is a vector of strictly decreasing integers $m_1 > m_2 > \dots$ such that $m_i = -i$ for large enough i. Partitions and Maya diagrams are in natural bijection. Given any partition λ, we consider the matrix $(\xi_{m_i,j})_{i,j \geq 1}$ whose row indices $m_1, m_2, m_3, \dots$ are the entries in the Maya diagram of λ. Thanks to the shape of the matrix ξ, it makes sense to take the determinant

$$\xi_\lambda \ := \ \det(\xi_{m_i,j}). \tag{2.1.16}$$

This Plücker coordinate is a scalar in $\mathbb{K}$ that can be computed as a maximal minor of the finite matrix to the lower right of $\xi_{-\ell,\ell}$ in (2.1.14). We summarize our discussion as a theorem.

Theorem 2.1.11. *The Sato Grassmannian SGM is the inverse limit of the classical Grassmannians $\mathrm{Gr}(k,n) \subset \mathbb{P}^{\binom{n}{k}-1}$ as both k and $n-k$ tend to infinity. A parameterization of SGM is given by the matrix minors $c_\lambda = \xi_\lambda$ in (2.1.16), where λ runs over all partitions. The equations of SGM are the quadratic Plücker relations, shown in [DE18, Example 4.1] and in Example 2.1.10.*

We now connect the Grassmannians above to our study of solutions to the KP equation. Fix positive integers $k < n$ and a vector of parameters $\kappa = (\kappa_1, \kappa_2, \ldots, \kappa_n)$. Our ansatz for solving (2.0.4) is now the τ function (2.0.6). Notice that even the case $k = 1$ is interesting. Writing $A = \begin{pmatrix} a_1 & a_2 & \cdots & a_n \end{pmatrix}$, the $(1, n)$-soliton equals

$$\tau(x, y, t) \;=\; \sum_{i=1}^{n} a_i \exp\big[\, x \cdot \kappa_i \,+\, y \cdot \kappa_i^2 \,+\, t \cdot \kappa_i^3 \,\big].$$

If we now set $n = g + 1$ and divide the sum above by its first exponential term then we obtain the tau function associated with the g-simplex in Lemma 2.1.7. Hence the KP solutions that arise when the Delaunay polytope is a simplex are precisely the $(1, n)$-solitons.

We now connect the Sato Grassmannian and the classical finite Grassmannians to our study of solutions to the KP equation. First, we derive the Sato representation in [Kod17, Definition 1.3], that is, we express $\tau(x, y, t)$ as a linear combination of Schur polynomials. Let λ be a partition with at most three parts, written $\lambda_1 \geq \lambda_2 \geq \lambda_3 \geq 0$. Following [Kod17, §1.2.2], the associated Schur polynomial $\sigma_\lambda(x, y, t)$ can be defined as follows. We first introduce the *elementary Schur polynomial* $\sigma_j(x, y, t)$ by the series $\exp\big[\, x\lambda + y\lambda^2 + t\lambda^3 \,\big] = \sum_{j=0}^{\infty} \sigma_j(x, y, t)\lambda^j$. The *Schur polynomial* σ_λ for the partition $\lambda = (\lambda_1, \lambda_2, \lambda_3)$ is the determinant of the Jacobi-Trudi matrix of size 3×3:

$$\sigma_\lambda(x, y, t) \;=\; \det\big(\sigma_{\lambda_i - i + j}(x, y, t)\big)_{1 \leq i, j \leq 3}.$$

To be completely explicit, we list Schur polynomials for partitions λ with $\lambda_1 + \lambda_2 + \lambda_3 \leq 4$:

$$\sigma_\varnothing = 1, \quad \sigma_1 = x, \quad \sigma_{11} = \tfrac{1}{2}x^2 - y, \quad \sigma_2 = \tfrac{1}{2}x^2 + y, \quad \sigma_{111} = \tfrac{1}{6}x^3 - xy + t, \quad \sigma_3 = \tfrac{1}{6}x^3 + xy + t,$$
$$\sigma_{21} = \tfrac{1}{3}x^3 - t, \; \sigma_{211} = \tfrac{1}{8}x^4 - \tfrac{1}{2}x^2 y - \tfrac{1}{2}y^2, \; \sigma_{22} = \tfrac{1}{12}x^4 - tx + y^2, \; \sigma_{31} = \tfrac{1}{8}x^4 + \tfrac{1}{2}x^2 y - \tfrac{1}{2}y^2, \ldots$$

For a partition λ as above, we set $\lambda_4 = \cdots = \lambda_k = 0$. For $I = \{i_1 < i_2 < \cdots < i_k\}$ we set

$$\Delta_\lambda(\kappa_i, i \in I) \;\;:=\;\; \det\begin{pmatrix} \kappa_{i_1}^{\lambda_1 + k - 1} & \kappa_{i_2}^{\lambda_1 + k - 1} & \cdots & \kappa_{i_k}^{\lambda_1 + k - 1} \\ \kappa_{i_1}^{\lambda_2 + k - 2} & \kappa_{i_2}^{\lambda_2 + k - 2} & \cdots & \kappa_{i_k}^{\lambda_2 + k - 2} \\ \vdots & \vdots & \ddots & \vdots \\ \kappa_{i_1}^{\lambda_k} & \kappa_{i_2}^{\lambda_k} & \cdots & \kappa_{i_k}^{\lambda_k} \end{pmatrix}.$$

The empty partition gives the Vandermonde determinant $\Delta_\varnothing(\kappa_i, i \in I) = \prod_{\substack{i,j \in I \\ i < j}} (\kappa_j - \kappa_i)$.

Lemma 2.1.12. *The exponential function indexed by I in the formula (2.0.6) has the expansion*

$$\exp\bigg[\, x \cdot \sum_{i \in I} \kappa_i \,+\, y \cdot \sum_{i \in I} \kappa_i^2 \,+\, t \cdot \sum_{i \in I} \kappa_i^3 \,\bigg] \;=\; \Delta_\varnothing(\kappa_i, i \in I)^{-1} \cdot \sum_{\lambda_1 \geq \lambda_2 \geq \lambda_3 \geq 0} \Delta_\lambda(\kappa_i, i \in I) \cdot \sigma_\lambda(x, y, t).$$

Proof. The unknowns x, y, t play the role of power sum symmetric functions in $r_1, r_2, \ldots$:

$$x = r_1 + r_2 + r_3 = p_1(r), \quad y = \frac{1}{2}(r_1^2 + r_2^2 + r_3^2) = \frac{1}{2}p_2(r), \quad t = \frac{1}{3}(r_1^3 + r_2^3 + r_3^3) = \frac{1}{3}p_3(r).$$

It suffices to prove the statement after this substitution since the ring of power series is graded according to the weights $\deg x = 1, \deg y = 2$, and $\deg t = 3$, and the substitution above preserves the grading. By [Kod17, Remark 1.5], we have $\sigma_\lambda(x, y, t) = s_\lambda(r_1, r_2, r_3)$, where s_λ is the usual Schur function as a symmetric polynomial, which satisfies $\Delta_\lambda(\kappa_i, i \in I) = s_\lambda(\kappa_i, i \in I) \cdot \Delta_\varnothing(\kappa_i, i \in I)$. Our identity can be rewritten as

$$\exp\bigg[p_1(w) \cdot p_1(\kappa) + \frac{1}{2}p_2(w) \cdot p_2(\kappa) + \frac{1}{3}p_3(w) \cdot p_3(\kappa) \bigg] \;=\; \sum_{\lambda_1 \geq \lambda_2 \geq \lambda_3 \geq 0} s_\lambda(\kappa_i, i \in I) \cdot s_\lambda(r_1, r_2, r_3).$$

This is precisely the classical Cauchy identity, as stated in [Sta01, page 386].   ∎

By substituting the formula in Lemma 2.1.12 into the right hand side of (2.0.6), we obtain the following:

Proposition 2.1.13. *The (k,n)-soliton has the following expansion into Schur polynomials*

$$\tau(x,y,t) \;=\; \sum_{\lambda_1 \geq \lambda_2 \geq \lambda_3 \geq 0} c_\lambda \cdot \sigma_\lambda(x,y,t)\,, \qquad \text{where} \quad c_\lambda = \sum_{I \in \binom{[n]}{k}} p_I \cdot \Delta_\lambda(\kappa_i, i \in I)\,. \quad (2.1.17)$$

For any point ξ in the Sato Grassmannian SGM we now define a tau function as follows:

$$\tau_\xi(x,y,t) \;=\; \sum_\lambda \xi_\lambda\, \sigma_\lambda(x,y,t)\,. \tag{2.1.18}$$

The sum is over all possible partitions. We can now state the main result of Sato's theory.

Theorem 2.1.14 (Sato)**.** *For any $\xi \in$ SGM, the tau function τ_ξ satisfies Hirota's bilinear form (2.0.4).*

Actually, Sato's theorem is much more general. From a frame ξ as in (2.1.14), we can define

$$\tau(t_1, t_2, t_3, t_4, \dots) \;=\; \sum_\lambda \xi_\lambda\, \sigma_\lambda(t_1, t_2, t_3, t_4, \dots)\,.$$

The sum is over all partitions. This function in infinitely many variables is a solution to the *KP hierarchy*. Moreover, every solution to the KP hierarchy arises from the Sato Grassmannian in this way. The tau functions that we consider here arise from the general case by setting

$$t_1 = x, \quad t_2 = y, \quad t_3 = t, \quad t_4 = t_5 = \dots = 0.$$

We refer to [Kod17, Theorem 1.3] for a first introduction and numerous references. We may also start with an ansatz $\tau(x,y,t) = \sum_\lambda c_\lambda\, \sigma_\lambda(x,y,t)$, and examine the quadratic equations in the unknowns c_λ that are imposed by (2.0.4). This leads to polynomials that vanish on the Sato Grassmannian.

Remark 2.1.15. We can view Proposition 2.0.1 as a special case of Theorem 2.1.14, given that the Sato Grassmannian contains all classical Grassmannians $\mathrm{Gr}(k,n)$. Here is an explicit description. We fix distinct scalars $\kappa_1, \dots, \kappa_n$ in $\mathbb{K}^*$. Points in $\mathrm{Gr}(k,n)$ are represented by matrices A in $\mathbb{K}^{k \times n}$. Following [KX21, §3.1] and [Nak19, §2.2], we turn A into an infinite matrix ξ as in (2.1.14). Let $\Lambda(\kappa)$ denote the $\infty \times n$ matrix whose rows are $(\kappa_1^\ell, \kappa_2^\ell, \dots, \kappa_n^\ell)$ for $\ell = 0, 1, 2, \dots$. We define $A(\kappa) \coloneqq \Lambda(\kappa) \cdot A^T$. This is the $\infty \times k$ matrix whose jth column is given by the coefficients of

$$\sum_{i=1}^n \frac{a_{ji}}{1 - \kappa_i z} \;=\; \sum_{\ell=0}^\infty \sum_{i=1}^n \kappa_i^\ell\, a_{ji} \cdot z^\ell.$$

This verifies [Nak19, Theorem 3.2]. Indeed, the double infinite matrix representing τ equals

$$\xi \;=\; \begin{bmatrix} \mathbf{1} & \mathbf{0} \\ \mathbf{0} & A(\kappa) \end{bmatrix},$$

where $\mathbf{0}$ and $\mathbf{1}$ are infinite zero and identity matrices. In particular, the first nonzero row of $A(\kappa)$ is at the row $-k$ of ξ. The corresponding basis $(f_1, f_2, f_3, \dots)$ of the space U is given by

$$f_j = \frac{1}{z^{k-1}} \sum_{i=1}^n \frac{a_{ji}}{1 - \kappa_i z}, \quad \text{for } j = 1, \dots, k, \qquad f_j = \frac{1}{z^{j-1}}, \quad \text{for } j \geq k+1. \tag{2.1.19}$$

The Plücker coordinates c_λ indexed by partitions with at most three parts are certain minors of $A(\kappa)$, and these are expressed in terms of maximal minors of A by the formula in (2.1.17).

2.1.3. Tau functions from algebraic curves

Let X be a smooth projective curve of genus g defined over a field $\mathbb{K}$ of characteristic zero. In this subsection we show how certain Riemann-Roch spaces on X define points in the Sato Grassmannian SGM. Using Theorem 2.1.14, we obtain KP solutions by choosing appropriate bases of these spaces. The relevant theory is known since the 1980s; see [Kod17, KX21, Sat81]. We begin with the exposition in [Nak19, §4]. Our aim is to develop tools to carry this out in practice.

Fix a divisor D of degree $g-1$ on X and a distinguished point $p \in X$, both defined over $\mathbb{K}$. For any integer $n \in \mathbb{N}$, we consider the Riemann-Roch space $H^0(X, D + np)$. For $m < n$ there is an inclusion $H^0(X, D + mp) \subseteq H^0(X, D + np)$. As n increases, we obtain a space $H^0(X, D + \infty p)$ of rational functions on the curve X whose pole order at p is unconstrained.

Let z denote a local coordinate on X at p. Each element in $H^0(X, D + \infty p)$ has a unique Laurent series expansion in z and hence determines an element in $V = \mathbb{K}((z))$. Let $m = \mathrm{ord}_p(D)$ be the multiplicity of p in D. Multiplication by z^{m+1} defines the $\mathbb{K}$-linear map:

$$\iota \colon H^0(X, D + \infty p) \to V, \qquad s = \sum_{n \in \mathbb{Z}} s_n z^n \mapsto \sum_{n \in \mathbb{Z}} s_n z^{n+m+1}.$$

Proposition 2.1.16. *The space* $U = \iota(H^0(X, D + \infty p)) \subset V$ *lies in SGM.*

Proof. The map ι is injective because a rational function on an irreducible curve X is uniquely determined by its Laurent series. Setting $V_n = z^{-n}\mathbb{K}[[z]] \subset V$ as in Subsection 2.1.2, we have

$$\dim U \cap V_n = h^0(X, D + (n+1)p) = n + 1 + h^1(X, D + (n+1)p). \tag{2.1.20}$$

The second equality is the Riemann-Roch Theorem, with $\deg(D) = g-1$. Hence (2.1.15) holds provided $h^1(X, D + (n+1)p) = 0$. This happens for $n \geq g - 1$, by degree considerations. ∎

Following [Nak19], we examine the case $g = 2$. A smooth genus two curve is hyperelliptic:

$$X = \left\{ y^2 = (x - \lambda_1)(x - \lambda_2) \cdots (x - \lambda_6) \right\}.$$

Here $\lambda_1, \lambda_2, \ldots, \lambda_6 \in \mathbb{K}$ are pairwise distinct. Let p be one of the two preimages of the point at infinity under the double cover $X \to \mathbb{P}^1$. Using the local coordinate $z = \frac{1}{x}$ at p, we write

$$y = \pm\sqrt{(x - \lambda_1) \cdots (x - \lambda_6)} = \pm\frac{1}{z^3} \cdot \sum_{n=0}^{+\infty} \alpha_n z^n,$$

where $\alpha_0 = 1$ and the α_i are polynomials in $\lambda_1, \ldots, \lambda_6$. We consider three kinds of divisors:

$$D_0 = p, \qquad D_1 = p_1, \qquad \text{and} \qquad D_2 = p_1 + p_2 - p,$$

where $p_1 = (c_1, y_1)$, $p_2 = (c_2, y_2)$ are general points on X. For $m \geq 3$, consider the functions

$$
\begin{aligned}
g_m(x) &= \sum_{j=0}^{m} \alpha_j x^{m-j}, \\
f_m(x, y) &= \tfrac{1}{2}\left(x^{m-3} y + g_m(x) \right), \\
h_j(x, y) &= \frac{f_3(x, y) - f_3(c_j, -y_j)}{x - c_j} = \frac{y + g_3(x) - (-y_j + g_3(c_j))}{2(x - c_j)} \qquad \text{for } j = 1, 2.
\end{aligned}
$$

These rational functions are series in z with coefficients that are polynomials in $\lambda_1, \ldots, \lambda_6$. We write U_i for the image of the Riemann-Roch space $H^0(X, D_i + \infty p)$ under the inclusion ι.

Lemma 2.1.17 ([Nak19, Lemma 5.2]). *The set $\{1, f_3, f_4, f_5, \ldots\}$ is a basis of U_0, the set $\{1, f_3, f_4, f_5, \ldots\} \cup \{h_1\}$ is a basis of U_1, and $\{1, f_3, f_4, f_5, \ldots\} \cup \{h_1, h_2\}$ is a basis of U_2.*

This lemma furnishes us with an explicit basis for the $\mathbb{K}$-vector space U in Proposition 2.1.16. This basis is a frame in the sense of Sato theory. It gives us the matrix ξ in (2.1.14), from which we compute the Plücker coordinates (2.1.16) and the tau function (2.1.18). This process is a symbolic computation over the ground field $\mathbb{K}$. No numerics are needed. For general curves of genus $g \geq 3$, the same is possible, but it requires computing a basis for U, e.g. using the concrete methods such as [Hes02, Algorithm 6.1 and 8.8].

Our approach differs greatly from the computation of KP solutions from the curve X via theta functions as in [AÇS21, Dub81, Kri77]. That would require the computation of the Riemann matrix of X, which cannot be done over $\mathbb{K}$. This is why we adopted the SGM approach in [KX21, Nak19].

We implemented the method described above in `Maple` for $D_0 = p$ on hyperelliptic curves over $\mathbb{K} = \mathbb{Q}(\epsilon)$. The code is available at the link

https://mathrepo.mis.mpg.de/KPSolitonsFromTropicalLimits.

If λ is a partition with n parts, then the Plücker coordinate ξ_λ is the minor given by the n right-most columns of ξ and the rows given by the first n parts in the Maya diagram of λ. Since the tau function (2.1.18) is an infinite sum over all partitions, our code does not provide an exact solution to the Hirota equation (2.0.4). Instead, it computes the truncated tau function

$$\tau[n] \coloneqq \sum_{i=1}^{n} \sum_{\lambda \vdash i} \xi_\lambda \, \sigma_\lambda(x, y, t), \qquad (2.1.21)$$

where n is the order of precision. In our experiments we evaluated (2.1.21) up to $n = 12$ on a range of hyperelliptic curves of genus $g = 2, 3, 4$. The first non-zero $\tau[n]$ is $\tau[g] = \sigma_{(g)}(x, y, t)$ [Nak19, Proposition 6.3]. When plugging (2.1.21) into the left hand side of (2.0.4), we get an expression in x, y, t whose terms of low order vanish. The following facts were observed for this expression. For $n > g + 2$, the term of lowest degree has degree $n + g - 3$, and the monomial that appears in that lowest degree $n + g - 3 = 1, 2, 3, \ldots$ is $x, y, t, xt, yt, t^2, xt^2, yt^2, t^3, xt^3, yt^3, t^4, \ldots$.

We use our `Maple` code to study (k, n)-solitons arising from the degenerations in [Nak19]. Namely, we explore the limit for $\epsilon \to 0$ for hyperelliptic curves of genus $g = n - 1$ given by

$$y^2 = (x - \kappa_1)(x - \kappa_1 - \epsilon) \cdot \cdots \cdot (x - \kappa_n)(x - \kappa_n - \epsilon). \qquad (2.1.22)$$

Set $h(z) = (1 - \kappa_1 z) \cdots (1 - \kappa_n z)$. For $\epsilon \to 0$ the frame found in Lemma 2.1.17 degenerates to

$$U = \left\{ 1, z^{-n} h(z), z^{-(n+1)} h(z), z^{-(n+2)} h(z), z^{-(n+3)} h(z), \ldots \right\}. \qquad (2.1.23)$$

Observe that $z^{-n} h(z)$ gets expanded to

$$z^{-n} + z^{-(n-1)} \Big(-\sum_{i=1}^{n} \kappa_i \Big) + z^{-(n-2)} \Big(\sum_{1 \leq i \leq j \leq n} \kappa_i \kappa_j \Big) + z^{-(n-3)} \Big(\sum_{1 \leq i \leq j \leq l \leq n} \kappa_i \kappa_j \kappa_l \Big) + O(z^{-(n-4)}).$$

Following [Nak19, §7], one multiplies all elements in U by $h(z)^{-1}$ in order to obtain a soliton solution. By [Nak19, Theorem 3.2], we obtain a $(1, n)$-soliton solution given by the matrix

$$A = \left(\Big(\prod_{i \neq 1} (\kappa_1 - \kappa_i) \Big)^{-1} \quad \Big(\prod_{i \neq 2} (\kappa_2 - \kappa_i) \Big)^{-1} \quad \cdots \quad \Big(\prod_{i \neq n} (\kappa_n - \kappa_i) \Big)^{-1} \right).$$

Example 2.1.18. The soliton that arises from the genus 2 curve given by the polynomial $f_2(x)$ in (2.1.1) is a $(1,3)$-soliton given by the matrix $A = \left(\begin{smallmatrix} \frac{1}{2} & -1 & \frac{1}{2} \end{smallmatrix}\right)$ and parameters $\kappa = (1,2,3)$.

We computed the tau function for a range of curves over $\mathbb{K} = \mathbb{Q}(\epsilon)$. Their limit as $\epsilon \to 0$ is not the same as the tau functions obtained from the combinatorial methods in Section 2.1:

Example 2.1.19. Let X be the hyperelliptic curve of genus 3 given by $y^2 = f(x)$ where $f(x)$ is given by

$$(x+1+\epsilon)(x+1+2\epsilon)(x+1+\epsilon+\epsilon^2)(x+1+2\epsilon+\epsilon^2)(x+2+\epsilon)(x+2+2\epsilon)(x+2+\epsilon+\epsilon^2)(x+2+2\epsilon+\epsilon^2).$$

In Figure 2.4 we exihibit the subtree with 8 leaves that arises from the 8 roots of $f(x)$ and the corresponding metric graph of genus 3 which maps to it under the hyperelliptic covering.
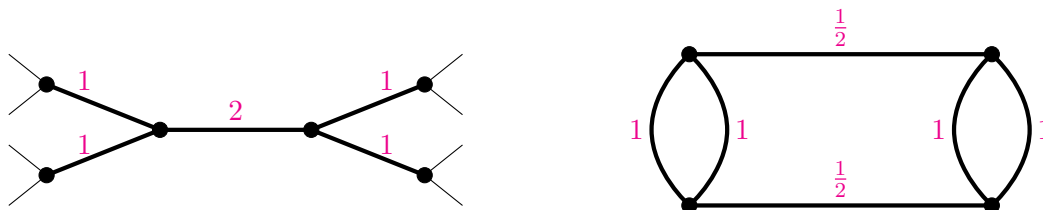
Figure 2.4. The metric tree (left) and the metric graph (right) for the curve X

For a suitable cycle basis, the tropical Riemann matrix equals $Q = \begin{bmatrix} 2 & -1 & 0 \\ -1 & 3 & -1 \\ 0 & -1 & 2 \end{bmatrix}$. This appears in the second row in [AÇSS21, Table 4]: the Voronoi polytope is the hexarhombic dodecahedron. This corresponds to the tropical degeneration from a smooth quartic to a conic and two lines in $\mathbb{P}^2$. According to [AÇSS21, Theorem 4] there are two types of Delaunay polytopes in this case, namely the tetrahedron (4 vertices) and the pyramid (5 vertices). The theta function (2.0.7) for the tetrahedron equals $\theta_\mathcal{C}(z) = a_{000} + a_{100}\exp[z_1] + a_{010}\exp[z_2] + a_{001}\exp[z_3]$. The Hirota variety lives in $(\mathbb{K}^*)^4 \times \mathbb{WP}^8$, and it is characterized by Theorem 2.1.8. Each point on the Hirota variety gives a KP solution. The theta function for the pyramid equals

$$\theta_{\mathcal{C}'}(z) = a_{000} + a_{100}\exp[z_1] + a_{001}\exp[z_3] + a_{101}\exp[z_1+z_3] + a_{111}\exp[z_1+z_2+z_3].$$

The Hirota variety $\mathcal{H}_{\mathcal{C}'} \subset (\mathbb{K}^*)^5 \times \mathbb{WP}^8$ is cut out by eight quadrics P_{ij} as in Section 2.1.1, plus

$$P(u_1+u_3, v_1+v_3, w_1+w_3)\, a_{000}a_{101} \;+\; P(u_1, v_1, w_1)\, a_{001}a_{101}.$$

The resulting tau functions differ from those obtained by setting $\epsilon = 0$ in our `Maple` output. This happens because $y^2 = f(x)$ is not a semistable model. The special fiber of that curve at $\epsilon = 0$ does not have ordinary singularities: it has two singular points of the form $y^2 = x^4$. On the other hand, if the curve at $\epsilon = 0$ is rational and has nodal singularities, as in (2.1.22), then we get soliton solutions at the limit. We shall see this more precisely in the next subsection.

After this combinatorial interlude, we now return to Proposition 2.1.16, and explore this for a singular curve X. Suppose X is connected, has arithmetic genus g, and all singularities are nodal. We recall briefly how to compute $H^0(X, E)$ when E is a divisor supported in the smooth locus of X. If X is irreducible, then we consider the normalization $\widetilde{X} \to X$, that separates the nodes of X. The divisor E lifts to $\widetilde{X}$, and $H^0(X, E)$ is a subspace of $H^0(\widetilde{X}, E)$.

It consists of rational functions which coincide on the points of $\widetilde{X}$ that map to the nodes of X. If $X = X_0 \cup \cdots \cup X_r$ is reducible, then $H^0(X, E)$ is a subspace of $\bigoplus_{i=0}^r H^0(X_i, E_{|X_i})$. Its elements are tuples $(f_0, f_1, \ldots, f_r)$ where f_i and f_j coincide on $X_i \cap X_j$.

Fix a divisor D of degree $g-1$ and a point p, where all the points in support of D and p are smooth on X and defined over $\mathbb{K}$. We wish to compute $H^0(X, D + \infty p)$. Riemann-Roch holds for X and hence so does (2.1.20). In order for the proof of Proposition 2.1.16 to go through, we need two conditions:

($*$) A rational function in $H^0(X, D + np)$ is uniquely determined by its Laurent series at p.

($**$) We have $h^1(X, D + np) = 0$ for $n \gg 0$.

Our next result characterizes when these two conditions hold. Let X_0 be the irreducible component of X that contains p, and let $X_0' = \overline{X \backslash X_0}$ be the curve obtained by removing X_0. Set $Z = X_0 \cap X_0'$ and denote the restrictions of the divisor D to X_0, X_0' by D_0, D_0' respectively.

Proposition 2.1.20. *Condition* ($*$) *holds if and only if* $H^0(X_0', D_0' - Z) = 0$. *Condition* ($**$) *holds if and only if* $H^1(X_0', D_0') = 0$. *These are vanishing conditions on the curve* X_0'.

Proof. If X is irreducible then ($*$) holds since rational functions are determined by their series on the normalization $\widetilde{X}$. If X is reducible then X_0' is nonempty. We need that the restriction

$$H^0(X, D + np) \longrightarrow H^0(X_0, D_0 + np)$$

is injective. The kernel of this map consists exactly of those rational functions in $H^0(X_0', D_0')$ which vanish on Z. In other words, the kernel is the space $H^0(X_0', D_0' - Z)$, as desired.

Also for the second statement, we can take X to be reducible. Consider the exact sequence

$$0 \longrightarrow \mathcal{O}_X(D + np) \longrightarrow \mathcal{O}_{X_0}(D_0 + np) \oplus \mathcal{O}_{X_0'}(D_0') \longrightarrow \mathcal{O}_Z(D_0 + np) \longrightarrow 0.$$

Taking global sections we see that $H^1(X, D + np)$ surjects onto $H^1(X_0', D_0')$, since $\dim(Z) = 0$. Hence $H^1(Z, D_0 + np) = 0$. In particular, if $H^1(X, D + np) = 0$ then $H^1(X_0', D_0') = 0$.

Conversely, suppose $H^1(X_0', D_0') = 0$. Since X_0 is irreducible, we have $H^1(X_0, D_0 + np) = 0$ for $n \gg 0$. The long exact sequence tells us that $H^1(X, D + np) = 0$ as soon as the map

$$H^0(X_0, D_0 + np) \oplus H^0(X_0', D_0') \longrightarrow H^0(Z, D + np), \qquad (f_0, f_0') \mapsto f_{0|Z} - f_{0|Z}'$$

is surjective. Actually, the map $H^0(X_0, D + np) \to H^0(Z, D + np)$ is surjective for $n \gg 0$. Indeed, $H^1(X_0, D - Z + np) = 0$ for $n \gg 0$ since p is an ample divisor on the curve X_0. ∎

Remark 2.1.21. Here we present the case of nodal curves for simplicity, but the same discussion holds true, with essentially the same proofs, for an arbitrary singular curve. This is precisely the focus of [AÇL21], where Agostini, Çelik, and Little study the case of singular curves whose theta divisors in their generalized Jacobians are algebraic.

Remark 2.1.22. The two conditions in Proposition 2.1.20 are automatically satisfied when the curve X is irreducible. In that case we always get a point U in the Sato Grassmannian.

2.1.4. Riemann–Roch spaces

Our long-term goal is to fully understand the points $U(\epsilon)$ in the Sato Grassmannian that represent Riemann-Roch spaces of a smooth curve over a valued field, such as $\mathbb{K} = \mathbb{Q}(\epsilon)$. We explained how these points are computed, and we implemented this in `Maple` for the case of hyperelliptic curves. Our approach is similar to [KX21, Nak18, Nak19]. For a given Mumford curve, it remains a challenge to lift the computation to the valuation ring (such as $\mathbb{Q}[\epsilon]$) and correctly encode the limiting process as $\epsilon \to 0$. In this section we focus on what happens in the limit.

Consider a nodal reducible curve $X = X_0 \cup \cdots \cup X_r$, where each irreducible component X_i is rational. The arithmetic genus g is the genus of the dual graph. We present an algorithm whose input is a divisor D of degree $g - 1$ and a point p, supported in the smooth locus of X. The algorithm checks the conditions in Proposition 2.1.20, and, if these are satisfied, it outputs a soliton solution that corresponds to $U = \iota(H^0(X, D + \infty p))$.

We start with some remarks on interpolation of rational functions on $\mathbb{P}^1$. Consider distinct points $\kappa_1, \ldots, \kappa_a$ and $\kappa_{1,1}, \kappa_{1,2}, \ldots, \kappa_{b,1}, \kappa_{b,2}$ on $\mathbb{P}^1$. We also choose a divisor $D_0 = m_1 p_1 + \cdots + m_s p_s + mp$, which is supported away from the previous points. Choose also scalars $\lambda_1, \ldots, \lambda_a, \mu_1, \ldots, \mu_b \in \mathbb{K}$. We wish to compute all functions f in $H^0(\mathbb{P}^1, D_0 + \infty p)$ satisfying

$$f(\kappa_j) = \lambda_j \text{ for } j = 1, \ldots, a \qquad \text{and} \qquad f(\kappa_{j,1}) = f(\kappa_{j,2}) = \mu_j \text{ for } j = 1, \ldots, b. \qquad (2.1.24)$$

To do so, we choose an affine coordinate x on $\mathbb{P}^1$ such that $p = \infty$. Then we define

$$P(x) := \prod_{j=1}^{s} (x - p_j)^{m_j} \qquad \text{and} \qquad K(x) := \prod_{j=1}^{a} (x - \kappa_j) \cdot \prod_{j=1}^{b} (x - \kappa_{j,1})(x - \kappa_{j,2}).$$

Write $K'(x)$ for the derivative of the polynomial $K(x)$. An interpolation argument shows:

Lemma 2.1.23. *A rational function f in $H^0(\mathbb{P}^1, D_0 + \infty p)$ satisfies condition (2.1.24) if and only if*

$$f(x) \;=\; \frac{K(x)}{P(x)} \left[\sum_{j=1}^{a} \lambda_j \frac{P(\kappa_j)}{K'(\kappa_j)} \frac{1}{x - \kappa_j} + \sum_{j=1}^{b} \mu_j \left(\frac{P(\kappa_{j,1})}{K'(\kappa_{j,1})} \frac{1}{x - \kappa_{j,1}} + \frac{P(\kappa_{j,2})}{K'(\kappa_{j,2})} \frac{1}{x - \kappa_{j,2}} \right) + H(x) \right],$$

where $\mu_1, \ldots, \mu_b \in \mathbb{K}$ and $H(x)$ is a polynomial in $\mathbb{K}[x]$.

Lemma 2.1.23 gives a way to compute the Riemann-Roch space $H^0(X, E)$ when E is a divisor on a nodal rational curve X as above. The normalization of such a curve is an union of projective lines. On each line we need to compute rational functions with prescribed values at certain points (corresponding to the intersection of two components of X) and at certain pairs of points (corresponding to the nodes in the components of X).

Algorithm 2.1.24. The following steps compute the soliton (2.0.6) associated to the curve data.

Input: A reducible curve $X = X_0 \cup \cdots \cup X_r$ as above, with a smooth point p and a divisor D of degree $g - 1$ supported also on smooth points. Everything is defined over $\mathbb{K}$.

(1) Let X_0, X_0', D_0, D_0', Z be as in Section 2.1.3. Write $Z = \{q_1, \ldots, q_a\}$ and let $n_1, \ldots, n_b$ be the nodes in X_0. If $\nu : \mathbb{P}^1 \to X_0$ is the normalization of X_0 we set $\kappa_j := \nu^{-1}(q_j)$ and $\{\kappa_{j,1}, \kappa_{j,2}\} = \nu^{-1}(n_j)$. We also write $D_0 = m_1 p_1 + \cdots + m_s p_s + mp$, we fix an affine coordinate x on $\mathbb{P}^1$ such that $p = \infty$, and we compute $P(x)$ and $K(x)$ as in (2.1.24).

(2) Compute a basis $Q_1, Q_2, \ldots, Q_\ell$ of $H^0(X_0', D_0')$. If $\ell = \deg D_0' + 1 - p_a(X_0')$ then proceed. Otherwise return "Condition ($**$) in Proposition 2.1.20 fails" and terminate.

(3) Compute the Riemann-Roch space $H^0(X_0', D_0' - Z)$. If this is zero then proceed. Otherwise return "Condition ($*$) in Proposition 2.1.20 fails" and terminate.

(4) Define the $\ell \times a$ matrix A and the $b \times 2b$ matrix B by

$$A_{i,j} := \frac{Q_i(p_j)P(\kappa_j)}{K'(\kappa_j)}, \; B_{j,2j-1} := \frac{P(\kappa_{j,1})}{K'(\kappa_{j,i})}, \; B_{j,2j} := \frac{P(\kappa_{j,2})}{K'(\kappa_{j,2})}, \; B_{i,j} := 0 \text{ otherwise.}$$

Output: The $(\ell + b) \times (a + 2b)$ matrix $\begin{pmatrix} A & 0 \\ 0 & B \end{pmatrix}$. This represents the soliton solution for the point $\iota(H^0(X, D + \infty p))$ in the Sato Grassmannian SGM, after a gauge transformation.

Proposition 2.1.25. *Algorithm 2.1.24 is correct.*

Proof. By Riemann-Roch, we have $h^0(X_0', D_0') = h^1(X_0', D_0') + \deg D_0' + 1 - p_a(X_0')$. Hence condition ($**$) in Proposition 2.1.20 is satisfied if and only if the condition in step (2) of Algorithm 2.1.24 is satisfied. Moreover, condition ($*$) in Proposition 2.1.20 is precisely the condition in step (3). Hence, we need to show that the output of the algorithm corresponds to $\iota(H^0(X, D + \infty p))$, after a gauge transformation. However, we know that any element of $H^0(X, D + \infty p)$ can be written as $(f, \sum_j \lambda_j Q_j)$ such that $f \in H^0(X_0, D_0 + \infty p)$ and

$$f(\kappa_j) = \sum_i \lambda_i Q_i(\kappa_j), \text{ for } j = 1, \ldots, a \qquad \text{and} \qquad f(\kappa_{j,1}) = f(\kappa_{j,2}) \text{ for } j = 1, \ldots, b.$$

At this point, Lemma 2.1.23 gives us a basis of $\iota(H^0(X, D + \infty p))$. Remark 2.1.15 shows that this corresponds exactly to the matrix given by the algorithm, after the gauge transformation given by multiplying with $P(x)/K(x)$. ∎

We illustrate the algorithm in the following examples.

Example 2.1.26. Let X be an irreducible rational curve with g nodes. Algorithm 2.1.24 returns a matrix B for a $(g, 2g)$-soliton. This is consistent with (2.2.14). Note that the dual graph associated to the curve X consists in one node with g loops and the associated Delaunay polytope is a g-dimensional cube. This fact is discussed in detail in Section 2.1.1.

Example 2.1.27 ($g = 2$). Let X be the union of two smooth rational curves X_0, X_1 meeting at three points $Z = \{q_1, q_2, q_3\}$. This curve is the special fiber of the genus 2 curve $\{y^2 = f_2(x)\}$ in Example 2.1.1. It corresponds to the graph on the right in Figure 2.2. We choose a smooth point $p \in X_0 \backslash Z$, and we consider three different divisors of degree one: p, $-2q + 3p$ and $3q - 2p$, where q is a smooth point in X_1. We apply Algorithm 2.1.24 to these three instances.

- Take $D = p$. Then $H^0(X_0', D_0') = H^0(\mathbb{P}^1, \mathcal{O}) = \mathbb{K}$ has the constant function 1 as basis. The conditions in steps (2) and (3) are both satisfied, and the algorithm gives us the soliton solution corresponding to the matrix $A = \left(\frac{1}{K'(\kappa_1)} \quad \frac{1}{K'(\kappa_2)} \quad \frac{1}{K'(\kappa_3)} \right)$. Note that the Delaunay polytope $\mathcal{C}$ is a triangle, and the approach in Section 2.1.1 leads to the gauge-equivalent matrix $A = \begin{pmatrix} 1 & 1 & 1 \end{pmatrix}$. This also arises for $z_1 = 0$ in Example 2.1.9.

- Take $D_2 = -2q + 3p$. Then $H^0(X_0', D_0') \cong H^0(\mathbb{P}^1, -2q) = 0$ and the condition in step (2) is not satisfied. Hence we do not get a point in the Sato Grassmannian.

- Take $D_3 = 3q - 2p$. Then $H^0(X_0', D_0') \cong H^0(\mathbb{P}^1, 3q)$ has dimension 4 and the condition in step (2) is satisfied. However, $H^0(X_0', D_0' - Z) \cong H^0(\mathbb{P}^1, \mathcal{O}) \neq 0$ so the condition in step (3) is not satisfied, and we do not get a point in the Sato Grassmannian.

Example 2.1.28 ($g = 3$)**.** Consider four general lines $X = X_0 \cup X_1 \cup X_2 \cup X_3$ in $\mathbb{P}^2$. Set $X_0 \cap X_i = \kappa_i$ and $X_i \cap X_j = q_{ij}$ for $i, j \in \{1, 2, 3\}$. We fix the divisor $D = p_1 + p_2 + p_3 - p$, for general points $p \in X_0$ and $p_i \in X_i$ for $i = 1, 2, 3$. After the preperatory set-up in step (1), we compute $H^0(X_0', D_0')$ in step (2). This is the space of functions (g_1, g_2, g_3) in $\bigoplus_{i=1}^3 H^0(X_i, p_i)$ such that $g_i(q_{ij}) = g_j(q_{ij})$ for $i, j \in \{1, 2, 3\}$. Choose affine coordinates x_i on X_i for $i = 1, 2, 3$ such that $p_i = \infty$. We compute the following basis for $H^0(X_0', D_0')$:

$$Q_1 = \left(0, \frac{x_2 - q_{12}}{q_{23} - q_{12}}, \frac{x_3 - q_{13}}{q_{23} - q_{12}}\right), \quad Q_2 = \left(\frac{x_1 - q_{12}}{q_{13} - q_{12}}, 0, \frac{x_3 - q_{23}}{q_{13} - q_{23}}\right), \quad Q_3 = \left(\frac{x_1 - q_{13}}{q_{12} - q_{13}}, \frac{x_2 - q_{23}}{q_{12} - q_{13}}, 0\right).$$

Hence $\ell = 3$ and the condition in step (2) holds. We also find that $H^0(X_0', D_0' - Z) = 0$, so that the condition in step (3) is satisfied as well. Algorithm 2.1.24 outputs the soliton matrix

$$A = \begin{pmatrix} 0 & \frac{\kappa_1 - q_{12}}{q_{13} - q_{12}} \frac{1}{K'(\kappa_1)} & \frac{\kappa_1 - q_{13}}{q_{12} - q_{13}} \frac{1}{K'(\kappa_1)} \\ \frac{\kappa_2 - q_{12}}{q_{23} - q_{12}} \frac{1}{K'(\kappa_2)} & 0 & \frac{\kappa_2 - q_{23}}{q_{12} - q_{13}} \frac{1}{K'(\kappa_2)} \\ \frac{\kappa_3 - q_{13}}{q_{23} - q_{12}} \frac{1}{K'(\kappa_3)} & \frac{\kappa_3 - q_{23}}{q_{13} - q_{23}} \frac{1}{K'(\kappa_3)} & 0 \end{pmatrix}. \tag{2.1.25}$$

The curve X is the last one in [AÇSS21, Figure 2]. The Delaunay polytope $\mathcal{C}$ is a tetrahedron, so Theorem 2.1.8 applies. It would be desirable to better understand the relationship between the soliton solution (2.1.25), the Hirota variety $\mathcal{H}_\mathcal{C}$, and the Dubrovin variety in [AÇS21, Example 6.2].

2.2. Rational nodal curves

For the rest of the chapter we assume X to be an irreducible rational nodal curve of genus g. Let Γ denote the metric graph associated to X introduced in Section 2.1. In general, the metric graph associated to an algebraic curve consists of a vertex for each irreducible component, an edge for each intersection point between two components, and a node on an irreducible component gives a loop on the corresponding vertex [Cha12]. Therefore, Γ consists of a unique node and g cycles. Figure 2.5 illustrates an example when $g = 5$.
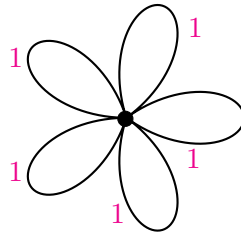
Figure 2.5. The metric graph of an irreducible rational nodal curve of genus 5

The way we read off the tropical Riemann matrix Q from a tropical curve is described in Section 2.1. When X is an irreducible rational nodal curve the matrices Λ and Δ both equal the identity matrix I_g, returning $Q = I_g$ as the tropical Riemann matrix. The distance induced on $\mathbb{R}^g$ is therefore the Euclidean distance, and we can fix the point $\mathbf{a} = \left(\frac{1}{2}, \frac{1}{2}, \ldots, \frac{1}{2}\right) \in \mathbb{R}^g$ as a vertex of the *Voronoi cell* for I_g given by the cube with vertices $\left(\pm\frac{1}{2}, \pm\frac{1}{2}, \ldots, \pm\frac{1}{2}\right)$. Under these hypotheses, the support of the degenerate theta function of Theorem 2.1.2 is the Delaunay set

$$\mathcal{C} = \mathcal{D}_{\mathbf{a}, I_g} = \left\{ \mathbf{c} \in \mathbb{Z}^g : \|\mathbf{a}\|^2 = \|\mathbf{a} - \mathbf{c}\|^2 \right\} = \{0, 1\}^g, \tag{2.2.1}$$

where $\|\cdot\|$ denotes the Euclidean norm. The degenerate theta function is then a finite sum of 2^g exponentials supported on the vertices of the g-dimensional cube $\mathcal{C}$ whose vertices are all possible binary g-dimensional vectors:

$$\theta_{\mathcal{C}}(\mathbf{z}) = \sum_{\mathbf{c}\in\{0,1\}^g} a_{\mathbf{c}} \exp\left[\mathbf{c}^T \mathbf{z}\right], \quad \text{where} \quad a_{\mathbf{c}} = \exp\left[\frac{1}{2}\mathbf{c}^T R_0 \mathbf{c}\right]. \tag{2.2.2}$$

Here the matrix R_0 is the limit of a matrix R_ϵ which is a symmetric $g \times g$ matrix with entries given by complex analytic functions in ϵ converging for $\epsilon \to 0$. This comes from degenerating the family of Riemann matrices given by $B_\epsilon = -\frac{1}{\epsilon}Q + R_\epsilon$. The matrices B_ϵ lie in the Schottky locus (see Subsection 1.1.2).

The Hirota variety $\mathcal{H}_{\mathcal{C}}$ lives in the space $(\mathbb{C}^*)^{2^g} \times \mathbb{WP}^{3g-1}$ with coordinate ring $\mathbb{C}[\mathbf{a}^{\pm 1}, \mathbf{u}, \mathbf{v}, \mathbf{w}]$, with grading as in (2.0.3). We want to investigate the subvariety denoted by $\mathcal{H}_{\mathcal{C}}^I$ of the Hirota variety $\mathcal{H}_{\mathcal{C}}$, where the superscript I stands for 'invertible'. We define this to be the Zariski closure of the set

$$\left\{ (\mathbf{a}, (\mathbf{u}, \mathbf{v}, \mathbf{w})) \in \mathcal{H}_{\mathcal{C}} \ : \ \mathbf{u} \neq \mathbf{0} \right\}. \tag{2.2.3}$$

This subvariety contains an irreducible subvariety of $\mathcal{H}_{\mathcal{C}}$ which we call the *main component*, denoted by $\mathcal{H}_{\mathcal{C}}^M$. In order to rigorously define $\mathcal{H}_{\mathcal{C}}^M$, consider the map from the affine space $\mathbb{C}^{3g}$ with coordinates $(\lambda_1, \ldots, \lambda_g, \kappa_1, \kappa_2, \ldots, \kappa_{2g})$ into the ambient space of the Hirota variety $\mathcal{H}_{\mathcal{C}}$ given by

$$\phi : \mathbb{C}^{3g} \ \dashrightarrow \ (\mathbb{C}^*)^{2^g} \times \mathbb{WP}^{3g-1} \tag{2.2.4}$$
$$(\lambda_1, \ldots, \lambda_g, \kappa_1, \kappa_2, \ldots, \kappa_{2g}) \mapsto (a_{\mathbf{c}_1}, a_{\mathbf{c}_2}, \ldots, a_{\mathbf{c}_{2g}}, \mathbf{u}, \mathbf{v}, \mathbf{w})$$

where the coordinates $\mathbf{a} = (a_{\mathbf{c}_1}, a_{\mathbf{c}_2}, \ldots, a_{\mathbf{c}_{2g}})$ are indexed by the points in $\mathcal{C} = \{0,1\}^g$. The image of ϕ is defined as follows

$$u_i = \kappa_{2i-1} - \kappa_{2i}, \quad v_i = \kappa_{2i-1}^2 - \kappa_{2i}^2, \quad w_i = \kappa_{2i-1}^3 - \kappa_{2i}^3 \quad \text{for all } i = 1, 2, \ldots, g,$$

$$a_{\mathbf{c}} = \prod_{\substack{i,j \in I \\ i<j}} (\kappa_i - \kappa_j) \prod_{i:c_i=1} \lambda_i, \quad \text{where } I = \{2i : c_i = 0\} \cup \{2i-1 : c_i = 1\} \quad \text{for all } \mathbf{c} \in \mathcal{C}. \tag{2.2.5}$$

We call the closure of the image of ϕ the *main component of $\mathcal{H}_{\mathcal{C}}$* and denote it by $\mathcal{H}_{\mathcal{C}}^M$.

The next subsection describes the geometric intuition that leads us to the definition of the main component $\mathcal{H}_{\mathcal{C}}^M$ by way of the *Abel-Jacobi map* for curves and the *theta divisor*, see [ACGH85]. Later we will focus on the study of the main component and its connection to the weak and the classical Schottky problem.

2.2.1. Theta divisor

The theta divisor of a smooth projective curve is a crucial object that controls significantly the geometry of the curve [ACGH85, §4]. This divisor is cut out in the Jacobian of the curve by the Riemann theta function (2.0.2) and has an important role in mathematical physics. Many geometric properties of the theta divisor hold because it can be parameterized through the Abel-Jacobi map of the curve. Furthermore, this parametrization also applies to any reasonably singular curve [AÇL21]. Broadly speaking, the theta divisor becomes less trascendental as the underlying curve becomes more singular. We refer to Chapter 1 and the references therein for an introduction to the Abal-Jacobi map and the theta divisor in the case of smooth curves.

In what follows, we study the theta divisor for the curve X as above, where $n_1, n_2, \ldots, n_g$ denote its nodes. The normalization $\nu : \tilde{X} \to X$ that separates the g nodes of X is given by a projective line. We consider $\kappa_1, \kappa_2, \ldots, \kappa_{2g}$ to be points on $\mathbb{P}^1$ and set $\nu^{-1}(n_i) := \{\kappa_{2i-1}, \kappa_{2i}\}$. Therefore, each rational curve with at worst nodal singularities corresponds to a copy of $\mathbb{P}^1$ and $2g$-many points on it. This explains why the moduli space of rational nodal curves has dimension $2g - 3$, where -3 accounts for the dimension of the automorphism group of $\mathbb{P}^1$. A basis $\boldsymbol{\omega} = (\omega_1, \omega_2, \ldots, \omega_g)$ of canonical differentials for such curves is given by

$$\omega_i \;=\; \frac{1}{y}\left(\frac{1}{1 - \kappa_{2i}y} - \frac{1}{1 - \kappa_{2i-1}y}\right)dy \qquad \text{for } i = 1, 2, \ldots, g,$$

where $y = 1/x$ denotes the choice of the local coordinate. The canonical differentials define a map $\alpha' : (\mathbb{P}^1)^{g-1} \dashrightarrow \mathbb{C}^g$ such that

$$(y_1, \ldots, y_{g-1}) \longmapsto \left(\sum_{i=1}^{g-1} \int_0^{y_i} \omega_j\right)_{j=1,2,\ldots,g} \qquad \text{where} \qquad \int_0^{y_i} \omega_j = \log\left(\frac{1 - \kappa_{2j-1}y_i}{1 - \kappa_{2j}y_i}\right).$$

The (generalized) Jacobian of X is an algebraic torus $(\mathbb{C}^*)^g$. Exponentiation allows to map in the Jacobian through the map $\mathbb{C}^g \to (\mathbb{C}^*)^g$ given by $((z_1, \ldots, z_g) \mapsto (\exp[z_1], \ldots, \exp[z_g]))$. The composition gives the Abel-Jacobi map $\mu^{g-1} : (\mathbb{P}^1)^{g-1} \dashrightarrow (\mathbb{C}^*)^g$ defined by

$$(y_1, \ldots, y_{g-1}) \longmapsto \left(\prod_{i=1}^{g-1}\frac{1 - \kappa_1 y_i}{1 - \kappa_2 y_i}, \prod_{i=1}^{g-1}\frac{1 - \kappa_3 y_i}{1 - \kappa_4 y_i}, \ldots, \prod_{i=1}^{g-1}\frac{1 - \kappa_{2g-1} y_i}{1 - \kappa_{2g} y_i}\right). \tag{2.2.6}$$

The theta divisor of X is the image of the Abel-Jacobi map μ up to translation. We will later justify why we expect each point in the main component of the Hirota variety $\mathcal{H}_{\mathcal{C}}^M$ to correspond (non-injectively) to a choice of a curve together with a theta divisor in the moduli space of rational nodal curves. Following this reasoning, the projection of $\mathcal{H}_{\mathcal{C}}^M$ into the space $(\mathbb{C}^*)^{2g}$ has dimension $3g - 3$, accounting for the choice of a rational nodal curve and its theta divisor. For each point in this projection, the fiber is a threefold (analogous to the Dubrovin threefold studied in [AÇS21]) given by

$$\left\{\, (\mathbf{u}, \mathbf{v}, \mathbf{w}) \in \mathbb{WP}^{3g-1} \;:\; \tau(x, y, t) = \theta_{\mathcal{C}}(\mathbf{u}x + \mathbf{v}y + \mathbf{w}t) \text{ solves } (2.1.5) \,\right\}.$$

Thus, the expected dimension of the main component is $2g - 3 + g + 3 = 3g$.

This discussion also provides a method to parameterize the main component of the Hirota variety. The idea is that the choice of the curve X yields $2g$ parameters $\kappa_1, \kappa_2, \ldots, \kappa_{2g}$, and the family of theta divisors corresponding to shifts of the unknown vector $\mathbf{z} \in \mathbb{C}^g$ yields g parameters $\boldsymbol{\lambda} = (\lambda_1, \lambda_2, \ldots, \lambda_g)$. Using `Macaulay2`, we can compute the theta divisor as a shift (through a change of variables) of the image of the map (2.2.6) up to genus 6. This is done following the method described in [MS21b, Corollary 4.8]. The equation of the theta divisor returned by the code coincides with (2.2.2) with coefficients $\mathbf{a} = (a_1, a_2, \ldots, a_{2g})$ parameterized in a way which can be shown, through a change of coordinates and some calculations, to be geometrically equivalent to (2.2.5), up to the parameters $\boldsymbol{\lambda}$. More precisely, this fact justifies the non-uniqueness of the parameterization in (2.2.4). The torus action on the theta divisor provides new suitable parameterizations. The approach for computing the theta divisor was inspired by [AÇL21].

To understand how the parameters $\boldsymbol{\lambda} = (\lambda_1, \lambda_2, \ldots, \lambda_g)$ arise, we evaluate the Riemann theta function (2.2.2) at the point $\mathbf{z} + \mathbf{h} \in \mathbb{C}^g$ and where $\mathbf{h} = (h_1, h_2, \ldots, h_g) \in \mathbb{C}^g$

$$\theta_{\mathcal{C}}(\mathbf{z} + \mathbf{h}) \;=\; \sum_{\mathbf{c} \in \mathcal{C}} a_{\mathbf{c}} \exp[\mathbf{c}^T \mathbf{h}] \exp[\mathbf{c}^T \mathbf{z}].$$

The two degenerate theta functions, $\theta_{\mathcal{C}}(\mathbf{z})$ and $\theta_{\mathcal{C}}(\mathbf{z} + \mathbf{h})$, both provide solutions to the KP equation (with nonzero u_i), hence they correspond to points in $\mathcal{H}_{\mathcal{C}}^M$. More explicitly, let $\lambda_i := \exp[h_i]$, for $i = 1, \ldots, g$, then the points

$$(\mathbf{a}, (\mathbf{u}, \mathbf{v}, \mathbf{w})), (\tilde{\mathbf{a}}, (\mathbf{u}, \mathbf{v}, \mathbf{w})) \in \mathcal{H}_{\mathcal{C}}^M \quad \text{where} \quad \tilde{\mathbf{a}} = (a_{\mathbf{c}} \exp[\mathbf{c}^T \mathbf{h}])_{\mathbf{c} \in \mathcal{C}} = \left(a_{\mathbf{c}} \prod_{i:c_i=1} \lambda_i \right)_{\mathbf{c} \in \mathcal{C}}.$$

Thus, we conclude that the choice of theta divisor is exactly represented by the parameterizing variables $\boldsymbol{\lambda} = (\lambda_1, \lambda_2, \ldots, \lambda_g)$.

Example 2.2.1. (g=3) This example is intended to clarify the role of the parameters in the case of the 3-cube. As in the discussion above, we fix points $\kappa_1, \kappa_2, \ldots, \kappa_6 \in \mathbb{P}^1$. The differentials $\boldsymbol{\omega} = (\omega_1, \omega_2, \omega_3)$, after the coordinate change $y = 1/x$, are given by

$$\omega_1 = \frac{1}{y}\left(\frac{1}{1-\kappa_2 y} - \frac{1}{1-\kappa_1 y}\right) dy, \qquad \omega_2 = \frac{1}{y}\left(\frac{1}{1-\kappa_4 y} - \frac{1}{1-\kappa_3 y}\right) dy,$$

$$\omega_3 = \frac{1}{y}\left(\frac{1}{1-\kappa_6 y} - \frac{1}{1-\kappa_5 y}\right) dy.$$

The Abel-Jacobi map $\mu^2 : (\mathbb{P}^1)^2 \dashrightarrow (\mathbb{C}^*)^3$ is defined by

$$(y_1, y_2) \mapsto \left(\left(\frac{1-\kappa_1 y_1}{1-\kappa_2 y_1}\right) \cdot \left(\frac{1-\kappa_1 y_2}{1-\kappa_2 y_2}\right), \left(\frac{1-\kappa_3 y_1}{1-\kappa_4 y_1}\right) \cdot \left(\frac{1-\kappa_3 y_2}{1-\kappa_4 y_2}\right), \left(\frac{1-\kappa_5 y_1}{1-\kappa_6 y_1}\right) \cdot \left(\frac{1-\kappa_5 y_2}{1-\kappa_6 y_2}\right)\right).$$

One can compute the implicitizing equation cutting out the image of this map in `Macaulay2` with the code

```
I = ideal(q1*(1-k2*y1)*(1-k2*y2)-(1-k1*y1)*(1-k1*y2),
q2*(1-k4*y1)*(1-k4*y2)-(1-k3*y1)*(1-k3*y2),
q3*(1-k6*y1)*(1-k6*y2)-(1-k5*y1)*(1-k5*y2));
J = eliminate(I,{y1,y2})
```

The resulting equation gives exactly the familiar theta function for $g = 3$, with the $a_{\mathbf{c}}$ parameterized by $\kappa_1, \kappa_2, \ldots, \kappa_6$. For the parameters $\boldsymbol{\lambda} = (\lambda_1, \lambda_2, \lambda_3)$, consider the theta functions

$$\theta_{\mathcal{C}}(\mathbf{z}) = a_{000} + a_{100}\exp[z_1] + a_{010}\exp[z_2] + a_{001}\exp[z_3] + a_{110}\exp[z_1 + z_2] \qquad (2.2.7)$$
$$+ a_{101}\exp[z_1 + z_3] + a_{011}\exp[z_2 + z_3] + a_{111}\exp[z_1 + z_2 + z_3],$$

and

$$\theta_{\mathcal{C}}(\mathbf{z} + \mathbf{h}) = a_{000} + a_{100}\exp[h_1]\exp[z_1] + a_{010}\exp[h_2]\exp[z_2] + a_{001}\exp[h_3]\exp[z_3]$$
$$+ a_{110}\exp[h_1 + h_2]\exp[z_1 + z_2] + a_{101}\exp[h_1 + h_3]\exp[z_1 + z_3]$$
$$+ a_{011}\exp[h_2 + h_3]\exp[z_2 + z_3] + a_{111}\exp[h_1 + h_2 + h_3]\exp[z_1 + z_2 + z_3].$$

Letting $\lambda_i := \exp[h_i]$, we have

$$\theta_{\mathcal{C}}(\mathbf{z} + \mathbf{h}) = a_{000} + \lambda_1 a_{100}\exp[z_1] + \lambda_2 a_{010}\exp[z_2] + \lambda_3 a_{001}\exp[z_3] + \lambda_1 \lambda_2 a_{110}\exp[z_1 + z_2]$$
$$+ \lambda_1 \lambda_3 a_{101}\exp[z_1 + z_3] + \lambda_2 \lambda_3 a_{011}\exp[z_2 + z_3] + \lambda_1 \lambda_2 \lambda_3 a_{111}\exp[z_1 + z_2 + z_3].$$

This gives us g parameterizing factors λ_i with $i = 1, 2, \ldots, g$ for the variables $a_{\mathbf{c}}$. The code used for this example is available at the link

https://mathrepo.mis.mpg.de/HirotaVarietyRationalNodalCurve.   (2.2.8)

2.2.2. Geometry of the main component

A further reason to introduce the Hirota variety and understanding its geometry is that it provides an additional formulation and approach to the Schottky problem for nodal curves. Proving the Schottky problem restricted to irreducible rational nodal curves is equivalent to showing that the irreducible subvariety of $\mathcal{H}_\mathcal{C}$, whose points correspond to soliton solutions arising from such curves, is a component of the expected dimension. This subsection explains this connection. The following result, in particular, validates the definition of the main component $\mathcal{H}_\mathcal{C}^M$ and establishes a link with soliton solutions to the KP equation.

Theorem 2.2.2. *Consider the map ϕ given in (2.2.4). This is a birational map onto its image, which is an irreducible subvariety of $\mathcal{H}_\mathcal{C}^M$ and has dimension $3g$.*

Proof. Let I be as in (2.2.5). Let $K \subseteq \mathbb{C}^{3g}$ be the closed set where at least two of the κ_i coincide. The expression of $\tau(x, y, t) = \theta_\mathcal{C}(\mathbf{u}x + \mathbf{v}y + \mathbf{w}t)$ where $(\mathbf{a}, (\mathbf{u}, \mathbf{v}, \mathbf{w}))$ is attained as the image of a point in $\mathbb{C}^{3g} \smallsetminus K$ through the map ϕ, described in (2.2.4), is a point in the Hirota variety $\mathcal{H}_\mathcal{C}$ since it can be expressed as a $(g, 2g)$-soliton [Kod04] for the matrix

$$
A = \begin{pmatrix}
\lambda_1 & 1 & 0 & 0 & 0 & 0 & \ldots & 0 & 0 \\
0 & 0 & \lambda_2 & 1 & 0 & 0 & \ldots & 0 & 0 \\
0 & 0 & 0 & 0 & \lambda_3 & 1 & \ldots & 0 & 0 \\
\vdots & \vdots & \vdots & \vdots & \vdots & \vdots & \ddots & \vdots & \vdots \\
0 & 0 & 0 & 0 & 0 & 0 & \ldots & \lambda_g & 1
\end{pmatrix}
\tag{2.2.9}
$$

Indeed, if we denote $E_i := \exp(\kappa_i x + \kappa_i^2 y + \kappa_i^3 t)$, plugging the parameterization in $\theta_\mathcal{C}(\mathbf{u}x + \mathbf{v}y + \mathbf{w}t)$ we obtain:

$$
\tilde{\tau}_\mathcal{C}(x, y, t) = \frac{1}{E_2 E_4 \cdots E_{2g}} \left(\sum_I \prod_{i < j \in I} (\kappa_i - \kappa_j) \prod_{i : c_i = 1} \lambda_i \prod_{i \in I} E_i \right),
\tag{2.2.10}
$$

where the sets I that define the sum are the same ones defined in (2.2.5). The extraneous exponential factor $(E_2 E_4 \cdots E_{2g})^{-1}$ disappears after we pass from $\tilde{\tau}(x, y, t)$ to $\partial_x^2 \log(\tilde{\tau}(x, y, t))$. Both versions of the $(g, 2g)$-soliton satisfy the Hirota's bilinear form and they represent the same solution to the KP equation. Hence, it follows that the image of $\mathbb{C}^{3g}$ through the map ϕ is contained in $\mathcal{H}_\mathcal{C}$.

Furthermore, the map ϕ is invertible outside the closed set where the u_i's vanish: given a point $(\mathbf{a}, (\mathbf{u}, \mathbf{v}, \mathbf{w}))$ in the image one can write

$$
\kappa_{2i-1} = \frac{u_i^2 + v_i}{2u_i} \qquad \text{and} \qquad \kappa_{2i} = \frac{v_i - u_i^2}{2u_i},
\tag{2.2.11}
$$

and the λ_i's can be obtained sequentially, starting from λ_1, by plugging in the values for the κ variables into the a_i's. Hence, we can conclude that the map ϕ is birational. This implies that the closure of the image is irreducible and of dimension $3g$. ∎

Notice that the method above provides a method to parameterize solutions arising from a genus g irreducible rational nodal curve as $(g, 2g)$-solitons. This is also consistent with Example 2.1.26.

In what follows, we show that $\mathcal{H}_\mathcal{C}^M$ is an irreducible component of $\mathcal{H}_\mathcal{C}$ whose points correspond to genus g rational nodal curves. This is equivalent to solving a version of the *weak Schottky problem*. In fact, $\mathcal{H}_\mathcal{C}^M$ parameterizes some solutions to the KP equation arising from irreducible rational nodal curves of genus g, and hence corresponds to a variety containing

the locus of Jacobians of such curves as an irreducible component. For an introduction to the Schottky problem see Subsection 2.2.4 and the references therein.

Theorem 2.2.3. *For genus $g \leq 9$, the subvariety $\mathcal{H}_{\mathcal{C}}^M$ is an irreducible component of the Hirota variety.*

Proof. The proof is mainly computational. A direct computation performed in `Macaulay2` shows that the Jacobian matrix of the Hirota variety $\mathcal{H}_{\mathcal{C}}$ evaluated at the image of a general point in $\mathbb{C}^{3g}$ through ϕ has rank $r - (3g)$, where r is the dimension of the space $(\mathbb{C}^*)^{2g} \times \mathbb{WP}^{3g-1}$. Hence the map ϕ is dominant into the main component $\mathcal{H}_{\mathcal{C}}^M$.   ∎

The code used for the proof above can be found at the link (2.2.8). The difficulty of extending the computation to higher genus mainly lies in the fast growth of the number of variables $\mathbf{a} = (a_{\mathbf{c}_1}, a_{\mathbf{c}_2}, \ldots, a_{\mathbf{c}_{2g}})$. One possibility to compute the ideal defining the variety $\mathcal{H}_{\mathcal{C}}$ consists in using the condition provided by the Hirota's bilinear form (2.1.5), which becomes computationally expensive when the genus is larger than 7. To avoid this computation, we implement the equations cutting out $\mathcal{H}_{\mathcal{C}}$ via the combinatorial description provided in Subsection 2.1.1.

Example 2.2.4 (The Cube). Let $g = 3$ and consider the tropical degeneration of a smooth plane quartic to a rational quartic. The 3-cube associated to the dual graph of a rational nodal quartic is the support of the degenerate theta function (2.2.7). This agrees with [AÇSS21, Example 6].

We compute the Hirota variety in $(\mathbb{K}^*)^8 \times \mathbb{WP}^8$. The set $\mathcal{C}^{[2]}$ consists of 19 points. Twelve are uniquely attained, one for each edge of the cube. These give rise to the three familiar quartics $u_j^4 - 4u_j w_j + 3v_j^2$, one for each edge direction $\mathbf{c}_k - \mathbf{c}_\ell$. Six points in $\mathcal{C}^{[2]}$ are attained twice. They contribute equations like (2.1.10), one for each of the six facets of the cube. Finally, the point $\mathbf{d} = (1, 1, 1)$ is attained four times. The polynomial (2.2.19) contributed by $\mathbf{d}$ equals

$$
\begin{aligned}
& P(\, u_1 + u_2 + u_3, \, v_1 + v_2 + v_3, \, w_1 + w_2 + w_3 \,) \, a_{000} a_{111} \\
+\ & P(\, u_1 + u_2 - u_3, \, v_1 + v_2 - v_3, \, w_1 + w_2 - w_3 \,) \, a_{001} a_{110} \\
+\ & P(\, u_1 - u_2 + u_3, \, v_1 - v_2 + v_3, \, w_1 - w_2 + w_3 \,) \, a_{010} a_{101} \\
+\ & P(\, -u_1 + u_2 + u_3, \, -v_1 + v_2 + v_3, \, -w_1 + w_2 + w_3 \,) \, a_{100} a_{011}.
\end{aligned}
\tag{2.2.12}
$$

If we restrict to the main component we can observe that the additional quartic relation

$$
a_{000} a_{110} a_{101} a_{011} \ = \ a_{100} a_{010} a_{001} a_{111}
\tag{2.2.13}
$$

holds. The main component has dimension 9, while its image in $\mathbb{WP}^8$ has dimension 5 and it is defined by the equations $u_1^4 + 3v_1^2 - 4u_1 w_1$, $u_2^4 + 3v_2^2 - 4u_2 w_2$, $u_3^4 + 3v_3^2 - 4u_3 w_3$, with fibers that are cones over $\mathbb{P}^1 \times \mathbb{P}^1 \times \mathbb{P}^1$. They are defined by seven equations arising from non-unique (k, ℓ). Six of these are binomials (2.1.10). Extending [Kod17, §2.5], we identify $\tau(x, y, t)$ with $(3, 6)$-solitons for

$$
A \ = \ \begin{pmatrix} 1 & 1 & 0 & 0 & 0 & 0 \\ 0 & 0 & 1 & 1 & 0 & 0 \\ 0 & 0 & 0 & 0 & 1 & 1 \end{pmatrix}.
\tag{2.2.14}
$$

By definition, a $(3, 6)$-soliton for the matrix A has the form

$$
\tilde{\tau}(x, y, t) \ = \ \sum_I \prod_{\substack{i, j \in I \\ i < j}} (\kappa_j - \kappa_i) \cdot \exp\left[x \cdot \sum_{i \in I} \kappa_i + y \cdot \sum_{i \in I} \kappa_i^2 + t \cdot \sum_{i \in I} \kappa_i^3 \right],
\tag{2.2.15}
$$

where I runs over the eight bases $135, 136, 145, 146, 235, 236, 245, 246$. To get from $(2.2.7)$ to this form, we use the following parametric representation of the main component in $\mathcal{H}_C$:

$$
\begin{aligned}
u_1 &= \kappa_1 - \kappa_2\,, \quad v_1 = \kappa_1^2 - \kappa_2^2\,, \quad w_1 = \kappa_1^3 - \kappa_2^3\,, \\
u_2 &= \kappa_3 - \kappa_4\,, \quad v_2 = \kappa_3^2 - \kappa_4^2\,, \quad w_2 = \kappa_3^3 - \kappa_4^3\,, \\
u_3 &= \kappa_5 - \kappa_6\,, \quad v_3 = \kappa_5^2 - \kappa_6^2\,, \quad w_3 = \kappa_5^3 - \kappa_6^3\,, \\
a_{111} &= (\kappa_3 - \kappa_5)(\kappa_1 - \kappa_5)(\kappa_1 - \kappa_3)\lambda_0\lambda_1\lambda_2\lambda_3\,, \quad a_{011} = (\kappa_3 - \kappa_5)(\kappa_2 - \kappa_5)(\kappa_2 - \kappa_3)\lambda_0\lambda_2\lambda_3\,, \\
a_{101} &= (\kappa_4 - \kappa_5)(\kappa_1 - \kappa_5)(\kappa_1 - \kappa_4)\lambda_0\lambda_1\lambda_3\,, \quad a_{001} = (\kappa_4 - \kappa_5)(\kappa_2 - \kappa_5)(\kappa_2 - \kappa_4)\lambda_0\lambda_3\,, \\
a_{110} &= (\kappa_3 - \kappa_6)(\kappa_1 - \kappa_6)(\kappa_1 - \kappa_3)\lambda_0\lambda_1\lambda_2\,, \quad a_{010} = (\kappa_3 - \kappa_6)(\kappa_2 - \kappa_6)(\kappa_2 - \kappa_3)\lambda_0\lambda_2\,, \\
a_{100} &= (\kappa_4 - \kappa_6)(\kappa_1 - \kappa_6)(\kappa_1 - \kappa_4)\lambda_0\lambda_1\,, \quad a_{000} = (\kappa_4 - \kappa_6)(\kappa_2 - \kappa_6)(\kappa_2 - \kappa_4)\lambda_0\,.
\end{aligned}
$$

If we multiply $(2.2.15)$ by $\exp\big[-(\kappa_2+\kappa_4+\kappa_6)\,x-(\kappa_2^2+\kappa_4^2+\kappa_6^2)\,y-(\kappa_2^3+\kappa_4^3+\kappa_6^3)\,t\big]$ then we obtain the desired function $\theta_{\mathcal{C}}(\mathbf{u}x + \mathbf{v}y + \mathbf{w}t)$ for the above generic point on the Hirota variety. The extraneous exponential factor disappears after we pass from $\tilde{\tau}(x,y,t)$ to $\partial_x^2 \log(\tilde{\tau}(x,y,t))$. Both versions of the $(3,6)$-soliton satisfy $(2.0.4)$ and they represent the same solution to the KP equation $(2.0.1)$.

An analogous construction works for the cube $\mathcal{C} = \{0,1\}^g$ in any dimension g. The description of the projection of the main component $\mathcal{H}_{\mathcal{C}}^M$ into the space $\mathbb{WP}^{3g-1}$ given in the example above reveals itself to be true for any genus:

Proposition 2.2.5. *The projection of $\mathcal{H}_{\mathcal{C}}^M$ into $\mathbb{WP}^{3g-1}$ is a $(2g-1)$-dimensional variety defined by the vanishing of $u_i^4 + 3v_i^2 - 4u_iw_i$ for $i = 1, 2, \ldots, g$.*

Proof. One direction (i.e., that the relations $u_i^4 + 3v_i^2 - 4u_iw_i$ hold in the projection) is immediate, as these are polynomials defining the Hirota variety (see Lemma 2.2.7) that do not include any a_i. For the other direction, it suffices to exhibit a point in $\mathcal{H}_{\mathcal{C}}^M$ for any $(\mathbf{u}, \mathbf{v}, \mathbf{w})$ which satisfy $u_i^4 + 3v_i^2 - 4u_iw_i$ for all $i \in [g]$. Using the inverse map given in $(2.2.11)$, given any u_i, v_i, w_i satisfying $u_i^4 + 3v_i^2 - 4u_iw_i = 0$, we uniquely determine (up to a scaling factor) $\kappa_{2i-1}, \kappa_{2i}$. We choose arbitrary $\lambda_1, \ldots, \lambda_g$ to get a point $(\mathbf{a}, (\mathbf{u}, \mathbf{v}, \mathbf{w}))$, so we are done. ∎

We conclude this subsection by stating two conjectures which consolidate and generalize the results above to any genus. Indeed, a generalization of Theorem 2.2.3 would provide a solution to the weak Schottky problem for rational nodal curves of genus g.

Weak Schottky Problem. For any genus g, the main component of the Hirota variety $\mathcal{H}_{\mathcal{C}}^M$ is a $3g$-dimensional irreducible component of $\mathcal{H}_{\mathcal{C}}$ with a parametric representation given in $(2.2.5)$.

Strong Schottky Problem. $\mathcal{H}_{\mathcal{C}}^M = \mathcal{H}_{\mathcal{C}}^I$.

Notice that one direction of the Schottky problem is immediate from the proof of Theorem 2.2.2: a sufficiently generic choice of κ_i ensures that, in the image, the u_i are nonzero, thus $\mathcal{H}_{\mathcal{C}}^M \subseteq \mathcal{H}_{\mathcal{C}}^I$. The other direction is more difficult. To prove it, one would need to show that any point in $\mathcal{H}_{\mathcal{C}}^I$ can be parameterized as in $(2.2.5)$.

2.2.3. Combinatorics of the main component

The results in this subsection describe in detail facts which we use in many of the proofs in Section 2.2. We aim to study in detail the Hirota variety $\mathcal{H}_{\mathcal{C}}$ in connection with the combinatorics of the support $\mathcal{C} = \{0,1\}^g$. Subsection 2.1.1 describes the equations defining the Hirota variety, a first step to better understand them in the case of the cube, consists in describing the set $\mathcal{C}^{[2]}$ from $(2.1.8)$.

Proposition 2.2.6. *A point $\mathbf{c} = (c_1, \ldots, c_g) \in \mathcal{C}^{[2]}$ is attained 2^{d-1} times, where $d = |\{i : c_i = 1\}|$.*

Proof. For a point $\mathbf{c} \in \mathcal{C}^{[2]}$, consider the set of indices $I = \{i : c_i \neq 1\}$. Suppose now $\mathbf{c} = \mathbf{c}_1 + \mathbf{c}_2$ for some points $\mathbf{c}_1, \mathbf{c}_2 \in \mathcal{C}$. Then, for any $i \in I$, if $c_i = 0$ then $c_{1i} = c_{2i} = 0$, while if $c_i = 2$ then $c_{1i} = c_{2i} = 1$. In the first case, this means that both $\mathbf{c}_1$ and $\mathbf{c}_2$ lie on the face of the g-cube defined by the i-th coordinate hyperplane $x_i = 0$. In the latter case, $\mathbf{c}_1, \mathbf{c}_2$ lie on the face defined by $x_i = 1$. The full set I of indices corresponding to elements $\neq 1$ defines a set of restrictions on x_i for $i \in I$. In fact, it defines a face of codimension $|I|$ (and thus dimension d) that $\mathbf{c}_1$ and $\mathbf{c}_2$ lie on. Let $[g] = \{1, \ldots, g\}$. For the indices $i \in [g] \smallsetminus I$, we have exactly one of c_{1i}, c_{2i} equal to 1. This gives exactly 2^{d-1} such pairs. These pairs can be viewed as diagonals of the faces defined by the restrictions given by I: they are the points which are distinct from one another in each coordinate except for the ones fixed by the face. ∎

As discussed in the proof, the points in $\mathcal{C}^{[2]}$ correspond to d-dimensional faces of the g-cube, where d is the number of coordinates equal to 1. Hence $|\mathcal{C}^{[2]}| = \sum_{d=1}^{g} 2^{g-d} \binom{g}{d}$ and the pairs that sum to points in $\mathcal{C}^{[2]}$ correspond to diagonals of the associated face. Another way to count $|\mathcal{C}^{[2]}|$ is to observe that it consists exactly of the points in $\{0, 1, 2\}^g$ which have at least one 1, so there are $3^g - 2^g$ of them.

We now investigate the polynomials arising from the points in $\mathcal{C}^{[2]}$. The points which are attained once correspond to the edges (one-dimensional faces) of the cube and the unique pair that adds up to such a point are the two vertices $\mathbf{c}_k, \mathbf{c}_\ell$ comprising the edge. Hence these points contribute the quartic

$$P_{k\ell}(\mathbf{u}, \mathbf{v}, \mathbf{w}) \ := \ P\big((\mathbf{c}_k - \mathbf{c}_\ell) \cdot \mathbf{u}, \ (\mathbf{c}_k - \mathbf{c}_\ell) \cdot \mathbf{v}, \ (\mathbf{c}_k - \mathbf{c}_\ell) \cdot \mathbf{w} \big).$$

Notice that this quartic depends only on the difference $\mathbf{c}_k - \mathbf{c}_\ell$, which is the same for all edges going in the same direction (that is, all edges whose corresponding point in $\mathcal{C}^{[2]}$ has the unique 1 at the same index). This reasoning yields the immediate result

Lemma 2.2.7. *The set $\mathcal{C}^{[2]}$ contains $g \cdot 2^{g-1}$ points which are uniquely attained. These contribute as generators of the ideal defining the Hirota variety $\mathcal{H}_\mathcal{C}$ with g quartics of the form $u_i^4 - 4u_i w_i + 3v_i^2$, for $i = 1, 2, \ldots, g$.*

Recall that the Hirota variety lies in the ambient space $(\mathbb{C}^*)^{2^g} \times \mathbb{WP}^{3g-1}$. The coordinate ring is $\mathbb{C}[\mathbf{a}^{\pm 1}, \mathbf{u}, \mathbf{v}, \mathbf{w}]$ and the ideal defining $\mathcal{H}_\mathcal{C}$ has $g + \sum_{d=2}^{g} 2^{g-d} \binom{g}{d}$ generators with respect to inclusion, one for each edge direction, and one for each face of every dimension from 2 up to g.

The combinatorics of the cube has already been shown to be important when studying the generators of the Hirota variety. In what follows, we will go over the combinatorics of the cube in relation to the main component, as well as present a more general version of Lemma 2.2.7. We begin with some definitions.

We denote by $\hat{\mathcal{C}}$ the convex hull of the set $\mathcal{C} = \{0, 1\}^g$ in $\mathbb{R}^g$ with coordinates $x_1, x_2, \ldots, x_g$. A d-dimensional face of the $\hat{\mathcal{C}}$ is determined by fixing $g - d$ indices of the vertices defining it. These indices are precisely the ones of the coordinate hyperplanes that define each face. We call the *direction* of the face the set of indices $I = \{i_1, i_2, \ldots, i_d\}$ that are not fixed. Furthermore, if two d-dimensional faces have the same direction, we define the *difference* between them to be the set J of fixed indices in the two faces which are different.

Example 2.2.8 ($g = 3, d = 1$)**.** Let $\mathcal{C} = \{0, 1\}^3$, the cube $\hat{\mathcal{C}}$ is displayed in Figure 2.6. The direction of an edge is given by a set with one element, namely the index of the standard basis vector to which the edge is parallel. For instance the edges $\mathrm{conv}((1, 0, 0), (1, 0, 1))$ and

$\text{conv}((1,1,0),(1,1,1))$ (in pink in Figure 2.6) are determined respectively by the hyperplanes $\{x_1 = 0, \ x_2 = 1\}$, and $\{x_1 = x_2 = 1\}$. Hence, they have the same direction given by $I = \{3\}$.

The difference of two edges on the same two dimensional face is also a one-element set, consisting of the index of the second standard basis vector defining the face (in addition to the standard basis vector given by the direction). Thus, the two edges above have difference $J = \{1\}$ corresponding to the coordinate hyperplane x_1 that determines different entries for the first coordinate of the vertices spanning the edges.
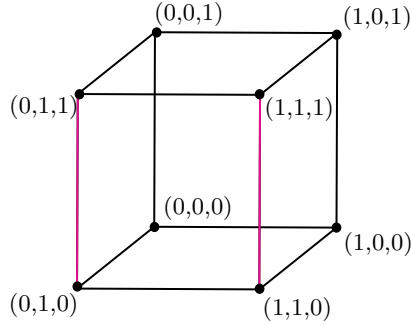
Figure 2.6. The 3-dimensional cube given by the vertices in $\mathcal{C} = \{0,1\}^3$.

In the following result, we restrict to the main component $\mathcal{H}_\mathcal{C}^M$ of the Hirota variety. We are interested in the points in $\mathcal{H}_\mathcal{C}^M$ that also verify the quartic relations

$$a_{\mathbf{c}_1} a_{\mathbf{c}_2} a_{\mathbf{c}_3} a_{\mathbf{c}_4} = a_{\mathbf{d}_1} a_{\mathbf{d}_2} a_{\mathbf{d}_3} a_{\mathbf{d}_4}, \quad \text{with } \sum_{i=1}^4 \mathbf{c}_i = \sum_{i=1}^4 \mathbf{d}_i, \ \sum_{i=1}^4 \mathbf{c}_i^2 = \sum_{i=1}^4 \mathbf{d}_i^2, \tag{2.2.16}$$

where $\mathbf{c}_i, \mathbf{d}_i$ are points in $\mathcal{C} = \{0,1\}^g$. Here, given a vector $\mathbf{c} \in \mathcal{C}$, we write $\mathbf{c}^2$ to denote the dot product $\mathbf{c}^T \cdot \mathbf{c}$. For $g = 3$, there exists a unique relation of this type, namely the one in (2.2.13). In particular, when the a_i are exponentials of the form $a_\mathbf{c} = \exp[\frac{1}{2}\mathbf{c}R_0\mathbf{c}^T]$, as in (2.2.2), then they verify these quartic relations. In general, one has

Lemma 2.2.9. *The closure of the image of the map* $\psi : Sym^2(\mathbb{C}^g) \to \mathbb{P}^{2^g-1}$ *defined by*

$$R \mapsto \left(a_\mathbf{c} = \exp\left[\frac{1}{2}\mathbf{c}^T R \mathbf{c} \right] \right)_{\mathbf{c} \in \{0,1\}^g} \tag{2.2.17}$$

is cut out by the equations in (2.2.16) and the additional equation $a_\mathbf{0} = 1$.

Proof. An immediate computation shows that the points in the image of ψ verify the relations in (2.2.16) and $a_\mathbf{0} = 1$. To show converse, we consider a point $\mathbf{a} = [a_{\mathbf{c}_1} : a_{\mathbf{c}_2} : \cdots : a_{\mathbf{c}_{2^g}}] \in \mathbb{P}^{2^g-1}$, with entries indexed by points in $\mathcal{C}$, such that it verifies the desired equations. Define the matrix $R \in \text{Sym}^2(\mathbb{C}^g)$ with entries given by

$$R_{ii} = 2\log a_{e_i} \quad \text{and} \quad R_{ij} = \log \frac{a_{e_i + e_j}}{a_{e_i} a_{e_j}} \quad \text{for } i, j \in [g], \ i \neq j,$$

where e_i denotes the i-th vector in the standard basis of $\mathbb{Z}^g$ and log denotes the natural logarithm. In this way, by definition we have that

$$a_{e_i} = \exp\left[\frac{1}{2}e_i^T R e_i \right] \quad \text{and} \quad a_{e_i + e_j} = \exp\left[\frac{1}{2}(e_i + e_j)^T R(e_i + e_j) \right] \quad \text{for } i, j \in [g], \ i \neq j.$$

Notice that the points in $\mathcal{C}$ are indexed by all possible subsets of the set $[g] = \{1, 2, \ldots, g\}$, and they are all of the form $\mathbf{c}_I = \sum_{i \in I} e_i$, with $\mathbf{c}_\varnothing = \mathbf{0}$. Hence we proceed by induction on the size n of the support I. The cases $n = 1, 2$ have been verified above. Hence, we assume that the a_{c_I} have the desired form for any $I \subset [g]$ with $|I| \leq n - 1$.

It is sufficient to prove the claim for the element $a_{e_1 + \cdots + e_n}$. By hypothesis, it verifies a relation of the form

$$a_{e_1 + \cdots + e_n} = \frac{a_{e_1 + \cdots + e_{n-1}} \cdot a_{e_1 + \cdots + e_{n-2} + e_n} \cdot a_{e_{n-1} + e_n} \cdot a_{\mathbf{0}}}{a_{e_1 + \cdots + e_{n-2}} \cdot a_{e_{n-1}} \cdot a_{e_n}}, \qquad (2.2.18)$$

where all the factors on the right-hand side of the equality are of the prescribed exponential form. Observe that, for $\mathbf{c}_I$ as above, in general one has

$$a_{\mathbf{c}_I} = \exp\left[\frac{1}{2} \left(\sum_{i \in I} e_i \right)^T R \left(\sum_{i \in I} e_i \right) \right] = \exp\left[\frac{1}{2} \left(\sum_{i \in I} R_{ii} + \sum_{\substack{i, j \in I \\ i \neq j}} R_{ij} \right) \right].$$

Substituting such exponentials in the right-hand side of Equation (2.2.18) we obtain that

$$a_{e_1 + \cdots + e_n} = \exp\left[\frac{1}{2} (e_1 + \cdots + e_n)^T R (e_1 + \cdots + e_n) \right].$$

This concludes the proof. ∎

Theorem 2.2.10. *There are $\binom{g}{d}$ face directions for each dimension d, and all faces with the same direction contribute the same quartic, up to a multiple, to the ideal defining $\mathcal{H}_{\mathcal{C}}^M$.*

Proof. Consider two d-dimensional faces of the g-cube with the same direction. This means that their corresponding points $\mathbf{c}_1, \mathbf{c}_2 \in \mathcal{C}^{[2]}$ have 1s in exactly the same positions. Both points have 2^{d-1} pairs which sum to them, and these pairs can be put in a correspondence. Namely, for a pair $\mathbf{c}_k, \mathbf{c}_\ell$ that sums to $\mathbf{c}_1$, the pair $\tilde{\mathbf{c}}_k, \tilde{\mathbf{c}}_\ell$ is a pair that sums to $\mathbf{c}_2$, where $\tilde{\mathbf{a}}$ is obtained from $\mathbf{a}$ by changing the entry from 0 to 1 (or vice-versa) for every index in the difference of the two faces. For the two pairs, $(\mathbf{c}_k, \mathbf{c}_\ell)$ and $(\tilde{\mathbf{c}}_k, \tilde{\mathbf{c}}_\ell)$, their corresponding quartic P_{kl} is the same, since it is easy to see that $\mathbf{c}_k - \mathbf{c}_\ell = \tilde{\mathbf{c}}_\ell - \tilde{\mathbf{c}}_k$.

Recall from Subsection 2.1.1, that the generators of the ideal $\mathcal{I}(\mathcal{H}_{\mathcal{C}})$ corresponding to d-dimensional faces with $d > 1$ are of the form

$$\sum_{\substack{1 \leq k < \ell \leq m \\ \mathbf{c}_k + \mathbf{c}_\ell = \mathbf{d}}} P_{k\ell}(\mathbf{u}, \mathbf{v}, \mathbf{w}) \, a_k a_\ell, \qquad (2.2.19)$$

where $\mathbf{d} \in \mathcal{C}^{[2]}$ is not uniquely attained. In what follows, we show that, when we restrict to the main component $\mathcal{H}_{\mathcal{C}}^M$, a d-dimensional face with direction D contributes the same quartic, up to a multiple, as the face corresponding to the point $\mathbf{c}_D = \sum_{i \in D} e_i$. We have already shown that the $P_{k\ell}$ are the same for faces with the same direction. Thus, it is sufficient to show that the polynomial

$$a_{\mathbf{c}_k} a_{\mathbf{c}_\ell} - d \cdot a_{\tilde{\mathbf{c}}_k} a_{\tilde{\mathbf{c}}_\ell}$$

is in the ideal defining $\mathcal{H}_{\mathcal{C}}^M$, where d is a factor (in fact, a product of some $a_{\mathbf{c}}$'s) which does not depend on k, ℓ, instead it depends only on the difference and direction of the two faces.

For ease of computations, we fix a direction D and we will take one of the faces (F_1) to be the face corresponding to the point $\mathbf{c}_1 = \sum_{i \in D} e_i$. The other face (F_2) is a face with direction D and difference E from F_1. Hence, the point corresponding to F_2 is $\mathbf{c}_2 = \sum_{i \in D} e_i + \sum_{i \in E} 2e_i$.

Since we will show that the quartic contributed by F_2 is the same as the one contributed by F_1 up to a multiple, this will show that all faces with the same direction contribute essentially the same polynomial to the ideal defining $\mathcal{H}_\mathcal{C}^M$.

Recall that the $a_\mathbf{c}$ are given by $\exp[\frac{1}{2}\mathbf{c}R\mathbf{c}^T]$, where we write R for R_0 from Equation (2.2.2). Consider a pair $\mathbf{c}_k, \mathbf{c}_\ell \in \mathcal{C}$ such that $\mathbf{c}_1 = \mathbf{c}_k + \mathbf{c}_\ell$. Then, there exist two disjoint subsets $D_1, D_2 \subseteq D$ such that $D = D_1 \cup D_2$, and $\mathbf{c}_k = \sum_{i \in D_1} e_i$ and $\mathbf{c}_\ell = \sum_{i \in D_2} e_i$. It follows that $\tilde{\mathbf{c}}_k = \sum_{i \in D_1 \cup E} e_i$ and $\tilde{\mathbf{c}}_\ell = \sum_{i \in D_2 \cup E} e_i$.

We will now use the linear algebra fact that for a symmetric $g \times g$ symmetric matrix, the following hold

$$\left(\sum_{i \in I} e_i \right) R \left(\sum_{j \in J} e_j \right)^T = \sum_{i \in I, j \in J} R_{ij}$$

Therefore, we have

$$a_{\tilde{\mathbf{c}}_k} a_{\tilde{\mathbf{c}}_\ell} = \exp\left[\frac{1}{2} \sum_{i,j \in D_1 \cup E} R_{ij} \right] \exp\left[\frac{1}{2} \sum_{i,j \in D_2 \cup E} R_{ij} \right] = \exp\left[\frac{1}{2} \sum_{i,j \in D \cup E} R_{ij} \right] \exp\left[\frac{1}{2} \sum_{i,j \in E} R_{ij} \right]$$

which one can easily see is a multiple of $\exp[\frac{1}{2} \sum_{i,j \in D} R_{ij}] = a_{\mathbf{c}_k} a_{\mathbf{c}_\ell}$ which only depends on the sets D and E, as desired. ∎

One can observe that Theorem 2.2.10 is a generalization of Lemma 2.2.7 to equations arising from points in $\mathcal{C}^{[2]}$ which correspond to higher dimensional faces. This holds for points in the main component $\mathcal{H}_\mathcal{C}^M$. Moreover, Theorem 2.2.10 reduces the number of potentially non-redundant relations holding in the ideal defining the variety $\mathcal{H}_\mathcal{C}^M$ to $2^g - 1$. This is also the codimension of $\mathcal{H}_\mathcal{C}^M$ inside its ambient space $(\mathbb{C}^*)^{2g} \times \mathbb{WP}^{3g-1}$. Our code in (2.2.8) verifies that this set of generators defines a variety which is a complete intersection, of which $\mathcal{H}_\mathcal{C}^M$ is a component for $g \leq 9$.

2.2.4. Quartic relations and the Schottky locus

This subsection provides a discussion relating quartic relations among the $\mathbf{a}$ parameters appearing in the degenerate theta function (2.2.2) and the Schottky problem. We write $\mathfrak{I}_g$ for the *Schottky locus* of abelian varieties corresponding to Jacobians of curves of genus g. The *second order theta constants*, [vG98] defined as

$$\Theta[m](\mathbf{z}, B) := \theta \begin{bmatrix} m \\ 0 \end{bmatrix} (2\mathbf{z}, 2B),$$

provide an embedding $\iota : \mathcal{A}_g \hookrightarrow \mathbb{P}^{2g-1}$ of $\mathcal{A}_g$ into a projective space. Recall that the theta function appearing on the right-hand side is the theta function with characteristic defined in (1.1.3). In the setting provided by the maps

$$\mathcal{M}_g \xrightarrow{J} \mathcal{A}_g \hookrightarrow \mathbb{P}^{2g-1}, \tag{2.2.20}$$

to solve the Schottky problem, one aims to determine the defining ideal of $\iota(\mathfrak{I}_g) \subset \iota(\mathcal{A}_g)$. In genus 4, we have $\dim \mathcal{M}_4 = 9 = 10 - 1 = \dim \mathcal{A}_4$, and hence the ideal $\mathfrak{I}_4$ is an analytic hypersurface in $\mathcal{A}_4$. In fact, in genus 3, the second order theta constants verify an equation of degree 16 which leads to the equation characterizing Jacobians of curves in genus 4, i.e., Igusa's equation, see [vG16, Example 6.2], [Igu82]. An analogous situation can be described when looking at the degenerate theta functions arising from irreducible rational nodal curves.

The map ψ in (2.2.17) provides an embedding of the space $Sym^2(\mathbb{C}^g)$ in the projective space $\mathbb{P}^{2^g-1}$. The dimension count for these spaces is analogous to the one for the spaces involved in (2.2.20). In particular, for genus 3, we find that $\overline{im(\psi)} = \overline{Sym^2(\mathbb{C}^3)}$ inside $\mathbb{P}^7$. Note that the image of the map ψ is contained in the locus $V(a_{111}a_{100}a_{010}a_{001} - a_{110}a_{101}a_{011}a_{000})$, where the relation among the a_i's comes from (2.2.13). Equality then follows by a direct computation since these are both irreducible varieties of equal dimension. We believe a similar situation should hold for higher genus. We aim to pursue this direction as a future project.

2.3. Conclusions

In this section, we outline the main research directions in the study of the connection between algebraic curves with nodal singularities and KP theory directed toward future work.

Analogously to what was done in Section 2.2 when the Delaunay set is the g-cube, a natural direction to investigate consists in studying the Hirota varieties for the 17 Delaunay polytopes in Table 2.1. This includes computing equations, irreducible decomposition, dimensions, and all the relevant geometric invariants.

Moreover, the Hirota variety provides a further way of attaining KP solutions. Nevertheless, the relationship between solutions obtained from the Sato Grassmannian and from the Hirota variety is not well understood. More precisely, having fixed an algebraic curve C, in both constructions, a choice is needed: studying the degeneration of the Riemann theta function requires one to pick a point $\mathbf{a} \in \mathbb{Z}^g$; analogously, to construct a point in the Sato Grassmannian a divisor D and a point p on the curve have to be fixed. Moreover, in Subsection 2.1.4 we presented examples of divisors on rational nodal curves from which one cannot build a point in the Sato Grassmannian. This discussion motivates the following open problem:

Problem 2.3.1. Given a complex algebraic curve C of genus g with at worst nodal singularities, understand the relation between the degeneration of the Riemann theta function via $\mathbf{a} \in \mathbb{Z}^g$ and the choice of the divisor D and point p on the curve.

In the same spirit of the previous problem, the following connection deserves further investigation:

Problem 2.3.2. Study how the choice of the pair (p, D) on the curve C corresponding to a soliton solution relates to the point in the positive Grassmannian and the soliton graphs studied by Kodama and Williams [KW14].

As discussed in the previous section, another reason for introducing the Hirota variety and understanding its geometry is that it provides an additional formulation and approach to the Schottky problem for nodal curves. Solving the Schottky problem restricting to irreducible rational nodal curves is, in fact, equivalent to showing that the irreducible subvariety of $\mathcal{H}_\mathcal{C}$, whose points correspond to soliton solutions arising from such curves, is a component of the expected dimension. Besides the conjectures stated at the end of Subsection 2.2.4, one can investigate the following

Combinatorial Schottky Problem. Determine the equations defining the locus of Jacobian varieties of irreducible rational nodal curves in genus 4 and 5.

In genus 4, one approach to attack this problem is to apply the degeneration from Theorem 2.1.2 to the theory developed to solve the Schottky problem for smooth algebraic curves.

In higher genus, partial results exist for smooth curves [FGSM21, vG16]. This also inspires further progress for the nodal case, with the advantage that, when the curve is singular, the theta function is a finite sum of exponentials, and understanding the combinatorics of the support $\mathcal{C}$ provides new approaches to the problem. This is essentially the rationale behind the adjective "combinatorial" being used to describe the Schottky problem for nodal curves.

Chapter 3

Particle physics and very affine varieties

By addressing unsolved problems regarding the geometric objects arising in scattering amplitudes from both the physics and mathematics perspectives, this chapter tries to forge links between algebraic geometry and particle physics. We present material from the papers [ABF+23] and [AFST22]. Both articles discuss how various physics questions can be reduced to studying properties and geometry of certain algebraic varieties. In either case, we deal with very affine varieties, that is, closed subvarieties of an algebraic torus. Very affine varieties have recently received considerable attention due to their central role in tropical geometry [Tev07] and to their connection to the problem of maximum likelihood estimation in algebraic statistics [Huh13].

In particle physics, very affine varieties arise when counting the number of critical points of the *potential function*, or equivalently, the number of solutions to the *scattering equations* [CEGM19, CHY14, CUZ20, ST21]. We connect the study of such solutions to computing the *maximum likelihood* (ML) *degree* of the likelihood function in algebraic statistics. In fact, in both fields, one aims to count the number of solutions to a system of rational equations over a very affine variety X. Huh [Huh13] proved that, when the variety is smooth, this number coincides with the Euler characteristic of X. When studying the potential function, the variety X is the moduli space of m points in $\mathbb{P}^{k-1}$ in linearly general position

$$X(k, m) = \mathrm{Gr}(k, m)^\circ / (\mathbb{C}^*)^m, \qquad \text{with } k \geq 2. \tag{3.0.1}$$

Section 3.1 answers several questions raised in the physics literature pertaining to bounded regions in discriminantal arrangements and to moduli spaces of point configurations. We introduce the *likelihood degenerations*, a type of degenerations in algebraic geometry and numerical nonlinear algebra, inspired by the *soft limits* in [CUZ20]. The study of such degenerations allows one to compute the Euler characteristic of $X(k, m)$ for several cases, proving some conjectures stated in [CUZ20].

A further crucial problem in scattering amplitudes and quantum field theory consists in finding basis for prescribed families of *Feynman integrals*. These are integrals associated with connected undirected graphs known as Feynman diagrams, which encode the interaction patterns in a scattering process mediated by internal particles, as explained in Appendix A. Numerical evaluation of Feynman integrals is a crucial step for computing scattering amplitudes. A first step in this direction is to define a finite-dimensional vector space of such integrals and establish linear relationships between them. Therefore, one expresses more complex integrals in terms of basis integrals, also referred to as *master integrals* in the physics literature. Implementing algorithms to compute basis of master integrals and linear relations among them is a topic undergoing intense study in particle physics [FGM+19, FGL+21, MM19].

Feynman integrals in the Lee–Pomeransky representation [LP13] are concrete, non-trivial examples of a class of well-studied and more general integrals called *generalized Euler integrals*. More explicitly, these are integrals of the form

$$\int_\Gamma f^{s+a}\, x^{\nu+b}\, \frac{\mathrm{d}x}{x} \;=\; \int_\Gamma \left(\prod_{j=1}^{\ell} f_j^{s_j+a_j}\right) \cdot \left(\prod_{i=1}^{n} x_i^{\nu_i+b_i}\right) \frac{\mathrm{d}x_1}{x_1} \wedge \cdots \wedge \frac{\mathrm{d}x_n}{x_n}. \tag{3.0.2}$$

Here, $x = (x_1, \ldots, x_n)$ are coordinates on $(\mathbb{C}^*)^n$ and $f = (f_1, \ldots, f_\ell)$ denotes a tuple of ℓ Laurent polynomials in x. We use multi-index notation, i.e., f^s denotes $f_1^{s_1} \cdots f_\ell^{s_\ell}$, and similarly for x^ν. The integration contour Γ is chosen compatibly with the polynomials f so that the integral (3.0.2) converges. We will later make this precise. The exponents ν_i, s_j take on complex values, whereas $a_i, b_j \in \mathbb{Z}$ are thought of as integer shifts.

Section 3.2 studies the vector spaces associated with a family of such integrals. Their dimension, which is the number of master integrals when (3.0.2) is a Feynman integral, is given by the Euler characteristic of a very affine variety. In this context, the relevant very affine variety is the complement of the vanishing locus of the product $f_1 \cdots f_\ell$ in the n-dimensional algebraic torus

$$X \;=\; \left\{\, x \in (\mathbb{C}^*)^n \mid f_1(x) \cdots f_\ell(x) \neq 0 \,\right\} \;=\; (\mathbb{C}^*)^n \smallsetminus V(f_1 \cdots f_\ell) \subset (\mathbb{C}^*)^n.$$

We investigate this number using tools from homological algebra and D-module theory, uncover new relations between these approaches, and provide new algorithmic tools.

The structure of this chapter is as follows. The novel approaches to compute the Euler characteristics of the very affine varieties (3.0.1) are illustrated in the Subsection 3.1.1, and Subsections 3.1.5 and 3.1.7. They rely on techniques from combinatorics and numerical nonlinear algebra, in addition to algebro-geometric tools. Subsection 3.1.1 concerns the deletion maps

$$\pi_{k,m} : X(k, m+1) \to X(k, m). \tag{3.0.3}$$

These maps are shown to be stratified fibrations. We discuss both the fibers (Subsection 3.1.2) and the strata (Subsection 3.1.3), setting the stage for the computation of Euler characteristics by combinatorial methods. Subsection 3.1.4 focuses on techniques to compute the Euler characteristic of the space $X(3, m)$ of m points in general position in the projective plane $\mathbb{P}^2$. Subsection 3.1.5 presents a detailed analysis of the tropical geometry of soft limits for configurations of eight points in projective 3-space. In Subsection 3.1.6 we turn to algebraic statistics, and we follow up on earlier work on likelihood degenerations due to Gross and Rodriguez [GR14]. We introduce the tropical version of maximum likelihood estimation for discrete statistical models. This arises by replacing the real numbers $\mathbb{R}$ by the Puiseux series field $\mathbb{R}\{\{t\}\}$, in both the data and the solutions. Our main result (Theorem 3.1.28) characterizes the tropical MLE for linear discrete models. In Subsection 3.1.7 we present numerical methods for likelihood degenerations, with an emphasis on recovering the description of tropical curves from floating point coordinates. This extends the tropical MLE approach in Subsection 3.1.6 from linear models to other very affine varieties, and it allows us to find tropical solutions to scattering equations in particle physics. The code used in this section together with computational results are available at https://mathrepo.mis.mpg.de/LikelihoodDegenerations.

Section 3.2 aims to provide all of the tools required to demonstrate the equalities in Theorem 3.2.1. We start by carefully introducing the three vector spaces $V_\Gamma, V_{s,\nu}, V_{c^*}$ of Euler integrals that can be distinguished depending on the choice of parameters one fixes. More explicitly, in Subsection 3.2.1, we recall twisted de Rham cohomology and homology

with coefficients in a local system. We study the vector space V_Γ and relations between its generators. Subsection 3.2.2 recalls definitions about algebras of differential and difference operators, and revisits the Mellin transform adapted to our setup. This is used to investigate $V_{s,\nu}$. We discuss how to algorithmically obtain relations between the generators of V_Γ and $V_{s,\nu}$, which is relevant in practice. Proposition 3.2.20 provides new insights in connections between the relations for these two different vector spaces. Subsection 3.2.3 presents the GKZ system leading to V_{c^*}, and recalls the background. At this point, our main result (Theorem 3.2.1) follows as a corollary of Theorems 3.2.7, 3.2.23, and 3.2.28, which state the result in different contexts. Subsection 3.2.4 presents numerical methods to compute $\chi(X)$, and to find relations among the integrals in the case of V_Γ. We also highlight what genericity means in each context. We provide examples illustrating the theory and demonstrate how to run computations using different software systems. Our setup applies to the generalized Euler integrals in (3.0.2), and is not restricted to Feynman integrals. However, we discuss this special case in several remarks.

The code used in Subsection 3.2.4, together with our other computational examples, can be found at the link https://mathrepo.mis.mpg.de/EulerIntegrals.

3.1. Point configurations

This section revolves around a very affine variety arising in particle physics [CEGM19, CUZ20], namely the moduli space $X(k,m)$ of m points in $\mathbb{P}^{k-1}$ in linearly general position. More explicitly, this moduli space parametrizes m-tuples $[P] = [P_1, \ldots, P_m]$ of points $P_i \in \mathbb{P}^{k-1}$ such that no k of them lie on a hyperplane. Moreover, the m-tuples are considered only up to the action of $\mathrm{GL}(k,\mathbb{C})$. The dimension of $X(k,m)$ equals $(k-1)(m-k-1)$. Observe that $X(2,m)$ is the familiar $(m-3)$-dimensional moduli space $\mathcal{M}_{0,m} = \mathrm{Gr}(2,m)^\circ/(\mathbb{C}^*)^m$ of genus zero curves with m marked points. These spaces are central to the Cachazo–He–Yuan (CHY) formulas for biadjoint scalar amplitudes [CHY14].

We next present a parametrization which shows that $X(k,m)$ is very affine. Taking homogeneous coordinates for the points P_i, any m-tuple $[P]$ as above can be represented by a complex $k \times m$ matrix whose $k \times k$ minors are all nonzero. Two such representations are equivalent if and only if they differ by left multiplication by $\mathrm{GL}(k,\mathbb{C})$, or by a rescaling of the columns by an element in the torus $(\mathbb{C}^*)^m$. Hence, this identifies $X(k,m)$ as the quotient

$$X(k,m) = \mathrm{Gr}(k,m)^\circ/(\mathbb{C}^*)^m, \tag{3.1.1}$$

where $\mathrm{Gr}(k,m)$ is the Grassmannian of k-dimensional subspaces in $\mathbb{C}^m$ and $\mathrm{Gr}(k,m)^\circ$ is the open cell where all Plücker coordinates $p_{i_1 \ldots i_k}$ are nonzero. We can uniquely write the homogeneous coordinates of an m-tuple $[P] \in X(k,m)$ as the columns of the $k \times m$ matrix

$$M_{k,m} = \begin{bmatrix} 0 & 0 & 0 & \ldots & 0 & (-1)^k & 1 & 1 & 1 & \ldots & 1 \\ 0 & 0 & 0 & \ldots & (-1)^{k-1} & 0 & 1 & x_{1,1} & x_{1,2} & \ldots & x_{1,m-k-1} \\ \vdots & \vdots & \vdots & \cdot^{\cdot^{\cdot}} & \vdots & \vdots & \vdots & \vdots & \vdots & \cdot^{\cdot^{\cdot}} & \vdots \\ 0 & 0 & -1 & \ldots & 0 & 0 & 1 & x_{k-3,1} & x_{k-3,2} & \ldots & x_{k-3,m-k-1} \\ 0 & 1 & 0 & \ldots & 0 & 0 & 1 & x_{k-2,1} & x_{k-2,2} & \ldots & x_{k-2,m-k-1} \\ -1 & 0 & 0 & \ldots & 0 & 0 & 1 & x_{k-1,1} & x_{k-1,2} & \ldots & x_{k-1,m-k-1} \end{bmatrix}, \tag{3.1.2}$$

provided all maximal minors $p_{i_1 \ldots i_k}$ of this matrix are nonzero. The antidiagonal matrix in the left $k \times k$ block was chosen so that each unknown $x_{i,j}$ equals such a minor for $i_1 < \cdots < i_k$.

This identifies $X(k,m)$ as an open subset of the torus $(\mathbb{C}^*)^{(k-1)(m-k-1)}$ with coordinates $x_{i,j}$. The Plücker embedding realizes $X(k,m)$ as a closed subvariety of a high-dimensional torus:

$$X(k,m) \hookrightarrow (\mathbb{C}^*)^{\binom{m}{k}}, \qquad M_{k,m} \mapsto (p_{i_1 \ldots i_k}). \tag{3.1.3}$$

As aforementioned, in particle physics, very affine varieties arise when computing critical points of the potential function on the moduli space $X(k,m)$. Such a function is analogous to the log-likelihood function in statistics, namely

$$\mathcal{L}_{k,m} = \sum_{i_1 \ldots i_k} u_{i_1 \ldots i_k} \cdot \log(p_{i_1 \ldots i_k}). \tag{3.1.4}$$

The critical point equations, known as *scattering equations* in physics, are given by

$$\frac{\partial \mathcal{L}_{k,m}}{\partial x_{i,j}} = 0 \qquad \text{for } 1 \le i \le k-1 \text{ and } 1 \le j \le m-k-1. \tag{3.1.5}$$

This is a system of rational function equations. One way to compute the ML degree of $X(k,m)$ is by counting the number of solutions for general values of the parameters $u_{i_1 \ldots i_k}$. This can be done by finding explicit solutions to (3.1.5), notably by the numerical approach described in [ST21, §3] which rests on the software `HomotopyContinuation.jl` [BT18]. The connection between maximum likelihood and scattering equations was first developed in [ST21]. While the maximum likelihood degree MLdegree($X(2,m)$) is known to be $(m-3)!$, see [ST21, §2], much less is known for $k \ge 3$. Cachazo, Umbert and Zhang [CUZ20] introduced a class of degenerations called *soft limits* to compute some of the unknown cases. In what follows, we develop novel techniques to gain a mathematical understanding of that construction from physics. We succeed in reaching this understanding, and we present our results using effective methods that connect complex geometry, tropical combinatorics, and numerical nonlinear algebra.

3.1.1. Likelihood degenerations

Recall that a very affine variety X is a closed subvariety of an algebraic torus $(\mathbb{C}^*)^n$. For any integer vector $\mathbf{u} = (u_1, \ldots, u_n) \in \mathbb{Z}^n$, the Laurent monomial $\mathbf{z}^{\mathbf{u}} = z_1^{u_1} \cdots z_n^{u_n}$ is a regular function on $(\mathbb{C}^*)^n$, and we are interested in the set of critical points of $\mathbf{z}^{\mathbf{u}}$ on X. The natural approach is via the gradient of the *log-likelihood function* $\log(\mathbf{z}^{\mathbf{u}}) = \sum_{i=1}^n u_i \log(z_i)$. This makes sense for any complex vector $\mathbf{u} \in \mathbb{C}^n$. The coordinates of $\nabla \log(\mathbf{z}^{\mathbf{u}})$ are rational functions, and we seek points $\mathbf{z} \in X$ at which that gradient vector lies in the normal space. This leads to a system of rational function equations whose solutions are the critical points. Their number is independent of $\mathbf{u}$, provided $\mathbf{u}$ is generic. This is an invariant of X, denoted MLdegree(X), and known as the maximum likelihood degree; see [CHKS06, GR14, Huh13, HS14]. Whenever X is smooth, we know from [Huh13, Theorem 1] that it coincides with the signed Euler characteristic of X:

$$\text{MLdegree}(X) = (-1)^{\dim X} \cdot \chi(X). \tag{3.1.6}$$

The term *likelihood* comes from statistics [PS05]. A discrete statistical model on $n-1$ states is a subset M of the probability simplex $\Delta_{n-2} = \{(z_1, \ldots, z_{n-1}) \in \mathbb{R}_{>0}^{n-1} : z_1 + \cdots + z_{n-1} = 1\}$. In algebraic statistics, the model M is a semialgebraic set, and one replaces M by its Zariski closure X. That closure is taken in the torus $(\mathbb{C}^*)^n$, where $z_n = z_1 + \cdots + z_{n-1}$. After

collecting data, we write $u_i \in \mathbb{N}$ for the number of samples in state i. The monomial $\mathbf{z}^{\mathbf{u}}$ is the likelihood function. The goal of likelihood inference is to maximize $\mathbf{z}^{\mathbf{u}}$ over M. Thus, statisticians seek those critical points of $\log(\mathbf{z}^{\mathbf{u}})$ that are real and positive. The ML degree of X is an algebraic complexity measure for performing likelihood inference with the model M.

The term *degeneration* comes from algebraic geometry. It represents the idea of studying the properties of a general object X_t for $t \neq 0$ by letting it degenerate to a more special object X_0, which is often easier to understand. This corresponds to finding a nice compactification of the variety $\mathcal{X}^0 = \cup_{t \neq 0} X_t$ to a variety $\mathcal{X}$, by adding the special fiber X_0. There are many possibilities for such constructions. Most relevant in our context are the tropical compactifications in [MS21a, §6.4] and their connection to likelihood inference in [vdVS22].

Likelihood degenerations arise when the coefficients $u_{i_1 \cdots i_k}$ depend on a parameter t, and one studies the behavior of the solutions in the limit $t \to 0$. A special instance are the soft limits of Cachazo et al. [CUZ20]. This likelihood degeneration is presented in (3.1.20). We explain in Subsection 3.1.5 how soft limits are related to the methods in this section. Subsections 3.1.6 and 3.1.7 explore arbitrary likelihood degenerations, with a view towards statistics and numerics.

Another approach to computing the ML degree is topological, through the Euler characteristic. Indeed, since the variety $X(k, m)$ is smooth, the formula (3.1.6) applies and gives

$$\text{MLdegree}(X(k, m)) = (-1)^{(k-1)(m-k-1)} \cdot \chi(X(k, m)). \tag{3.1.7}$$

Our strategy to compute the Euler characteristic is to exploit the deletion map in (3.0.3):

$$\pi_{k,m} \colon X(k, m+1) \longrightarrow X(k, m), \qquad [P_1, \ldots, P_m, P_{m+1}] \mapsto [P_1, \ldots, P_m].$$

This approach relies on the fact that the Euler characteristic is multiplicative along fibrations.

Example 3.1.1 ($k = 2$)**.** The space $X(2, 3)$ is a single point, so $\chi(X(2, 3)) = 1$. For $m \geq 3$ we consider the map $\pi_{2,m} \colon X(2, m+1) \longrightarrow X(2, m)$. A point below is identified with an m-tuple $[P_1, \ldots, P_m]$, where $P_i \in \mathbb{P}^1$ are pairwise distinct, and $P_1 = (0 : -1), P_2 = (1 : 0), P_3 = (1 : 1)$ are fixed. The fiber over this point equals $F = \mathbb{P}^1 \setminus \{P_1, \ldots, P_m\}$. This has Euler characteristic $2 - m$. All fibers are homeomorphic to F, so the map $\pi_{2,m}$ is a fibration. Multiplicativity of the Euler characteristic along fibrations implies

$$\chi(X(2, m+1)) = \chi(F) \cdot \chi(X(2, m)) = (2 - m) \cdot \chi(X(2, m)).$$

By induction on m, we conclude that $\chi(X(2, m)) = (-1)^{m-3}(m-3)!$.

Our main difficulty for $k \geq 3$ is that the deletion map $\pi_{k,m}$ is generally not a fibration. But it is a *stratified fibration*, that is, it is a map $f \colon X \to Y$ of complex algebraic varieties such that Y has a stratification $\mathcal{S} = \{S \subseteq Y\}$ by finitely many closed strata, with the property that, over each open stratum $S^\circ = S \setminus \bigcup_{S' \subsetneq S} S'$, the map is a fibration with fiber F_S.

The set $\mathcal{S}$ of all strata S in a stratified fibration $f \colon X \to Y$ is naturally a poset, ordered by inclusion. We can use this combinatorial structure to compute the Euler characteristic of X. The following result is standard but we include it here for the sake of reference.

Lemma 3.1.2. *Let $f \colon X \to Y$ be a stratified fibration and μ the Möbius function of $\mathcal{S}$. Then*

$$\chi(X) = \sum_{S \in \mathcal{S}} \chi(S) \cdot \sum_{S' \in \mathcal{S}, S' \supseteq S} \mu(S, S') \chi(F_{S'})$$

$$= \chi(Y) \cdot \chi(F_Y) + \sum_{S \in \mathcal{S}} \chi(S) \cdot \sum_{S' \in \mathcal{S}, S' \supseteq S} \mu(S, S') \cdot (\chi(F_{S'}) - \chi(F_Y)).$$

Proof. By the excision property of the Euler characteristic, together with the multiplicativity along fibrations, we know that $\chi(X) = \sum_{S' \in \mathcal{S}} \chi(S'^\circ) \cdot \chi(F_{S'})$. We can rewrite this as follows: for any closed stratum $S' \in \mathcal{S}$ we have $\chi(S') = \sum_{S' \supseteq S} \chi(S^\circ)$. The Möbius inversion formula yields $\chi(S'^\circ) = \sum_{S' \supseteq S} \mu(S, S')\chi(S)$. Plugging this into the previous formula, we obtain the first equality in Lemma 3.1.2. The second equality comes from the definition of the Möbius function, which stipulates that $\sum_{S' \supseteq S} \mu(S, S') = 0$, for a fixed stratum $S \in \mathcal{S} \smallsetminus \{Y\}$. ∎

Lemma 3.1.2 can be used to compute the ML degree of a very affine variety X that is smooth. If we are given a stratified fibration $X \to Y$, then the computation reduces to the topological task of computing the Euler characteristics of the fibers and of the strata, together with the combinatorial task of computing the Möbius function of the poset.

We shall apply this method to the deletion map in (3.0.3). For this, we need to argue that this map is a stratified fibration, which requires us to identify the strata and the fibers. The fibers are complements of discriminantal arrangements, to be discussed thoroughly in Section 3.1.2. The strata are given by a certain matroidal stratification, see Section 3.1.3. We describe the general setting here, and we will give explicit computations for the case $k = 3$ in Section 3.1.4.

First, let us consider the fibers. Given a representative $[P] = [P_1, \ldots, P_m]$ for an element of $X(k, m)$, the corresponding discriminantal arrangement is the set $\mathcal{B}(P)$ of all hyperplanes linearly spanned by any set of $k-1$ points $P_{i_1}, \ldots, P_{i_{k-1}}$. Observe that these span a hyperplane because of the requirement that the points are in linearly general position. The fiber of $\pi_{k,m}$ over $[P]$ is the complement of this hyperplane arrangement:

$$\pi_{k,m}^{-1}([P]) \;\cong\; \mathbb{P}^{k-1} \smallsetminus \bigcup_{H \in \mathcal{B}(P)} H. \tag{3.1.8}$$

The Euler characteristic of such a complement is found with the methods in Section 3.1.2. One subtle aspect of this computation is that all objects are taken up to the action of $\mathrm{GL}(k, \mathbb{C})$.

This description also indicates the appropriate stratification of $X(k, m)$: it depends on the linear dependencies satisfied by the $\binom{m}{k-1}$ hyperplanes in the arrangement $\mathcal{B}(P)$. This comes from a certain matroid stratification. Let us give an example for the case $k = 3$:

Example 3.1.3. Consider $\pi_{3,6} \colon X(3, 7) \to X(3, 6)$. To any $[P]$ in $X(3, 6)$ we associate the arrangement of 15 lines $\overline{P_i P_j}$. Move one of them to the line at infinity in $\mathbb{P}^2$. For generic $[P]$, the number of bounded regions in the resulting arrangement of 14 lines is the Euler characteristic of the fiber $\pi_{3,6}^{-1}([P])$. This number is 42, as we shall see in Section 3.1.2. For special fibers the Euler characteristic drops. Consider $[P]$ where the lines $\overline{P_1 P_2}, \overline{P_3 P_4}, \overline{P_5 P_6}$ are concurrent. These three lines are not in general position [BS06, Figure 4-3]. The Euler characteristic of the fiber of $\pi_{3,6}$ over $[P]$ is 41. Our stratification of $X(3, 6)$ must account for this.

In general, the situation is as follows. Each point of $X(k, m)$ is represented by a $k \times m$ matrix $M_{k,m}$ as in (3.1.2). We consider the $(k-1)$st exterior power $\wedge_{k-1} M_{k,m}$ of that matrix. That new matrix has k rows and $\binom{m}{k-1}$ columns, and its entries are the signed $(k-1) \times (k-1)$ minors of $M_{k,m}$. Each column of $\wedge_{k-1} M_{k,m}$ is the normal vector to the hyperplane spanned by $k-1$ points $P_{i_1}, \ldots, P_{i_{k-1}}$. Here we allow for the possibility that the column vector is zero, which means that $P_{i_1}, \ldots, P_{i_{k-1}}$ lie on a $(k-2)$-plane in $\mathbb{P}^{k-1}$. Taking the exterior power is equivariant with respect to the action of $\mathrm{GL}(k, \mathbb{C})$, so we obtain a map of Grassmannians

$$\mathrm{Gr}(k, m) \to \mathrm{Gr}\big(k, \binom{m}{k-1}\big). \tag{3.1.9}$$

We now consider the matroid stratification [BS06, §4.4] of the big Grassmannian $\mathrm{Gr}\big(k, \binom{m}{k-1}\big)$. The strata correspond to arrangements of $\binom{m}{k-1}$ hyperplanes in $\mathbb{P}^{k-1}$ that have a fixed intersection lattice. We next consider the pullback of this matroid stratification under the map (3.1.9). This is a very fine stratification of $\mathrm{Gr}(k, m)$. Its strata correspond to point configurations whose discriminantal hyperplane arrangement has a fixed intersection lattice. This stratification is much finer than the matroid stratification of $\mathrm{Gr}(k, m)$. In particular, it defines a highly nontrivial stratification of the open cell $\mathrm{Gr}(k, m)^\circ$. This stratification of $\mathrm{Gr}(k, m)^\circ$ is compatible with the action of the torus $(\mathbb{C}^*)^m$, given that all our constructions are based on projective geometry. Passing to the quotient in (3.1.1), let $\mathcal{S}_{k,m}$ denote the induced stratification of $X(k, m)$. We call this the *discriminantal stratification* of the space $X(k, m)$.

Proposition 3.1.4. *The deletion map $\pi_{k,m} \colon X(k, m+1) \to X(k, m)$ defines a stratified fibration with respect to the discriminantal stratification on the very affine variety $X(k, m)$.*

Proof and discussion. Each fiber of $\pi_{k,m}$ is the complement of a discriminantal hyperplane arrangement. These arrangements have fixed intersection lattice as the base point $[P]$ ranges over an open stratum of $\mathcal{S}_{k,m}$. This implies that the Euler characteristic is constant on each fiber. This is what we need to be a fibration on each stratum. It is possible that the homotopy type varies across such fibers [Ryb11]. This would require further subdivisions into constructible sets. But, all we need here is for the Euler characteristic to be constant. ∎

In conclusion, the topological approach to computing the ML degree of $X(k, m)$ consists of two parts: computing the Euler characteristic of the fibers, which is done in Subsection 3.1.2, and computing the Euler characteristic of the matroid strata, which is done in Subsection 3.1.3.

3.1.2. Discriminantal hyperplane arrangements

The fibers of the deletion map (3.0.3) are complements of discriminantal hyperplane arrangements, see (3.1.8). By Varchenko's Theorem [CHKS06, Theorem 3], the ML degree is the number of bounded regions. In this subsection we focus on the generic fiber. This arises from the $\binom{m}{k-1}$ hyperplanes spanned by m generic points in $\mathbb{P}^{k-1}$. Such arrangements have been studied for decades, e.g. in [Cra85, Fal94, KNT12, OT13]. Our general reference on the relevant combinatorics is [Sta01]. We show that, for fixed k, the number of bounded regions is a polynomial in m of degree $(k-1)^2$. This polynomial was denoted $\mathrm{Soft}_{k,m}$ in [CUZ20]. We display it explicitly for $k \leq 7$. Our result extends to all coefficients of the characteristic polynomial (Theorem 3.1.7). Its proof rests on constructions of Koizumi, Numata and Takemura in [KNT12].

We work with two models in real affine space. First, fix m general points in $\mathbb{R}^{k-1}$. We write $\mathcal{A}(k, m)$ for the arrangement of $\binom{m}{k-1}$ hyperplanes spanned any $k-1$ of these points. Second, we consider the set $\widetilde{\mathcal{B}}(k, m)$ of $\binom{m}{k-1}$ hyperplanes through the origin in $\mathbb{R}^k$ that are spanned by any $k-1$ of the columns of the matrix $M_{k,m}$ in (3.1.2), where the $x_{i,j}$ are generic. Let $\mathcal{B}(k, m)$ be the restriction of this hyperplane arrangement to $\mathbb{R}^{k-1} \simeq \{x_1 = 1\}$. Thus $\mathcal{B}(k, m)$ is an affine arrangement of $\binom{m}{k-1} - 1$ hyperplanes in $\mathbb{R}^{k-1}$. As pointed out by Falk in [Fal94], the combinatorics of the arrangement $\mathcal{A}(k, m)$ is not independent of the choice of the m general points as for some choices the dependencies among those points admit "second-order" dependencies beyond the Grassmann-Plücker relations. Following Bayer and Brandt [BB97] we assume that the m points are *very generic* in the sense that such dependencies do not appear. All such very generic choices yield combinatorially equivalent

arrangements $\mathcal{A}(k, m)$, see also [SY22] for a discussion of non-very generic discriminantal arrangements.

In Subsection 3.1.4 we will explore non-very generic degenerations of these discriminantal arrangements. Both $\mathcal{A}(k, m)$ and $\mathcal{B}(k, m)$ are induced by the open cell in the large Grassmannian under an embedding of the form (3.1.9). But their combinatorial structures are different.
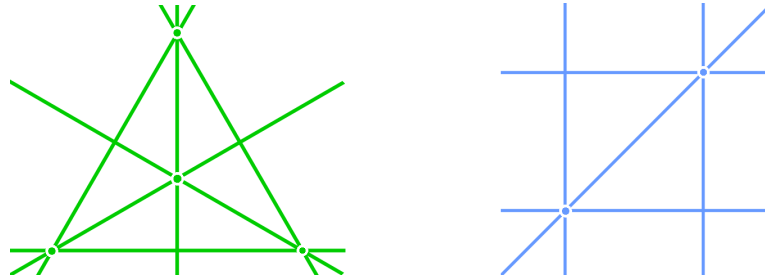
Figure 3.1. The discriminantal line arrangements $\mathcal{A}(3,4)$ (left) and $\mathcal{B}(3,4)$ (right).

Example 3.1.5 ($k = 3, m = 4$). The arrangement $\mathcal{A}(3,4)$ consists of the six lines that are spanned by four general points in the affine plane $\mathbb{R}^2$. Its complement in $\mathbb{R}^2$ consists of 18 regions, of which six are bounded. The arrangement $\mathcal{B}(3,4)$ is obtained from $\mathcal{A}(3,4)$ by moving one of the six lines to infinity. Thus $\mathcal{B}(3,4)$ consists of five lines, which divide $\mathbb{R}^2$ into 12 regions, of which two are bounded. The two arrangements are shown in Figure 3.1. Their characteristic polynomials (3.1.10) are $\chi_{\mathcal{A}(3,4)}(t) = t^2 - 6t + 11$ and $\chi_{\mathcal{B}(3,4)}(t) = t^2 - 5t + 6$.

	$m = 2$	3	4	5	6	7	8	9
$k = 2$	0	1	2	3	4	5	6	7
3		0	2	13	42	101	205	372
4			0	6	192	1858	10644	44595
5				0	24	5388	204117	3458276
6					0	120	255180	46545915
7						0	720	18699210

Table 3.1. The number of bounded regions of $\mathcal{B}(k, m)$ for various k and m. See Remark 3.1.6.

It is the second arrangement, $\mathcal{B}(k, m)$, which plays the center stage for our application. We shall reduce its analysis to that of $\mathcal{A}(k, m)$, so we can use results of Koizumi et al. [KNT12].

Remark 3.1.6. The generic fiber of the map $\pi_{k,m}$ is the complement of a hyperplane arrangement in complex projective space $\mathbb{P}^{k-1}$ that is combinatorially isomorphic to $\mathcal{B}(k, m)$. Hence the Euler characteristic of the generic fiber equals the number of bounded regions of $\mathcal{B}(k, m)$.

We begin with some basics from [S+04]. Given an arrangement $\mathcal{A}$ of hyperplanes $H_1, \ldots, H_N$ in real affine space $\mathbb{R}^d$, we write $F_I = \bigcap_{i \in I} H_i$ for any subset I of $[N] := \{1, \ldots, N\}$. The collection of nonempty F_I forms a poset $L(\mathcal{A})$ by reverse inclusion. This is called the *intersection poset*, and it is graded by the codimension of F_I. The *characteristic polynomial* is

$$\chi_{\mathcal{A}}(t) \;=\; \sum_{F_I \in L(\mathcal{A})} \mu(F_I) \cdot t^{d - \mathrm{codim}(F_I)} \;=:\; \sum_{i=0}^{d} (-1)^d \cdot b_i(\mathcal{A}) \cdot t^{d-i} \qquad (3.1.10)$$

where $\mu(F_I) = \mu(\mathbb{R}^d, F_I)$ is the Möbius function of $L(\mathcal{A})$. The coefficients $\{b_i(\mathcal{A})\}_{i=0}^d$ are the *Betti numbers* of $\mathcal{A}$. They are nonnegative integers. The components of the complement of the arrangement in $\mathbb{R}^d$ are called the *regions* of $\mathcal{A}$. Zaslavsky [Zas97] showed that the regions are counted, up to sign, by $\chi_{\mathcal{A}}(-1)$. The bounded regions of $\mathcal{A}$ are counted by $|\chi_{\mathcal{A}}(1)|$.

We are interested in the characteristic polynomials of the generic discriminantal arrangements $\mathcal{A}(k,m)$ and $\mathcal{B}(k,m)$ defined above. The following is our main result in this subsection.

Theorem 3.1.7. *For fixed k, the Betti numbers of $\mathcal{A}(k,m)$ and $\mathcal{B}(k,m)$ are polynomials in the parameter m. Here the i-th Betti number is a polynomial of degree $i(k-1)$. The number of bounded regions of either arrangement is given by a polynomial in m of degree $(k-1)^2$.*

In light of Remark 3.1.6, we are primarily interested in the number of bounded regions of $\mathcal{B}(k,m)$. Cachazo et al. [CUZ20, §3] wrote these as polynomials of degree 4 and 9 for $k = 3, 4$. This led to the polynomiality conjecture that is proved here. We list our polynomials for $k \le 7$:

$k = 3$: $\quad \frac{1}{(2!)^3}(m-4)(m^3 - 6m^2 + 11m - 14)$

$k = 4$: $\quad \frac{1}{(3!)^4}(m-5)(m^8 - 13m^7 - 5m^6 + 1019m^5 - 7934m^4 + 29198m^3 - 57510m^2 + 57276m - 20736)$

$k = 5$: $\quad \frac{1}{(4!)^5}(m-6)(m^{15} - 34m^{14} + 536m^{13} - 6016m^{12} + 56342m^{11} - 324124m^{10} - 737436m^9 + 33755560m^8 - 324772079m^7$
$\qquad + 1784683822m^6 - 6330080036m^5 + 14844484456m^4 - 22600207744m^3 + 21093515136m^2 - 10696725504m + 2188394496)$

$k = 6$: $\quad \frac{1}{(5!)^6}(m-7)(m^{24} - 68m^{23} + 2199m^{22} - 44982m^{21} + 643996m^{20} - 6596728m^{19} + 44404954m^{18} - 71800572m^{17} - 3127304119m^{16}$
$\qquad + 54378585092m^{15} - 490514132181m^{14} + 1776590470858m^{13} + 18487658083746m^{12} - 378944155004728m^{11} + 3596483286643204m^{10}$
$\qquad - 23256569552060072m^9 + 111789542126956376m^8 - 412236512413133568m^7 + 1177950138000941824m^6 - 2598297935794415232m^5$
$\qquad + 4348400923758960000m^4 - 5332505009742720000m^3 + 4499090747884800000m^2 - 2314865713121280000m + 540696010752000000)$

$k = 7$: $\quad \frac{1}{(6!)^7}(m-8)(m^{35} - 118m^{34} + 6721m^{33} - 246112m^{32} + 6510988m^{31} - 132696712m^{30} + 2174185716m^{29} - 29636017152m^{28}$
$\qquad + 347341371054m^{27} - 3619686930036m^{26} + 34412884983870m^{25} - 297168540668160m^{24} + 2163013989971700m^{23} - 9541316565707160m^{22}$
$\qquad - 57505724652057900m^{21} + 2082608669563706400m^{20} - 30141885880045284135m^{19} + 290868328355522261370m^{18}$
$\qquad - 1789045412885731209655m^{17} + 2410419545362804828960m^{16} + 98045335860104486976824m^{15} - 1463950567334046862107632m^{14}$
$\qquad + 13043235985765459517500784m^{13} - 86372694744783734157998048m^{12} + 451792193002382546052610752m^{11}$
$\qquad - 1910783375678688560288108928m^{10} + 6590586320126085204961058304m^9 - 18548788372955608600206309888m^8$
$\qquad + 42375051122462107996615842816m^7 - 77750332979800481270501750784m^6 + 112672771830431700211895132160m^5$
$\qquad - 125767704870432247378231296000m^4 + 104081289628186508359680000000m^3 - 60012326911967527500840960000m^2$
$\qquad + 21475615998699753858662400000m - 2^2 53^1 55^7 235936983)$

Each polynomial gives the values in one row of Table 3.1. See also the list at the end of [KNT12].

We now embark towards the proof of Theorem 3.1.7, beginning with the following lemma.

Lemma 3.1.8. *The characteristic polynomials of $\mathcal{A}(k,m)$ and $\mathcal{B}(k,m)$ are related as follows:*

$$\chi_{\mathcal{A}(k,m)}(t) \cdot t - \chi_{\mathcal{A}(k,m)}(1) = \chi_{\mathcal{B}(k,m)}(t) \cdot (t-1).$$

Proof. The central arrangement $\widetilde{\mathcal{B}}(k,m)$ is the cone over $\mathcal{B}(k,m)$. This gives the relation

$$\chi_{\widetilde{\mathcal{B}}(k,m)}(t) = \chi_{\mathcal{B}(k,m)}(t) \cdot (t-1).$$

The restriction $\mathcal{C}^H$ of any central arrangement $\mathcal{C}$ to a hyperplane H not containing the origin satisfies $\chi_{\mathcal{C}^H}(t) \cdot t - \chi_{\mathcal{C}^H}(1) = \chi_{\mathcal{C}}(t)$. We apply this fact to $\mathcal{C} = \widetilde{\mathcal{B}}(k,m)$ and $H = \{x_1 = 1\}$. This implies the assertion because the restriction of $\mathcal{C}$ to H is precisely $\mathcal{C}^H = \mathcal{A}(k,m)$. ∎

Example 3.1.9. The discriminantal arrangement $\widetilde{\mathcal{B}}(3,4)$ given by four vectors in $\mathbb{R}^3$ satisfies

$$\chi_{\widetilde{\mathcal{B}}(3,4)}(t) \;=\; t^3 - 6t^2 + 11t - 6.$$

The characteristic polynomials in Example 3.1.5 are derived from this. We obtain $\chi_{\mathcal{A}(3,4)}(t)$ by deleting the constant term and dividing by t. We obtain $\chi_{\mathcal{B}(3,4)}(t)$ by dividing by $t-1$.

Corollary 3.1.10. *The number of bounded regions of $\mathcal{B}(k,m)$ is given, up to a sign, by*

$$\chi_{\mathcal{B}(k,m)}(1) \;=\; \frac{d}{dt}\chi_{\mathcal{A}(k,m)}(1) + \chi_{\mathcal{A}(k,m)}(1).$$

Koizumi et al. [KNT12] provide formulas for $\chi_{\mathcal{A}(k,m)}$ for $1 \le k \le 7$ and general m. The coefficients of their characteristic polynomials, i.e. the Betti numbers, are polynomials in m. We show that this trend continues. The extension to $\mathcal{B}(k,m)$ follows from Lemma 3.1.8.

Lemma 3.1.11. *The Betti numbers of both $\mathcal{A}(k,m)$ and $\mathcal{B}(k,m)$ are polynomials in m.*

Proof. We shall use [KNT12] to derive the result for $\mathcal{A}(k,m)$. We set $d = k - 1$ and write $L(d,m)$ for the intersection poset of $\mathcal{A}(k,m)$, with Möbius function $\mu_{d,m}$. Note that $\mu_{d,m}(\{\varnothing\})$ is the number of bounded regions in $\mathcal{A}(k,m)$. In [KNT12], the elements F of $L(d,m)$ are grouped according to partitions $\gamma = (\gamma_1, \dots, \gamma_\ell)$, called the *type* of F. The number of elements of type γ is denoted $\lambda_{d,m}(\gamma)$. A main result of [KNT12] is that the Möbius function applied to F depends only on the type of F. Hence, the characteristic polynomial of $L(d,m)$ equals

$$\chi_{d,m}(t) \;=\; \sum_{i=0}^{d} \sum_{\gamma \vdash i} \lambda_{d,m}(\gamma)\mu_{d,m}(\gamma)t^{d-i}. \tag{3.1.11}$$

We will show that $\lambda_{d,m}(\gamma)$ and $\mu_{d,m}(\gamma)$ are both polynomials in m for fixed d. Then (3.1.11) implies that the coefficients of the characteristic polynomial are polynomials in m as well. Proposition 4.7 of [KNT12] gives the following formula:

$$\lambda_{d,m}(\gamma) \;=\; \frac{1}{\prod_{k=1}^{d} m_k(\gamma)!} \sum_{\nu} \frac{(\nu(I_2) + \dots + \nu(I_{2^\ell}))!}{\nu(I_2)!\cdots\nu(I_{2^\ell})!} \binom{m}{\nu(I_2) + \dots + \nu(I_{2^\ell})}. \tag{3.1.12}$$

Here, $m_k(\gamma)$ is a constant depending on k and γ, and $2^{[\ell]}$ is the power set of $[\ell]$. This set is ordered $\{I_1, \dots, I_{2^\ell}\}$ with $I_1 = \varnothing$. The sum in (3.1.12) is over all maps $\nu : 2^{[\ell]} \to \mathbb{N}$ satisfying

(i) $\sum_{i \in I} \nu(I) = d + 1 - \gamma_i$ for all $i \in [\ell]$,

(ii) $\sum_{I \subset I'} \nu(I') < d + 1 - \sum_{i \in I} \gamma_i$ for all I with $|I| > 1$, and

(iii) $\sum_{I \in 2^{[\ell]}} \nu(I) = m$.

Note that as m grows by one, the indexing set of these maps essentially remains the same; the only difference is that $\nu(\varnothing)$ is also incremented by one. Since $\nu(\varnothing) = \nu(I_1)$ does not appear in the binomial in (3.1.12), the expression (3.1.12) is polynomial in m.

Proposition 4.1 of [KNT12] gives a recursive definition for $\mu_{d,m}(\gamma)$ in terms of $\mu_{d',m'}(\{\varnothing\})$ for strictly smaller d' and m'. Since these are the numbers of bounded regions of $\mathcal{A}(k',m')$ for strictly smaller k' and m', their polynomiality follows inductively, proving the result. ∎

Proof of Theorem 3.1.7. The Betti number b_i of interest is the coefficient of t^{d-i} in $\chi_{d,m}(t)$. We know that this is a polynomial in m. We first argue that the degree of this polynomial is at most $d \cdot i$, and then we show that it has degree at least $d \cdot i$. For the upper bound, we note that the i-th Betti number of a generic arrangement with $\binom{m}{d}$ hyperplanes in $\mathbb{R}^d$ is a polynomial in m of degree $d \cdot i$. Any other arrangement with the same number of hyperplanes, including discriminantal ones, must have Betti numbers bounded by these generic Betti numbers.

To derive the lower bound, we recall that, by definition of the Betti numbers in (3.1.10),

$$b_i = \sum_{\substack{F \in L(d,m) \\ \mathrm{codim}(F)=i}} \mu_{d,m}(F). \tag{3.1.13}$$

All terms in this sum have the same sign. Suppose $m > d \cdot i$ and consider all $T_{e_1}, \ldots, T_{e_i} \subset [m]$ where each T_{e_j} consists of d points and $T_{e_j} \cap T_{e_k} = \varnothing$ for $1 \leq j < k \leq i$. These collections correspond to the codimension i flats $\bigcap_{j=1}^{i} H_j$ where H_j is the hyperplane spanned by the points indexed by T_{e_j}. These are special flats in our arrangement. Their number is

$$\frac{1}{d!} \underbrace{\binom{m}{d} \cdot \binom{m-d}{d} \cdot \ldots \cdot \binom{m-id+d}{d}}_{i \text{ factors}}.$$

This product of i binomial coefficients is a polynomial in m of degree $d \cdot i$. Therefore, the degree of b_i as polynomial in m is at least $d \cdot i$. This completes the proof of Theorem 3.1.7. ∎

Corollary 3.1.12. *The ML degree of the generic fiber of $\pi_{k,m}$ is a polynomial of degree $(k-1)^2$.*

We presented formulas for these ML degrees for $k \leq 7$ and arbitrary m. These play a major role in the stratified fibration approach of Subsection 3.1.1. However, in addition to the generic fiber, we also need to know the Euler characteristic for the fiber over each stratum in the base space $X(k,m)$. All of these fibers are discriminantal arrangements, arising from lower-dimensional matroid strata in the large Grassmannian on the right hand side of (3.1.9). In other words, we need to compute $\chi_{\mathcal{A}}(1)$ for many large hyperplane arrangements $\mathcal{A}$.

In practise, this task can now be accomplished easily, thanks to the software recently presented in [BEK21]. This implementation was essential to us in getting this project started, and in validating the polynomial formulas for $\mathcal{B}(k,m)$ displayed above. We expect it to be useful for a wide range of applications, not just in mathematics, but also in physics and statistics.

3.1.3. Matroid strata

In our topological approach to computing the ML degree of $X(k,m)$, we encountered special strata of points and lines in $\mathbb{P}^{k-1}$ with prescribed incidence conditions. Such strata can be modeled as matroid strata. Such matroid strata are very affine varieties. In Theorem 3.1.14 we furnish a comprehensive study for small matroids of rank k on m elements. Note that the uniform matroid corresponds to $X(k,m)$. We compute the ML degrees for all matroids in the range $k = 3, m \leq 9$ and $k = 4, m = 8$. For larger matroids this would become infeasible by *Mnëv's Universality Theorem* [BS06, §6.3]. Our result is achieved by integrating software tools from computer algebra [BKLH], combinatorics [MMIB12a], and certified numerics [BRT20, BT18].

From now on, all matroids are assumed to be simple, so the term "matroid" will mean "simple matroid". We shall comprehensively study all small matroids. For a matroid M of

rank k on m elements, we consider the points in $\mathrm{Gr}(k, m)$ whose nonzero Plücker coordinates are precisely those indexed by the bases of M. Let $X(M)$ be the quotient of that constructible set modulo the action of $(\mathbb{C}^*)^m$. One represents $X(M)$ by a $k \times m$ matrix with at least one entry 1 per column and some unknown entries that satisfy equations and inequations of degree $\leq k-1$ arising from nonbases and bases. This encoding shows that $X(M)$ is a very affine variety. If M is the uniform matroid then $X(M) = X(k, m)$. The aim of this subsection is to compute the ML degree of $X(M)$ for every matroid of small size.

Example 3.1.13 ($k = 3, m = 9$)**.** The *Pappus matroid M* (shown in Figure 3.2a) has the nonbases

$$123 \quad 148 \quad 159 \quad 247 \quad 269 \quad 357 \quad 368 \quad 456 \quad 789.$$

These are precisely the triples that index the vanishing 3×3 minors of the matrix

$$\begin{bmatrix} 1 & 0 & 1 & 0 & 1 & y & 0 & 1 & y \\ 0 & 1 & x & 0 & 1 & y & 1 & 0 & 1 \\ 0 & 0 & 0 & 1 & 1 & 1 & 1/(1-x) & x/(y(x-1)) & 1 \end{bmatrix}. \tag{3.1.14}$$

Indeed, the stratum $X(M)$ for the Pappus matroid is the set of pairs $(x, y) \in (\mathbb{C}^*)^2$ such that all $\binom{9}{3} - 9 = 75$ other maximal minors are nonzero. The log-likelihood function equals

$$u_1\log(x) + u_2\log(y) + u_3\log(1-x) + u_4\log(1-y) + u_5\log(1-x-y) + u_6\log(1-xy) + u_7\log(xy-x-y).$$

The two partial derivatives of this expression are rational functions in x and y. By equating these to zero, we obtain a system of equations that has precisely eight solutions in $(\mathbb{C}^*)^2$, provided $u_1, u_2, \ldots, u_7$ are general enough. Hence the stratum of the Pappus matroid M is a very affine variety $X(M)$ of dimension 2 whose ML degree is equal to 8. It is one of the 12 matroids of rank 3 on 9 elements with these invariants, marked 8_{12} in Theorem 3.1.14.

We now present the result of our computations for matroids of rank k on m elements. For fixed k, m, we list the matroid strata by dimension, and we list all occurring ML degrees together with their multiplicity of occurrences. For instance, the string $2_5[1, 2_4]$ accounts for five strata of dimension 2: four have ML degree 2 and one has ML degree 1. If the variety $X(M)$ is reducible, then we list the ML degree for each component, e.g. in the format $(3, 3)_2$.

Below we follow the convention in the applied algebraic geometry literature (e.g. [OS16]) to assign a star to a theorem obtained by a numerical computation which was not fully certified.

Theorem* 3.1.14. *The strata $X(M)$ are smooth for all matroids M with $k = 2$ or ($k = 3$ and $m \leq 9$) or ($k = 4$ and $m = 8$). Their ML degrees are given in the following lists.*

For $k = 3, m = 5$ there are 4 matroids, up to permuting labels, and all are realizable over $\mathbb{C}$:
$$2_1[2_1] \qquad 1_2[1_2] \qquad 0_1[1_1].$$

For $k = 3, m = 6$ there are 9 matroids, up to permuting labels, and all are realizable over $\mathbb{C}$:
$$4_1[26_1] \qquad 3_1[6_1] \qquad 2_4[1_1, 2_3] \qquad 1_2[1_2] \qquad 0_1[1_1].$$

For $k = 3, m = 7$ there are 22 orbits of $\mathbb{C}$-realizable matroids:
$$6_1[1272_1] \quad 5_1[192_1] \quad 4_3[24_2, 38_1] \quad 3_7[2_1, 6_4, 10_1, 12_1] \quad 2_6[1_1, 2_3, 4_2] \quad 1_3[1_2, 2_1] \quad 0_1[1_1]$$

For $k = 3, m = 8$ there are 66 orbits of $\mathbb{C}$-realizable matroids:
$$8_1[188112_1] \quad 7_1[21240_1] \quad 6_3[1560_1, 2136_1, 2976_1] \quad 5_7[120_2, 264_2, 368_1, 520_1, 568_1]$$
$$4_{16}[4_1, 6_1, 24_5, 38_1, 55_1, 56_2, 72_1, 80_1, 88_1, 120_2] \quad 3_{16}[2_1, 6_4, 10_2, 16_3, 17_1, 18_2, 24_1, 25_1, 32_1]$$
$$2_{14}[2_4, 4_3, 5_1, 6_3, 7_1, 8_2] \qquad 1_6[1_1, 2_4, 3_1] \qquad 0_2[1_1, 2_1]$$

For $k = 3, m = 9$ there are 368 *orbits of $\mathbb{C}$-realizable matroids:*

$$10_1[74570400_1] \quad 9_1[\underline{6750000_1}] \quad 8_3[349920_1, 565706_1, 730656_1],$$
$$7_8[13920_1, 24624_1, 43512_1, 44496_1, 56448_1, 73024_1, 94668_1, 99808_1]$$
$$6_{22}[720_3, 2040_2, 2856_2, 3696_1, 5160_1, 6648_1, 6700_1, 6708_1, 6796_1, 7752_1, 8646_1,$$
$$8684_1, 9152_1, 11392_1, 11972_1, 14880_1, 15132_1, 18768_1]$$
$$5_{45}[0_2, 12_1, 24_1, 120_6, 264_2, 360_2, 480_1, 500_1, 512_2, 672_1, 712_2, 720_1, 780_1, 922_1, 948_1, 956_1, 960_1, 1092_1,$$
$$1220_1, 1264_1, 1294_1, 1296_3, 1316_1, 1364_1, 1672_1, 1736_1, 1744_1, 1756_1, 1806_1, 2274_1, 2292_1, 2628_1, 2648_1]$$
$$4_{77}[0_1, 4_1, 6_1, 24_5, 38_1, 56_3, 80_4, 82_2, 96_2, 116_2, 118_2, 119_1, 120_1, 124_3, 132_1, 144_1, 150_1, 156_1, 162_2, 166_1,$$
$$168_1, 172_2, 174_1, 186_1, 192_1, 200_1, 222_1, 224_1, 228_2, 232_3, 236_1, 238_1, 240_1, 242_2, 243_1, 244_1, 262_1,$$
$$272_1, 280_1, 292_1, 302_1, 306_1, 312_1, 318_1, 324_1, 330_2, 336_1, 342_1, 376_1, 416_1, 424_2, 434_1, 456_1, 460_1]$$
$$3_{93}[0_2, 6_4, 10_3, 16_6, 17_1, 18_2, 24_6, 25_1, 26_4, 27_1, 30_1, 32_1, 34_2, 35_2, 36_5, 37_3, 38_3, 39_1, 40_5, 42_2, 44_2, 46_2,$$
$$47_2, 51_1, 52_4, 54_2, 55_1, 56_4, 58_2, 60_1, 64_1, 66_2, 68_2, 70_3, 72_2, 76_2, 84_1, 86_1, 102_1, 104_1, 108_1]$$
$$2_{78}[0_1, 2_3, 4_4, 6_8, 7_3, 8_{12}, 9_3, 10_{10}, 11_4, 12_7, 13_3, 14_2, 15_3, 16_7, 17_1, 18_3, 19_2, 30_1, (18, 18)_1],$$
$$1_{34}[0_3, 2_{10}, 3_8, 4_7, 5_2, 6_2, (3, 3)_2] \qquad 0_8[1_3, 2_5]$$

For $k = 4, m = 8$ there are 554 *orbits of $\mathbb{C}$-realizable matroids:*

$$9_1[\underline{5211816}] \qquad 8_1[\underline{516673_1}] \qquad 7_5[21240_2, 46392_1, 52392_1, 63040_1]$$
$$6_{14}[1272_2, 1560_2, 2136_1, 2976_2, 5136_1, 6976_1, 7600_1, 9424_1, 103368_2]$$
$$5_{40}[26_1, 120_4, 192_4, 264_6, 368_3, 488_1, 520_2, 568_2, 692_1, 708_1, 770_1, 936_1, 950_1,$$
$$1080_3, 1294_1, 1296_2, 1322_1, 1400_1, 1710_1, 1768_1, 1812_2]$$
$$4_{89}[0_3, 4_1, 6_2, 24_{14}, 26_1, 38_9, 55_1, 56_8, 72_3, 80_3, 88_4, 104_1, 115_2, 120_6, 122_1, 134_2, 136_1, 154_3,$$
$$162_2, 180_2, 181_1, 216_1, 220_1, 224_1, 226_1, 232_2, 236_2, 272_1, 282_3, 288_2, 308_2, 384_2, 410_1]$$
$$3_{153}[1_1, 2_8, 6_{30}, 10_{15}, 12_5, 16_{13}, 17_5, 18_{10}, 24_9, 25_5, 27_2, 28_1, 32_7, 34_1, 35_3, 36_5, 38_1,$$
$$39_2, 40_1, 45_1, 46_2, 48_1, 50_6, 51_1, 52_3, 53_2, 55_1, 56_2, 58_2, 64_2, 66_2, 67_1, 72_2, 104_1]$$
$$2_{153}[1_8, 2_{35}, 4_{29}, 5_1, 6_{18}, 7_{10}, 8_{16}, 9_2, 10_6, 11_6, 12_8, 13_3, 14_3, 15_3, 18_2, 19_1, 24_2]$$
$$1_{81}[0_4, 1_{20}, 2_{36}, 3_9, 4_9, 5_2, (2, 2)_1] \qquad 0_{18}[1_{15}, 2_3]$$

Proof. This was obtained by exhaustive computations. The matroids were taken from the database [MMIB12a] that is described in [MMIB12b]. The GAP packages alcove [Leu20] and ZariskiFrames [BKLH] were used to obtain a representing $k \times m$ matrix, such as (3.1.14), along with further equations for nonbases and inequations for bases, whenever needed. The details of the underlying algorithm are described in [BK21]. From this matrix, together with the defining equations, we compute the ML degree as the number of critical points of the log-likelihood function. This is illustrated in Example 3.1.13. These computations were performed using the Julia package HomotopyContinuation.jl [BT18]. See also [ST21]. The ML degrees of the uniform matroids $U_{3,7}$, $U_{3,8}$, $U_{3,9}$, $U_{4,8}$ are derived and discussed in Subsections 3.1.4 and 3.1.5. ∎

Remark 3.1.15. As the method of homotopy continuation is numerical, it is inherently subject to rounding errors. Hence, the numbers in Theorem 3.1.14 come with this disclaimer as well. For those numbers which are not underlined, we successfully performed the certification method described in [BRT20], using the implementation conveniently available in [BT18]. Subsection 4.2.4 goes into greater detail about how this method works. Such a certified result delivers a mathematical *proof* that our number bounds the true ML degree from below. Of the six underlined entries, two are the uniform matroids $U_{3,9}$ and $U_{4,8}$ (discussed in Subsections 3.1.4 and 3.1.5) and another is a matroid whose ML degree is computed in Example 3.1.23. The certificates proving the correctness of our results can be found at https://zenodo.org/record/7454826#.Y6DCdezMKdY.

We now briefly discuss some special matroids that appear in our lists, shown in Figure 3.2.

Example 3.1.16. The *Pappus matroid* was seen in Example 3.1.13. The *non-Fano matroid* has $k = 3$ and $m = 7$. It is projectively unique, so its stratum has dimension 0 and ML degree 1. The *affine geometry $AG(2, 3)$* has $k = 3$ and $m = 9$. It is also known as the dual Hessian configuration. Its stratum is 0-dimensional of degree 2. Hence, its ML degree is 2. The

(a) Pappus matroid   **(b)** Non Fano matroid   **(c)** $AG(2,3)$ **(d)** ML degree 0 matroid
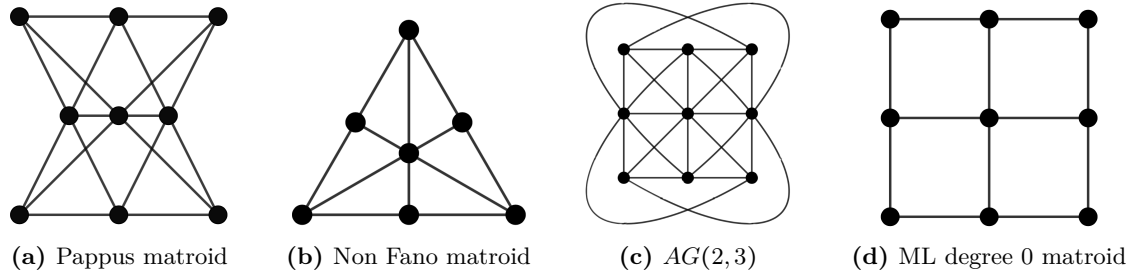
Figure 3.2. Geometric representations of the matroids discussed in Examples 3.1.13 and 3.1.16.

table for $k = 3, m = 9$ lists nine $\mathbb{C}$-realizable matroids with ML degree 0. The one with the fewest nonbases has 6 nonbases; its stratum is 4-dimensional and has degree 4. A geometric representation of this matroid has the form of 3×3 grid and is depicted in Figure 3.2d.

3.1.4. Points and lines in the plane

We now study the moduli space $X(3,m)$ of m labeled points in $\mathbb{P}^2$ in linearly general position. Cachazo, Umbert and Zhang [CUZ20] report that the ML degree of $X(3,m)$ equals 26 for $m = 6$, $1\,272$ for $m = 7$, and $188\,112$ for $m = 8$. These numbers are denoted $\mathcal{N}_m^{(3)}$ in [CUZ20]. Thomas Lam [ABF$^+$23, Appendix A] derived them using finite field methods, and he also computed

$$\mathcal{N}_9^{(3)} \; = \; \mathrm{MLdegree}(X(3,9)) \; = \; 74\,570\,400.$$

We present a topological proof of these results, and we prove the conjecture in [CUZ20, §6]. This involves a careful study of the stratified fibration (3.0.3). The combinatorics we develop along the way, such as posets of strata and Möbius functions, should be of independent interest.

The moduli space $X(3,m)$ is very affine of dimension $2m - 8$. Here is what we know about its Euler characteristic.

Theorem 3.1.17. *The ML degree of $X(3,m)$ is given by the following table for $m \le 9$:*

m	4	5	6	7	8	9
$\chi(X(3,m))$	1	2	26	$1\,272$	$188\,112$	$74\,570\,400$

These numbers are easy to prove for $m \le 6$. A computational proof for $m = 6$ appeared in [CEGM19, Appendix C]. The numbers for $m = 7, 8$ were derived with the soft limit argument in [CUZ20]. This was a proof in the sense of physics but perhaps not in the sense of mathematics. The verification by numerical computation was presented in [ST21, Proposition 5]. Thomas Lam had derived and proved all numbers, including the $m = 9$ case, using finite field methods, see [ABF$^+$23, Appendix A].

The aim of this subsection is to solve this problem for general m using the stratified fibration approach in Subsection 3.1.1. Our techniques will be of independent interest. In particular, they can be adapted to give a geometric proof for each of the ML degrees of matroids in Theorem 3.1.14. As a warm-up, here are geometric proofs for the first three numbers in Theorem 3.1.17.

Example 3.1.18 ($m = 4, 5, 6$)**.** The space $X(3,4)$ is just a point, hence $\chi(X(3,4)) = 1$. The very affine surface $X(3,5)$ is the complement of the arrangement $\mathcal{B}(3,4)$ in Example 3.1.5. We have $\chi(X(3,5)) = 2$, by Varchenko's Theorem, as there are two bounded regions on the right in Figure 3.1. For $m = 6$, we consider the deletion map $\pi_{3,6} : X(3,6) \to X(3,5)$. The discriminantal arrangement for any five points in $\mathbb{P}^2$, with no three on a line, is isomorphic to $\mathcal{B}(3,5)$. All fibers of $\pi_{3,6}$ are homotopy equivalent to the complement of $\mathcal{B}(3,5)$. Hence $\pi_{3,6}$ is a fibration, where each fiber has Euler characteristic 13, by Table 3.1. The base $X(3,5)$ has Euler characteristic 2. Hence their product 26 is the Euler characteristic of $X(3,6)$.

We now consider $m \geq 6$. Following Subsection 3.1.1, we study the stratification $\mathcal{S}_{3,m}$ of $X(3,m)$. The codimension one strata are all combinatorially equivalent: they are the loci of configurations $[P] = [P_1, \ldots, P_m]$ where three lines $\overline{P_iP_j}$, $\overline{P_kP_l}$, $\overline{P_rP_s}$ meet in a new point in $\mathbb{P}^2$. We write $S_{(ij)(kl)(rs)}$ for this stratum in $X(3,m)$. All other strata are intersections of those, hence they can be denoted by a collection of triples $(ij)(kl)(rs)$. For $m = 6$, there are 15 distinct codimension one strata $S_{(ij)(kl)(rs)}$, one for each tripartition of $\{1, \ldots, 6\}$. All other strata in $\mathcal{S}_{3,6}$ are obtained by intersecting these 15 divisors. We found that $\mathcal{S}_{3,6}$ has two combinatorially distinct codimension two strata, two codimension three strata and two codimension four strata. In Table 3.2 we list all strata explicitly, up to combinatorial equivalence. Figure 3.3 shows point configurations $[P_1, \ldots, P_6]$ for three among the seven strata in our list.

Type	Codim	Representatives for the divisors $(i,j)(k,l)(r,s)$ that intersect in the stratum
I	1	$(12)(34)(56)$
II	2	$(12)(34)(56),(12)(35)(46)$
III	2	$(12)(34)(56),(15)(23)(46),(14)(26)(35)$
IV	3	$(12)(34)(56),(15)(23)(46),(14)(26)(35),(15)(26)(34)$
V	3	$(12)(34)(56),(12)(35)(46),(13)(26)(45),(14)(25)(36),(15)(24)(36),(16)(23)(45)$
VI	4	$(12)(34)(56),(12)(35)(46),(14)(23)(56),(14)(26)(35),(15)(23)(46),(15)(26)(34)$
VII	4	$(12)(34)(56),(12)(35)(46),(13)(24)(56),(13)(26)(45),(14)(25)(36),$
		$(14)(26)(35),(15)(23)(46),(15)(24)(36),(16)(23)(45),(16)(25)(36)$

Table 3.2. All types of strata in the 4-dimensional very affine variety $X(3,6)$.
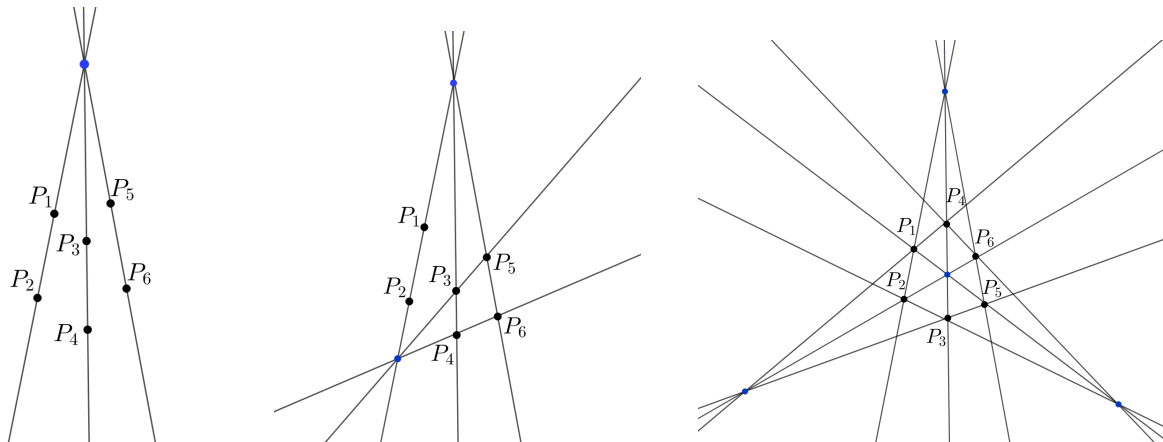
Figure 3.3. Geometric representation of the strata of Type I, II, and IV in Table 3.2

For our proof of Theorem 3.1.17, we shall use Lemma 3.1.2, here rewritten in the specific

form

$$\chi(X(3, m+1)) \;=\; \chi(X(3,m)) \cdot \chi(F_{X(3,m)}) - \sum_{S \in \mathcal{S}} \chi(S) \cdot \rho(S), \qquad (3.1.15)$$

where we define

$$\rho(S) \;:=\; \sum_{S' \in \mathcal{S}, S' \supseteq S} \mu(S, S') \cdot (\chi(F_{X(3,m)}) - \chi(F_{S'})). \qquad (3.1.16)$$

For a fixed stratum S, the sum in (3.1.16) is over all S' that contain S. These form a subposet $\mathcal{P}_S$ (actually, a filter) of the poset $\mathcal{S}_{3,m}$. It turns out that for many strata S, the factor $\rho(S)$ is zero. This drastically simplifies the computation. Let us illustrate this with an example.

Example 3.1.19. Consider the map $\pi_{3,6} : X(3,7) \to X(3,6)$. Figure 3.4 shows the subposets for the two codimension three strata, of type IV and V, together with the Möbius function values at each node. The poset is ranked by codimension: zero for the top stratum, and three for the bottom stratum. Our aim is to compute $\rho(S)$. Let us look at the left poset $\mathcal{P}_S$. The codimension zero stratum S' has $\chi(F_{S'}) = \chi(F_{X(3,6)})$ by definition. The codimension one strata have $\chi(F_{X(3,m)}) - \chi(F_{S'}) = 1$, by Example 3.1.3. Looking at the strata of codimension two, we find that those of type III have $\chi(F_{X(3,6)}) - \chi(F_{S'}) = 3$, whereas those of type II have $\chi(F_{X(3,6)}) - \chi(F_{S'}) = 2$. Finally, the stratum of type IV has $\chi(F_{X(3,6)}) - \chi(F_{S'}) = 4$. With this, one computes

$$\rho(S) \;=\; -2 \cdot 0 + 3 \cdot (1 \cdot 1) + 2 \cdot 1 + (-1) \cdot 3 + 3 \cdot (-1 \cdot 2) + 1 \cdot 4 = 0.$$
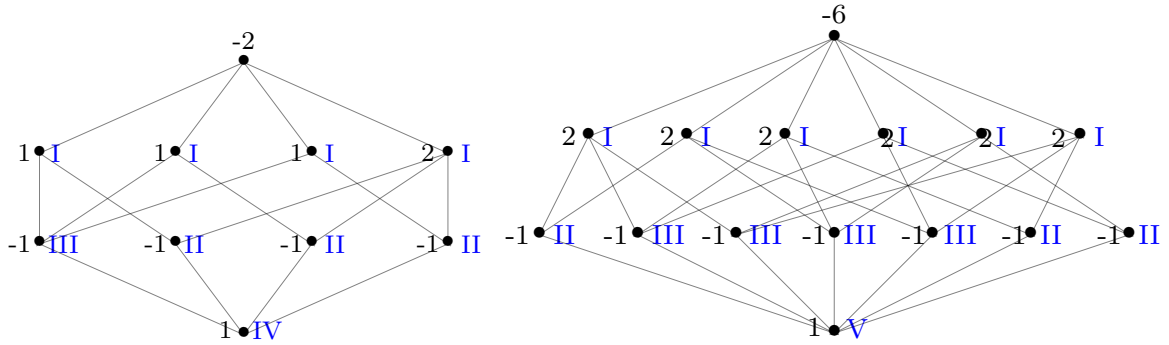
Figure 3.4. The posets $\mathcal{P}_S$ for the codimension three strata in $X(3,6)$. The numbers in black are the values of the Möbius function. The types of the strata are shown in blue.

This phenomenon generalizes to other strata and to all spaces $X(3,m)$. Indeed, the only strata $S \in \mathcal{S}_{3,m}$ for which $\rho(S) \neq 0$ are those whose lines meet in only one extra special point apart from the original ones. This is illustrated in [CUZ20, Figure 8]. More precisely, for each stratum S, let $[P] = [P_1, \ldots, P_m]$ be a general element in S, and for each $h \geq 3$ denote by $n_h(S)$ the number of points, apart from $P_1, \ldots, P_m$, where exactly h lines of the discriminantal arrangement $\mathcal{B}(P)$ meet. The following result proves the conjecture in [CUZ20, §6]:

Theorem 3.1.20. *Every stratum $S \in \mathcal{S}_{3,m}$ satisfies $\rho(S) \in \{-1, 0, +1\}$. More precisely:*

(a) *If $n_h(S) = 1$ for some h and $n_i(S) = 0$ for all $i \neq h$, then $\rho(S) = (-1)^{h-1}$.*

(b) *In all other cases, we have $\rho(S) = 0$.*

Item (b) is the punchline: a stratum S does not contribute to the Euler characteristic unless it looks like [CUZ20, Figure 8]. To prove this, we introduce some further notation. For any stratum $S \in \mathcal{S}_{3,m}$ let $\sigma(S) := \chi(F_{X(3,m)}) - \chi(F_S)$. When the discriminantal arrangement in the fiber F_S over S is realizable over $\mathbb{R}$, this denotes the difference between the numbers of bounded regions in $\mathcal{B}(3,m)$ and in F_S. Applying the Möbius inversion formula to (3.1.16) yields

$$\sigma(S) \;=\; \rho(S) \;+\; \sum_{S' \in \mathcal{P}_S \smallsetminus \{S\}} \rho(S'). \tag{3.1.17}$$

We start by computing the function $\sigma(S)$ in terms of the counting function $n_h(S)$:

Lemma 3.1.21. *Every stratum $S \in \mathcal{S}_{3,m}$ satisfies $\sigma(S) = \sum_{h=3}^{\infty} \binom{h-1}{2} \cdot n_h(S)$.*

Proof. Let $\mathcal{B}$ be the discriminantal arrangement associated to the fiber F_S. Let $\mathcal{B}(3,m)$ be as in Subsection 3.1.2. Its characteristic polynomial is $\chi_{\mathcal{B}(3,m)} = t^2 - \left(\binom{m}{2} - 1\right)t + b_2(\mathcal{B}(3,m))$ where $b_2(\mathcal{B}(3,m))$ is the second Betti number of $\mathcal{B}(3,m)$. Using (3.1.10), the characteristic polynomial of the special arrangement $\mathcal{B}$ equals

$$\chi_{\mathcal{B}}(t) \;=\; t^2 - \left(\binom{m}{2} - 1\right)t + b_2(\mathcal{B}(3,m)) - \sum_{h=3}^{\infty} n_h(S)\binom{h}{2} + \sum_{h=3}^{\infty} n_h(S)(h-1),$$

since every additional intersection point of h lines in $\mathcal{B}$ removes $\binom{h}{2}$ many generic codimension two elements of $L(\mathcal{B}(3,m))$ and adds a summand with Möbius value $h-1$. Evaluating these two polynomials at $t = 1$ and taking their difference yields the claim. ∎

We now show that σ is monotonic with respect to the poset $\mathcal{S}$ in the following sense.

Lemma 3.1.22. *Let $S', S \in \mathcal{S}_{3,m}$ be two strata such that $S' \supsetneqq S$. Then $\sigma(S') < \sigma(S)$.*

Proof. The assertion is equivalent to $\chi(F_{S'}) = \chi_{\mathcal{B}_{S'}}(1) > \chi(F_S) = \chi_{\mathcal{B}_S}(1)$ where $\mathcal{B}_S$ and $\mathcal{B}_{S'}$ are the discriminantal arrangements corresponding to the fibers F_S and $F_{S'}$, respectively. Since each arrangement has the same number of lines, it suffices to prove $b_2(\mathcal{B}_{S'}) > b_2(\mathcal{B}_S)$.

We will establish a general statement, namely a strict inequality between the Betti numbers of two arrangements where one is a strict weak image of the other in the sense of matroid theory. Let $\mathcal{A} = \{H_1, \ldots, H_n\}$ and $\mathcal{A}' = \{H'_1, \ldots, H'_n\}$ be two affine arrangements of lines in $\mathbb{C}^2$ with $n \geq 3$. We claim that $b_2(\mathcal{A}) < b_2(\mathcal{A}')$ holds under the following two assumptions:

  (i) If for $I \subseteq [n]$ the lines $\{H'_i\}_{i \in I}$ meet in $\mathcal{A}'$ then the lines $\{H_i\}_{i \in I}$ also meet in $\mathcal{A}$,

  (ii) The lines H_1, H_2, H_3 intersect but the lines H'_1, H'_2, H'_3 do not intersect.

We prove this claim by induction on n. If $n = 3$ then the statement is trivial since (ii) forces $\mathcal{A}'$ to consist of three generic lines and $\mathcal{A}$ of three concurrent lines, so $b_2(\mathcal{A}) = 2 < 3 = b_2(\mathcal{A}')$.

Now fix some $n > 3$. The deletion–restriction relation for the characteristic polynomial (cf. [OT13, Corollary 2.57]) implies $b_2(\mathcal{A}) = b_2(\mathcal{A} \smallsetminus \{H_n\}) + |\mathcal{A}^{H_n}|$ where $\mathcal{A}^{H_n}$ is the restriction of $\mathcal{A}$ to H_n. The analogous relation holds for $\mathcal{A}'$. Since removing the last hyperplane preserves both assumptions (i) and (ii), we have $b_2(\mathcal{A} \smallsetminus \{H_n\}) < b_2(\mathcal{A}' \smallsetminus \{H'_n\})$ by induction. Moreover, assumption (i) implies $|\mathcal{A}^{H_n}| \leq |\mathcal{A}'^{H'_n}|$. So in total this proves $b_2(\mathcal{A}) < b_2(\mathcal{A}')$. ∎

Proof of Theorem 3.1.20. Note that $\rho(X(3,m)) = 0$ by definition. Let S be a stratum with the property that $n_h(S) = 1$ and all other are zero. Observe that the only $S' \subsetneqq X(3,m)$ strictly containing S are the $\binom{h}{j}$ strata S' with $n_j(S') = 1$ and all others zero for $j = 3, \ldots h-1$.

If $h = 3$ then S is a codimension one stratum and is only strictly contained in $X(3, m)$, so Lemma 3.1.21 and formula (3.1.17) show that $\rho(S) = 1$. We now rewrite (3.1.17) via Lemma 3.1.21 as

$$\binom{h-1}{2} = \rho(S) + \binom{h}{3} - \binom{h}{4} + \ldots + (-1)^h \binom{h}{h-1}$$

by induction on h. This shows that $\rho(S) = (-1)^{h-1}$.

We prove part (b) by induction on $\sigma(S)$. The base case $\sigma(S) = 0$ corresponds to the stratum $X(3, m)$, for which we know already that $\rho(S) = 0$. For the induction step, let $S \in \mathcal{S}_{3,m}$ be another stratum that is not one of those considered in part (a). For all strata $S' \in \mathcal{P}_S \smallsetminus \{S\}$ we have $\sigma(S') < \sigma(S)$ by Lemma 3.1.22. The induction hypothesis shows that $\rho(S') = 0$ for all strata that are not of the type of part (a). Thus, we have

$$\sigma(S) = \sum_{h=3}^{\infty} \binom{h-1}{2} \cdot n_h(S) = \rho(S) + \sum_{h=3}^{\infty} N_h(S) \cdot (-1)^{h-1},$$

where $N_h(S)$ is the number of strata $S' \in \mathcal{P}_S \smallsetminus \{S\}$ like those in part (a). This number is given directly by $N_h(S) = \sum_{k=3}^{\infty} n_k(S) \cdot \binom{k}{h}$. We conclude that

$$\sum_{h=3}^{\infty} \binom{h-1}{2} \cdot n_h(S) = \rho(S) + \sum_{k=3}^{\infty} n_k(S) \cdot \sum_{h=3}^{\infty} (-1)^{h-1} \binom{k}{h} = \rho(S) + \sum_{k=3}^{\infty} n_k(S) \cdot \binom{k-1}{2}.$$

This implies $\rho(S) = 0$ for all strata S other than those in case (a).   ∎

Equipped with Theorem 3.1.20, we can prove Theorem 3.1.17 with few calculations.

Proof of Theorem 3.1.17. We want to use the formula (3.1.15). By Theorem 3.1.20, we need to consider only those strata $S \in \mathcal{S}_{3,m}$ where $n_h(S) = 1$ for a certain h and $n_i(S) = 0$ for all $i \neq h$. The number of these strata in $X(3, m)$ is $\frac{1}{h!}\binom{m}{2} \cdot \binom{m-2}{2} \ldots \binom{m-2h+2}{2}$. Furthermore, all these strata are combinatorially equivalent, so we write $\chi(3, m; h)$ for the Euler characteristic of any of them. Using Theorem 3.1.20, we rewrite the formula (3.1.15) as follows:

$$\chi(X(3, m+1)) = \chi(X(3, m)) \cdot \chi(F_{X(3,m)}) + \sum_{h=3}^{\infty} \frac{(-1)^h}{h!} \binom{m}{2} \cdot \binom{m-2}{2} \cdots \binom{m-2h+2}{2} \cdot \chi(3, m; h).$$

In particular, when $m = 6, 7$ the formula becomes

$$\chi(X(3, 7)) = \chi(X(3, 6)) \cdot \chi(F_{X(3,6)}) - 15 \cdot \chi(3, 6; 3),$$
$$\chi(X(3, 8)) = \chi(X(3, 7)) \cdot \chi(F_{X(3,7)}) - 105 \cdot \chi(3, 7; 3).$$

The Euler characteristic $\chi(X(3, 6)) = 26$ is obtained in Example 3.1.3, whereas the bounded chamber counts $\chi(F_{X(3,6)}) = 42$ and $\chi(F_{X(3,7)}) = 101$ are taken from Table 3.1. To compute $\chi(3, m; 3)$, we note that the corresponding stratum in $X(3, m)$ is isomorphic to a matroid stratum of codimension 3 in $X(3, m+1)$, obtained by requiring that the new point P_{m+1} lies on the three special lines. Those matroid strata have Euler characteristic $\chi(3, 6; 3) = -12$ for $m = 6$ and $\chi(3, 7; 3) = -568$. This is proved either geometrically, or by computer algebra. Note that these strata are identified uniquely in Theorem 3.1.14, namely for $m = 6$ under $3_5[\ldots, 12]$, and for $m = 7$ under $5_7[\ldots, 568]$. In conclusion, we can write $\chi(X(3, 7)) = 26 \cdot 42 + 15 \cdot 12 = 1\,272$ and

$$\chi(X(3, 8)) = 1\,272 \cdot 101 + 105 \cdot 568 = 188\,112.$$

If instead $m = 8$ the formula becomes

$$\chi(X(3,9)) = \chi(X(3,8)) \cdot \chi(F_{X(3,8)}) - 420 \cdot \chi(3,8;3) + 105 \cdot \chi(3,8;4).$$

Table 3.1 shows that $\chi(F_{X(3,8)}) = 205$. The numbers $\chi(3,8;3) = -81\,040$ and $\chi(3,8;4) = 18\,768$ can be computed using `HomotopyContinuation.jl` [BT18] as the ML degrees of the corresponding strata. Note that $18\,768$ appears in Theorem 3.1.14 as the ML degree of the rank 3 matroid on 9 elements corresponding to four lines meeting in a point. The number $81\,040$ does not appear in this theorem. However, $81\,040 = 99\,808 - 18\,768$ where $99\,808$ is the ML degree of the matroid on 9 elements where three lines meet in a point. Thus, the contribution above stems from this matroid strata where one needs to remove the locus of four concurrent lines. In conclusion, we have

$$\chi(X(3,9)) \;=\; 188\,112 \cdot 205 + 420 \cdot 81\,040 + 105 \cdot 18\,768 \;=\; 74\,570\,400.$$

∎

As a proof of concept, we show how this story extends to nonuniform matroids.

Example 3.1.23. Let M be the matroid of rank 3 on 9 elements with one nonbasis 789. The map $X(M) \to X(3,8)$ which forgets the ninth point is a surjection. The generic fiber is no longer the complement of $\mathcal{B}(3,8)$, but rather its restriction to the line $\overline{P_7 P_8}$. That restricted arrangement has 15 bounded regions. The nongeneric fiber over $S_{(ij)(kl)(rs)}$ has 14 bounded regions provided $(78) \in \{(ij), (kl), (rs)\}$, and 15 otherwise. There are 45 strata of the form $S_{(ij)(kl)(78)}$. Similarly, the fiber over a stratum of four concurrent lines has 13 bounded regions provided $\overline{P_7 P_8}$ is one of those lines. There are 15 such codimension 2 strata. This gives

$$\chi(X(M)) \;=\; 188\,112 \cdot 15 + 45 \cdot 81\,040 + 15 \cdot 18768 \;=\; 6\,750\,000,$$

as a decomposition of $6\,750\,000$, verifying the entry $9_1[6750000_1]$ in Theorem 3.1.14.

3.1.5. Eight points in 3-space

We now turn to configurations in $\mathbb{P}^3$. For $k = 4$ and $m \le 7$, we can apply Grassmann duality, which shows that $X(4,m) = X(m-4,m)$. Hence the ML degrees for few points in $\mathbb{P}^3$ are

$$|\chi(X(4,6))| = |\chi(X(2,6))| = 6 \quad \text{and} \quad \chi(X(4,7)) = \chi(X(3,7)) = 1\,272.$$

This subsection is devoted to the 9-dimensional very affine variety $X(4,8)$. Here is our result:

Theorem* 3.1.24. *The Euler characteristic of $X(4,8)$ equals $-5\,211\,816$.*

The number $5\,211\,816$ is new. Unlike the ML degrees in Theorem 3.1.17, it did not yet appear in the physics literature. Also, Lam's finite field method [ABF+23, Appendix A] did not yield this number. Thus far, the $(4,8)$ case was out of reach for all available techniques, in spite of the progress in [CUZ20, §6]. Our result proves the conjecture stated tacitly in [CUZ20, Table 2].

Our derivation of Theorem* 3.1.24 rests on numerical computations with the software `HomotopyContinuation.jl` [BT18]. However, the methodology is closely related to the topological approach seen in previous subsections. We exploit a specific likelihood degeneration, i.e., the soft limits [CUZ20], to analyze $X(4,8)$ in a similar way to Lemma 3.1.2

We start by describing our computational setup. For each quadruple (i, j, k, ℓ), where $1 \le i < j < k < \ell \le 8$, let $p_{ijk\ell}$ be the determinant of the corresponding 4×4 submatrix of

$$M_{4,8} = \begin{bmatrix} 0 & 0 & 0 & 1 & 1 & 1 & 1 & 1 \\ 0 & 0 & -1 & 0 & 1 & x_1 & x_2 & x_3 \\ 0 & 1 & 0 & 0 & 1 & y_1 & y_2 & y_3 \\ -1 & 0 & 0 & 0 & 1 & z_1 & z_2 & z_3 \end{bmatrix}. \tag{3.1.18}$$

Let $\mathcal{I}$ be the set of all such quadruples with $k \ge 4$ and $\ell \ge 6$. We write (x, y, z) for the nine variables appearing in (3.1.18). Note that $X(4, 8)$ is the complement of the union of hypersurfaces $\mathcal{H} = \bigcup_{(i,j,k,\ell) \in \mathcal{I}} V(p_{ijk\ell}) \subset \mathbb{C}^9$. This is a very affine variety in $(\mathbb{C}^*)^{62}$ with parametrization $\mathbb{C}^9 \smallsetminus \mathcal{H} \to (\mathbb{C}^*)^{62}$ given by $(x, y, z) \mapsto (p_{ijk\ell}(x, y, z))_{(i,j,k,\ell) \in \mathcal{I}}$. By [Huh13, Theorem 1], the quantity $|\chi(X(4, 8))|$ is the number of critical points of the log-likelihood function

$$\mathcal{L}_{4,8}(x, y, z) = \sum_{(i,j,k,\ell) \in \mathcal{I}} u_{ijk\ell} \cdot \log(p_{ijk\ell}(x, y, z)).$$

Here we count critical points in $\mathbb{C}^9 \backslash \mathcal{H}$, for generic data $u_{ijk\ell} \in \mathbb{C}$. In other words, we seek the number of solutions to the following system of 9 rational function equations in 9 unknowns:

$$\frac{\partial \mathcal{L}_{4,8}}{\partial x_i} = \frac{\partial \mathcal{L}_{4,8}}{\partial y_i} = \frac{\partial \mathcal{L}_{4,8}}{\partial z_i} = 0 \qquad \text{for} \quad i = 1, 2, 3. \tag{3.1.19}$$

In particle physics, these are the *scattering equations* for $X(4, 8)$ in the CEGM model [CEGM19]. The projection of the likelihood correspondence [HS14, vdVS22] to the space of data is a branched covering of degree $|\chi(X(4, 8))|$. For generic complex numbers $u_{ijk\ell}$, the fiber can be computed using the command `monodromy_solve` in `HomotopyContinuation.jl`, as explained in [ST21, §3]. In principle, we can use the `certify` command [BRT20] to give a proof of the inequality

$$|\chi(X(4, 8))| \ge 5\,211\,816.$$

In practice, we missed 218 solutions. In our run, the method quickly certified that $5\,211\,598$ paths correspond to distinct true solutions, giving a proof that $|\chi(X(4, 8))| \ge 5\,211\,598$.

The main idea in this subsection is to follow up this brute force monodromy computation by a likelihood degeneration of (3.1.19) to study $X(4, 8)$ in a more structured way. In particular, the degeneration will help us to decompose the number $|\chi(X(4, 8))|$ into positive summands, much like what we did in the Subsection 3.1.4. We keep assuming that the data $u_{ijk\ell}$ are generic.

We introduce a parameter t into the log-likelihood function $\mathcal{L}_{4,8}$ by setting

$$\tilde{\mathcal{L}}_{4,8}(x, y, z, t) = \sum_{\substack{(i,j,k,\ell) \in \mathcal{I} \\ \ell < 8}} u_{ijk\ell} \cdot \log(p_{ijk\ell}(x, y, z)) + \sum_{(i,j,k,8) \in \mathcal{I}} u_{ijk8} \cdot t \cdot \log(p_{ijk8}(x, y, z)). \tag{3.1.20}$$

The limit for $t \to 0$ is the soft limit in [CUZ20]. Taking partial derivatives, we obtain rational function equations in the unknowns x, y, z with coefficients in the rational function field $\mathbb{C}(t)$:

$$\frac{\partial \tilde{\mathcal{L}}_{4,8}(x, y, z; t)}{\partial x_i} = \frac{\partial \tilde{\mathcal{L}}_{4,8}(x, y, z; t)}{\partial y_i} = \frac{\partial \tilde{\mathcal{L}}_{4,8}(x, y, z; t)}{\partial z_i} = 0 \quad \text{for} \quad i = 1, 2, 3. \tag{3.1.21}$$

There are $|\chi(X(4, 8))|$ solutions $(\hat{x}(t), \hat{y}(t), \hat{z}(t))$ over the field of Puiseux series $K = \mathbb{C}\{\{t\}\}$. We are interested in computing the valuations of the Plücker coordinates for these solutions. In other words, suppose we knew these solutions, and suppose we were to substitute them

into the 4×8 matrix (3.1.18). Each of its 4×4 minors is then a Puiseux series $\hat{p}_\bullet(t)$, and we could consider the lowest order exponent of that series. This is the t-adic valuation of $\hat{p}_\bullet = \hat{p}_\bullet(t)$, denoted $\mathrm{val}_t(\hat{p}_\bullet)$. The result of this process would be the tropical Plücker vector

$$\hat{q} = \left(\mathrm{val}_t\left(p_{ijk\ell}(\hat{x}(t), \hat{y}(t), \hat{z}(t)) \right) \right)_{1 \le i < j < k < \ell \le 8} \in \mathbb{Q}^{70}. \tag{3.1.22}$$

Recall from (3.1.1) that $X(4,8)$ is the quotient of $\mathrm{Gr}(4,8)^\circ$ by the action of the torus $(K^\star)^8$. On the tropical side, where the vector $\hat{q}$ lives, this corresponds to an additive action of $\mathbb{R}^8$ on $\mathbb{R}^{70}$. We take the quotient of this additive action by setting to 0 the eight coordinates not in $\mathcal{I}$. Thus our choice of 62 coordinates is compatible with tropicalization [MS21a], and we get $\mathrm{trop}(X(4,8))$ as a 9-dimensional pointed fan in $\mathbb{R}^{62}$, with coordinates indexed by $\mathcal{I}$.

Now, here is the punchline: we cannot compute solutions over K, and we have no access to the Puiseux series in the argument of val_t in (3.1.22). Instead, we carry out floating point computations over $\mathbb{R}$. This will give us enough information to identify the coordinates of $\hat{q}$. Indeed, from the point of view of complex geometry, the equations (3.1.21) define an affine curve

$$C \subset X(4,8) \times \mathbb{C} \subset (\mathbb{C}^\star)^{62} \times \mathbb{C},$$

where the second factor is the line with coordinate t. The vectors $\hat{q}$ in (3.1.22), which will be called *tropical critical points* in Subsection 3.1.6, span the rays in the partial tropical curve

$$\mathrm{trop}(C) \subset \mathrm{trop}(X(4,8)) \times \mathbb{R}_{\ge 0} \subset \mathbb{R}^{62} \times \mathbb{R}_{\ge 0}.$$

The solution $\hat{q} = 0$ represents classical solutions $(x(t), y(t), z(t))$ which, in the soft limit $t \to 0$, converge in $X(4,8)$. The corresponding ray in $\mathrm{trop}(C)$ is $\rho_0 = \mathbb{R}_{\ge 0} \cdot (0, \dots, 0, 1)$.

Proposition 3.1.25. *The ray $\rho_0 = \mathbb{R}_{\ge 0} \cdot (0, \dots, 0, 1)$ has multiplicity $2\,363\,376$ in $\mathrm{trop}(C)$.*

Proof. The multiplicity of ρ_0 is the number of classical solutions converging in $X(4,8)$ for $t \to 0$. In this limit, the equations for $i = 1, 2$ in (3.1.21) are the likelihood equations for $X(4,7)$. Plugging any solution of these equations into those for $i = 3$, we find, up to division by t, the likelihood equations for the complement in $\mathbb{C}^3$ of the discriminantal arrangement $\mathcal{B}(4,7)$. The ML degree of that arrangement complement is $1\,858$, as seen in Table 3.1. This gives the formula $\chi(X(4,7)) \cdot |\chi(\mathbb{C}^3 \smallsetminus \mathcal{B}(4,8))| = 1\,272 \cdot 1\,858$ for the multiplicity of ρ_0. ∎

The number $2\,363\,376$ is the number of *regular solutions* in [CUZ20]. In the spirit of Subsections 3.1.1 and 3.1.4, it is the contribution to $\chi(X(4,8))$ coming from the dense stratum in $X(4,7)$. The nonzero tropical critical points $\hat{q}$ correspond to the *singular solutions* in [CUZ20]. For $t \to 0$, these curves move to the boundary of $X(4,8)$. The following result verifies a conjecture in [CUZ20].

Theorem* 3.1.26. *There are $3\,150$ distinct nonzero tropical critical points $\hat{q}$. All of them are given by $\{0,1\}$-vectors in $\mathbb{R}^{70}$ and they come in 7 combinatorial types, summarized in Table 3.3.*

We here assume that the $u_{ijk\ell}$ are generic complex numbers. The result is derived by computations with `HomotopyContinuation.jl`. The t-adic order of each numerical solution was found using Algorithm 1. The nonzero tropical critical points $\hat{q}$ span the rays in $\mathrm{trop}(C)$, other than ρ_0, whose generator has a positive last coordinate. The ML degree equals

$$|\chi(X(4,8))| = 2\,363\,376 + A_\mathrm{I} \cdot B_\mathrm{I} + A_\mathrm{II} \cdot B_\mathrm{II} + \cdots + A_\mathrm{VII} \cdot B_\mathrm{VII}, \tag{3.1.23}$$

Type	representative $((i,j,k,\ell)$ for which $\mathrm{val}_t(p_{ijk\ell}) = 1)$	# configurations
I	(1,4,7,8),(2,5,7,8),(3,6,7,8)	105
II	(1,2,3,8),(3,4,5,8),(5,6,1,8),(2,4,6,8)	210
III	(1,2,3,8),(3,4,5,8),(5,6,7,8),(2,4,6,8)	1260
IV	(1,4,7,8),(2,5,7,8),(3,6,7,8),(1,2,3,8),(4,5,6,8)	420
V	(1,2,3,8),(1,4,5,8),(1,6,7,8),(2,4,6,8),(2,5,7,8)	630
VI	(1,2,3,8),(1,4,5,8),(1,6,7,8),(2,4,6,8),(2,5,7,8),(3,4,7,8)	210
VII	(1,2,3,8),(1,2,4,8),(1,2,5,8),(1,2,6,8),(1,2,7,8),(3,4,5,8),(3,6,7,8)	315

Table 3.3. Combinatorial types contributing singular solutions to (3.1.21). The second column shows a representative for each type indicating which Plücker coordinates have valuation 1. The third column shows the cardinality of the orbit of the action of S_7 on the first 7 indices.

where $A_{\mathrm{I}} = 105$ is the number of configurations of type I, B_{I} is the multiplicity of each A_{I} ray in $\mathrm{trop}(C)$, and likewise for the other types. In other words, B_{I} is the number of Puiseux series solutions to (3.1.21) whose t-adic valuation is the representative of type I in Table 3.3.

We use numerical computation to obtain the multiplicities $B_{\mathrm{I}}, \ldots, B_{\mathrm{VII}}$. This is done without any prior knowledge about $\mathrm{trop}(X(4,8))$ or the fibration $\pi_{4,8}$. Approximate solutions of (3.1.19) are tracked numerically along the soft limit degeneration to learn the tropical critical points (3.1.22). We explain the details of this computation in a more general context in Subsection 3.1.7.

We filter the obtained list of candidate critical points by recording the regression error in (3.1.34) and by checking that the solutions come in S_7-orbits. This gives a total of $3\,151$ successfully found vectors $\hat{q}$ in $\mathbb{Q}^{70}$. One of them is $0 \in \mathbb{R}^{70}$. This establishes Theorem* 3.1.26. To learn the multiplicities $B_{\bullet}$ in (3.1.23), we record, for each tropical solution $\hat{q}$ of type $\bullet$, the number of classical solutions that were found to have valuation $\hat{q}$. The multiplicities are

$$B_{\mathrm{I}} = 5\,680, \quad B_{\mathrm{II}} = 1\,704, \quad B_{\mathrm{III}} = 988, \quad B_{\mathrm{IV}} = 832,$$
$$B_{\mathrm{V}} = 308, \quad B_{\mathrm{VI}} = 240, \quad B_{\mathrm{VII}} = 72. \tag{3.1.24}$$

Plugging these values into (3.1.23) leads to Theorem* 3.1.24. Additional strong support arises from the fact that the number $5\,211\,816$ is also the number of approximate solutions found in a stand-alone run of `monodromy_solve`, although not all of them could be certified via [BRT20].

Remark 3.1.27. The decomposition (3.1.23) is strongly related to the sum in Lemma 3.1.2. For instance, the formula $\chi(X(3,7)) = 26 \cdot 42 + 15 \cdot 12$ from the proof of Theorem 3.1.17 partitions the $1\,272$ critical points of the log-likelihood function into $1\,092$ solutions that converge in $X(3,7)$ and 180 solutions that move to the boundary in the soft limit. These boundary solutions escape from the open variety $X(3,7)$ in 15 groups of 12. Here $A_{\mathrm{I}} = 15$ is a combinatorial number, and $B_{\mathrm{I}} = 12$ is the ML degree of a stratum in $X(3,6)$. This is isomorphic to the codimension 3 matroid stratum in $X(3,7)$ with ML degree 12 in Theorem 3.1.14. A similar interpretation holds for $X(3,8)$ and $X(3,9)$. In the case of $X(4,8)$, however, not all ray multiplicities $B_{\bullet}$ are equal to the ML degree of a corresponding stratum in $X(4,7)$. A notable difference to the $k = 3$ case is that the matroid stratum of type I, seen for $k = 4, m = 8$ in Table 3.3, differs in dimension from its corresponding stratum in $X(4,7)$.

3.1.6. Statistical models and their tropicalization

We consider maximum likelihood estimation (MLE) for discrete statistical models [HS14, PS05]. Our conventions and notation will be as in [ST21]. The given model is a d-dimensional subvariety X of the projective space $\mathbb{P}^n$, which is assumed to intersect the simplex $\Delta_n \subset \mathbb{RP}^n$ of positive points. We seek to compute the critical points on X of the log-likelihood function

$$\mathcal{L}_u = u_0 \cdot \log(p_0) + u_1 \cdot \log(p_1) + \cdots + u_n \cdot \log(p_n) - (u_0 + u_1 + \cdots + u_n) \cdot \log(p_0 + p_1 + \cdots + p_n).$$

For any positive constants $u_0, u_1, \ldots, u_n$, representing data in statistics, this is a well-defined function on Δ_n. The aim of likelihood inference is to maximize $\mathcal{L}_u$ over all points p in the model $X \cap \Delta_n$. The number of all complex critical points, for generic u, is the ML degree of the model X. If X is smooth then this equals the signed Euler characteristic of the open variety X°, which is the complement of the divisor in X defined by $p_0 p_1 \cdots p_n (\sum_{i=0}^n p_i) = 0$.

Likelihood degenerations were first introduced in the setting of algebraic statistics by Gross and Rodriguez in [GR14], who studied the behavior of the MLE when some of the u_i approach zero. They distinguish between model zeros, structural zeros and sampling zeros. These statistical concepts can serve as a guide for interpreting likelihood degenerations.

We draw samples independently from some unknown distribution that is in $X \cap \Delta_n$. The probabilities in the following definitions refer to that sampling distribution. The data are summarized in a vector $u \in \mathbb{N}^{n+1}$, where u_i denotes the number of observations found to be in state i. Suppose that state i was never observed in our sample. The entry $u_i = 0$ is called:

- a *structural zero* if the probability of it being zero is equal to one;
- a *sampling zero* if the probability of it being zero is less than one;
- a *model zero* if the maximizer of $\mathcal{L}_u$ over $X \cap \Delta_n$ is a critical point of the restriction of $\mathcal{L}_u$ to the hyperplane section $X \cap \{p_i = 0\}$.

Structural zeros may mean that the wrong model was chosen, so we exclude this possibility. What remains is a consideration of sampling zeros and model zeros. These statistical concepts led Huh and Sturmfels to propose the following formula in [HS14, Conjecture 3.19]:

$$\mathrm{MLdegree}(X) = \mathrm{MLdegree}(X \cap \{p_j = 0\}) + \mathrm{MLdegree}(X|_{u_j=0}). \tag{3.1.25}$$

The last summand counts critical points of $\mathcal{L}_u$ on X when $u_j = 0$ and the other u_i are generic. The identity (3.1.25) holds under suitable smoothness and transversality assumptions. They ensure that the ML degrees are signed Euler characteristics of very affine varieties, obtained by removing the arrangement $\mathcal{H} = \{p_0 p_1 \cdots p_n (\sum_{i=0}^n p_i) = 0\}$ of $n + 2$ hyperplanes from $\mathbb{P}^n$. For the last summand we remove only $n + 1$ hyperplanes. The Euler characteristic is additive relative to the additional hyperplane $\{p_j = 0\}$. The sum becomes a minus for the signed Euler characteristic, as the dimensions differ by one, so the identity (3.1.25) follows.

Familiar combinatorics arises when X is a linear space. In this case, X° is the complement of $n + 1$ hyperplanes in affine d-space. The number of bounded regions can be computed by deletion-restriction. This is precisely the formula in (3.1.25). Moreover, all critical points are real, and there is one critical point per bounded region. An example from [ST21] is the space $X = X(2, m)$ of m points on the line $\mathbb{P}^1$, modulo projective transformations. Here $d = m - 3$, $n = m(m - 3)/2$, and the ML degree equals $(m - 3)!$. Formula (3.1.25) is essentially that for soft limits in [CEGM19, CUZ20]. We count solutions in (3.1.25) as singular solutions plus regular solutions.

In this subsection, we consider a vast generalization of soft limits, namely *tropical degenerations*. We examine MLE for discrete statistical models through the lens of tropical

geometry. In what follows, the real numbers $\mathbb{R}$ are replaced by the real Puiseux series $R = \mathbb{R}\{\{t\}\}$. This is a real closed field, and it comes with the t-adic valuation. The uniformizer t is positive and infinitesimal. A scalar u in R can be viewed as the germ of a function $u(t)$ near $t \to 0$.

We are now given $u_0, \ldots, u_n \in R$, with valuations $w_i = \text{val}_t(u_i)$. We call $w = (w_0, \ldots, w_n)$ the *tropical data vector*. Each critical point $\hat{p}$ of $\mathcal{L}_u$ has its coordinates $\hat{p}_i$ in the algebraic closure $K = \mathbb{C}\{\{t\}\}$ of R. We set $\hat{q}_i = \text{val}_t(\hat{p}_i)$, and we refer to $\hat{q} = (\hat{q}_0, \ldots, \hat{q}_n)$ as a *tropical critical point*. Given any model X, we would like to describe the multivalued map that takes any tropical data vector w to the set of its tropical critical points $\hat{q}$.

The following theorem accomplishes this goal for the class of linear models [PS05, §1.2]. We augment the homogeneous linear forms defining X by the equation $p_0 + p_1 + \cdots + p_n = 1$, and we identify X with the resulting d-dimensional affine-linear subspace in $\mathbb{R}^{n+1}$. We write $X^\perp$ for the linear subspace of $\mathbb{R}^{n+1}$ that consists of all vectors perpendicular to X, with respect to the usual dot product. Thus $X^\perp$ is a vector space of dimension $n - d + 1$ in $\mathbb{R}^{n+1}$.

The tropical affine space $\text{trop}(X)$ is a pointed cone of dimension d in $\mathbb{R}^{n+1}$. Combinatorially, this is the Bergman fan [MS21a, §4.2] of the rank $d + 1$ matroid on $n + 2$ elements defined by X. Here the matroid is associated with the hyperplane arrangement $X \backslash X^\circ$. The tropical linear space $\text{trop}(X^\perp)$ has dimension $n - d + 1$. It is a fan with 1-dimensional lineality space spanned by $(1, 1, \ldots, 1)$. Combinatorially, it is the Bergman fan of the rank $n - d + 1$ matroid on $n + 1$ elements defined by $X^\perp$. Here the matroid of $X^\perp$ is the dual of a one-element contraction of the matroid of X. The contracted element corresponds to the hyperplane at infinity, namely $\{p_0 + p_1 + \cdots + p_n = 0\}$. It is very important to distinguish this element.

Theorem 3.1.28. *If the tropical data vector w is sufficiently generic then there are exactly* $\text{MLdegree}(X)$ *many distinct tropical critical points. They are given by the intersection*

$$\hat{q} \in \text{trop}(X) \cap (w - \text{trop}(X^\perp)). \tag{3.1.26}$$

We call the subspace X *general* if both of the above matroids are uniform. In that case we have $\text{MLdegree}(X) = \binom{n}{d}$; see [ST21, Example 4]. The matroid of X is the uniform matroid $U_{d+1,n+2}$, and the matroid of $X^\perp$ is the uniform matroid $U_{n-d+1,n+1}$. We abbreviate $e_{n+1} = -e_0 - e_1 - \cdots - e_n$, the negated sum of all unit vectors in $\mathbb{R}^{n+1}$. The tropical affine space $\text{trop}(X)$ is the union of all $\binom{n+2}{d}$ cones $\text{pos}(e_i : i \in I)$ where I runs over d-element subsets of $\{0, 1, \ldots, n, n+1\}$. The tropical linear space $\text{trop}(X^\perp)$ is the union of all $\binom{n+1}{n-d}$ cones $\mathbb{R}e_{n+1} + \text{pos}(e_j : j \in J)$, where J runs over $(n-d)$-element subsets of $\{0, 1, \ldots, n\}$. Let $w \in \mathbb{R}^{n+1}$ and suppose w_0 is its smallest coordinate. Then $w + w_0 e_{n+1}$ is a nonnegative vector with first coordinate 0. Replacing w by $w + w_0 e_{n+1}$ does not change tropical critical points.

Corollary 3.1.29. *If X is general then (3.1.26) consists of the $\binom{n}{d}$ points $\hat{q} = \sum_{i \in I}(w_i - w_0)e_i$, where I runs over all d-element subsets of $\{1, 2, \ldots, n\}$. These are the tropical critical points.*

Proof. By construction, the vector $\hat{q}$ lies in $\text{trop}(X)$. We also have

$$w - \hat{q} = w - \sum_{i \in I} w_i e_i + \sum_{i \in I} w_0 e_i = \sum_{j \notin I}(w_j - w_0)e_j - w_0 e_{n+1}.$$

This vector is visibly in $\text{trop}(X^\perp)$. We have thus constructed $\binom{n}{d}$ distinct vectors in the intersection (3.1.26). The corollary hence follows from Theorem 3.1.28, applied to general X. ∎

Example 3.1.30 ($n = 3, d = 2$)**.** We consider the 2-parameter linear model X for the state space $\{A, C, G, T\}$ discussed in [PS05, Example 11]. This model is defined by one homogeneous linear constraint $c_A p_A + c_C p_C + c_G p_G + c_T p_T = 0$. Its coefficients c_i are nonzero real numbers. Consider the data vector $u = (t^{w_A}, t^{w_C}, t^{w_G}, t^{w_T})$. The four exponents are nonnegative integers, and we assume that w_A is the smallest among them. The log-likelihood function has three critical points $\hat{p} = (\hat{p}_A, \hat{p}_C, \hat{p}_G, \hat{p}_T)$, one for each bounded polygon. These are functions in t, and we seek their behavior for $t \to 0$. This is given by the three tropical critical points:

$$\hat{q} = (0, w_C - w_A, w_G - w_A, 0),\ (0, w_C - w_A, 0, w_T - w_A)\ \text{or}\ (0, 0, w_G - w_A, w_T - w_A).$$

We change the model by setting $c_A = 0$, so X is no longer general. The number of bounded regions drops from 3 to 2. The matroid of X changes, and so does $\mathrm{trop}(X)$. We now find $\hat{q} = (0, w_C - w_A, w_C - w_A, w_G - w_A)$ or $(0, w_C - w_A, w_G - w_A, w_C - w_A)$ provided $w_C < \min(w_G, w_T)$.

Proof of Theorem 3.1.28. We use the formulation of the likelihood correspondence given in [HS14, Proposition 1.19]. This states, in our notation, that the critical points $\hat{p}$ are the elements of

$$X \cap (u^{-1} \star X^{\perp})^{-1}. \tag{3.1.27}$$

Here, $\star$ is the Hadamard product, and u^{-1} is the coordinatewise reciprocal of the vector u. The intersection in (3.1.27) commutes with tropicalization, provided $w = \mathrm{val}_t(u)$ is generic:

$$\mathrm{trop}(X \cap (u^{-1} \star X^{\perp})^{-1}) = \mathrm{trop}(X) \cap -\mathrm{trop}(u^{-1} \star X^{\perp}) = \mathrm{trop}(X) \cap (w - \mathrm{trop}(X^{\perp})). \tag{3.1.28}$$

Indeed, the left expression is contained in the middle expression, and they are equal in the sense of stable intersection. This is the content of [MS21a, Theorem 3.6.1]. In (3.1.28) we intersect polyhedral spaces of dimensions d and $n + 1 - d$ in $\mathbb{R}^{n+1}$. The second equation follows from [MS21a, Proposition 5.5.11]. Since w is generic, the intersection is transverse at any intersection point and each intersection point is isolated. Lemma 3.1.31 below shows that the multiplicity of every tropical intersection is 1, even in the more general case of a nonrealizable matroid. ∎

Fix a matroid X of rank $d + 1$ on the elements $\{0, 1, \ldots, n + 1\}$. Let $X^{\perp} = (X/(n+1))^*$ be the dual of the contraction of X by the element $n + 1$. Furthermore, let $\mathcal{F} := \{F_1 \subsetneq \cdots \subsetneq F_d\}$ and $\mathcal{F}^{\perp} := \{F_1^{\perp} \subsetneq \cdots \subsetneq F_{n-d}^{\perp}\}$ be flags of flats of X and $X^{\perp}$, respectively with $\mathrm{rank}(F_i) = i$ and $\mathrm{rank}(F_j^{\perp}) = j$ for all i, j. Since X has rank $d + 1$, we can assume $F_d \subseteq \{0, \ldots, n\}$.

Lemma 3.1.31. *Each intersection in (3.1.28) has multiplicity* 1*. It is the signed determinant of an* $(n + 1) \times (n + 1)$ *matrix whose columns are indicator vectors of flats in flags as above:*

$$M_{\mathcal{F}, \mathcal{F}^{\perp}} := \begin{pmatrix} | & \cdots & | & | & \cdots & | & | \\ e_{F_1} & \cdots & e_{F_d} & e_{F_1^{\perp}} & \cdots & e_{F_{n-d}^{\perp}} & e_{\{0,\ldots,n\}} \\ | & \cdots & | & | & \cdots & | & | \end{pmatrix}.$$

Such a matrix $M_{\mathcal{F}, \mathcal{F}^{\perp}}$ *has determinant* 0 *or* ± 1*. Moreover, if* $M_{\mathcal{F}, \mathcal{F}^{\perp}}$ *is invertible, there exist complementary bases of the matroids* $X/(n+1)$ *and* $X^{\perp}$ *generating the flags* $\mathcal{F}$ *and* $\mathcal{F}^{\perp}$*.*

Proof. We proceed along the following four steps.

(i) We can assume that $\{0, \ldots, d-1, n+1\}$ is a basis of X, and

$$M_{\mathcal{F}, \mathcal{F}^{\perp}} = \begin{pmatrix} 1 & 1 & 1 & 1 & & \\ 0 & 1 & 1 & 1 & & * \\ 0 & 0 & \ddots & 1 & & \\ 0 & 0 & 0 & 1 & & \\ \hline & & & & & \\ & & * & & & * \\ & & & & & \end{pmatrix}, \qquad (3.1.29)$$

where the left block has d columns and the symbols '$*$' represent arbitrary $\{0, 1\}$-entries. The definition of flag ensures that within each column block, a 1-entry is followed by only 1's in the same row. Therefore, rows in each column block are uniquely determined by their number of 1-entries.

(ii) Let I_j be the set of row indices corresponding to rows having precisely j 1-entries in the left block. For each row index i, let $\gamma(i)$ be the smallest column index in the right block such that the entry $(i, \gamma(i))$ is 1. By permuting rows of $M_{\mathcal{F}, \mathcal{F}^{\perp}}$ we can ensure that all rows indexed by I_j are sorted by increasing number of 1's in the right block. Since a 1-entry in the right block is followed by 1's in the same row, we have that

$$\text{if } i, i' \in I_j \text{ are such that } i' < i, \text{ then } \gamma(i) \le \gamma(i'). \qquad (3.1.30)$$

If equality holds for some $i \in I_j \smallsetminus \{i'\}$, then two rows are equal and $M_{\mathcal{F}, \mathcal{F}^{\perp}}$ has determinant 0, in which case we are done. Hence, in what follows we assume that the last inequality in (3.1.30) is strict for all distinct $i, i' \in I_j$.

(iii) We perform the following elementary row operations. Each row r_i indexed by $i > d$ is replaced by $r_i - r_{i'}$, where $i \in I_{i'}$. After this operation, the lower left block in $M_{\mathcal{F}, \mathcal{F}^{\perp}}$ is zero, all entries are still 0 or 1 and the function γ is unchanged.

(iv) It remains to show that the determinant of the lower right block matrix is ± 1. Since the matrix $M_{\mathcal{F}, \mathcal{F}^{\perp}}$ is still of the form (3.1.29), the elements $\{0, \ldots, d-1, n+1\}$ are still a basis of X (after the above permutations). Therefore by definition of $X^{\perp}$, the set $\{d, \ldots, n\}$ is a basis of $X^{\perp}$. This implies that, up to a permutation of rows, the lower right block is an upper triagonal matrix with 1-entries on the diagonal. ∎

We now apply Theorem 3.1.28 to the CHY model $X^{\circ} = X(2, m)$, where $n = m(m-3)/2$. The tropical linear space $\text{trop}(X)$ consists of ultrametrics on $m-1$ points [MS21a, Lemma 4.3.9]. The matroid of X is the graphic matroid of the complete graph K_{m-1}; see [MS21a, Example 4.2.14]. Using (3.1.2) with $k = 2$, the vertices of K_{m-1} are labeled by $2, 3, \ldots, m$. The special edge $e = \{2, 3\}$ corresponds to the hyperplane at infinity. The matroid of $X^{\perp}$ is the cographic matroid of the graph K_{m-1}/e obtained by contracting e. This is dual to the graphic matroid of K_{m-1}/e. Vectors in $\text{trop}(X)$ have the minimum attained twice on every circuit of K_{m-1}, where the edge e has weight 0. Vectors in $\text{trop}(X^{\perp})$ attain their minimum twice on every cocircuit of K_{m-1}/e. Thus tropical MLE amounts to writing the vector w as a sum of two such minimum-attained-twice vectors. The number of such decompositions equals $(m-3)!$.

Example 3.1.32 ($m = 6$). Following [ST21, Example 2], we consider the CHY model $X(2, 6)$. This corresponds to an arrangement of 9 planes in $\mathbb{R}^3$, with six bounded regions,

namely the tetrahedron of a triangulated 3-cube. We coordinatize this model by the matrix (3.1.2), so that $e = \{2, 3\}$ is the special edge of K_5. Our data are the Mandelstam invariants

$$u_{24} = t^{12}, \; u_{25} = t^6, \; u_{26} = t^9, \; u_{34} = t^{12}, \; u_{35} = t^5, \; u_{36} = t, \; u_{45} = t^{10}, \; u_{46} = t^{11}, \; u_{56} = t^3.$$

Hence the tropical data vector equals $w = (w_{24}, w_{25}, \ldots, w_{45}) = (12, 6, 9, 12, 5, 1, 10, 11, 3)$. Our task is to find all additive decompositions $w = \hat{q} + (w - \hat{q})$ where the two summands lie in the respective Bergman fans $\mathrm{trop}(X)$ and $\mathrm{trop}(X^\perp)$. One such decomposition equals

$$w = \hat{q} + (w - \hat{q}) = (7, 5, 2, 0, 0, 0, 5, 2, 2) + (5, 1, 7, 12, 5, 1, 5, 9, 1). \tag{3.1.31}$$

This solution is verified in Figure 3.5: the minimum over each circuit is attained at least twice.
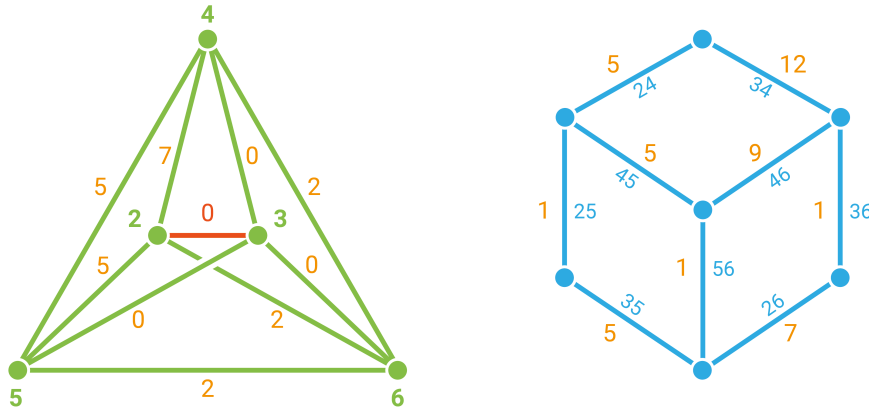
Figure 3.5. Contracting the edge 23 in the green graph K_5 yields a planar graph whose dual is the blue graph on the right. The orange edge weights are the entries in (3.1.31). The key property is that the minimum is attained at least twice in each cycle of the respective graph.

The intersection (3.1.26) consists of six points. The tropical critical points $\hat{q}$ are

$$(0, 0, 8, 4, 2, 0, 2, 0, 0), \quad (0, 5, 2, 2, 0, 0, 0, 0, 2), \quad (1, 0, 8, 0, 2, 0, 0, 1, 0),$$
$$(2, 5, 2, 0, 0, 0, 2, 3, 2), \quad (7, 5, 2, 0, 0, 0, 5, 2, 2), \quad (9, 0, 8, 0, 2, 0, 0, 8, 0).$$

Each $\hat{q}$ gives a decomposition as in (3.1.31), where the two summands are compatible with the cycles of the two graphs in Figure 3.5. These solutions specify small arcs that lie in the six tetrahedra. These arcs converge for $t \to 0$ with the given rates to vertices of the arrangement.

What we have outlined here is the combinatorial theory of *tropical CHY scattering*. This works for all $m \geq 5$. The soft limits of [CUZ20] arise as the very special case when the tropical Mandelstam invariants w satisfy $w_{im} = 1$ and $w_{ij} = 0$ for $i \leq j \leq m - 1$. The key player in tropical CHY scattering is the space $\mathrm{trop}(X)$ of ultrametric phylogenetic trees. In the case $m = 5$, this space is a cone over the Petersen graph. See [MS21a, §4.3] for details.

In this subsection we presented the theory of tropical MLE for linear models. A more general combinatorial version of Theorem 3.1.28 has been recently proved in [AMEP22]. At this point, it is natural to ask what happens when the model X is an arbitrary (nonlinear) projective variety in $\mathbb{P}^n$. A partial answer based on homotopy techniques is given in the next subsection. The role of (3.1.27) is now played by the likelihood correspondence. According to [HS14, Theorem 1.6], this is an n-dimensional subvariety in $\mathbb{P}^n \times \mathbb{P}^n$. An ambitious goal is to

determine the tropicalization of that subvariety. The desired pairs $(w, \hat{q})$ are points in that *tropical likelihood correspondence.* This leads to very interesting geometry and combinatorics. For instance, it is closely related to the Bernstein-Sato slopes studied by van der Veer and Sattelberger [vdVS22].

3.1.7. Learning valuations numerically

The previous subsections developed two techniques for obtaining the ML degree of a very affine variety: Euler characteristics via stratified fibrations, and tropical geometry. Each method leads to a meaningful combinatorial description of the ML degree, but it requires significant combinatorial efforts. In this subsection we propose a numerical method which computes the tropical solutions $\hat{q}$ discussed in Subsections 3.1.5 and 3.1.6 directly, while avoiding any combinatorial overhead. A decomposition of the ML degree as a positive sum of integers naturally emerges as a byproduct. We used this method to verify the multiplicities (3.1.24) as detailed in Subsection 3.1.5.

Let $K = \mathbb{C}\{\{t\}\}$ and consider a very affine variety $X \subset (K^*)^n$ that is defined over $\mathbb{C}$. Fix a data vector $u \in K^n$. The problem of tropical MLE is to compute the coordinate-wise valuations $\hat{q} = \mathrm{val}_t(\hat{p})$ of the critical points $\hat{p}$ of the log-likelihood function $\mathcal{L}_u$ restricted to X. Note that each $\hat{q}$ is a vector in $\mathbb{Q}^n$, so the output can be written in exact arithmetic.

In this subsection, we think of t as a coordinate for $\mathbb{C}^*$. We assume for simplicity that $u \in \mathbb{C}[t, t^{-1}]^n$ is given by Laurent polynomials. The following incidence variety is a curve:

$$C = \left\{ (\hat{p}, t) \in X \times \mathbb{C}^* \mid \hat{p} \text{ is a critical point of } (\mathcal{L}_{u(t)})\big|_X \right\},$$

The generalization to the case where the u_i are Laurent series, convergent in the punctured disk $\{t \in \mathbb{C}^* \mid |t| < 1\}$, is straightforward. We assume that u is sufficiently generic, so that:

- the projection map $\pi_{\mathbb{C}^*} : C \to \mathbb{C}^*$ is an $\mathrm{MLdegree}(X)$-to-one branched covering,

- the half-open real line segment $(0, 1] \subset \mathbb{C}^*$ avoids the branch locus of $\pi_{\mathbb{C}^*}$.

Any point $(\hat{p}(1), 1)$ of the curve C lies on a unique path in $\pi_{\mathbb{C}^*}^{-1}((0, 1])$ which corresponds to a critical point $\hat{p}(t) = (\hat{p}_1(t), \ldots, \hat{p}_n(t)) \in K^n$. Each coordinate of $\hat{p}(t)$ is a Puiseux series

$$\hat{p}_i(t) = c_i t^{\hat{q}_i} + \text{ higher order terms,} \tag{3.1.32}$$

where $\hat{q} = (\hat{q}_1, \ldots, \hat{q}_n)$ is its corresponding tropical critical point.

For any real constant $t' \in (0, 1]$ with $t' \ll 1$, the following approximation holds:

$$\log |\hat{p}_i(t')| \approx \log |c_i| + \hat{q}_i \cdot \log t'. \tag{3.1.33}$$

Hence, for all values of t' that are small enough, the points $(a_{t'}, b_{t'}) = (\log t', \log |\hat{p}_i(t')|) \in \mathbb{R}^2$ lie approximately on a line with slope $\hat{q}_i = \mathrm{val}_t(\hat{p}_i(t))$. We wish to learn that slope.

Using standard numerical predictor-corrector techniques on the critical point equations, one can compute $(\hat{p}(t'), t') \in \pi_{\mathbb{C}^*}^{-1}(t')$ for any $t' \in (0, 1]$. This amounts to evaluating the solution $\hat{p}(t)$ at t'. We used `HomotopyContinuation.jl` for this computation.

By evaluating $\hat{p}(t)$ at many t' near 0, we may approximate the ith coordinate $\hat{q}_i$ by fitting a line through the points $(a_{t'}, b_{t'})$, see (3.1.33). We find $\hat{q}$ by doing this for $i = 1, 2, \ldots, n$. This discussion is summarized in Algorithm 1 for computing the tropical critical point $\hat{q}$.

Algorithm 1: Numerical computation of tropical critical points

---

Input: Data u and a critical point $\hat{p}(1) \in (\mathbb{C}^*)^n$ of the log-likelihood function $\mathcal{L}_{u(1)}$.
Output: The tropical critical point $\hat{q}$ associated to the solution $\hat{p}(t)$, together with some measure ρ of trust in this result.

1 With $\hat{p}(1)$ as the start solution, use numerical predictor-corrector techniques to compute $\hat{p}(t')$ for a finite set $T \subset (0,1]$ of values t', all sufficiently close to 0.

2 Fit lines ℓ_i through the data points $\{(\log t, \log|\hat{p}_i(t)|) \mid t \in T\}$ for each coordinate $\hat{p}_i$, using standard regression techniques.

3 Using any rationalization heuristic, such as the built-in function `rationalize` in `Julia`, round the slope of the line ℓ_i to obtain the rational number $\hat{q}_i$.

4 As a measure of trust, record the *regression error*

$$\rho \;:=\; \sum_{t' \in T}\big(\log|\hat{p}_i(t')| - (\log|c_i| + \hat{q}_i \cdot \log t')\big)^2. \qquad (3.1.34)$$

5 return $(\hat{q}, \rho)$

Example 3.1.33 (Soft limits)**.** We apply this to the CEGM model $X(3,7)$. It is parametrized by the 3×3 minors p_{ijk} of the matrix $M_{3,7}$ given in (3.1.2). Consider the log-likelihood function

$$\mathcal{L}_{u(t)} \;=\; \tilde{\mathcal{L}}_{3,7}(x,t) \;=\; \sum_{1 \leq i < j < k \leq 6} u_{ijk} \cdot \log p_{ijk} \;+\; \sum_{1 \leq i < j \leq 6} t \cdot u_{ij7} \cdot \log p_{ij7} \qquad (3.1.35)$$

for generic complex parameters u_{ijk}. The numerical computation in [ST21, §4] provides $1\,272$ start solutions $\hat{p}(1)$. Each of these now serves as the input to Algorithm 1. That algorithm performs the likelihood degeneration (soft limit) purely numerically for $t \to 0$.

The $1\,272$ runs of Algorithm 1 lead to only 16 distinct tropical critical points $\hat{q}$. This means that different start solutions $\hat{p}(1)$ yield the same output. The multiplicity of $\hat{q}$ in the tropical curve $\mathrm{trop}(C)$ is the number of runs that yield output $\hat{q}$. The coordinates and multiplicities of all tropical critical points are shown in the columns of Table 3.4. We stress that this table was computed blindly, without any prior knowledge about the model $X(3,7)$.

Remarkably, one learns the geometry of the stratified fibration $\pi_{3,7}$ from the output in Table 3.4. The first column corresponds to the $1\,092$ regular solutions, i.e., those which converge in $X(3,7)$. The others correspond to 15 groups of 12 boundary solutions, whose limit for $t \to 0$ lies on the boundary in the tropical compactification of $X(3,7)$. Thus, by using Algorithm 1, we discover the ML degrees in Theorem 3.1.17 in a purely automatic manner.

Recall that the action of $(\mathbb{C}^*)^7$ on the Plücker coordinates tropicalizes to an additive action of $\mathbb{R}^7$ on $\mathbb{R}^{35}$. Modulo this $\mathbb{R}^7$-action, each column of Table 3.4, except the first one, can be represented by a $\{0,1\}$ vector that has precisely three nonzero entries. For instance, the second column has its entries 1 in the rows $p_{137}, p_{267}, p_{457}$, so it identifies the divisor $S_{(13),(26),(45)}$ in the stratification of $X(3,6)$. This corresponds to a codimension 3 matroid stratum for $k = 3, m = 7$. In this manner, one automatically learns the 15 strata of type I in Table 3.2. On average, the regression error (3.1.34) for all $1\,272$ paths was ~ 0.0045, the largest one being ~ 0.162. The computation took no more than a couple of minutes.

Extending Example 3.1.33 to a more challenging scenario, we applied Algorithm 1 to each of the $5\,211\,816$ solutions to the maximum likelihood equations (3.1.19) for $k = 4, m = 8$. This led us to the multiplicities (3.1.24) and the derivation of Theorem* 3.1.26 as discussed in Subsection 3.1.5.

p_{123}	0	0	0	0	0	0	0	0	0	0	0	0	0	0	0	0
p_{124}	0	0	0	0	0	0	0	0	0	0	0	0	0	0	0	0
p_{125}	0	0	0	0	0	0	0	0	0	0	0	0	0	0	0	0
p_{126}	0	0	0	0	0	0	0	0	0	0	0	0	0	0	0	0
p_{127}	0	0	0	0	0	0	0	0	0	0	0	0	0	0	0	0
p_{134}	0	0	0	0	0	0	0	0	0	0	0	0	0	0	0	0
p_{135}	0	0	0	0	0	0	0	0	0	0	0	0	0	0	0	0
p_{136}	0	0	0	0	0	0	0	0	0	0	0	0	0	0	0	0
p_{137}	0	1	0	0	-1	0	1	0	1	0	0	0	0	-1	0	-1
p_{145}	0	0	0	0	0	0	0	0	0	0	0	0	0	0	0	0
p_{146}	0	0	0	0	0	0	0	0	0	0	0	0	0	0	0	0
p_{147}	0	0	0	1	-1	1	0	0	0	0	0	0	0	-1	1	-1
p_{156}	0	0	0	0	0	0	0	0	0	0	0	0	0	0	0	0
p_{157}	0	0	0	0	-1	0	0	1	0	0	1	1	0	-1	0	-1
p_{167}	0	0	1	0	-1	0	0	0	0	1	0	0	1	-1	0	-1
p_{234}	0	0	0	0	0	0	0	0	0	0	0	0	0	0	0	0
p_{235}	0	0	0	0	0	0	0	0	0	0	0	0	0	0	0	0
p_{236}	0	0	0	0	0	0	0	0	0	0	0	0	0	0	0	0
p_{237}	0	0	0	0	-1	0	0	0	0	1	0	1	0	-1	1	-1
p_{245}	0	0	0	0	0	0	0	0	0	0	0	0	0	0	0	0
p_{246}	0	0	0	0	0	0	0	0	0	0	0	0	0	0	0	0
p_{247}	0	0	0	0	-1	0	0	1	1	0	0	0	1	-1	0	-1
p_{256}	0	0	0	0	0	0	0	0	0	0	0	0	0	0	0	0
p_{257}	0	0	1	0	-1	1	1	0	0	0	0	0	0	-1	0	-1
p_{267}	0	1	0	1	-1	0	0	0	0	0	1	0	0	-1	0	-1
p_{345}	0	0	0	0	0	0	0	0	0	0	0	0	0	0	0	0
p_{346}	0	0	0	0	0	0	0	0	0	0	0	0	0	0	0	0
p_{347}	0	0	1	0	-1	0	0	0	0	0	1	0	0	-1	0	0
p_{356}	0	0	0	0	0	0	0	0	0	0	0	0	0	0	0	0
p_{357}	0	0	0	1	-1	0	0	0	0	0	0	0	1	0	0	-1
p_{367}	0	0	0	0	0	1	0	1	0	0	0	0	0	-1	0	-1
p_{456}	0	0	0	0	0	0	0	0	0	0	0	0	0	0	0	0
p_{457}	0	1	0	0	0	0	0	0	0	1	0	0	0	-1	0	-1
p_{467}	0	0	0	0	-1	0	1	0	0	0	0	1	0	0	0	-1
p_{567}	0	0	0	0	-1	0	0	0	1	0	0	0	0	-1	1	0
$m_{\hat{q}}$	1 092	12	12	12	12	12	12	12	12	12	12	12	12	12	12	12

Table 3.4. Columns represent the 16 numerically obtained tropical critical points of the log-likelihood function in the soft limit for $X(3,7)$. The last row represents their multiplicities.

3.2. Hypersurface complements

As stated at the beginning of this chapter, this section studies vector spaces of generalized Euler integrals. These are integrals of the form

$$\int_\Gamma f^{s+a}\, x^{\nu+b}\, \frac{\mathrm{d}x}{x} \;=\; \int_\Gamma \left(\prod_{j=1}^{\ell} f_j^{s_j+a_j}\right) \cdot \left(\prod_{i=1}^{n} x_i^{\nu_i+b_i}\right) \frac{\mathrm{d}x_1}{x_1}\wedge\cdots\wedge\frac{\mathrm{d}x_n}{x_n}. \tag{3.2.1}$$

For the sake of clarity, recall that $x=(x_1,\ldots,x_n)$ are coordinates on $(\mathbb{C}^*)^n$, $f=(f_1,\ldots,f_\ell)$ denotes a tuple of ℓ Laurent polynomials in x, and we use multi-index notation, i.e., f^s denotes $f_1^{s_1}\cdots f_\ell^{s_\ell}$, and similarly for x^ν. The choice of the integration contour will be made precise in Subsection 3.2.1. The exponents ν_i, s_j take on complex values, whereas $a_i, b_j \in \mathbb{Z}$ are thought of as integer shifts. Our motivation for studying generalized Euler integral comes from particle physics, where they arise as Feynman integrals in the Lee–Pomeransky representation (see Appendix A). These are evaluated to make predictions for particle scattering experiments [Wei22].

It well known in the physics literature that, when (3.2.1) represents a Feynman integral, varying the integer vectors a, b in (3.2.1) gives Feynman integrals for different space-time dimensions, which are known to satisfy linear relations. In fact, there exists a finite set $\{(a^{(k)}, b^{(k)})\}_{k=1,\ldots,\chi} \subset \mathbb{Z}^\ell \times \mathbb{Z}^n$ such that any integral of the form (3.0.2) can be written as a linear combination of the corresponding χ Euler integrals.

This discussion hints at the fact that the integrals (3.2.1), for varying $(a,b)\in\mathbb{Z}^\ell\times\mathbb{Z}^n$, generate a finite-dimensional vector space. We present two ways of formalizing this statement. We start with a homological interpretation. Let $s_j \in \mathbb{C}$, $\nu_i \in \mathbb{C}$ be fixed, generic complex numbers and $f \in \mathbb{C}[x, x^{-1}]^\ell$ fixed, nonzero Laurent polynomials such that none of the f_j is a multiplicative unit in $\mathbb{C}[x, x^{-1}]$. The complement of the vanishing locus of their product

$f_1 \cdots f_\ell$ in the algebraic torus $(\mathbb{C}^*)^n$ defines the very affine variety

$$X \;=\; \{\, x \in (\mathbb{C}^*)^n \mid f_1(x) \cdots f_\ell(x) \neq 0 \,\} \;=\; (\mathbb{C}^*)^n \smallsetminus V(f_1 \cdots f_\ell) \subset (\mathbb{C}^*)^n. \tag{3.2.2}$$

The variety X fits into the framework of very affine varieties because the graph embedding

$$X \hookrightarrow (\mathbb{C}^*)^\ell \times (\mathbb{C}^*)^n, \qquad x \mapsto (f_1(x), \ldots, f_\ell(x), x_1, \ldots, x_n)$$

is a closed embedding that identifies X with the smooth closed subvariety

$$U \;=\; \left\{ (y, x) \in (\mathbb{C}^*)^{\ell + n} \mid y_j = f_j(x) \;\; \text{for } j = 1, \ldots, \ell \right\} \subset (\mathbb{C}^*)^{\ell + n}.$$

Regular functions on X are precisely elements of $\mathbb{C}[x^{\pm 1}, f_1^{-1}, \ldots, f_\ell^{-1}]$. We are interested in the twisted homology of X, where the twist is defined by the logarithmic differential 1-form

$$\omega \;:=\; \mathrm{dlog}(f^s x^\nu) \;=\; \sum_{j=1}^{\ell} s_j \cdot \mathrm{dlog}\,(f_j) \;+\; \sum_{i=1}^{n} \nu_i \cdot \mathrm{dlog}\,(x_i) \;\in\; \Omega_X^1(X). \tag{3.2.3}$$

For each $(a, b) \in \mathbb{Z}^\ell \times \mathbb{Z}^n$, the integral (3.2.1) defines a linear map on the space of n-cycles. We define the $\mathbb{C}$-vector space

$$V_\Gamma \;:=\; \mathrm{Span}_{\mathbb{C}} \left\{ [\Gamma] \longmapsto \int_\Gamma f^{s+a}\, x^{\nu+b} \frac{\mathrm{d}x}{x} \right\}_{(a,b) \in \mathbb{Z}^\ell \times \mathbb{Z}^n} \;\subseteq\; \mathrm{Hom}_{\mathbb{C}}\,(\,H_n(X, \omega)\,, \mathbb{C}\,). \tag{3.2.4}$$

Here, $H_n(X, \omega)$ is the n-th homology of the twisted chain complex associated to ω [AKKI11, Chapter 2]. We recall the definition in Subsection 3.2.1. Another way to obtain a vector space by varying $(a, b) \in \mathbb{Z}^\ell \times \mathbb{Z}^n$ is to view (3.2.1) as a function of s and ν. We fix an integration contour $\Gamma \in H_n(X, \omega)$ and also keep $f \in \mathbb{C}[x, x^{-1}]^\ell$ fixed. We obtain the $\mathbb{C}(s, \nu)$-vector space

$$V_{s,\nu} \;:=\; \mathrm{Span}_{\mathbb{C}(s,\nu)} \left\{ (s, \nu) \longmapsto \int_\Gamma f^{s+a}\, x^{\nu+b} \frac{\mathrm{d}x}{x} \right\}_{(a,b) \in \mathbb{Z}^\ell \times \mathbb{Z}^n}. \tag{3.2.5}$$

The cycle Γ depends on (s, ν), as we will clarify in Subsection 3.2.2. The vector spaces V_Γ and $V_{s,\nu}$, as well as the relations between their generators, are connected in an intriguing way. This is explored in the rest of the chapter. In the context of Feynman integrals, the vector space V_Γ was studied by Mizera and Mastrolia in [Miz18, MM19], and $V_{s,\nu}$ for the case of a single polynomial f is the central object in the article [BBKP19] by Bitoun, Bogner, Klausen, and Panzer. Variations of $V_{s,\nu}$, in which the Feynman integral depends on some extra physical parameters, appear in [BGL$^+$18].

The motivation in [GKZ90] for studying generalized Euler integrals comes from the theory of GKZ systems. It turns out that (3.2.1) gives a natural description of the stalk V_{c^*} of the solution sheaf of a certain system of linear PDEs at the point c^*. We set $a = b = 0$ and fix generic complex values for the parameters $s \in \mathbb{C}^\ell, \nu \in \mathbb{C}^n$. We now think of (3.2.1) as a function of the coefficients of the f_j and generate a $\mathbb{C}$-vector space by varying the integration contour Γ:

$$V_{c^*} \;:=\; \mathrm{Span}_{\mathbb{C}} \left\{ c \longmapsto \int_\Gamma f(x; c)^s\, x^\nu \frac{\mathrm{d}x}{x} \right\}_{[\Gamma] \in H_n(X, \omega)}, \tag{3.2.6}$$

where c lies in a small neighborhood of c^* and two functions are identified when they agree on a neighborhood of c^*. The space X depends on c^*, as we explain in Subsection 3.2.3.

Here, the monomial supports of the Laurent polynomials f_j are fixed, and their coefficients are listed in a vector $c \in \mathbb{C}^A$ of complex parameters. The notation $\mathbb{C}^A$ indicates that

the entries of c are indexed by a set of exponents $A \subset \mathbb{Z}^n$. The vector space V_{c^*} is a subspace of the hypergeometric functions on $\mathbb{C}^A$. It consists of local solutions to a GKZ system, which is a D_A-ideal later denoted by $H_A(\kappa)$ with $\kappa = (-\nu, s)$. Here D_A is the Weyl algebra whose variables are indexed by A. We recall definitions and notation in Subsections 3.2.2 and 3.2.3. A classical result by Cauchy, Kovalevskaya, and Kashiwara in D-module theory (see Theorem 1.2.9) relates the dimension of V_{c^*} to that of the $\mathbb{C}(c)$-vector space $R_A/(R_A \cdot H_A(\kappa))$, which is the quotient of the rational Weyl algebra R_A by the R_A-ideal generated by the GKZ system. The connection between V_{c^*} and V_Γ is investigated in the works of Matsubara-Heo [MH22, MH21] in a more general setup. In the recent article [CGM$^+$22], the authors present a fast algorithm to compute Macaulay matrices to efficiently derive Pfaffian systems of GKZ systems.

Fixing generic parameters in each context, all vector spaces seen above share the same dimension. Moreover, this dimension is governed by the topology of X in (3.2.2).

Theorem 3.2.1. *Let $X \subset (\mathbb{C}^*)^n$ be the very affine variety* (3.2.2), *where f_j are Laurent polynomials with fixed monomial supports and generic coefficients. Let $V_\Gamma, V_{s,\nu}, V_{c^*}, H_A(\kappa)$ be as defined above, with generic choices of parameters each. We have*

$$\dim_{\mathbb{C}}(V_\Gamma) = \dim_{\mathbb{C}(s,\nu)}(V_{s,\nu}) = \dim_{\mathbb{C}}(V_{c^*}) = \dim_{\mathbb{C}(c)}(R_A/(R_A \cdot H_A(\kappa))) = (-1)^n \cdot \chi(X),$$

where $\chi(X)$ denotes the topological Euler characteristic of X.

Although the statement of Theorem 3.2.1 in the case of $V_{s,\nu}$ appears in the literature only for $\ell = 1$, the rest of its content summarizes known results. Other than allowing $\ell > 1$ for the vector space $V_{s,\nu}$, we also consider it part of our contribution to bring together scattered results in the literature on this important topic, leading to an accessible, complete proof of Theorem 3.2.1. The following subsections study in detail the three vector spaces of integrals introduced above. Finally, Theorem 3.2.1 follows as a corollary of Theorems 3.2.7, 3.2.23, and 3.2.28, which state the result in different contexts.

3.2.1. Twisted de Rham cohomology

Throughout this subsection, $s \in \mathbb{C}^\ell$, $\nu \in \mathbb{C}^n$, and $f \in \mathbb{C}[x, x^{-1}]^\ell$ are fixed. None of the f_j are zero or a unit in $\mathbb{C}[x, x^{-1}]$. We focus on the $\mathbb{C}$-vector space

$$V_\Gamma = \mathrm{Span}_{\mathbb{C}} \left\{ [\Gamma] \longmapsto \int_\Gamma f^{s+a} \, x^{\nu+b} \frac{\mathrm{d}x}{x} \right\}_{(a,b) \in \mathbb{Z}^\ell \times \mathbb{Z}^n} \tag{3.2.7}$$

previously introduced. In particular, we are interested in interpreting its dimension as that of a (co-)homology vector space. We denote by $I_{a,b}(\Gamma)$ the integral in (3.2.1) to stress the dependence on the integer shifts $(a,b) \in \mathbb{Z}^\ell \times \mathbb{Z}^n$ and on the integration contour Γ in this context. This subsection views $I_{a,b}(\Gamma)$ as the pairing between the *twisted cycle* Γ and the *co-cycle* $f^a x^b \frac{\mathrm{d}x}{x}$. We now introduce the relevant (co-)chain complexes, and refer to [AKKI11] for more details.

Let X be the very affine variety defined in (3.2.2). We start by briefly discussing twisted chains, and later switch to co-chains. Since the parameters s_j and ν_i are complex numbers, $f^s x^\nu = f_1^{s_1} \cdots f_\ell^{s_\ell} x_1^{\nu_1} \cdots x_n^{\nu_n}$ is a multi-valued function on X. To compute our integral (3.2.1), a branch of this function needs to be specified. A twisted chain Γ in (3.2.7) comes with this information: it belongs to the *twisted chain group* $C_n(X, \mathcal{L}_\omega^\vee)$, defined as follows. Let $\mathcal{L}_\omega^\vee$ be the line bundle on X whose sections are local solutions ϕ to the differential equation $\mathrm{d}\phi - \omega \wedge \phi = 0$. Here ω is the differential form in (3.2.3). One checks that these local sections

are $\mathbb{C}$-linear combinations of branches of $f^s x^\nu$ (see Example 3.2.2). For $k = 0, \ldots, 2n$, we define the *k-dimensional twisted chain group* $C_k(X, \mathcal{L}_\omega^\vee)$ as the $\mathbb{C}$-vector space spanned by elements of the form $\Delta \otimes_{\mathbb{C}} \phi$, where $\Delta \in C_k(X)$ is a singular chain of dimension k on X, and $\phi \in \mathcal{L}_\omega^\vee(U_\Delta)$ is a local section of $\mathcal{L}_\omega^\vee$ on an open neighborhood U_Δ of Δ. Two such sections are identified if they coincide on some open neighborhood. The tensor sign indicates bilinearity of $C_k(X) \times \mathcal{L}_\omega^\vee \to C_k(X, \mathcal{L}_\omega^\vee)$ in this construction. The *twisted boundary operator* $\partial_\omega : C_k(X, \mathcal{L}_\omega^\vee) \to C_{k-1}(X, \mathcal{L}_\omega^\vee)$ naturally remembers the choice of branch: $\partial_\omega(\Delta \otimes_{\mathbb{C}} \phi) = \partial\Delta \otimes_{\mathbb{C}} \phi$, where $\partial : C_k(X) \to C_{k-1}(X)$ is the usual boundary operator. An element in $C_k(X, \mathcal{L}_\omega^\vee) \cap \ker(\partial_\omega)$ is called a *k-cycle*. We obtain the following chain complex:

$$(C_\bullet(X, \mathcal{L}_\omega^\vee), \partial_\omega) \colon 0 \longrightarrow C_{2n}(X, \mathcal{L}_\omega^\vee) \xrightarrow{\partial_\omega} C_{2n-1}(X, \mathcal{L}_\omega^\vee) \xrightarrow{\partial_\omega} \cdots \xrightarrow{\partial_\omega} C_0(X, \mathcal{L}_\omega^\vee) \longrightarrow 0.$$

Its homology vector spaces are

$$H_k(X, \mathcal{L}_\omega^\vee) \coloneqq \ker(C_k(X, \mathcal{L}_\omega^\vee) \xrightarrow{\partial_\omega} C_{k-1}(X, \mathcal{L}_\omega^\vee)) / \operatorname{im}(C_{k+1}(X, \mathcal{L}_\omega^\vee) \xrightarrow{\partial_\omega} C_k(X, \mathcal{L}_\omega^\vee)).$$

To simplify the notation, we will write $H_k(X, \omega) \coloneqq H_k(X, \mathcal{L}_\omega^\vee)$ in what follows. As indicated in (3.2.4), the class $[\Gamma]$ in (3.2.7) lives in the n-th homology vector space $H_n(X, \omega)$. Before proceeding with co-chain complexes, we work out an example.

Example 3.2.2 ($\ell = 2, n = 1$)**.** Let $f = (x - 1, x - 2) \in \mathbb{C}[x, x^{-1}]^2$, $s = (\frac{1}{2}, \frac{1}{2})$ and $\nu = \frac{1}{2}$. The very affine variety X is $\mathbb{P}^1 \smallsetminus \{0, 1, 2, \infty\}$. Let $\mathcal{C}$ be the elliptic curve given by

$$\{y^2 z - x(x - z)(x - 2z) = 0\} \subset \mathbb{P}^2.$$

There is a double covering $\mathcal{C} \smallsetminus \{4 \text{ points}\} \to X$ whose sheets represent the branches of the multi-valued function $f^s x^\nu = \sqrt{x(x-1)(x-2)}$. These are the solutions to the differential equation $(\mathrm{d} - \omega)\phi = 0$, where

$$\omega = \left(\frac{1}{2(x-1)} + \frac{1}{2(x-2)} + \frac{1}{2x} \right) \mathrm{d}x. \tag{3.2.8}$$

It is instructive to think of twisted 1-cycles on X as projections of singular cycles on $\mathcal{C} \smallsetminus \{4 \text{ points}\}$. This is illustrated in Figure 3.6. We view the elliptic curve $\mathcal{C}$ as two copies of $\mathbb{P}^1$, glued along the branch cuts between $0, 1$ and $2, \infty$, drawn in black. The green loops in the left part of the figure lift to the standard basis of the first homology of $\mathcal{C}$, seen on the right. See for instance [Bob11, Section 1.3.3, p. 27]. The dotted part of the cycle encircling $1, 2$ lies on a different branch of the covering. The small red loop, even though it is a singular cycle on X, does not lift to a closed loop on $\mathcal{C}$. Hence, to obtain a twisted cycle, this loop needs to be run through twice. The reader who is unfamiliar with twisted cycles might appreciate the discussion in Subsection 3.2.4, where we discuss numerical evaluation of $I_{a,b}(\Gamma)$ when $n = 1$.
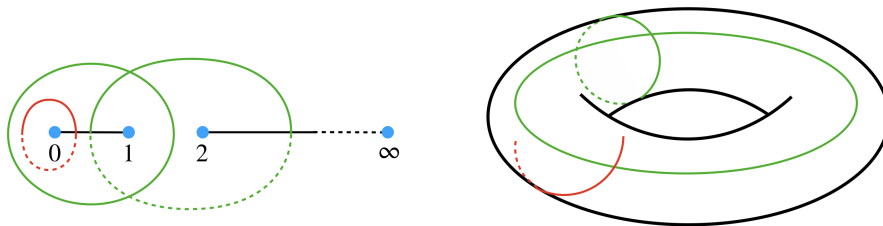
Figure 3.6. Twisted cycles in $\mathbb{P}^1 \smallsetminus \{0, 1, 2, \infty\}$ are singular cycles on an elliptic curve.

One then sets up the *twisted de Rham complex* dual to the chain complex $C_\bullet(X, \mathcal{L}_\omega^\vee)$. This uses the vector spaces $\mathcal{A}^k(X)$ of smooth k-forms on X. The co-chain complex is

$$(\mathcal{A}^\bullet(X), \nabla_\omega) \colon 0 \longrightarrow \mathcal{A}^0(X) \xrightarrow{\nabla_\omega} \mathcal{A}^1(X) \xrightarrow{\nabla_\omega} \mathcal{A}^2(X) \xrightarrow{\nabla_\omega} \cdots \xrightarrow{\nabla_\omega} \mathcal{A}^n(X) \xrightarrow{\nabla_\omega} 0. \quad (3.2.9)$$

The *twisted differential* is defined as $\nabla_\omega := \mathrm{d} + \omega \wedge$. That is,

$$\nabla_\omega \colon \mathcal{A}^k(X) \to \mathcal{A}^{k+1}(X), \qquad \phi \mapsto \mathrm{d}\phi + \omega \wedge \phi.$$

Note that $\omega \in \mathcal{A}^1(X)$ is indeed a smooth 1-form on X. For this complex, the cohomology vector spaces are given by

$$H_{\mathrm{dR}}^k(X, \omega) := H^k(\mathcal{A}^\bullet(X), \nabla_\omega) = \ker\left(\mathcal{A}^k(X) \xrightarrow{\nabla_\omega} \mathcal{A}^{k+1}(X)\right) / \operatorname{im}\left(\mathcal{A}^{k-1}(X) \xrightarrow{\nabla_\omega} \mathcal{A}^k(X)\right).$$

By [AKKI11, Lemma 2.9(1)], there is a perfect pairing between twisted homology and cohomology, justifying our claim that the complexes are dual. For $k = n$, this is given by

$$\langle \cdot, \cdot \rangle \colon H_{\mathrm{dR}}^n(X, \omega) \times H_n(X, \omega) \longrightarrow \mathbb{C}, \quad ([\phi], [\Gamma]) \mapsto \langle [\phi], [\Gamma] \rangle := \int_\Gamma f^s \, x^\nu \, \phi. \quad (3.2.10)$$

This also shows, since $[f^a x^b \frac{\mathrm{d}x}{x}] \in H_{\mathrm{dR}}^n(X, \omega)$, that $I_{a,b} \colon [\Gamma] \to I_{a,b}(\Gamma)$ in (3.2.7) are elements in $\operatorname{Hom}_\mathbb{C}(H_n(X, \omega), \mathbb{C})$. This is the inclusion (3.2.4), which we will show to be an equality.

A drawback of the twisted de Rham complex (3.2.9) is that its vector spaces $\mathcal{A}^k(X)$ are not amenable to computations. This is why one uses a twisted *algebraic* de Rham complex for X, whose vector spaces have more explicit descriptions. Moreover, we will see that this complex has the same cohomology spaces as $(\mathcal{A}^\bullet(X), \nabla_\omega)$. We use the vector spaces $\Omega_X^k(X)$ of *regular k-forms* on X. An element of $\Omega_X^0(X)$ is a $\mathbb{C}$-linear combination of $f^a x^b$, where $(a, b) \in \mathbb{Z}^\ell \times \mathbb{Z}^n$. More generally, a regular k-form on X is given by $\sum_{i_1 < \cdots < i_k} h_{i_1,\ldots,i_k} \, \mathrm{d}x_{i_1} \wedge \cdots \wedge \mathrm{d}x_{i_k}$, where $h_{i_1,\ldots,i_k} \in \Omega_X^0(X)$ are global regular functions on X. This defines the *twisted algebraic de Rham complex*

$$(\Omega_X^\bullet(X), \nabla_\omega) \colon 0 \longrightarrow \Omega_X^0(X) \xrightarrow{\nabla_\omega} \Omega_X^1(X) \xrightarrow{\nabla_\omega} \cdots \xrightarrow{\nabla_\omega} \Omega_X^n(X) \xrightarrow{\nabla_\omega} 0, \quad (3.2.11)$$

whose twisted differential is defined as before: $\nabla_\omega = \mathrm{d} + \omega \wedge$. Here, we view ω as a regular 1-form. Note that ∇_ω defines an integrable connection on $\mathcal{O}_X$ with logarithmic poles on the boundary of a compactification of X. Taking cohomology of (3.2.11) gives $\mathbb{C}$-vector spaces

$$H^k(X, \omega) := H^k(\Omega_X^\bullet(X), \nabla_\omega) = \ker\left(\Omega_X^k(X) \xrightarrow{\nabla_\omega} \Omega_X^{k+1}(X)\right) / \operatorname{im}\left(\Omega_X^{k-1}(X) \xrightarrow{\nabla_\omega} \Omega_X^k(X)\right).$$

Remark 3.2.3. In passing from the algebraic twisted de Rham complex $\Omega_X^\bullet(X)$ to the analytic version $\mathcal{A}^\bullet(X)$, one actually needs to replace the algebraic variety X by its *analytification* X^{an}. This is to emphasize that regular functions should now be thought of in an analytic, rather than algebraic, sense. In this paper, we drop the superscript $(\cdot)^{\mathrm{an}}$ to simplify notation. We write $H_k(X, \omega)$ for the twisted homology of X^{an} and distinguish the cohomology of the two cochain complexes by using the subscript $(\cdot)_{\mathrm{dR}}$ to mean the analytic context.

By the Deligne–Grothendieck comparison theorem [Del70, Corollaire 6.3], we have an isomorphism $H_{\mathrm{dR}}^n(X, \omega) \simeq H^n(X, \omega)$. We now relate $H^n(X, \omega)$ to our vector space V_Γ.

Lemma 3.2.4. *The $\mathbb{C}$-vector spaces V_Γ, $H^n(X, \omega)$, and $H_{\mathrm{dR}}^n(X, \omega)$ are isomorphic.*

Proof. Let $H_n(X, \omega)$ be the twisted homology defined above. By the perfect pairing (3.2.10) and $H_{\mathrm{dR}}^n(X, \omega) \simeq H^n(X, \omega)$, every $\mathbb{C}$-linear map $H_n(X, \omega) \to \mathbb{C}$ is given by a $\mathbb{C}$-linear combination of $I_{a,b}$'s. We conclude $V_\Gamma = \mathrm{Hom}_\mathbb{C}(H_n(X, \omega), \mathbb{C}) \simeq H_{\mathrm{dR}}^n(X, \omega) \simeq H^n(X, \omega)$.   ∎

By Lemma 3.2.4, the dimension $\dim_\mathbb{C}(V_\Gamma)$ is equal to that of the twisted top cohomology groups. To relate this to the topology of X, we make use of the following vanishing theorem.

Theorem 3.2.5. *Fix $f \in \mathbb{C}[x, x^{-1}]^\ell$ and let X be defined as in* (3.2.2). *For general $(s, \nu) \in \mathbb{C}^{\ell+n}$, we have that $H^\star(X, \omega) = H_{\mathrm{dR}}^\star(X, \omega) = 0$ whenever $\star \neq n$.*

Remark 3.2.6. Theorem 3.2.5 is proven in work of Douai and Sabbah [DS03] for non-degenerate functions with isolated singularities and by Douai [Dou] for cohomologically tame functions. A proof for our setup is included in [AFST22, Appendix A]. The precise meaning of *general* in Theorem 3.2.5 follows from the proof of [AFST22, Theorem A.1].

Theorem 1.4 in [AS97] is close to Theorem 3.2.5, but makes extra assumptions on the Laurent polynomials f. First, it is required that the Newton polytope $\mathrm{NP}(h) \subset \mathbb{R}^{n+\ell}$ of

$$h := \sum_{j=1}^\ell x_{n+j}\, f_j \in \mathbb{C}[x_1, \ldots x_{n+\ell}, x_1^{-1}, \ldots, x_{n+\ell}^{-1}] \tag{3.2.12}$$

is of maximal dimension $n + \ell - 1$. It is easy to verify that $\mathrm{NP}(h)$ is contained in an affine hyperplane, so its dimension is indeed bounded by $n + \ell - 1$. Second, it is assumed that h is *non-degenerate with respect to* $\mathrm{NP}(h)$. This can be phrased as a concrete Zariski open condition on the coefficients of f_j. Namely, it is equivalent to the non-vanishing of the *principal A-determinant* from [GKZ94b, Chapter 10] at h. The exponents A appearing in h will be seen as columns of the matrix A in Subsection 3.2.3. Under these assumptions on f, the integer $\dim_\mathbb{C}(V_\Gamma)$ can be interpreted as the *normalized volume* $\mathrm{vol}(\mathrm{NP}(h))$ of the Newton polytope $\mathrm{NP}(h)$. This equals $(n+\ell)!$ times the volume of $\mathrm{Conv}(\{0\} \cup \mathrm{NP}(h))$ induced by the lattice spanned by the columns of the matrix A.

Theorem 3.2.7. *Fix $f \in \mathbb{C}[x, x^{-1}]^\ell$ and let X be defined as in* (3.2.2). *For general $(s, \nu) \in \mathbb{C}^{\ell+n}$, we have*

$$\dim_\mathbb{C}(V_\Gamma) = |\chi(X)|. \tag{3.2.13}$$

Moreover, if f is such that the polynomial h from (3.2.12) *is non-degenerate with respect to $\mathrm{NP}(h)$ and $\dim(\mathrm{NP}(h)) = n + \ell - 1$, then the number* (3.2.13) *equals* $\mathrm{vol}(\mathrm{NP}(h))$.

Proof. Lemma 3.2.4 implies $\dim_\mathbb{C}(V_\Gamma) = \dim_\mathbb{C}(H_{\mathrm{dR}}^n(X, \omega))$. By Theorem 3.2.5, the alternating sum $\sum_{k=0}^{2n}(-1)^k \dim_\mathbb{C}(H_{\mathrm{dR}}^k(X, \omega))$ equals $(-1)^n \dim_\mathbb{C}(H_{\mathrm{dR}}^n(X, \omega))$. This coincides with the Euler characteristic $\chi(X)$ by [AKKI11, Theorem 2.2]. Finally, Lemma 3.2.4 gives $\dim_\mathbb{C}(H^n(X, \omega)) = \dim_\mathbb{C}(H_{\mathrm{dR}}^n(X, \omega))$ and the equality $\dim_\mathbb{C}(H^n(X, \omega)) = \mathrm{vol}(\mathrm{NP}(h))$ is [AS97, Theorem 1.4].   ∎

We reiterate that the equality (3.2.13) holds for arbitrary choices of f, since no extra assumptions are needed in Theorem 3.2.5. The equality $|\chi(X)| = \mathrm{vol}(\mathrm{NP}(h))$ needs the assumptions from [AS97, Theorem 1.4] discussed above. We illustrate this with an example.

Example 3.2.8 ($n = 2, \ell = 1$)**.** We consider the very affine surface $X = (\mathbb{C}^*)^2 \setminus V(f)$ with

$$f = -xy^2 + 2xy^3 + 3x^2y - x^2y^3 - 2x^3y + 3x^3y^2. \tag{3.2.14}$$

The polynomial h in $n + \ell = 3$ variables is given by $z \cdot f$. The Newton polytope $\mathrm{NP}(h)$ is the convex hull of the six exponents. It has dimension $n + \ell - 1 = 2$, and is contained in the plane with third coordinate equal to 1. This is shown in dark blue color in Figure 3.7. Appending the origin results in a hexagonal pyramid with Euclidean volume 1. Multiplying by $(n + \ell)! = 6$ gives $\mathrm{vol}(\mathrm{NP}(h))$. We will compute in Subsection 3.2.4 that $\chi(X) = 6$. Now consider

$$f = -xy^2 + xy^3 + x^2 y - x^2 y^3 - x^3 y + x^3 y^2 = xy(x-1)(y-1)(x-y). \qquad (3.2.15)$$

The polytope $\mathrm{NP}(h)$ did not change. The very affine variety X is the complement of an arrangement of five lines in $\mathbb{C}^2$, shown in Figure 3.1. Its Euler characteristic is 2, which is the number of bounded regions in that figure, and the number seen in entry $(k = 3, m = 4)$ of Table 3.1. The discrepancy $2 < 6$ is due to the fact that h is now no longer non-degenerate with respect to $\mathrm{NP}(h)$. The vanishing of the principal $\mathcal{A}$-determinant at h follows from $h = \frac{\partial h}{\partial x} = \frac{\partial h}{\partial y} = \frac{\partial h}{\partial z} = 0$ at the point $(x, y, z) = (1, 1, 1)$.
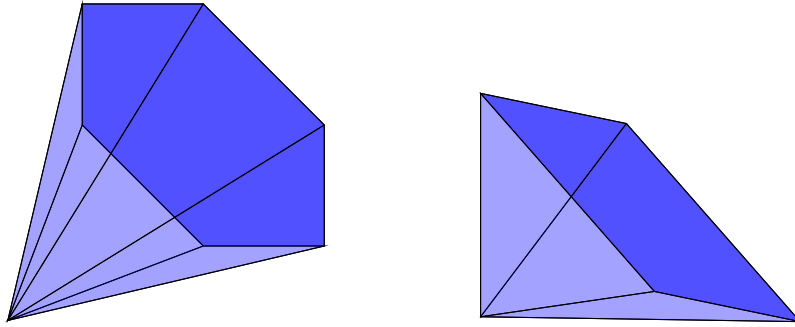
Figure 3.7. The polytopes $\mathrm{NP}(h)$ and $\mathrm{Conv}(\{0\} \cup \mathrm{NP}(h))$ from Example 3.2.8 (left) and Example 3.2.10 (right).

In what follows, we show how the twisted de Rham complex $(\Omega^\bullet_X(X), \nabla_\omega)$ leads to $\mathbb{C}$-linear relations among the functions $I_{a,b} : [\Gamma] \mapsto I_{a,b}(\Gamma)$ spanning the vector space V_Γ. In the proof of Lemma 3.2.4, we have used the perfect pairing (3.2.10) between homology and cohomology. The isomorphism $H^n(X, \omega) \simeq \mathrm{Hom}_{\mathbb{C}}(H_n(X, \omega), \mathbb{C})$ is explicitly given by $[f^a x^b \frac{dx}{x}] \mapsto I_{a,b}$. From this we conclude that for all complex constants $C_{a,b}$

$$
\begin{aligned}
\sum_{a,b} C_{a,b} \cdot I_{a,b} = 0 \text{ in } V_\Gamma \;\Longleftrightarrow\; & \left[\sum_{a,b} C_{a,b} \cdot f^a x^b \frac{dx}{x} \right] = 0 \text{ in } H^n(X, \omega) \\
\Longleftrightarrow\; & \sum_{a,b} C_{a,b} \cdot f^a x^b \frac{dx}{x} \in \mathrm{im}(\nabla_\omega).
\end{aligned}
\qquad (3.2.16)
$$

Hence for any $\phi \in \Omega^{n-1}_X(X)$, we find linear relations between the generators $I_{a,b}$ by expanding

$$\nabla_\omega(\phi) = \sum_{a,b} C_{a,b}(\phi) \cdot f^a x^b \frac{dx}{x}. \qquad (3.2.17)$$

Remark 3.2.9. In the physics literature, relations obtained in this way are commonly referred to as *IBP relations*. They are typically derived using Stokes' theorem in the setup of dimensional regularization, e.g. [Eti99, Proposition 12]. We stress that we deduce our relations exploiting purely cohomological arguments. See Appendix A for further details.

We clarify this procedure with two examples.

Example 3.2.10 (Example 3.2.2 continued)**.** Let $f = (x-1, x-2) \in \mathbb{C}[x, x^{-1}]^2$, so that $X = \mathbb{P}^1 \smallsetminus \{0, 1, 2, \infty\}$ is a punctured Riemann sphere with Euler characteristic $\chi(\mathbb{P}^1) - 4 = 2 - 4 = -2$. We can obtain this also via a volume computation by setting $h = xy - y + xz - 2z$. Appending 0 to $\mathrm{NP}(h)$ gives the pyramid shown in the right part of Figure 3.7. We compute $\mathrm{vol}(\mathrm{NP}(h)) = 2 = -\chi(X)$. For a concrete example of (3.2.17), we take s, ν as in Example 3.2.2 and set $\phi = 1$. Applying $\nabla_\omega = \mathrm{d} + \omega \wedge : \Omega^0_X(X) \to \Omega^1_X(X)$ with ω as in (3.2.8) to $1 \in \Omega^0_X(X)$, we get

$$\nabla_\omega(1) = \frac{1}{2} f_1^{-1} f_2^0 x^1 \frac{\mathrm{d}x}{x} + \frac{1}{2} f_1^0 f_2^{-1} x^1 \frac{\mathrm{d}x}{x} + \frac{1}{2} f_1^0 f_2^0 x^0 \frac{\mathrm{d}x}{x}.$$

In the notation (3.2.17), this means $C_{(-1,0),1}(1) = C_{(0,-1),1}(1) = C_{(0,0),0}(1) = \frac{1}{2}$. We remind the reader that this entails that, for every choice of the twisted cycle Γ, we have

$$\int_\Gamma \frac{\sqrt{(x-1)(x-2)x}}{x-1} \, \mathrm{d}x + \int_\Gamma \frac{\sqrt{(x-1)(x-2)x}}{x-2} \, \mathrm{d}x + \int_\Gamma \frac{\sqrt{(x-1)(x-2)x}}{x} \, \mathrm{d}x = 0.$$

In what follows, we denote by $x_{\widehat{k}} := x_1 \cdots x_{k-1} \cdot x_{k+1} \cdots x_n$ and by $\mathrm{d}x_{\widehat{k}}$ the $(n-1)$-form $\mathrm{d}x_{\widehat{k}} := \mathrm{d}x_1 \wedge \cdots \wedge \mathrm{d}x_{k-1} \wedge \mathrm{d}x_{k+1} \wedge \cdots \wedge \mathrm{d}x_n$, i.e., the (differential with respect to the) k-th coordinate is omitted. In this notation,

$$\frac{\mathrm{d}x_{\widehat{k}}}{x_{\widehat{k}}} = \frac{\mathrm{d}x_1}{x_1} \wedge \cdots \wedge \frac{\mathrm{d}x_{k-1}}{x_{k-1}} \wedge \frac{\mathrm{d}x_{k+1}}{x_{k+1}} \wedge \cdots \wedge \frac{\mathrm{d}x_n}{x_n} \quad \text{and} \quad \frac{\mathrm{d}x_{\widehat{k}}}{x} = \frac{\mathrm{d}x_{\widehat{k}}}{x_1 \cdots x_n}. \tag{3.2.18}$$

Example 3.2.11 ($\ell = 1$)**.** Let $f \in \mathbb{C}[x, x^{-1}]$ be a Laurent polynomial in n variables, and let $X = (\mathbb{C}^*)^n \smallsetminus V(f)$ be the associated very affine variety. For $1 \le k \le n$, consider the $(n-1)$-form $\phi = p \, f^a x^b \frac{\mathrm{d}x_{\widehat{k}}}{x} \in \Omega^{n-1}_X(X)$, with $p \in \mathbb{C}[x]$. Applying $\nabla_\omega = \mathrm{d} + \omega \wedge$ with ω as in (3.2.3) to ϕ, we obtain the following relation in $H^n(X, \omega)$:

$$\left(\frac{\partial p}{\partial x_k} f^a x^b + (a+s) p \frac{\partial f}{\partial x_k} f^{a-1} x^b + (b_k + \nu_k - 1) p f^a x^{b-e_k} \right) \frac{\mathrm{d}x}{x} = 0, \tag{3.2.19}$$

where $e_k \in \mathbb{N}^n$ denotes the k-th standard unit vector. By expanding p as a sum of monomials, the equivalence in (3.2.16) gives a linear relation among the integrals $I_{a,b}$.

For any regular $(n-1)$-form ϕ, the method illustrated above provides a relation among some of the $I_{a,b}$. However, this does not (directly) allow to compute a relation among a set of given generators $\{I_{a,b}\}_{(a,b) \in S}$, where $|S| > \chi(X)$. Doing so—using tools from numerical nonlinear algebra—is one of our topics in Subsection 3.2.4.

3.2.2. Mellin transform

Let $f = (f_1, \ldots, f_\ell) \in \mathbb{C}[x_1, \ldots, x_n]^\ell$ be a tuple of polynomials. This subsection studies the $\mathbb{C}(s, \nu)$-vector space

$$V_{s,\nu} := \mathrm{Span}_{\mathbb{C}(s,\nu)} \left\{ (s, \nu) \longmapsto \int_\Gamma f^{s+a} \, x^{\nu+b} \frac{\mathrm{d}x}{x} \right\}_{(a,b) \in \mathbb{Z}^\ell \times \mathbb{Z}^n}, \tag{3.2.20}$$

defined in the beginning of Section 3.2 . For the sake of simplicity, throughout this subsection, we denote the integral in (3.2.1) by $I_{a,b}$. It is to be read as a function of the variables $s \in \mathbb{C}^\ell$ and $\nu \in \mathbb{C}^n$. Hence, the vector space (3.2.20) can be equivalently expressed as

$$V_{s,\nu} = \sum_{(a,b) \in \mathbb{Z}^\ell \times \mathbb{Z}^n} \mathbb{C}(s, \nu) \cdot I_{a,b}. \tag{3.2.21}$$

We comment on how to interpret the functions $I_{a,b}$. For fixed general (s^*, ν^*), let $\Gamma(s^*, \nu^*)$ be a twisted cycle in $H_n(X, \omega(s^*, \nu^*))$. We here emphasize the dependence of ω from (3.2.3) on s, ν. To compute $I_{a,b}(s, \nu)$ for (s, ν) in a small open neighborhood of (s^*, ν^*), one integrates over the unique cycle $\Gamma(s, \nu)$ obtained from $\Gamma(s^*, \nu^*)$ by analytic continuation. That is, $I_{a,b}(s, \nu) = \langle [f^a x^b \frac{\mathrm{d}x}{x}], [\Gamma(s, \nu)] \rangle$, with $\langle \cdot, \cdot \rangle$ as in (3.2.10). This defines $I_{a,b}$ on an open neighborhood of some fixed (s^*, ν^*). The results in this subsection do not depend on the choice of (s^*, ν^*) or the choice of cycle $\Gamma(s^*, \nu^*)$. In what follows, we tacitly assume that these are fixed.

Throughout this subsection, we assume that $f = (f_1, \ldots, f_\ell)$ is a tuple of polynomials instead of Laurent polynomials. There is no loss of generality: for some $m \in \mathbb{N}^n$, $\tilde{f} := x^m f \in \mathbb{C}[x_1, \ldots, x_n]^\ell$ consists of polynomials. Let $\tilde{\nu} := \nu - m \cdot (s_1 + \cdots + s_\ell)$ so that $\mathbb{C}(s, \nu) = \mathbb{C}(s, \tilde{\nu})$. The $\mathbb{C}(s, \nu)$-vector space $V_{s,\nu}$ (3.2.20) is equal to the $\mathbb{C}(s, \tilde{\nu})$-vector space $V_{s,\tilde{\nu}}$ defined by $\tilde{f}$.

The key tool to determine the dimension of the vector space $V_{s,\nu}$ is the *Mellin transform*. This allows to connect the integrals $I_{a,b}$ with the language of differential and shift operators.

Definition 3.2.12. Let $f \in \mathbb{C}[x_1, \ldots, x_n]^\ell$ be a tuple of polynomials and fix $s \in \mathbb{C}^\ell$. We define the *Mellin transform* of f^s to be the function in the variables $\nu = (\nu_1, \ldots, \nu_n)$ given by

$$\mathfrak{M}\{f^s\}(\nu) := \int_\Gamma f^s x^\nu \frac{\mathrm{d}x}{x} = I_{0,0}(s, \nu), \qquad (3.2.22)$$

where $\Gamma := \Gamma(s, \nu) \in H_n(X, \omega(s, \nu))$ is a twisted cycle, as defined in Subsection 3.2.1.

The operator $\mathfrak{M}$ is naturally extended to functions $f^{s+a} x^b$, i.e., $\mathfrak{M}(f^{s+a} x^b) = I_{a,b}(s, \nu)$.

Lemma 3.2.13. *The Mellin transform obeys the following rules:*

$$\mathfrak{M}\{x_i \cdot f^s\}(\nu) = \mathfrak{M}\{f^s\}(\nu + e_i),$$
$$\mathfrak{M}\left\{x_i \cdot \frac{\partial f^s}{\partial x_i}\right\}(\nu) = -\nu_i \cdot \mathfrak{M}\{f^s\}(\nu). \qquad (3.2.23)$$

Proof. The first equality follows immediately from the definition. For the second, we again use the notation $\mathrm{d}x_{\widehat{i}} \in \Omega^{n-1}(X)$ introduced in (3.2.18) and write out

$$\mathfrak{M}\left\{x_i \cdot \frac{\partial f^s}{\partial x_i}\right\}(\nu) = \int_\Gamma \frac{\partial f^s}{\partial x_i} x^{\nu + e_i} \frac{\mathrm{d}x}{x} = \int_\Gamma \sum_{j=1}^n s_j \frac{1}{f_j} \frac{\partial f_j}{\partial x_i} f^s x^{\nu + e_i} \frac{\mathrm{d}x}{x}$$

$$= (-1)^{i-1} \int_\Gamma \mathrm{d}\left(f^s x^\nu \frac{\mathrm{d}x_{\widehat{i}}}{x_{\widehat{i}}}\right) - \nu_i \cdot \mathfrak{M}(f^s)(\nu),$$

where the last equality follows from Leibniz' rule. An explicit computation shows that $(-1)^{i-1}\mathrm{d}(f^s x^\nu \frac{\mathrm{d}x_{\widehat{i}}}{x_{\widehat{i}}}) = f^s x^\nu \nabla_\omega(\frac{\mathrm{d}x_{\widehat{i}}}{x_{\widehat{i}}})$, hence

$$(-1)^{i-1} \cdot \int_\Gamma \mathrm{d}\left(f^s x^\nu \frac{\mathrm{d}x_{\widehat{i}}}{x_{\widehat{i}}}\right) = \left\langle [\Gamma], \left[\nabla_\omega\left(\frac{\mathrm{d}x_{\widehat{i}}}{x_{\widehat{i}}}\right)\right]\right\rangle = 0$$

by the perfect pairing introduced in (3.2.10). This proves the second equality in (3.2.23). ∎

Therefore, the Mellin transform turns multiplication by $x_i^{\pm 1}$ into shifting the new variable ν_i by ± 1 and the action of the ith Euler operator $\theta_i := x_i \partial_i$ into multiplication by $-\nu_i$.

The techniques we are going to use to study the vector space $V_{s,\nu}$ come from D-module and Bernstein–Sato theory. The basic definitions can be found in Section 1.2. In the study of the Mellin transform, we will use algebras of *shift operators*—also commonly called *finite difference operators*—with polynomial coefficients.

Definition 3.2.14. The (n-th) *shift algebra* with polynomial coefficients

$$S_n := \mathbb{C}[\nu_1, \ldots, \nu_n]\langle \sigma_1^{\pm 1}, \ldots, \sigma_n^{\pm 1}\rangle$$

is the free $\mathbb{C}$-algebra generated by $\{\nu_i, \sigma_i, \sigma_i^{-1}\}_{i=1,\ldots,n}$ modulo the following relations: all generators commute, except ν_i and the shift-operators σ_i. They obey the rule

$$\sigma_i^{\pm 1}\nu_i = (\nu_i \pm 1)\sigma_i^{\pm 1}. \tag{3.2.24}$$

This implies that $\sigma^a \nu^b = (\nu + a)^b \sigma^a$ for any $a \in \mathbb{Z}^n$, $b \in \mathbb{N}^n$, where we use multi-index notation, e.g., $(\nu + a)^b = (\nu_1 + a_1)^{b_1} \cdots (\nu_n + a_n)^{b_n}$. The shift algebra naturally comes into play when studying the Mellin transform of functions. Mimicking the rules in Equation (3.2.23), the *(algebraic) Mellin transform* (cf. [LS91b]) is the isomorphism of $\mathbb{C}$-algebras

$$\mathfrak{M}\{\cdot\} \colon D_{\mathbb{G}_m^n} \longrightarrow S_n, \quad x_i^{\pm 1} \mapsto \sigma_i^{\pm 1}, \ \theta_i \mapsto -\nu_i, \tag{3.2.25}$$

where $D_{\mathbb{G}_m^n}$ is the global ring of differential operators introduced in Equation (1.2.3). We conventionally use the notation $\mathfrak{M}\{\cdot\}$ both for the Mellin transform of *functions* (Definition 3.2.12) and that of *operators* (Equation (3.2.25)). Note that $\mathfrak{M}\{\cdot\}$ naturally extends to an isomorphism of $D_{\mathbb{G}_m^n}[s_1, \ldots, s_\ell]$ and $S_n[s_1, \ldots, s_\ell]$ by mapping s_j to itself.

Remark 3.2.15. Via the map $\mathfrak{M}\{\cdot\}$, one can also define the Mellin transform $\mathfrak{M}\{M\}$ of a $D_{\mathbb{G}_m^n}$-module M. It is the following module over S_n. As abelian groups, $\mathfrak{M}\{M\} = M$, and S_n acts by $\nu_i \bullet m := -\theta_i \bullet m$ and $\sigma_i^{\pm 1} \bullet m := x_i^{\pm 1} \bullet m$ for $m \in M$, $i = 1, \ldots, n$.

Let us first assume $\ell = 1$. Let $b_f \in \mathbb{C}[s]$ denote the Bernstein–Sato polynomial of $f \in \mathbb{C}[x_1, \ldots, x_n]$. Therefore, there exists an operator $P_f \in D_n[s]$ such that

$$P_f(s) \bullet f^{s+1} = b_f(s) \cdot f^s. \tag{3.2.26}$$

Applying the Mellin transform to both sides of Equation (3.2.26) yields

$$b_f(s) \cdot \mathfrak{M}\{f^s\} = \mathfrak{M}\{P_f\} \bullet \mathfrak{M}\{f^{s+1}\}. \tag{3.2.27}$$

We refer to this relation as being *lowering in s*. This means that it provides a way for writing the integral $I_{0,0}(s, \nu)$ as a linear combination of integrals of type $I_{0,b}(s+1, \nu)$ for some $b \in \mathbb{Z}^n$. One obtains a *raising* relation by the simple trick of considering $f \in \mathbb{C}[x]$ as a differential operator of order 0:

$$\mathfrak{M}\{f^{s+1}\} = \mathfrak{M}\{f \cdot f^s\} = \underbrace{\mathfrak{M}\{f\}}_{\in S_n} \bullet \mathfrak{M}\{f^s\}. \tag{3.2.28}$$

Moreover, for any operator $P \in \mathrm{Ann}_{D_n[s]}(f^s)$, (see Equation (1.2.5))applying the Mellin transform to the equation $P \bullet f^s = 0$, one attains a $\mathbb{C}(s, \nu)$-linear relation among integrals $I_{a,b}$. The following example shows how to compute this ideal in practice.

Example 3.2.16. Let $f = (x - 1)(x - 2) \in \mathbb{C}[x]$. As showed in Example 1.2.10, in this case, the $D_n[s]$-ideal $\mathrm{Ann}_{D_n[s]}(f^s)$ is generated by the operator $P = f \partial_x - s \partial_x \bullet f$. A linear relation in $V_{s,\nu}$ among integrals of the form $I_{a,b}$ can be attained by expanding the equation $\mathfrak{M}\{P\} \bullet \mathfrak{M}\{f^s\} = 0$. The same relation is given with the method as in Example 3.2.2 by taking the 0-form $\phi = f$.

Proposition 3.2.17. *Fix $f \in \mathbb{C}[x_1, \ldots, x_n]$ and $\Gamma \in H_n(X, \omega)$. The following $\mathbb{C}(s, \nu)$-vector spaces coincide:*

$$V_{s,\nu} = \sum_{a \in \mathbb{Z}^\ell} \mathbb{C}(s, \nu) \otimes_{\mathbb{C}[s,\nu]} (S_n \bullet I_{a,0}) = \mathbb{C}(s, \nu) \otimes_{\mathbb{C}[s,\nu]} (S_n[s] \bullet I_{0,0}).$$

Proof. The first equality follows from $\sigma^b \bullet I_{a,0} = I_{a,b}$. The second equality follows from the fact that via the Mellin transform, one obtains both lowering and increasing shift relations in s as in Equations (3.2.27) and (3.2.28).   ∎

This statement is contained in [BBKP19] for the special case that $\Gamma = \mathbb{R}_{>0}^n$ and f is a polynomial. Elements of a basis of $V_{s,\nu}$ are called *master integrals* in physics literature. We now present the main result of [BBKP19], which relates the number of master integrals to the topological Euler characteristic of our very affine variety for the case $\ell = 1$.

Theorem 3.2.18 ([BBKP19, Corollary 37])**.** *The dimension of $V_{s,\nu}$ is given by the signed topological Euler characteristic of the hypersurface complement $(\mathbb{C}^*)^n \smallsetminus V(f)$, i.e.,*

$$\dim_{\mathbb{C}(s,\nu)}(V_{s,\nu}) = (-1)^n \cdot \chi\left((\mathbb{C}^*)^n \smallsetminus V(f)\right).$$

The proof of this statement in [BBKP19, Section 3] builds on work of Loeser and Sabbah [LS91a, LS92]. Interested readers can find more details in the proof of Theorem 3.2.23, in which we generalize Theorem 3.2.18 to arbitrary $\ell > 1$.

The following example illustrates how to obtain shift relations among integrals when $f \in \mathbb{C}[x_1 \ldots, x_n]$ is smooth, starting from a Bernstein–Sato operator. We also exhibit the $(n-1)$-form to which the very same relation corresponds via the method presented in Subsection 3.2.1.

Example 3.2.19. Let $f \in \mathbb{C}[x_1, \ldots, x_n]$ be smooth. Hence $b_f = (s+1) \in \mathbb{C}[s]$. Since f and its partial derivatives are coprime, there exist polynomials $p_1, \ldots, p_n, q \in \mathbb{C}[x]$ such that $(\sum_{k=1}^n p_k \partial_k \bullet f) + qf = 1$. Then $P_f = (\sum_k p_k \partial_k) + b_f q \in D_n[s]$ is a Bernstein–Sato operator of f since

$$P_f \bullet f^{s+1} = (s+1)f^s \cdot \sum_{k=1}^n p_k \frac{\partial f}{\partial x_k} + (s+1)q \cdot f^{s+1}$$

$$= (s+1) \cdot \big(\underbrace{\sum_{k=1}^n p_k \frac{\partial f}{\partial x_k} + qf}_{=1}\big) \cdot f^s = b_f \cdot f^s.$$

Hence $P_f f - b_f \in \mathrm{Ann}_{D_n[s]}(f^s)$. Given a polynomial $p \in \mathbb{C}[x]$, we denote by $p(\sigma)$ its image under the isomorphism (3.2.25). The Mellin transform of P_f is

$$\mathfrak{M}\{P_f\} = \sum_{k=1}^n \left((1-\nu_k)p_k(\sigma)\sigma_k^{-1} - \frac{\partial p_k}{\partial x_k}(\sigma)\right) + (s+1)q(\sigma) \in S_n[s].$$

Applying the Mellin transform to Equation (3.2.26) induces the shift relation

$$\sum_{k=1}^n \left((1-\nu_k)p_k(\sigma)\sigma_k^{-1} - \frac{\partial p_k}{\partial x_k}(\sigma)\right) \bullet \mathfrak{M}\{f^{s+1}\} + (s+1)q(\sigma) \bullet \mathfrak{M}\{f^{s+1}\} = (s+1)\mathfrak{M}\{f^s\}.$$

Expanding this equality, one obtains a $\mathbb{C}(s,\nu)$-linear combination of integrals of type (3.2.20). Precisely the same relation among integrals is attained with the method illustrated in (3.2.16) for the $(n-1)$-form $\phi = f \cdot \sum_{k=1}^n p_k \frac{\mathrm{d}x_{\widehat{k}}}{x} \in \Omega_X^{n-1}(X)$. The image under ∇_ω of a single summand of ϕ is displayed in Equation (3.2.19). The correspondence between annihilating operators and $(n-1)$-forms is stated more clearly in the next result.

Proposition 3.2.20. *Let $\ell = 1$ and consider a differential operator $P \in \mathrm{Ann}_{D_n[s]}(f^s)$ which is of degree at most 1 in $\partial_1, \ldots, \partial_n$, i.e.,*

$$P = \sum_{i=1}^{n} p_i(x, s) \cdot \partial_i + q(x, s), \quad \text{where } p_1, \ldots, p_n, q \in \mathbb{C}[x_1, \ldots, x_n, s].$$

Then the equalities $\mathfrak{M}\{P\} \bullet \mathfrak{M}\{f^s\} = 0$ and (3.2.16) with $\phi = \sum_{i=1}^{n}(-1)^{i-1} p_i \frac{\mathrm{d}x_{\hat{i}}}{x}$ lead to the same linear relation of integrals $I_{a,b}$.

Proof. Since $P \in \mathrm{Ann}_{D_n[s]}(f^s)$, we can determine the polynomial q in terms of the p_i:

$$\left(\sum_{i=1}^{n} s_i p_i f^{s-1} \partial_i \bullet f \right) f^s + q f^s = 0 \iff q = -\sum_{i=1}^{n} s_i p_i f^{s-1} \partial_i \bullet f.$$

An explicit computation shows that the relation obtained from $\mathfrak{M}\{P \bullet f^s\} = 0$, where

$$\mathfrak{M}\{P\} = -\left(\sum_{i=1}^{n}(\nu_i - 1) p_i(\sigma) \sigma_i^{-1} + \sum_{i=1}^{n} \frac{\partial p_i}{\partial x_i}(\sigma) + s \frac{1}{f(\sigma)} \sum_{i+1}^{n} \frac{\partial f}{\partial x_i}(\sigma) p_i(\sigma) \right), \quad (3.2.29)$$

coincides with the one in cohomology obtained from (3.2.17). This is immediate when computing explicitly

$$\nabla_\omega \left(\sum_{i=1}^{n}(-1)^{i-1} p_i \frac{\mathrm{d}x_{\hat{i}}}{x} \right) = \left(\sum_{i=1}^{n}(\nu_i - 1) p_i x_i^{-1} + \sum_{i=1}^{n} \frac{\partial p_i}{\partial x_i} + s \frac{1}{f} \sum_{i=1}^{n} \frac{\partial f}{\partial x_i} p_i \right) \frac{\mathrm{d}x}{x},$$

where $\nabla_\omega(\phi) = \mathrm{d}\phi + \omega \wedge \phi$, and ω is our 1-form from (3.2.3). To be precise, in this last computation, we take $s = s^*$ and $\nu = \nu^*$ to be fixed, general complex numbers. The coefficients $C_{a,b}(\phi)$ in the relation (3.2.17) are obtained from evaluating the rational function coefficients of $I_{a,b}$ in $\mathfrak{M}\{P\} \bullet \mathfrak{M}\{f^s\} = 0$ at $(s, \nu) = (s^*, \nu^*)$. ∎

For $\ell > 1$ polynomials $f_1, \ldots, f_\ell$, one needs to study Bernstein–Sato *ideals* instead. These where introduced in Subsection 1.2.2. However, in (1.2.7), no individual shifts in the variables s_i can be taken into account; only a simultaneous shift by the all-one vector. A remedy is provided by the following ideals of Bernstein–Sato type, which also enter the study of the monodromy conjecture in [BvdVVW21, BvdVWZ21].

Definition 3.2.21. Let $a \in \mathbb{N}^\ell$ be a non-negative integer vector. The *a-Bernstein–Sato ideal* of $(f_1, \ldots, f_\ell)$ is the ideal $B^a_{(f_1, \ldots, f_\ell)} \lhd \mathbb{C}[s_1, \ldots, s_\ell]$ consisting of all polynomials $p \in \mathbb{C}[s_1, \ldots, s_\ell]$ for which there exists $P \in D_n[s_1, \ldots, s_\ell]$ such that

$$P \bullet \left(f_1^{s_1 + a_1} \cdots f_\ell^{s_\ell + a_\ell} \right) = p \cdot f_1^{s_1} \cdots f_\ell^{s_\ell}. \quad (3.2.30)$$

Again by [Sab87], the *a*-Bernstein–Sato ideal is non-trivial. In this notation, for $a = (1, \ldots, 1)$ the all-one vector, $B^{(1, \ldots, 1)}_{(f_1, \ldots, f_\ell)} = B_{(f_1, \ldots, f_\ell)}$. At present, the computation of *a*-Bernstein–Sato ideals using computer algebra software is out of reach. Yet, we can use *a*-Bernstein–Sato ideals to generalize Proposition 3.2.17 to a tuple of ℓ polynomials as follows.

Proposition 3.2.22. *Fix $\Gamma \in H_n(X, \omega)$ and let $f_1, \ldots, f_\ell \in \mathbb{C}[x_1, \ldots, x_n]$. The following $\mathbb{C}(s, \nu) = \mathbb{C}(s_1, \ldots, s_\ell, \nu_1, \ldots, \nu_n)$-vector spaces coincide:*

$$\begin{aligned}
V_{s,\nu} &= \sum_{(a,b) \in \mathbb{Z}^\ell \times \mathbb{Z}^n} \mathbb{C}(s, \nu) \cdot I_{a,b} = \sum_{a \in \mathbb{Z}^\ell} \mathbb{C}(s, \nu) \otimes_{\mathbb{C}[s,\nu]} (S_n \bullet I_{a,0}) \\
&= \mathbb{C}(s, \nu) \otimes_{\mathbb{C}[s,\nu]} (S_n[s_1, \ldots, s_\ell] \bullet I_{0,0}).
\end{aligned} \quad (3.2.31)$$

Proof. Let $e_i \in \mathbb{N}^\ell$ denote the i-th standard unit vector. Then

$$\mathfrak{M}\{f^{s+e_i}\} = \mathfrak{M}\{f_i \cdot f^s\} = \mathfrak{M}\{f_i\} \bullet \mathfrak{M}\{f^s\}$$

is an increasing relation in s_i. To construct lowering relations in the s_i, we study a-Bernstein–Sato ideals for $a = e_i$. Applying the Mellin transform to both sides of Equation (3.2.30) yields

$$\mathfrak{M}\{P\} \bullet \mathfrak{M}\{f^{s+e_i}\} = p \cdot \mathfrak{M}\{f^s\},$$

a lowering shift relation in s_i. ∎

With those tools at hand, we can now generalize Theorem 3.2.18 to $\ell > 1$. Denote by $D_n(s) \coloneqq D_n[s] \otimes_{\mathbb{C}[s]} \mathbb{C}(s)$ the n-th Weyl algebra over the field $\mathbb{C}(s) = \mathbb{C}(s_1, \ldots, s_\ell)$.

Theorem 3.2.23. *Let $f \in \mathbb{C}[x_1, \ldots, x_n]^\ell$ and denote by $\mathcal{M}$ the $D_n(s)$-module $D_n(s) \bullet f^s$. Then*

$$\dim_{\mathbb{C}(s,\nu)} (V_{s,\nu}) = |\chi(\iota^* \mathcal{M})| = |\chi((\mathbb{C}^*)^n \smallsetminus V(f_1 \cdots f_\ell))|,$$

where $\iota \colon \mathbb{G}^n_{\mathbb{C}(s),m} \hookrightarrow \mathbb{A}^n_{\mathbb{C}(s)}$ denotes the embedding of the algebraic n-torus over $\mathbb{C}(s)$ into the affine n-space over $\mathbb{C}(s)$, and $\iota^* \mathcal{M}$ is the D-module pullback of $\mathcal{M}$ via ι.

Proof. We first prove that $\iota^* \mathcal{M} = \mathcal{M}[x^{-1}] = D_{\mathbb{G}^n_m}(s) \bullet f^s$ is holonomic. Note that the operator

$$P_i(s) \coloneqq f_1 \cdots f_\ell \cdot \partial_i - \sum_{j=1}^\ell s_j f_{\widehat{j}} \frac{\partial f_j}{\partial x_i} \in \mathrm{Ann}_{D_n[s_1, \ldots, s_\ell]}(f^s)$$

annihilates $f^s = f_1^{s_1} \cdots f_\ell^{s_\ell}$ for all $i = 1, \ldots, n$, where $f_{\widehat{j}}$ denotes $f_1 \cdots f_{j-1} \cdot f_{j+1} \cdots f_\ell$. Denote by I the $D_n[s]$-ideal generated by $P_1(s), \ldots, P_n(s)$. Clearly, $I \subseteq \mathrm{Ann}_{D_n[s]}(f^s)$. Hence, for every $s^* \in \mathbb{C}^\ell$, the D_n-ideal $I_{s^*} \coloneqq \langle P_1(s^*), \ldots, P_n(s^*) \rangle$ has finite holonomic rank and therefore its Weyl closure $W(I_{s^*}) = R_n I_{s^*} \cap D_n$ is holonomic by [SST00, Theorem 1.4.15]. Since $I_{s^*} \subseteq W(I_{s^*}) \subseteq \mathrm{Ann}_{D_n}(f^{s^*})$, this proves that for all $s^* \in \mathbb{C}^\ell$, the D_n-ideal $\mathrm{Ann}_{D_n}(f^{s^*})$ is holonomic. Hence $D_n(s) \bullet f^s \cong D_n(s)/\mathrm{Ann}_{D_n(s)}(f^s)$ is a holonomic $D_n(s)$-module. Now denote by $D_{\mathbb{G}^n_m}(s) = D_{\mathbb{G}^n_m}[s] \otimes_{\mathbb{C}[s]} \mathbb{C}(s)$ the Weyl algebra over the algebraic n-torus over $\mathbb{C}(s)$. By [HTT08, Theorem 3.2.3], also the $D_{\mathbb{G}^n_m}(s)$-module $\iota^* \mathcal{M} = \mathcal{M}[x^{-1}] = D_{\mathbb{G}^n_m}(s)/\mathrm{Ann}_{D_{\mathbb{G}^n_m}(s)}(f^s)$ is holonomic. Therefore, by a classical result of Kashiwara, its solution complex—or, equivalently, its de Rham complex—is an element of the bounded derived category of constructible sheaves. Therefore, $\iota^* \mathcal{M}$ has finite Euler characteristic by Kashiwara's index theorem for constructible sheaves [Kas85].

For the rest of the proof, we follow and adapt the strategy of proof of [BBKP19, Section 3] to the case $\ell > 1$. The next step is to show that $\dim_{\mathbb{C}(s,\nu)}(V_{s,\nu})$ equals the Euler characteristic of the de Rham complex of $\iota^* \mathcal{M}$. Recall that $\mathrm{Ann}_{D_{\mathbb{G}^n_m}[s]}(f^s)$ turns into $\mathrm{Ann}_{S_n[s]}(I_{0,0})$ via the Mellin transform (3.2.25). By Proposition 3.2.22, we hence obtain the equality

$$\begin{aligned}
\dim_{\mathbb{C}(s,\nu)} (V_{s,\nu}) &= \dim_{\mathbb{C}(s,\nu)} \left(\mathbb{C}(s,\nu) \otimes_{\mathbb{C}[s,\nu]} (S_n[s] \bullet I_{0,0}) \right) \\
&= \dim_{\mathbb{C}(s,\theta)} \left(\mathbb{C}(s,\theta) \otimes_{\mathbb{C}[s,\theta]} (D_{\mathbb{G}^n_m}[s] \bullet f^s) \right),
\end{aligned}$$

where $\theta = (\theta_1, \ldots, \theta_n)$. By [LS92, Théorème 2] and noting that we work over the torus over $\mathbb{C}(s)$,

$$\dim_{\mathbb{C}(s,\theta)} \left(\mathbb{C}(s,\theta) \otimes_{\mathbb{C}[s,\theta]} (D_{\mathbb{G}^n_m}[s] \bullet f^s) \right) = \chi(\iota^* \mathcal{M}).$$

Now note that each element of $D_{\mathbb{G}_m^n}(s) \bullet f^s$ can be uniquely written as $h \cdot f^s$ for some $h \in \mathbb{C}(s)[x^{\pm 1}, f_1^{-1}, \ldots, f_\ell^{-1}]$. The natural action of $D_{\mathbb{G}_m^n}(s)$ on $\iota^* \mathcal{M}$ is given by

$$\partial_i \bullet (h f^s) = \frac{\partial h}{\partial x_i} f^s + \sum_{j=1}^{\ell} h s_j \frac{1}{f_j} \frac{\partial f_j}{\partial x_i} f^s.$$

Moreover, the morphism

$$D_{\mathbb{G}_m^n}(s) \bullet f^s \longrightarrow \mathbb{C}(s) \left[x^{\pm 1}, f_1^{-1}, \ldots, f_\ell^{-1} \right], \quad h \cdot f^s \mapsto h$$

is an isomorphism of $\mathbb{C}(s)[x^{\pm 1}]$-modules. It remains to prove that $\chi(\iota^* \mathcal{M})$ is equal to the signed Euler characteristic of $(\mathbb{C}^*)^n \smallsetminus V(f_1 \cdots f_\ell)$. For that, we first prove that the $D_{\mathbb{G}_m^n}(s)$-module $\iota^* \mathcal{M}$ and the D_n-module $\mathbb{C}[x^{\pm 1}, f_1^{-1}, \ldots, f_\ell^{-1}]$ have the same Euler characteristic.

Denote by $\mathcal{N}$ the D_n-module $\mathbb{C}[x^{\pm 1}]$ and by $\mathcal{N}[f^{-1}] = \mathcal{N}[f_1^{-1}, \ldots, f_\ell^{-1}]$. Then $D_{\mathbb{G}_m^n} \bullet f^s$ and $\mathcal{N}[f^{-1}][s]$ are isomorphic as $\mathbb{C}$-vector spaces. We now introduce new variables $t_1, \ldots, t_\ell$ that commute with $x_1, \ldots, x_n$ and consider $D_{\mathbb{G}_m^n} \bullet f^s$ as module over $D_{\mathbb{G}_m^{n+\ell}} = \mathbb{C}[x^{\pm 1}, t^{\pm 1}]\langle \partial_x, \partial_t \rangle$ via

$$t_i^{\pm 1} \bullet (n(s) f^s) := n(s \pm e_i) f^s f_i^{\pm 1} \quad \text{and} \quad \partial_{t_i} \bullet (n(s) f^s) := -s_i \cdot n(s - e_i) f^s \frac{1}{f_i}. \tag{3.2.32}$$

Since $\partial_{t_i} t_i = -s_i$, the following $D_{\mathbb{G}_m^{n+\ell}}$-modules are isomorphic by the rules in (3.2.32):

$$\left(\left(\left(D_{\mathbb{G}_m^n} \bullet f^s / \partial_{t_\ell} \bullet \left(D_{\mathbb{G}_m^n} \bullet f^s \right) \right) / \partial_{t_{\ell-1}} \bullet \left[D_{\mathbb{G}_m^n} \bullet f^s \right] \right) / \cdots \right) / \partial_{t_1} \bullet \left[D_{\mathbb{G}_m^n} \bullet f^s \right]$$

$$= \frac{D_{\mathbb{G}_m^n} \bullet f^s}{\partial_{t_1} \bullet \left(D_{\mathbb{G}_m^n} \bullet f^s \right) + \cdots + \partial_{t_\ell} \bullet \left(D_{\mathbb{G}_m^n} \bullet f^s \right)}$$

$$= \frac{D_{\mathbb{G}_m^n} \bullet f^s}{s_1 t_1^{-1} \bullet \left(D_{\mathbb{G}_m^n} \bullet f^s \right) + \cdots + s_\ell t_\ell^{-1} \bullet \left(D_{\mathbb{G}_m^n} \bullet f^s \right)}$$

$$= \frac{D_{\mathbb{G}_m^n} \bullet f^s}{s_1 \cdot D_{\mathbb{G}_m^n} \bullet f^s + \cdots + s_\ell \cdot D_{\mathbb{G}_m^n} \bullet f^s} \cong \mathcal{N}[f^{-1}].$$

Since ∂_{t_ℓ} is injective on $D_{\mathbb{G}_m^n} \bullet f^s$, the proof of [BBKP19, Theorem 35] shows that $\chi(D_{\mathbb{G}_m^n} \bullet f^s) = \chi(D_{\mathbb{G}_m^n} \bullet f^s / \partial_{t_\ell} \bullet (D_{\mathbb{G}_m^n} \bullet f^s))$. By iterating this reasoning, we conclude that

$$\chi \left(D_{\mathbb{G}_m^n} \bullet f^s \right) = \chi \left(\mathcal{N}[f^{-1}] \right). \tag{3.2.33}$$

Now denote by $\mathfrak{M}^t \{ D_{\mathbb{G}_m^n} \bullet f^s \}$ the Mellin transform of $D_{\mathbb{G}_m^n} \bullet f^s$ with respect to the variables $t_1, \ldots, t_\ell$. Then $\mathfrak{M}^t \{ D_{\mathbb{G}_m^n} \bullet f^s \}(s) \cong (D_{\mathbb{G}_m^n} \bullet f^s)(t_1 \partial_{t_1}, \ldots, t_\ell \partial_{t_\ell})$, since tensoring with $\mathbb{C}(t \partial_t)$ just extends the coefficients to $\mathbb{C}(s)$. Again by [LS92],

$$\chi \left(D_{\mathbb{G}_m^n} \bullet f^s \right) = \dim_{\mathbb{C}(\theta, t\partial_t)} \left(\left(D_{\mathbb{G}_m^n} \bullet f^s \right) (\theta, t\partial_t) \right) = \dim_{\mathbb{C}(\theta, s)} \left(\left(D_{\mathbb{G}_m^n} \bullet f^s \right) (s, t\partial_t) \right)$$

$$= \dim_{\mathbb{C}(s, \theta)} \left(\mathfrak{M}^t (D_{\mathbb{G}_m^n} \bullet f^s)(s, \theta) \right) = \chi \left(\mathfrak{M}^t \left(D_{\mathbb{G}_m^n} \bullet f^s \right) (s) \right),$$

see in particular [BBKP19, Theorem 35] for the first equality. Therefore,

$$\mathfrak{M}^t (D_{\mathbb{G}_m^n} \bullet f^s)(s) \cong \mathbb{C}(s)[x^{\pm 1}, f_1^{-1}, \ldots, f_\ell^{-1}] \cdot f^s$$

is $\iota^* \mathcal{M}$. Hence, by (3.2.33), $\chi(\iota^* \mathcal{M}) = \chi(\mathbb{C}[x^{\pm 1}, f_1^{-1}, \ldots, f_\ell^{-1}])$, concluding the proof. ∎

Remark 3.2.24. Alternatively, one can prove Theorem 3.2.23 by an inductive argument. We demonstrate how to reduce the proof of the statement from ℓ to $\ell - 1$ polynomials. Let $\mathcal{M}$ be a D_n-module and $f_1, f_2 \in \mathbb{C}[x_1, \ldots, x_n]$ two polynomials. Consider the module $\mathcal{M}_1 :=$

$\mathcal{M}[f_1^{-1}]$. By applying [BBKP19, Equation (3.13)] to $\mathcal{M}_1$, we see that $\chi(\mathcal{M}_1[s_2, f_2^{-1}]f_2^{s_2}) = \chi(\mathcal{M}_1[f_2^{-1}])$. More precisely, one gets

$$\chi(\mathcal{M}[s_2, f_1^{-1}, f_2^{-1}]f_2^{s_2}) = \chi(\mathcal{M}[f_1^{-1}, f_2^{-1}]).$$

Now denote $\mathcal{M}_2 := \mathcal{M}[s_2, f_2^{-1}]f_2^{s_2}$. Again by [BBKP19, (3.13)], we get that $\chi(\mathcal{M}_2[f_1^{-1}]) = \chi(\mathcal{M}_2[s_1, f_1^{-1}]f_1^{s_1})$ and hence

$$\chi(\mathcal{M}[s_1, s_2, f_1^{-1}, f_2^{-1}]f_1^{s_1}f_2^{s_2}) = \chi(\mathcal{M}[f_1^{-1}, f_2^{-1}]).$$

Iterating this process and setting $\mathcal{M}$ to be $\mathbb{C}[x_1^{\pm 1}, \dots, x_n^{\pm 1}]$ concludes the reasoning.

3.2.3. GKZ systems

It is well known that generalized Euler integrals provide a full description of the solutions to systems of linear PDEs called *GKZ systems* or *A-hypergeometric systems* [GKZ90]. Recent works by Matsubara-Heo and Takayama [MH22, MH20, MH21, MHT22] expose connections with the previous subsections. In what follows, we review some of these results and demonstrate how to compute with GKZ systems.

Throughout this subsection, we consider the parameters $\nu \in \mathbb{C}^n$, $s \in \mathbb{C}^\ell$, and the integers $a = b = 0$ to be fixed. We view the integrals (3.2.1) as functions of the coefficients of the Laurent polynomials f_j. Before making this precise, we introduce some additional notation.

We fix finite subsets $\{A_j\}_{j=1,\dots,\ell}$ of $\mathbb{Z}^n$ representing the monomial supports of the f_j:

$$f_j(x; c_j) = \sum_{\alpha \in A_j} c_{\alpha,j} \, x^\alpha. \tag{3.2.34}$$

The parameters $c_j = (c_{\alpha,j})_{\alpha \in A_j}$ take values in $\mathbb{C}^{A_j} := \mathbb{C}^{|A_j|}$. The *Cayley configuration* of $\{A_j\}_{1 \leq j \leq \ell}$ is $\{(\alpha, e_j) \mid \alpha \in A_j\}$, given by the columns of the $(n + \ell) \times \sum_{j=1}^\ell |A_j|$ matrix

$$A = \begin{pmatrix} \overbrace{1 \quad \cdots \quad 1}^{A_1} & \overbrace{0 \quad \cdots \quad 0}^{A_2} & & \overbrace{0 \quad \cdots \quad 0}^{A_\ell} \\ 0 \quad \cdots \quad 0 & 1 \quad \cdots \quad 1 & \cdots & 0 \quad \cdots \quad 0 \\ \vdots & \vdots & & \vdots \\ 0 \quad \cdots \quad 0 & 0 \quad \cdots \quad 0 & & 1 \quad \cdots \quad 1 \end{pmatrix}. \tag{3.2.35}$$

Here, A_j is represented by an $n \times |A_j|$ matrix, and e_j is the j-th standard unit vector in $\mathbb{N}^\ell$. It will be convenient to view A as the disjoint union of $A_1, \dots, A_\ell$ and to collect all coefficients in a vector $c = (c_\alpha)_{\alpha \in A}$, with entries indexed by A. The parameters c take values in $\mathbb{C}^A := \mathbb{C}^{A_1} \times \cdots \times \mathbb{C}^{A_\ell} = \mathbb{C}^{|A_1| + \cdots + |A_\ell|}$.

The very affine variety X from (3.2.2) now depends on the choice of coefficients. We write

$$X(c) := (\mathbb{C}^*)^n \smallsetminus V\left(\prod_{j=1}^\ell f_j(x; c_j)\right). \tag{3.2.36}$$

For fixed $c^* \in \mathbb{C}^A$, let $\Gamma_{c^*} = \Delta \otimes_{\mathbb{C}} \phi_{c^*}$ be a cycle in the vector space $C_n(X(c^*), \mathcal{L}_{\omega(c^*)}^\vee)$ from the twisted chain complex introduced in Subsection 3.2.1. For c in a sufficiently small neighborhood $U_{c^*} \subset \mathbb{C}^A$ of c^*, the singular chain Δ is contained in $X(c)$ as well. The 1-form $\omega(c)$ depends rationally on c, and there is a unique section ϕ_c of $\mathcal{L}_{\omega(c)}^\vee$ such that ϕ_c

is obtained from ϕ_{c^*} by analytic continuation. Varying c in a small neighborhood U_{c^*}, we obtain a function

$$I_{\Gamma_{c^*}} := \left(c \mapsto \int_{\Gamma_{c^* \to c}} f(x;c)^s \, x^\nu \, \frac{\mathrm{d}x}{x} \right), \tag{3.2.37}$$

with $f(x;c) = (f_j(x;c_j))_{1 \le j \le \ell}$. The twisted cycle $\Gamma_{c^* \to c} = \Delta \otimes_{\mathbb{C}} \phi_c$ over which is integrated depends on c, as well as on Γ_{c^*}. The vector space V_{c^*} from the introduction is generated by the functions (3.2.37), where $[\Gamma_{c^*}]$ ranges over the twisted homology vector space $H_n(X(c^*), \omega(c^*))$ and two such functions are identified if they coincide on an open subset containing c^*.

We will now write down differential operators which annihilate the functions (3.2.37). We consider the Weyl algebra $D_A = \mathbb{C}[c_\alpha \,|\, \alpha \in A]\langle \partial_a \,|\, \alpha \in A \rangle$ whose variables are indexed by the columns of A. The *toric ideal* associated to A is the binomial ideal

$$I_A := \langle \partial^u - \partial^v \,|\, u - v \in \ker(A), \ u, v \in \mathbb{N}^A \rangle \triangleleft \mathbb{C}[\partial_\alpha \,|\, \alpha \in A]. \tag{3.2.38}$$

Here we use the notation $u = (u_\alpha)_{\alpha \in A} \in \mathbb{N}^A$ and $\partial^u = \prod_{\alpha \in A} \partial_\alpha^{u_\alpha}$, and similarly for v. For the convenience of the reader, we now verify that any operator in I_A indeed annihilates $I_{\Gamma_{c^*}}$. One checks that

$$\partial^u \bullet I_{\Gamma_{c^*}}(c) = \int_{\Gamma_{c^* \to c}} s(s-1)\cdots(s-|u|+1) \, f(x;c)^{s-|u|} \, x^{Au+\nu} \, \frac{\mathrm{d}x}{x}, \tag{3.2.39}$$

where $|u| = \sum_{\alpha \in A} u_a$. If $u - v \in \ker(A)$, we have $|u| = |v|$, and $Au = Av$, which proves $(\partial^u - \partial^v) \bullet I_{\Gamma_{c^*}} = 0$. The ideal I_A is called *toric* because, viewed as an ideal in the polynomial ring, it defines a toric variety. We will show how to compute its generators in Example 3.2.26.

We now define another D-ideal of differential operators annihilating our integral functions (3.2.37). This ideal, in contrast to I_A, will depend on the exponents s and ν. We write $\kappa \in \mathbb{C}^{n+\ell}$ for the vector $(-\nu, s)^\top$. Let $J_{A,\kappa}$ be the ideal generated by the entries of $A\theta - \kappa$ where $\theta := (\theta_\alpha)_{\alpha \in A}$ and $\theta_\alpha = c_\alpha \partial_\alpha$. It is well known that $P \bullet I_{\Gamma_{c^*}} = 0$ for all $P \in J_{A,\kappa}$ [GKZ90, Theorem 2.7]. Nevertheless, it is instructive to prove this using results from Subsection 3.2.1.

Lemma 3.2.25. *Let I_A and $J_{A,\kappa}$ be as defined above. The D_A-ideal $H_A(k) := I_A + J_{A,\kappa}$ annihilates the function (3.2.37) for any choice of the twisted cycle Γ_{c^*}.*

Proof. We argued above that I_A annihilates $I_{\Gamma_{c^*}}$. The i-th entry of the vector $A\theta - \kappa$, with $1 \le i \le n$, is $\sum_{j=1}^{\ell} \sum_{\alpha \in A_j} \alpha_i \, c_\alpha \partial_\alpha + \nu_i$. Applying (3.2.39), we compute that

$$\begin{aligned} (A\theta - \kappa)_i \bullet I_{\Gamma_{c^*}} &= \sum_{j=1}^{\ell} \sum_{\alpha \in A_j} \alpha_i \, c_\alpha \int_{\Gamma_{c^* \to c}} s_j f^{s-e_j} x^{\alpha+\nu} \frac{\mathrm{d}x}{x} + \nu_i \int_{\Gamma_{c^* \to c}} f^s x^\nu \frac{\mathrm{d}x}{x} \\ &= \sum_{j=1}^{\ell} \int_{\Gamma_{c^* \to c}} s_j f^s x^\nu f_j^{-1} \left(\sum_{\alpha \in A_j} \alpha_i c_\alpha x^\alpha \right) \frac{\mathrm{d}x}{x} + \nu_i \int_{\Gamma_{c^* \to c}} f^s x^\nu \frac{\mathrm{d}x}{x} \\ &= \left\langle \left[\left(\sum_{j=1}^{\ell} s_j f_j^{-1} \frac{\partial f_j}{\partial x_i} x_i + \nu_i \right) \frac{\mathrm{d}x}{x} \right], [\Gamma_{c^* \to c}] \right\rangle, \end{aligned}$$

where we use the pairing between $H_n(X(c), \omega(c))$ and $H^n(X(c), \omega(c))$ seen in (3.2.10). This evaluates to zero by the fact that the cocycle is zero in cohomology: it is $\nabla_\omega(\frac{\mathrm{d}x_{\hat{i}}}{x_{\hat{i}}})$. The entry $(A\theta - \kappa)_{n+j}$ is $\sum_{\alpha \in A_j} c_\alpha \partial_\alpha - s_j$. Using (3.2.39), one checks that $(A\theta - \kappa)_{n+j}$ annihilates $I_{\Gamma_{c^*}}$. $\blacksquare$

Example 3.2.26. ($n = 2, \ell = 1$) We consider the polynomial $f \in \mathbb{C}[x, y]$ defined in (3.2.14), but replace its coefficients by indeterminates $c_1, \ldots, c_6$. The matrix $A \in \mathbb{Z}^{3 \times 6}$ in this case is

$$A = \begin{pmatrix} 1 & 1 & 2 & 2 & 3 & 3 \\ 2 & 3 & 1 & 3 & 1 & 2 \\ 1 & 1 & 1 & 1 & 1 & 1 \end{pmatrix}. \tag{3.2.40}$$

Using the `Macaulay2` [GS] package `Dmodules` [LT], one computes that the toric ideal I_A is generated by 9 binomials:

$$I_A = \langle \partial_2 \partial_5 - \partial_1 \partial_6, \partial_3 \partial_4 - \partial_1 \partial_6, \partial_4 \partial_5^2 - \partial_3 \partial_6^2, \partial_1 \partial_5^2 - \partial_3^2 \partial_6, \partial_4^2 \partial_5 - \partial_2 \partial_6^2,$$
$$\partial_1 \partial_4 \partial_5 - \partial_2 \partial_3 \partial_6, \partial_1 \partial_4^2 - \partial_2^2 \partial_6, \partial_2 \partial_3^2 - \partial_1^2 \partial_5, \partial_2^2 \partial_3 - \partial_1^2 \partial_4 \rangle.$$

The ideal $J_{A,\kappa}$ is generated by the 3 operators

$$\theta_1 + \theta_2 + 2\theta_3 + 2\theta_4 + 3\theta_5 + 3\theta_6 + \nu_1, \ 2\theta_1 + 3\theta_2 + \theta_3 + 3\theta_4 + \theta_5 + 2\theta_6 + \nu_2, \ \theta_1 + \theta_2 + \theta_3 + \theta_4 + \theta_5 + \theta_6 - s.$$

Together, these 12 operators generate $H_A(\kappa)$.

The D_A-ideal $H_A(\kappa)$ from Lemma 3.2.25 is called a *GKZ system* or *A-hypergeometric system* of degree κ. Such systems are examples of regular singular D-modules. Solution functions of the GKZ system $H_A(\kappa)$ are called *A-hypergeometric functions*. Lemma 3.2.25 implies that our functions (3.2.37) are A-hypergeometric. Under some *non-resonance* conditions on κ (see Definition 3.2.27), the converse is also true: all A-hypergeometric functions can be written in the form (3.2.37). To make this precise, let $\mathcal{S}ol$ be the sheaf of solutions of the D_A-module $D_A/H_A(\kappa)$ and let $\mathcal{S}ol_{c^*}$ be the stalk at c^*. By Lemma 3.2.25, there is a map $H_n(X(c^*), \omega(c^*)) \to \mathcal{S}ol_{c^*}$ which sends Γ_{c^*} to the image of $I_{\Gamma_{c^*}}$ in $\mathcal{S}ol_{c^*}$. The image of this map is $V_{\Gamma_{c^*}}$.

Definition 3.2.27. A vector $\kappa \in \mathbb{C}^{n+\ell}$ is *non-resonant* if it does not belong to $\mathbb{C} \cdot F + \mathbb{Z} \cdot A$ for any facet F of the cone $\sum_{\alpha \in A} \mathbb{R}_{\geq 0} \cdot \alpha$ generated by A.

Theorem 3.2.28. *If $\kappa = (-\nu, s)^\top$ is non-resonant, the $\mathbb{C}$-linear map $H_n(X(c^*), \omega(c^*)) \to \mathcal{S}ol_{c^*}$ is an isomorphism, and $\dim_{\mathbb{C}}(\mathcal{S}ol_{c^*}) = \dim_{\mathbb{C}}(V_{\Gamma_{c^*}}) = |\chi(X(c^*))|$.*

Proof. The first claim is [GKZ90, Theorem 2.10]. The statement about the dimension of $\mathcal{S}ol_{c^*}$ follows from the perfect pairing (3.2.10), Lemma 3.2.4, and Theorem 3.2.7. ∎

By the CKK theorem (see Theorem 1.2.9)) the dimension of the space of solutions of a D-ideal I on any simply connected domain U outside the *singular locus* $\text{Sing}(I)$ is equal to the *holonomic rank* of I. The definition of the singular locus of a D-ideal can be found in [SST00, (1.32)]. In the case of $I = H_A(\kappa)$, the holonomic rank is given by the dimension of $R_A/(R_A \cdot H_A(\kappa))$ as a $\mathbb{C}(c)$ vector space, where $\mathbb{C}(c)$ is the field of rational functions in the coefficients $(c_\alpha)_{\alpha \in A}$, and R_A denotes the Weyl algebra with rational function coefficients. This was outlined in the introduction. The singular locus of our A-hypergeometric system is the principal A-determinant [GKZ94b, Remark 1.8]. We denote this by $\{E_A(c) = 0\}$.

Remark 3.2.29. A relevant case in physics is where $f = \mathcal{F}$ is the second *Symanzik polynomial*. The singular locus in this specialization is closely related to the *Landau discriminant* from [MT22]. Feynman integrals in the Lee–Pomeransky representation were studied using GKZ theory in [dlC19]. There, $f = \mathcal{U} + \mathcal{F}$ is the sum of the first and second Symanzik polynomial.

The fact that the dimension of the space of local solutions of $H_A(\kappa)$ is constant on an open dense subset of $\mathbb{C}^A$ follows from Theorem 3.2.28 by observing that $\chi(X(c))$ is constant on an open dense subset. We have related this open condition to the principal A-determinant in Subsection 3.2.1, and described the *generic Euler characteristic* as the volume of a polytope $\mathrm{NP}(h)$, see Theorem 3.2.7. It is not surprising that the same polytope appears also here.

Theorem 3.2.30. *Let $c^* \in \mathbb{C}^A$ be such that $E_A(c^*) \neq 0$ and let κ be non-resonant. For any simply connected domain $U_{c^*} \ni c^*$ such that $U_{c^*} \cap \{E_A(c) = 0\} = \varnothing$, we have that*

$$\dim_{\mathbb{C}}\left(V_{c^*}\right) = \dim_{\mathbb{C}(c)}\left(R_A/(R_A \cdot H_A(\kappa))\right) = |\chi(X(c^*))| = \mathrm{vol}\left(\mathrm{NP}(h)\right),$$

where V_{c^*} is defined as in (3.2.6), and $\mathrm{NP}(h)$ is the Newton polytope of h from (3.2.12).

Remark 3.2.31. The volume $\mathrm{vol}\left(\mathrm{NP}(h)\right)$ in Theorem 3.2.30 has to be intended as the volume form induced by the lattice spanned by the row-space of the matrix A, see [GKZ94a, §5.3]. If A does not span the full-dimensional lattice $\mathbb{Z}^{n+\ell}$, in order for the equalities in Theorem 3.2.30 to hold true, one needs to multiply the numbers $\dim_{\mathbb{C}(c)}\left(R_A/(R_A \cdot H_A(\kappa))\right)$ and $\mathrm{vol}\left(\mathrm{NP}(h)\right)$ by the index of the lattice spanned by A inside $\mathbb{Z}^{n+\ell}$.

Example 3.2.32. Using the command `holonomicRank` in `Macaulay2`, we check that the holonomic ideal $H_A(\kappa)$ from Example 3.2.26 is 6. This number coincides with the degree of the toric ideal I_A associated to the matrix A from (3.2.40), and the normalized volume of the hexagonal pyramid from Figure 3.7.

We point out that, for any choice of parameters $\kappa = (-\nu, s)^\top$, we have the inequality

$$\dim_{\mathbb{C}(c)}\left(R_A/(R_A \cdot H_A(\kappa))\right) \geq \mathrm{vol}(\mathrm{NP}(h)), \tag{3.2.41}$$

see for instance [SST00, Theorem 3.5.1]. Equality holds for non-resonant parameters, but the holonomic rank may *jump up* for special κ. The Euler characteristic of $X(c^*)$ may *drop* for special choices of the coefficients c^*; this is what happened in Example 3.2.8.

Following [MH22, Sections 3, 4], we now explain which D_A-modules are behind these constructions. This will lead to an explicit connection between this subsection and Subsection 3.2.1. Define

$$\mathcal{X} := \left\{ (x, c) \in (\mathbb{C}^*)^n \times \mathbb{C}^A \mid \prod_{i=1}^{\ell} f_i(x; c) \neq 0 \right\} \tag{3.2.42}$$

and let $\pi: \mathcal{X} \to \mathbb{C}^A$ be the projection to $\mathbb{C}^A$. For $c \in \mathbb{C}^A$, the fiber of π is $X(c)$. Note that $H^n(X(c), \omega(c))$ depends rationally on the c_i. Denote by $\mathcal{H}^n$ the n-th cohomology group of the relative de Rham complex $(\Omega^\bullet_{\mathcal{X}/\mathbb{C}^A}, \nabla_x)$, where $\Omega^k_{\mathcal{X}/\mathbb{C}^A}$ is the sheaf of relative differential k-forms. This sheaf is locally defined by its sections $\sum_{|I|=k} s(x, c)\, \mathrm{d}x^I$, where $s(x, c)$ are sections of the structure sheaf $\mathcal{O}_{\mathcal{X}}$. The differential $\nabla_x = \mathrm{d}_x + \mathrm{dlog}_x(f^s x^\nu)$ only takes derivatives with respect to x. For every $c^* \in \mathbb{C}^A$, there is an evaluation map

$$\mathrm{ev}_{c^*}: \mathcal{H}^n_{c^*} \to H^n(X(c^*), \omega(c^*)). \tag{3.2.43}$$

We now recall that $\mathcal{H}^n$ is naturally endowed with the structure of a D_A-module via the *Gauß–Manin connection* $\nabla^{\mathrm{GM}} := \nabla_c = \mathrm{d}_c + \mathrm{dlog}_c(f^s x^\nu)$.

Denote by $M_A(\kappa)$ the regular holonomic D_A-module $D_A/H_A(\kappa)$.

Proposition 3.2.33 ([MH22]). *For non-resonant κ (see Definition 3.2.27) and $s \notin \mathbb{Z}^\ell$, the morphism*

$$M_A(\kappa) \xrightarrow{\cong} \mathcal{H}^n, \quad [1] \mapsto \left[\frac{\mathrm{d}x}{x}\right]$$

is an isomorphism of D_A-modules.

The isomorphism from Proposition 3.2.33 explains how to use GKZ theory to obtain relations between the generators of V_Γ. It extends $[1] \mapsto \left[\frac{\mathrm{d}x}{x}\right]$ D_A-linearly. Explicitly, $[P] \in M_A(\kappa)$ is sent to $P \bullet \left[\frac{\mathrm{d}x}{x}\right]$, where ∂_α acts on an element $[\phi(c)] \in \mathcal{H}^n$ as follows (cf. [MHT22]):

$$\partial_\alpha \bullet [\phi(c)] = \left[\partial_\alpha(\phi(c)) + \left(\sum_{j=1}^{\ell} s_j \frac{x^\alpha}{f_j(x;c)}\right)\phi(c)\right]. \tag{3.2.44}$$

The image of an element in $H_A(\kappa)$ is zero in $\mathcal{H}^n$ by Proposition 3.2.33. Applying the evaluation map (3.2.43) gives a zero-element in $H^n(X(c^*), \omega(c^*))$.

Example 3.2.34. The image of the differential operator $(A\theta - \kappa)_i$ under the isomorphism in Proposition 3.2.33 is

$$\left[\left(\sum_{j=1}^{\ell} s_j f_j^{-1} \frac{\partial f_j}{\partial x_i} x_i + \nu_i\right)\frac{\mathrm{d}x}{x}\right],$$

which is precisely the zero-cocycle seen at the end of the proof of Lemma 3.2.25.

3.2.4. Numerical methods

In previous subsections, we have focused on symbolic techniques for computing with generalized Euler integrals. We now switch gears and present some ideas for the use of numerical methods. We believe that integrating these different approaches will be of key importance to compute larger instances. A first, well-known observation is that the dimension of our vector spaces can be computed by solving a system of rational function equations. Fix $f \in \mathbb{C}[x, x^{-1}]^\ell$, $s \in \mathbb{C}^\ell$, and $\nu \in \mathbb{C}^n$, and let X be as in (3.2.2). We say that $x^* \in X$ is a *complex critical point* of $\log(f^s x^\nu)$ on X if $\omega(x^*) = 0$, where ω is the 1-form defined in (3.2.3).

Theorem 3.2.35. *Fix $f \in \mathbb{C}[x, x^{-1}]^\ell$ and let X be as in (3.2.2). The integer $(-1)^n \cdot \chi(X)$ equals the number of complex critical points of $\log(f^s x^\nu)$ on X, for generic $s \in \mathbb{C}^\ell$, $\nu \in \mathbb{C}^n$.*

Proof. Since X is smooth and very affine, this follows from [Huh13, Theorem 1]. ∎

Concretely, one obtains the Euler characteristic of X by counting complex solutions of

$$\frac{s_1 \cdot \frac{\partial f_1}{\partial x_i}}{f_1} + \cdots + \frac{s_\ell \cdot \frac{\partial f_\ell}{\partial x_i}}{f_\ell} + \frac{\nu_i}{x_i} = 0, \qquad i = 1, \dots, n. \tag{3.2.45}$$

This has been applied to count master integrals in [MT22], and to compute Euler characteristics of point configuration spaces in [ABF$^+$23, ST21] with a view towards physics and statistics. One way to solve the equations in (3.2.45) is by using numerical homotopy methods. For the computations in this subsection, we use the `Julia` package `HomotopyContinuation.jl` (v2.6.3) [BT18].

Example 3.2.36. We compute the Euler characteristic of the very affine surface X from Example 3.2.8, with f as in (3.2.14). The equations in (3.2.45) are generated in `Julia` as follows:

```
using HomotopyContinuation
@var x y s ν[1:2]
f = -x*y^2 + 2*x*y^3 + 3*x^2*y - x^2*y^3 - 2*x^3*y + 3*x^3*y^2
L = s*log(f) + ν[1]*log(x) + ν[2]*log(y)
F = System(differentiate(L,[x;y]), parameters = [s;ν])
```

The variable `F` is viewed as a system of two equations in two unknowns `x` and `y`, parameterized by `s`, `ν[1]`, and `ν[2]`. Solving for generic parameter values is done using the command `monodromy_solve(F)`. The output confirms that there are 6 complex solutions. We encourage the reader to check that the analogous computation with f as in (3.2.15) returns only 2 solutions. The equations (3.2.45) in this case coincide with [ST21, Equation (5)] for $m = 5$. For a tutorial on solving (3.2.45) in `Julia`, see [ST21, Section 3] and the references therein.

Another use for these tools is the computation of $\mathbb{C}$-linear relations among the generators

$$\left(I_{a,b} : [\Gamma] \longmapsto \int_\Gamma f^{s+a}\, x^{\nu+b}\, \frac{\mathrm{d}x}{x} \right) \in \operatorname{Hom}_\mathbb{C}(\, H_n(X,\omega), \mathbb{C}\,) \tag{3.2.46}$$

of our vector space V_Γ, discussed in Subsection 3.2.1. We present the ideas in the case where $n = 1$ and leave general methodology for future research. In particular, we reproduce the relation found in Example 3.2.10. We start with a discussion on numerically computing the integral $I_{a,b}(\Gamma)$. Since Γ is a *twisted* 1-cycle, it is encoded by a singular 1-cycle Δ and a choice of branch ϕ for the multi-valued function $f^s x^\nu$. We take Δ to be a triangle ABC, i.e., a sum $AB + BC + CA$ of line segments, with $A, B, C \in X \subset \mathbb{C}^*$. The cycle Γ is

$$\Gamma = AB \otimes_\mathbb{C} \phi_{AB} + BC \otimes_\mathbb{C} \phi_{BC} + CA \otimes_\mathbb{C} \phi_{CA}, \tag{3.2.47}$$

where $\phi_{AB} : U_{AB} \to \mathbb{C}$ is a section of $\mathcal{L}_\omega^\vee$, defined on the open neighborhood U_{AB} of the line segment AB, and similarly for ϕ_{BC} and ϕ_{CA}. Note that ϕ_{AB} is completely determined by its value $\phi_{AB}(A)$ at A, and $\phi_{AB}(B) = \phi_{BC}(B), \phi_{BC}(C) = \phi_{CA}(C)$. Moreover, we also have $\phi_{CA}(A) = \phi_{AB}(A)$ because Γ is a twisted cycle. Hence, the data specifying Γ are the points A, B, C, and the complex number $\phi_{AB}(A)$. The integral is

$$\int_\Gamma f^{s+a}\, x^{\nu+b}\, \frac{\mathrm{d}x}{x} = \int_{AB} \phi_{AB}(x) f^a x^b \frac{\mathrm{d}x}{x} + \int_{BC} \phi_{BC}(x) f^a x^b \frac{\mathrm{d}x}{x} + \int_{CA} \phi_{CA}(x) f^a x^b \frac{\mathrm{d}x}{x},$$

where the three integrals on the right are usual complex integrals over singular 1-chains on X, with a single-valued integrand. These can be approximated using the trapezoidal rule. Fixing a large integer N and writing $x_i = (N-1)^{-1} \cdot ((N-i)A + (i-1)B)$, we get

$$\int_{AB} \phi_{AB}(x) f^a x^b \frac{\mathrm{d}x}{x} \approx \frac{(B-A)}{N-1} \left(\frac{\phi_{AB}(x_1)\psi_1}{2} + \sum_{i=2}^{N-1} \phi_{AB}(x_i)\psi_i + \frac{\phi_{AB}(x_N)\psi_N}{2} \right), \tag{3.2.48}$$

where $\psi_i := f(x_i)^a x_i^{b-1}$ is the evaluation of the single-valued part of the integrand at x_i.

To evaluate (3.2.48), we need to evaluate the section ϕ_{AB} at the nodes $x_i \in AB$ of the numerical integration. To this end, recall that ϕ_{AB} satisfies a differential equation

$$\frac{\mathrm{d}\phi_{AB}(x) - \omega \cdot \phi_{AB}(x)}{\mathrm{d}x} = 0, \quad x \in AB, \tag{3.2.49}$$

with initial condition specified by $\phi_{AB}(x_1) = \phi_{AB}(A)$. One can use any standard method for numerically solving ODEs to approximate $\phi_{AB}(x_i)$, $i = 1, \ldots, N$. Furthermore, $\phi_{AB}(x_N) = \phi_{AB}(B)$ can be used as the initial condition for the next integral over the line segment BC.

When the parameters s, ν are rational numbers, we can make use of the fact that the graph $(x, \phi_{AB}(x))$, $x \in AB$, satisfies an algebraic equation $F(x, y) = 0$. Indeed, let k be the smallest integer such that $k\nu \in \mathbb{Z}^n$ and $ks \in \mathbb{Z}^\ell$. We have $F(x, \phi_{AB}(x)) = \phi_{AB}(x)^k - f(x)^{ks} x^{k\nu} = 0$. Consider the algebraic curve $\mathcal{C} = \{(x, y) \in (\mathbb{C}^*)^2 \mid y^k - f(x)^{ks} x^{k\nu} = 0\}$ with marked points $Z = \{(x, 0) \mid f(x) = 0\}$. There is a degree k covering

$$\pi : \mathcal{C} \smallsetminus Z \longrightarrow X, \quad (x, y) \mapsto x.$$

Suppose that, using (3.2.49), we have computed an approximation $\tilde{y}_i$ for $y_i := \phi_{AB}(x_i) \in \pi^{-1}(x_i)$. We can use $\tilde{y}_i$ as a starting point for Newton iteration on the nonlinear equation $F(x_i, y) = 0$ in the variable y. If $\tilde{y}_i$ is a reasonable approximation, the iteration will converge to y_i, and reduce the approximation error of our numerical ODE solver significantly in each discretization step. This is illustrated in Figure 3.8. The procedure is much like the standard *predict-and-correct* technique used in polynomial homotopy continuation [AG12, Chapter 3].

Suppose we know a basis of twisted cycles $[\Gamma_1], \ldots, [\Gamma_\chi]$ for $H_1(X, \omega)$, where Γ_i are as
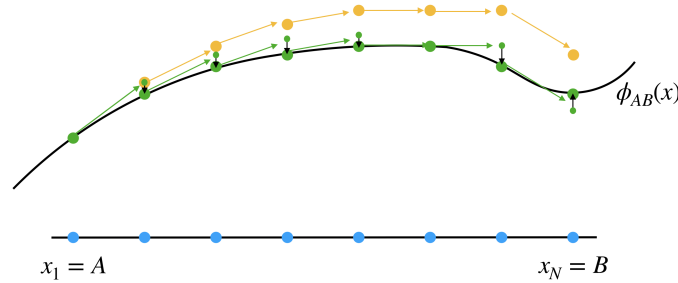
Figure 3.8. Estimating $\phi_{AB}(x_i)$ using a numerical ODE solver (yellow) with initial condition at $x_1 = A$. Results are improved by adding Newton iterations in each step (green).

in (3.2.47) and $\chi = |\chi(X)|$. Given $\chi + 1$ cocycles

$$\left[f^{a^{(1)}} x^{b^{(1)}} \frac{\mathrm{d}x}{x} \right], \ldots, \left[f^{a^{(\chi+1)}} x^{b^{(\chi+1)}} \frac{\mathrm{d}x}{x} \right] \in H^1(X, \omega),$$

we would like to compute a $\mathbb{C}$-linear relation between the corresponding $I_{a^{(j)}, b^{(j)}}$ from (3.2.46). Assume

$$M_{ij} := I_{a^{(j)}, b^{(j)}}(\Gamma_i) = \left\langle \left[f^{a^{(j)}} x^{b^{(j)}} \frac{\mathrm{d}x}{x} \right], [\Gamma_i] \right\rangle \in \mathbb{C}$$

is given by the perfect pairing (3.2.10). These are approximated numerically using the techniques outlined above. We then arrange these numbers in a matrix $M = (M_{ij})_{1 \le i \le \chi, 1 \le j \le \chi+1}$.

Proposition 3.2.37. *Any vector* $(c_1, \ldots, c_{\chi+1})$ *in the kernel of* M, *viewed as a linear map* $\mathbb{C}^{\chi+1} \to \mathbb{C}^\chi$, *gives a linear relation* $\sum_{j=1}^{\chi+1} c_j \cdot I_{a^{(j)}, b^{(j)}} = 0$.

Proof. For any twisted cycle $[\Gamma] = d_1 [\Gamma_1] + \cdots + d_\chi [\Gamma_\chi]$ we have

$$\sum_{j=1}^{\chi+1} c_j \, I_{a^{(j)}, b^{(j)}}(\Gamma) = \sum_{i=1}^{\chi} \sum_{j=1}^{\chi+1} d_i c_j I_{a^{(j)}, b^{(j)}}(\Gamma_i) = \sum_{i=1}^{\chi} d_i \sum_{j=1}^{\chi+1} c_j M_{ij} = 0. \qquad \blacksquare$$

Example 3.2.38. Let $f = (x - 1, x - 2)$, $s = (\frac{1}{2}, \frac{1}{2})$ and $\nu = \frac{1}{2}$ be as in Examples 3.2.2 and 3.2.10. The green cycles in Figure 3.6 form a basis for $H_1(X, \omega)$. We replace them by triangles Γ_1, Γ_2 as in (3.2.47). These are specified by the data

$$A_1 = \tfrac{1}{2} + \sqrt{-1}, \quad B_1 = \tfrac{1}{2} - \sqrt{-1}, \quad C_1 = 3, \quad \phi_{A_1 B_1}(A_1) = -1.436744 + 0.435011\sqrt{-1},$$
$$A_2 = -1, \quad B_2 = \tfrac{3}{2} + \sqrt{-1}, \quad C_2 = \tfrac{3}{2} - \sqrt{-1}, \quad \phi_{A_2 B_2}(A_2) = -2.449490\sqrt{-1}.$$

We integrate against the cocycles $[f^{a^{(j)}} x^{b^{(j)}} \frac{\mathrm{d}x}{x}]$, $j = 1, \ldots, 3$, with $a^{(1)} = (-1, 0)$, $a^{(2)} = (0, -1)$, $a^{(3)} = (0, 0)$ and $b^{(1)} = 1$, $b^{(2)} = 1$, $b^{(3)} = 0$. We do this using an implementation in Julia of the ideas discussed above. The code can be found in [AFST22, Appendix B]. Here is how to use it in this particular example:

```
f = x -> [x-1; x-2]
s = [1/2;1/2]; ν = 1/2; N = 1000; k = 2;
ω = x -> s[1]/(x-1) + s[2]/(x-2) + ν/x
cocycles = [[[-1;0],1], [[0,-1],1], [[0,0],0]]

A1 = 1/2+im; B1 = 1/2-im; C1 = 3+0im
phiA1B1_at_A1 = A1^ν*prod(f(A1).^s)
I1 = integrate_loop(A1,B1,C1,phiA1B1_at_A1,N,f,ω,s,ν,k,cocycles)

A2 = -1+0im; B2 = 3/2+im; C2 = 3/2-im
phiA2B2_at_A2 = A2^ν*prod(f(A2).^s)
I2 = integrate_loop(A2,B2,C2,phiA2B2_at_A2,N,f,ω,s,ν,k,cocycles)
```

The variable `I1` contains the first row $(M_{11} \; M_{12} \; M_{13})$ of our 2×3 matrix M. The second row is `I2`. We obtain the matrix

$$M = \begin{pmatrix} -3.496\sqrt{-1} & 4.144\sqrt{-1} & -0.648\sqrt{-1} \\ 3.496 & 0.648 & -4.144 \end{pmatrix},$$

whose kernel is spanned by $(\frac{1}{2}, \frac{1}{2}, \frac{1}{2})^\top$. This is the relation seen in Example 3.2.10.

3.3. Conclusions

We conclude Section 3.2 with some pertinent research questions. Our final long-term goal is to fully connect the various previously discussed approaches and to provide new methods for computing integral bases in physics and beyond.

Allowing integer shifts in the exponents of the tuple $f = (f_1, \ldots, f_\ell)$ of Laurent polynomials is one way to produce a finite-dimensional vector space of integrals of type as in (3.0.2). An integral basis is indexed by a subset of the integer lattice $\mathbb{Z}^\ell$. A long-term goal is to develop a combinatorial procedure to compute such integral basis. A natural case to begin with is resumed in the following:

Problem 3.3.1. *Describe an integral basis for vector spaces of integrals as in* (3.0.2) *when the tuple* $f = (f_1, \ldots, f_\ell)$ *consists of linear forms.*

This situation looks promising to disclose intriguing combinatorial structures even in the planar case, i.e., $n = 2$, where the dimension of the basis equals the number of bounded chambers in the lines arrangement determined by the linear forms in f. This connection

reveals a fascinating correspondence between bounded chambers and basis integrals that we aim to understand at a deeper level.

An additional useful point to consider in scattering amplitudes is that each Feynman integral comes with a Feynman diagram associated with it, as explained in Appendix A. In the physics literature, it is claimed the existence of a relation between the graph and the master integrals. More precisely, in some cases where a basis is known, it is conjectured that a basis can be computed from the subgraphs of the graph one starts with, e.g. [BGL⁺18]. Therefore we propose the following

Problem 3.3.2. *Characterize the family of Feynman graphs whose subgraphs are in bijection with the master integrals. Formulate an analogous version of this fact for generalized Euler integrals where the graph is replaced by the very affine variety X.*

The mildly noncommutative setting of D-modules provides new methods to compute linear relations among integrals. In Subsection 3.2.2 we learned that the Mellin transform not only plays a central role in understanding the dimension of the vector space of integrals but also provides an effective way to generate linear relations between integrals. Alternatively, the same relation can be computed using homological algebra for one of the other vector spaces, as showed in Subsection 3.2.1. Proposition 3.2.20 provides new insights about the connection between the relations for these two different vector spaces. A further goal is to understand this interplay in complete generality:

Problem 3.3.3. *Understand the connections between the relations for the vector spaces in [AFST22], and provide algorithmic methods to compute such relations.*

Chapter 4

Computation with quadrics

The main goal of this chapter is to approach classical problems in algebraic geometry by using modern techniques, such as relying on symbolic and numerical computations, and adding points of view and questions coming from different fields, such as algebraic statistics, real algebraic geometry, and related areas.

This chapter is divided into two main parts: Section 4.1 studies *pencils of quadrics*, namely two-dimensional linear subspaces in the space $\mathbb{S}^n$ of (real or complex) symmetric $n \times n$ matrices, according to the classification by Segre symbols [HP52], addressing questions motivated by algebraic statistics and optimization; Section 4.2 revisits a classical problem in enumerative geometry, namely the count of quadrics in the projective space that are tangent to nine given figures among points, lines, planes, or quadrics, with the purpose of showing that the instances of such quadratic surfaces can be fully real.

The common theme of both sections is the study *linear spaces of symmetric matrices* with the aim of expanding the comprehension of these matrix spaces by approaching them from various viewpoints. These objects, although seemingly elementary, possess a substantial influence and are utilized in a wide range of areas within mathematics. For example, they constitute spaces of smooth quadrics satisfying specific tangency conditions in enumerative algebraic geometry; they serve as linear Gaussian or concentration models in the realm of algebraic statistics; they establish the spectrahedra on which optimization problems are examined in semidefinite programming; and finally, they encode partially symmetric tensors in nonlinear algebra. This discussion is also the motivation for writing the volume [MMRS21].

Here are the chapter's major aspects. Section 4.1 begins by revisiting the history of the study of pencils of quadrics that lead to the classification by Segre symbols, with a linear algebra perspective on Theorem 4.1.1. We denote by $\mathcal{L}^{-1}$ the set of the inverses of all invertible matrices in $\mathcal{L}$. Since we exclude singular pencils, namely the ones with identically zero determinant, the set $\mathcal{L}^{-1}$ is nonempty. Its closure in $\mathbb{P}(\mathbb{S}^n)$ is a projective curve, called the *reciprocal curve* and denoted $\mathbb{P}\mathcal{L}^{-1}$. In Subsection 4.1.1 we prove that, when $\mathcal{L}$ is nonsingular, $\mathbb{P}\mathcal{L}^{-1}$ is a rational normal curve, we express its degree in terms of the Segre symbol $\sigma(\mathcal{L})$, and determine its prime ideal.

In Subsection 4.1.2 we turn to maximum likelihood estimation for Gaussians. A linear Gaussian model is a set of multivariate Gaussian probability distributions whose covariance or concentration matrices are linear combinations of some fixed symmetric matrices. Hence, when restricting to two-dimensional models, a pencil $\mathcal{L}$ plays two different roles in statistics, depending on whether it lives in the space of concentration matrices (as in [SU10]) or in the space of covariance matrices (as in [CMR20]). This yields two numerical invariants, the ML degree $\mathrm{mld}(\mathcal{L})$ and the reciprocal ML degree $\mathrm{rmld}(\mathcal{L})$. We give formulas for these as

expressed by Segre symbols in Theorem 4.1.13. Finally, in Subsection 4.1.3 we study the constructible set Gr_σ in the Grassmannian $\mathrm{Gr}(2, \mathbb{S}^n)^{\mathrm{reg}}$ defined by all nonsingular pencils with fixed Segre symbol. Its closure $\overline{\mathrm{Gr}}_\sigma$ is a variety. We study these varieties and their poset of inclusions, seen in Figure 4.1.

In Subsection 4.2.1 we move to quadratic surfaces in projective space. We introduce coordinates for points, lines, planes and quadrics, and derive the polynomials that describe our tangency conditions. Subsection 4.2.2 is dedicated to the space of complete quadrics, a variety in $\mathbb{P}^9 \times \mathbb{P}^{20} \times \mathbb{P}^9$. We determine its prime ideal, we recover Schubert's triangle as its multidegree, and we write our tangency conditions in that setting. In Subsection 4.2.3 we argue that Schubert's triangle is mostly real. We present explicit instances where all tangent quadrics are real. These instances were found by substantial computations using the software `HomotopyContinuation.jl` [BT18]. Our computations and the certification process are described in Subsection 4.2.4. To conclude, Subsection 4.2.5 describes the Schubert's pyramid. It gives the numbers $p^\alpha \ell^\beta h^\gamma q^\delta$ of quadrics through α points that are tangent to β lines, γ planes and δ quadrics; see Figure 4.3. At the top of this pyramid lives $q^9 = 666841088$, namely the number of quadrics tangent to nine given quadrics in $\mathbb{P}^3$. We discuss the associated polynomial systems, and we state two conjectures about their reality.

4.1. Pencils of quadrics

A pencil of quadrics is a two-dimensional linear subspace $\mathcal{L}$ in the space $\mathbb{S}^n$ of (real or complex) symmetric $n \times n$ matrices. It can also be interpreted as a point in the Grassmannian $\mathrm{Gr}(2, \mathbb{S}^n)$, and it specifies a line $\mathbb{P}\mathcal{L}$ in the projective space $\mathbb{P}(\mathbb{S}^n) \simeq \mathbb{P}^{\binom{n+1}{2}-1}$. The group $\mathrm{GL}(n)$ acts on $\mathbb{S}^n$ by congruence:

$$\mathrm{GL}(n) \times \mathbb{S}^n \to \mathbb{S}^n, \ (g, A) \mapsto gAg^T, \tag{4.1.1}$$

and this induces an action on $\mathrm{Gr}(2, \mathbb{S}^n)$. We say that two pencils are *isomorphic* if they lie in the same $\mathrm{GL}(n)$-orbit.

Fix a pencil $\mathcal{L}$ with basis $\{A, B\}$. The determinant $\det(\mathcal{L}) = \det(\lambda A + \mu B)$ is well-defined up to the action of $\mathrm{GL}(2)$ by changing basis in $\mathcal{L}$. The zeros of this binary form are a divisor of degree n in the line $\mathbb{P}^1$, well-defined up to isomorphism of $\mathbb{P}^1$. We exclude pencils $\mathcal{L}$ that are *singular*, meaning that the determinant $\det(\mathcal{L})$ is identically equal to zero. The singular pencils form a subvariety $\mathrm{Gr}(2, \mathbb{S}^n)^{\mathrm{sing}}$ in the Grassmannian. We are interested in a natural stratification of the open set of all regular pencils:

$$\mathrm{Gr}(2, \mathbb{S}^n)^{\mathrm{reg}} \ = \ \mathrm{Gr}(2, \mathbb{S}^n) \setminus \mathrm{Gr}(2, \mathbb{S}^n)^{\mathrm{sing}}.$$

Each stratum is indexed by a *Segre symbol σ*. This is a multiset of partitions whose parts add up to n in total. One exception: the singleton $[(1, 1, \ldots, 1)]$ is not a Segre symbol (see Remark 4.1.4). The number $S(n)$ of Segre symbols was already of interest to Arthur Cayley in 1855. In [Cay55, p. 316], he derived the generating function

$$\sum_{n=1}^\infty S(n)x^n \ = \ \prod_{k \geq 1} \frac{1}{(1 - x^k)^{P(k)}} - \frac{1}{1-x} \ = \ 2x^2 + 5x^3 + 13x^4 + 26x^5 + 57x^6 + 110x^7 + \cdots,$$

where $P(k)$ is the number of partitions of the integer k. The two Segre symbols for $n = 2$ are $[1, 1]$ and $[2]$. For $n = 3$ and $n = 4$ they are shown in Figure 4.1.

The Segre symbol $\sigma = \sigma(\mathcal{L})$ of a given pencil $\mathcal{L}$ can be computed as follows. Pick a basis $\{A, B\}$ of $\mathcal{L}$, where B is invertible, and find the Jordan canonical form of AB^{-1}. Each

eigenvalue of AB^{-1} determines a partition, according to the sizes of its Jordan blocks. Then σ is the associated multiset of partitions. It turns out that σ does not depend on the choice of basis $\{A, B\}$. For the relevant background in linear algebra see [DE95, Tho91, Uhl76].

The role of Segre symbols in projective geometry can be stated as follows.

Theorem 4.1.1 (Weierstrass-Segre). *Two pencils of quadrics in $\mathbb{S}^n$ are isomorphic if and only if their Segre symbols agree and their determinants define the same multiset of n points on the projective line $\mathbb{P}^1$, up to isomorphism of $\mathbb{P}^1$.*

Example 4.1.2 ($n = 2$). All pencils $\mathcal{L}$ are regular. There are two GL(2)-orbits, given by the rank of a matrix X that spans $\mathcal{L}^\perp = \{X \in \mathbb{S}^2 : \mathrm{trace}(AX) = \mathrm{trace}(BX) = 0\}$. If X has rank 2 then $\det(\mathcal{L})$ has two distinct roots in $\mathbb{P}^1$ and the Segre symbol is $\sigma(\mathcal{L}) = [1, 1]$. If X has rank 1 then it is a double root in $\mathbb{P}^1$ and $\sigma(\mathcal{L}) = [2]$.

We learned about Theorem 4.1.1 from an unpublished note by Pieter Belmans, titled *Segre symbols*, which credits the 1883 PhD thesis of Corrado Segre. It appears in the textbooks on algebraic geometry by Dolgachev [Dol12, §8.6.1] and Hodge-Pedoe [HP52, §XIII.10]. The idea goes back to at least the 1850s, in works of Cayley [Cay55] and Sylvester [Syl51].

One advantage of using Segre symbols relies in the fact that they determine a basis of canonical representatives for the pencil they index. To define such a basis, we first fix the field to be $\mathbb{C}$ and identify symmetric $n \times n$ matrices A with quadratic forms $\mathbf{x} A \mathbf{x}^T$ in unknowns $\mathbf{x} = (x_1, \ldots, x_n)$. Notice that the $\binom{n+1}{2}$-dimensional vector space $\mathbb{S}^n$ is also equipped with the trace inner product

$$\mathbb{S}^n \times \mathbb{S}^n \to \mathbb{C}, \quad (A, B) \mapsto \mathrm{trace}(AB).$$

The group $\mathrm{GL}(n)$ acts on quadratic forms by linear changes of coordinates, via $\mathbf{x} \mapsto \mathbf{x}g$. This corresponds to the action (4.1.1) of $\mathrm{GL}(n)$ on symmetric matrices.

Let $\mathcal{L} = \mathbb{C}\{A, B\}$ be a regular pencil in $\mathrm{Gr}(2, \mathbb{S}^n)$, with $\det(B) \neq 0$. The polynomial ring $\mathbb{C}[\lambda]$ in one variable λ is a principal ideal domain. The cokernel of the matrix $A - \lambda B$ is a module over this principal ideal domain (PID). Consider its *elementary divisors*

$$(\lambda - \alpha_1)^{e_1}, (\lambda - \alpha_2)^{e_2}, \ldots, (\lambda - \alpha_s)^{e_s}. \tag{4.1.2}$$

Here $e_1, \ldots, e_s$ are positive integers whose sum equals n. The list (4.1.2) is unordered and its product is $\det(\mathcal{L}) = \pm \det(A - \lambda B)$. The complex numbers α_i are the *eigenvalues* of the pair (A, B). They form a multiset of cardinality n in $\mathbb{P}^1$.

Suppose there are r distinct eigenvalues α_i. We have $r \leq s \leq n$. The exponents e_i corresponding to one fixed eigenvalue form a partition. This gives a multiset of r partitions, with s parts in total, where the sum of all parts is n. This multiset of partitions is the Segre symbol $\sigma = \sigma(\mathcal{L})$. It is thus visible in (4.1.2). We now paraphrase Theorem 4.1.1 using the elementary divisors of the matrix $A - \lambda B$.

Corollary 4.1.3. *Consider two quadrics $\mathbf{x} A \mathbf{x}^T$ and $\mathbf{x} B \mathbf{x}^T$ with $\det(B) \neq 0$. There exists a change of coordinates $\mathbf{x} \mapsto \mathbf{x}g$ which transforms them to $\mathbf{x} C \mathbf{x}^T$ and $\mathbf{x} D \mathbf{x}^T$ if and only if the matrices $A - \lambda B$ and $C - \lambda D$ have the same elementary divisors.*

Proof. For a textbook proof of this classical fact see [HP52, Theorem 1, p. 278]. ∎

Corollary 4.1.3 is used to construct a canonical form for pencils. For $e \in \mathbb{N}$ and $\alpha \in \mathbb{C}$, we

define a pair of symmetric $e \times e$ matrices by filling their antidiagonals:

$$P_e(\alpha) = \begin{pmatrix} 0 & 0 & \cdots & 0 & \alpha \\ 0 & 0 & \cdots & \alpha & 1 \\ \vdots & \vdots & \reflectbox{$\ddots$} & \reflectbox{$\ddots$} & \vdots \\ 0 & \alpha & 1 & \vdots & 0 \\ \alpha & 1 & \cdots & 0 & 0 \end{pmatrix} \quad \text{and} \quad Q_e = \begin{pmatrix} 0 & \cdots & 0 & 0 & 1 \\ 0 & \cdots & 0 & 1 & 0 \\ 0 & \cdots & 1 & 0 & 0 \\ \vdots & \reflectbox{$\ddots$} & \vdots & \vdots & \vdots \\ 1 & \cdots & 0 & 0 & 0 \end{pmatrix}. \tag{4.1.3}$$

The $e \times e$ matrix $P_e(\alpha) - \lambda Q_e$ has only one elementary divisor, namely $(\lambda - \alpha)^e$.

Let us now start with the list in (4.1.2). For each elementary divisor $(\lambda - \alpha_i)^{e_i}$ we form the $e_i \times e_i$ matrices in (4.1.3), and we aggregate these blocks as follows:

$$P = \begin{pmatrix} P_{e_1}(\alpha_1) & 0 & \cdots & 0 \\ 0 & P_{e_2}(\alpha_2) & \cdots & 0 \\ \vdots & \vdots & \ddots & \vdots \\ 0 & 0 & \cdots & P_{e_s}(\alpha_s) \end{pmatrix} \quad \text{and} \quad Q = \begin{pmatrix} Q_{e_1} & 0 & \cdots & 0 \\ 0 & Q_{e_2} & \cdots & 0 \\ \vdots & \vdots & \ddots & \vdots \\ 0 & 0 & \cdots & Q_{e_s} \end{pmatrix}. \tag{4.1.4}$$

The matrices $A - \lambda B$ and $P - \lambda Q$ have the same elementary divisors. Hence, by Corollary 4.1.3, the pair $(\mathbf{x}A\mathbf{x}^T, \mathbf{x}B\mathbf{x}^T)$ is isomorphic to $(\mathbf{x}P\mathbf{x}^T, \mathbf{x}Q\mathbf{x}^T)$ under the action by $\mathrm{GL}(n)$. As in Example 4.1.19, every regular pencil $\mathcal{L} \in \mathrm{Gr}(2, \mathbb{S}^n)$ has a normal form $\mathbb{C}\{P, Q\}$, where the matrices P and Q are defined by the unordered list (4.1.2). Given any Segre symbol σ, its canonical representative is $\mathcal{L} = \mathbb{C}\{P, Q\}$ where $\alpha_1, \ldots, \alpha_r$ are parameters. In what follows, we often use index-free notation for unknowns, like $\mathbf{x} = (x, y, z)$ and $(\alpha_1, \alpha_2, \alpha_3) = (a, b, c)$.

Remark 4.1.4. The canonical representatives of a pencil $\mathcal{L}$ also explain why the symbol $[(1, 1, \ldots, 1)]$ is not to a Segre symbol. The matrices P, Q corresponding to such partition would in fact be linearly dependent diagonal matrices that do not span a two dimensional linear subspace of $\mathbb{S}^n$.

Example 4.1.5 ($n = 5$)**.** Let $\sigma = [(2, 1), 2]$. The list of elementary divisors equals

$$(\lambda - a)^2, \ (\lambda - a), \ (\lambda - b)^2.$$

Our canonical representative (4.1.4) for this class of pencils $\mathcal{L}$ is the matrix pair

$$P = \begin{pmatrix} 0 & a & 0 & 0 & 0 \\ a & 1 & 0 & 0 & 0 \\ 0 & 0 & a & 0 & 0 \\ 0 & 0 & 0 & 0 & b \\ 0 & 0 & 0 & b & 1 \end{pmatrix} \quad \text{and} \quad Q = \begin{pmatrix} 0 & 1 & 0 & 0 & 0 \\ 1 & 0 & 0 & 0 & 0 \\ 0 & 0 & 1 & 0 & 0 \\ 0 & 0 & 0 & 0 & 1 \\ 0 & 0 & 0 & 1 & 0 \end{pmatrix}.$$

The quadrics $P = 2axy + y^2 + az^2 + 2buv + v^2$ and $Q = 2xy + z^2 + 2uv$ define a degenerate del Pezzo surface of degree four in $\mathbb{P}^4$. This surface has two singular points, $(0 : 0 : 0 : 1 : 0)$ and $(1 : 0 : 0 : 0 : 0)$; their multiplicities are one and three.

Remark 4.1.6. To appreciate Theorem 4.1.1 and Corollary 4.1.3, it helps to distinguish the two geometric figures associated with a pencil of quadrics, and how the groups $\mathrm{GL}(2)$ and $\mathrm{GL}(n)$ act on these. First, there is the configuration of n points in $\mathbb{P}^1$ defined by $\det(\mathcal{L})$. This configuration undergoes projective transformations via $\mathrm{GL}(2)$ but it is left invariant by $\mathrm{GL}(n)$. Second, there is the codimension 2 variety in $\mathbb{P}^{n-1}$ defined by the intersection of the two quadrics in $\mathcal{L}$. This variety undergoes projective transformations via $\mathrm{GL}(n)$ but it is left invariant by $\mathrm{GL}(2)$. Hence, combining Theorem 4.1.1 and Corollary 4.1.3, we want these two geometric figures to be invariant when looking at isomorphic pencils, and this is possible by acting on pencils with the two groups $\mathrm{GL}(2)$ and $\mathrm{GL}(n)$.

In this section, pencils $\mathcal{L} = \mathbb{C}\{A, B\}$ are studied by linear algebra over a PID. We use the relationship between elementary divisors and invariant factors. One can compute these with the *Smith normal form* algorithm over $\mathbb{C}[\lambda]$. We apply this to a specific torsion module, namely the cokernel of our matrix $A - \lambda B$.

Fix n and a Segre symbol $\sigma = [\sigma_1, \ldots, \sigma_r]$, where each entry is now a weakly decreasing vector $\sigma_i = (\sigma_{i1}, \sigma_{i2}, \ldots, \sigma_{in})$ of nonnegative integers. With this convention, the Segre symbol $\sigma = [\sigma_1, \sigma_2]$ in Example 4.1.5, with $n = 5, s = 3, r = 2$, has $\sigma_1 = (2, 1, 0)$ and $\sigma_2 = (2, 0, 0)$. Write $\alpha_1, \ldots, \alpha_r \in \mathbb{C}$ for the distinct roots of $\det(A - \lambda B)$. Then the elementary divisors are $(\lambda - \alpha_i)^{\sigma_{ij}}$ for $i = 1, \ldots, r$ and $j = 1, \ldots, n$. Only s of these are different from 1. The invariant factors are

$$d_j := \prod_{i=1}^{r} (\lambda - \alpha_i)^{\sigma_{ij}} \quad \text{for } j = 1, \ldots, n.$$

Note that $d_n \,|\, d_{n-1} \,|\, \cdots \,|\, d_2 \,|\, d_1$. The number of nontrivial invariant factors is the maximum number of parts among the r partitions σ_i. For instance, in Example 4.1.5, the invariant factors are $d_1 = (\lambda - a)^2 (\lambda - b)^2$, $d_2 = \lambda - a$, $d_3 = d_4 = d_5 = 1$.

The ideal of $k \times k$ minors of $A - \lambda B$ is generated by the greatest common divisor D_k of these minors. The theory of modules over a PID tells us that

$$D_k := \prod_{j=1}^{k} d_{n+1-j} = \prod_{i=1}^{r} (\lambda - \alpha_i)^{\sigma_{i,n-k+1}+\cdots+\sigma_{i,n-1}+\sigma_{i,n}}. \tag{4.1.5}$$

The Segre symbol of a pencil $\mathcal{L} = \mathbb{C}\{A, B\}$ is determined by the ideal of $k \times k$ minors of $A - \lambda B$ for $k = 1, \ldots, n$. In practice, we use the Smith normal form of $A - \lambda B$. Observe that the method introduced above, making use of the Jordan canonical form of AB^{-1}, uses only linear algebra over $\mathbb{C}$, unlike the Smith normal form. To see that the Jordan canonical form of AB^{-1} reveals the Segre symbol, consider the transformation from (A, B) to (P, Q) in Corollary 4.1.3. This preserves the conjugacy class of AB^{-1}. Therefore, AB^{-1} and PQ^{-1} have the same Jordan canonical form. We see in (4.1.4) that Q is a permutation matrix, and hence so is Q^{-1}. Furthermore, P is already in Jordan canonical form, after permuting rows and columns, and σ is clearly visible in P.

4.1.1. The reciprocal curve

The object of study of this subsection is the reciprocal curve $\mathbb{P}\mathcal{L}^{-1}$ associated to a regular pencil $\mathcal{L}$. This is defined as the variety in $\mathbb{P}(\mathbb{S}^n)$ parametrizing the inverses of all invertible matrices in $\mathcal{L}$. In Theorem 4.1.9 we prove that this is a rational normal curve, express its degree $\deg(\mathcal{L}^{-1})$ in terms of Segre symbols, and give an algorithm for computing generators of the homogeneous prime ideal defining it.

Example 4.1.7 ($n = 3$)**.** For the five Segre symbols corresponding to pencils of conics in the projective plane $\mathbb{P}^2$, we have $\deg(\mathcal{L}^{-1}) = 2$ in three cases, so $\mathbb{P}\mathcal{L}^{-1}$ is a plane conic. In the other two cases, $\mathbb{P}\mathcal{L}^{-1}$ is a line in $\mathbb{P}^5$. Here are the homogeneous prime ideals of these curves:

Segre symbol	Ideal of the reciprocal curve $\mathbb{P}\mathcal{L}^{-1}$	mingens
$[1,1,1]$	$\langle x_{12}, x_{13}, x_{23}, (c{-}b)x_{11}x_{22} + (a{-}c)x_{11}x_{33} + (b{-}a)x_{22}x_{33}\rangle$	$(3,1)$
$[2,1]$	$\langle\, x_{13}, x_{22}, x_{23}, x_{12}^2 + (c-a)x_{11}x_{33} - 2x_{12}x_{33}\,\rangle$	$(3,1)$
$[3]$	$\langle\, x_{23}, x_{33}, x_{13} - 2x_{22}, x_{12}^2 - x_{11}x_{22}\,\rangle$	$(3,1)$
$[(1,1),1]$	$\langle\, x_{12}, x_{13}, x_{23}, x_{11} - x_{22}\,\rangle$	$(4,0)$
$[(2,1)]$	$\langle\, x_{13}, x_{22}, x_{23}, x_{12} - 2x_{33}\,\rangle$	$(4,0)$

The column "mingens" gives the numbers of linear and quadratic generators.

Example 4.1.8 ($n = 4$)**.** Two quadrics P and Q in $\mathbb{P}^3$ meet in a quartic curve. There are 13 cases, one for each Segre symbol. Here, x, y, z, u are coordinates on $\mathbb{P}^3$.

symbol	codims	degrees	mingens	quadrics P, Q	variety in $\mathbb{P}^3$
$[1,1,1,1]$	$0,0,0$	$(\mathbf{3},3,5)$	$(6,3)$	$\begin{matrix} ax^2+by^2+cz^2+du^2 \\ x^2+y^2+z^2+u^2 \end{matrix}$	*elliptic curve*
$[2,1,1]$	$1,1,1$	$(\mathbf{3},2,4)$	$(6,3)$	$\begin{matrix} 2axy+y^2+cz^2+du^2 \\ 2xy+z^2+u^2 \end{matrix}$	*nodal curve*
$[(1,1),1,1]$	$3,2,2$	$(\mathbf{2},2,3)$	$(7,1)$	$\begin{matrix} a(x^2+y^2)+cz^2+du^2 \\ x^2+y^2+z^2+u^2 \end{matrix}$	*two conics meet twice*
$[3,1]$	$2,2,2$	$(\mathbf{3},1,3)$	$(6,3)$	$\begin{matrix} 2axz+ay^2+2yz+du^2 \\ 2xz+y^2+u^2 \end{matrix}$	*cuspidal curve*
$[2,2]$	$2,2,2$	$(\mathbf{3},1,3)$	$(6,3)$	$\begin{matrix} 2axy+y^2+2bzu+u^2 \\ 2xy+2zu \end{matrix}$	*twisted cubic with secant*
$[(2,1),1]$	$4,3,3$	$(\mathbf{2},1,2)$	$(7,1)$	$\begin{matrix} 2axy+y^2+az^2+du^2 \\ 2xy+z^2+u^2 \end{matrix}$	*two tangent conics*
$[4]$	$3,3,3$	$(\mathbf{3},0,2)$	$(6,3)$	$\begin{matrix} 2axu+2ayz+2yu+z^2 \\ 2xu+2yz \end{matrix}$	*twisted cubic with tangent*
$[2,(1,1)]$	$4,3,3$	$(\mathbf{2},1,2)$	$(7,1)$	$\begin{matrix} 2axy+y^2+c(z^2+u^2) \\ 2xy+z^2+u^2 \end{matrix}$	*conic meets two lines*
$[(3,1)]$	$5,4,4$	$(\mathbf{2},0,1)$	$(7,1)$	$\begin{matrix} 2axz+ay^2+2yz+au^2 \\ 2xz+y^2+u^2 \end{matrix}$	*conic and two lines concur*
$[(1,1),(1,1)]$	$6,4,4$	$(\mathbf{1},1,1)$	$(8,0)$	$\begin{matrix} a(x^2+y^2)+c(z^2+u^2) \\ x^2+y^2+z^2+u^2 \end{matrix}$	*quadrangle of lines*
$[(1,1,1),1]$	$8,5,5$	$(\mathbf{1},1,1)$	$(8,0)$	$\begin{matrix} a(x^2+y^2+z^2)+du^2 \\ x^2+y^2+z^2+u^2 \end{matrix}$	*double conic*
$[(2,2)]$	$7,5,5$	$(\mathbf{1},0,0)$	$(8,0)$	$\begin{matrix} 2axy+y^2+2azu+u^2 \\ 2xy+2zu \end{matrix}$	*double line and two lines*
$[(2,1,1)]$	$9,6,6$	$(\mathbf{1},0,0)$	$(8,0)$	$\begin{matrix} 2axy+y^2+a(z^2+u^2) \\ 2xy+z^2+u^2 \end{matrix}$	*two double lines*

The bold numbers in the third column show that $\mathbb{P}\mathcal{L}^{-1} \subset \mathbb{P}^9$ is either a line, a plane conic, or a twisted cubic curve. This is explained by the next theorem, which is our main result in Subsection 4.1.1.

Theorem 4.1.9. *Let $\mathcal{L}$ be a regular pencil in $\mathbb{S}^n$ with Segre symbol $\sigma = [\sigma_1, \ldots, \sigma_r]$. Then $\mathbb{P}\mathcal{L}^{-1}$ is a rational normal curve of degree d in $\mathbb{P}(\mathbb{S}^n)$, where $d = \sum_{i=1}^r \sigma_{i1} - 1$ is one less than the sum of the first parts of the partitions in σ. The ideal of $\mathbb{P}\mathcal{L}^{-1}$ is generated by $\binom{n+1}{2} - d - 1$ linear forms and $\binom{d}{2}$ quadrics in $\binom{n+1}{2}$ unknowns.*

Proof. The curve $\mathbb{P}\mathcal{L}^{-1}$ is parametrized by $\binom{n+1}{2}$ rational functions in one unknown λ, namely the entries in the inverse of matrix $P - \lambda Q$, with P and Q as in (4.1.4). We scale each entry by $D_n = \pm\det(P - \lambda Q)$ to get a polynomial parametrization by the adjoint of $P - \lambda Q$. This is an $n \times n$ matrix whose entries are the $(n-1) \times (n-1)$ minors of $P - \lambda Q$. These are polynomials of degree $\leq n - 1$ in λ, which are divisible by the invariant factor D_{n-1}. Note that D_{n-1} has degree $\sum_{i=1}^r \sum_{j=2}^n \sigma_{ij}$ in λ. Subtracting this from the expected degree $n - 1$, we obtain $d = \sum_{i=1}^r \sigma_{i1} - 1$. We remove the factor D_{n-1} from each entry of the adjoint. The resulting matrix $(D_n/D_{n-1}) \cdot (P - \lambda Q)^{-1}$ also parametrizes $\mathbb{P}\mathcal{L}^{-1}$. The entries of that matrix are polynomials in λ of degree $\leq d$. As a key step, we will show that these span the $(d + 1)$-dimensional space $\mathbb{C}[\lambda]_{\leq d}$ of all polynomials in λ of degree $\leq d$.

The inverse of $P - \lambda Q$ is a block matrix, where the blocks are the inverses of the $e \times e$ matrices $P_e(\alpha) - \lambda Q_e$ in (4.1.3), one for each elementary divisor. A computation shows that the entry of $(P_e(\alpha) - \lambda Q_e)^{-1}$ in row i and column j is

$$-(\lambda - \alpha)^{i+j-e-2} \quad \text{if } i + j \leq e + 1 \qquad \text{and} \qquad 0 \quad \text{if } i + j \geq e + 2. \qquad (4.1.6)$$

It follows that the distinct nonzero entries in the $n \times n$ matrix $(P - \lambda Q)^{-1}$ are

$$\pm(\lambda - \alpha_i)^{-k} \quad \text{where } 1 \le k \le \sigma_{i1} \text{ and } 1 \le i \le r. \tag{4.1.7}$$

The common denominator of these $d + 1 = \sum_{i=1}^{r} \sigma_{i1}$ rational functions in λ is equal to $D_n/D_{n-1} = \prod_{i=1}(\lambda - \alpha_i)^{\sigma_{i1}}$. Multiplying by that common denominator, we obtain $d + 1$ polynomials in λ of degree $\le d$. Lemma 4.1.10 below tells us that these polynomials are linearly independent. Hence they span $\mathbb{C}[\lambda]_{\le d} \simeq \mathbb{C}^{d+1}$.

The proof of Theorem 4.1.9 now concludes as follows. By recording which entries of $(P - \lambda Q)^{-1}$ are zero, and which pairs of entries are equal, we obtain $\binom{n+1}{2} - d - 1$ independent linear forms that vanish on $\mathbb{P}\mathcal{L}^{-1}$. We know that there exist linear forms u_i in the matrix entries which evaluate to λ^i for $i = 0, 1, 2, \ldots, d$. The $\binom{d}{2}$ quadrics that vanish on $\mathbb{P}\mathcal{L}^{-1}$ are the 2×2 minors of the $2 \times d$ matrix

$$\begin{pmatrix} u_0 & u_1 & u_2 & \cdots & u_{d-1} \\ u_1 & u_2 & u_3 & \cdots & u_d \end{pmatrix}. \tag{4.1.8}$$

We have thus constructed an isomorphism between our curve $\mathbb{P}\mathcal{L}^{-1}$ and the rational normal curve $\{(1 : \lambda : \cdots : \lambda^d)\}$, whose prime ideal is given by (4.1.8). ∎

Notice that the final part of the proof gives an algorithm for computing generators of the homogeneous prime ideal that defines the reciprocal curve.

Lemma 4.1.10. *A finite set of distinct rational functions $(\lambda - \alpha_j)^{-s_{ij}}$, each a negative power of one of the expressions $\lambda - \alpha_1, \ldots, \lambda - \alpha_r$, is linearly independent.*

Proof. We use induction on r. The base case is $r = 1$. We claim that $(\lambda - \alpha)^{-s_1}, \ldots, (\lambda - \alpha)^{-s_n}$ are linearly independent when $0 < s_1 < \cdots < s_n$. Suppose

$$k_1(\lambda - \alpha)^{-s_1} + \cdots + k_n(\lambda - \alpha)^{-s_n} = 0 \quad \text{for some } k_1, \ldots, k_n \in \mathbb{C}.$$

Clearing denominators, we obtain $k_1(\lambda - \alpha)^{s_n - s_1} + \cdots + k_n = 0$. Setting $\lambda = \alpha$ we find $k_n = 0$. Repeating this computation n times, we conclude $k_1 = k_2 = \cdots = k_n = 0$.

For the induction step from $r - 1$ to r, we consider distinct negative powers

$$\begin{array}{cccc} (\lambda - \alpha_1)^{-s_{1,1}}, & (\lambda - \alpha_1)^{-s_{1,2}}, & \ldots, & (\lambda - \alpha_1)^{-s_{1,n_1}}, \\ \vdots & \vdots & & \vdots \\ (\lambda - \alpha_r)^{-s_{r,1}}, & (\lambda - \alpha_r)^{-s_{r,2}}, & \ldots, & (\lambda - \alpha_r)^{-s_{r,n_r}}, \end{array} \tag{4.1.9}$$

where $0 \le s_{i,j} < s_{i,j+1}$ for $i = 1, \ldots, r$ and $j = 1, \ldots, n_i$. Consider a linear combination of (4.1.9) with coefficients $k_{1,1}, \ldots, k_{r,n_r}$. Multiplying by $(\lambda - \alpha_r)^{s_{r,n_r}}$ and setting $\lambda = \alpha_r$, we find $k_{r,n_r} = 0$. Repeating with $(\lambda - \alpha_r)^{s_{r,i}}$ for $i = n_r-1, n_r-2, \ldots, 1$, we get $k_{r,1} = \cdots = k_{r,n_r} = 0$. By the induction hypothesis, the first $r - 1$ rows of (4.1.9) are linearly independent. This proves that all $k_{i,j}$ are zero. Lemma 4.1.10 follows. ∎

The last paragraph in the proof of Theorem 4.1.9 gives an algorithm for computing generators of the ideal of $\mathbb{P}\mathcal{L}^{-1}$. We show this for our running example.

Example 4.1.11. Let $\sigma = [(2, 1), 2]$ as in Example 4.1.5. We have $d = \sigma_{11} + \sigma_{21} - 1 = 3$, so $\mathbb{P}\mathcal{L}^{-1}$ is a twisted cubic curve in $\mathbb{P}^{14}$. The inverse of $P - \lambda Q$ satisfies the $\binom{6}{2} - 3 - 1 = 11$ linear

forms $x_{13}, x_{14}, x_{15}, x_{22}, x_{23}, x_{24}, x_{25}, x_{34}, x_{35}, x_{55}, x_{12} - x_{33}$. The quadratic ideal generators are $u_0 u_2 - u_1^2$, $u_0 u_3 - u_1 u_2$ and $u_1 u_3 - u_2^2$, where

$$
\begin{aligned}
u_0 &= & (a-b)x_{11} - 2x_{12} + (a-b)x_{44} + 2x_{45}\,, \\
u_1 &= & (a^2 - ab)x_{11} - (a+b)x_{12} + (ab - b^2)x_{44} + (a+b)x_{45}\,, \\
u_2 &= & (a^3 - a^2 b)x_{11} - 2ab x_{12} + (ab^2 - b^3)x_{44} + 2ab x_{45}\,, \\
u_3 &= & (a^4 - a^3 b)x_{11} + (a^3 - 3a^2 b)x_{12} + (ab^3 - b^4)x_{44} + (3ab^2 - b^3)x_{45}.
\end{aligned}
$$

Note that $x_{11} = -(\lambda - a)^{-2}$, $x_{12} = (\lambda - a)^{-1}$, $x_{44} = -(\lambda - b)^{-2}$, $x_{45} = (\lambda - b)^{-1}$.

4.1.2. Maximum likelihood degrees

Let $\mathbb{S}_{>0}^n$ denote the open convex cone of positive definite real symmetric $n \times n$ matrices. For any fixed $S \in \mathbb{S}^n$, we consider the following *log-likelihood function*:

$$
\ell_S : \mathbb{S}_{>0}^n \to \mathbb{R}, \qquad M \mapsto \log(\det(M)) - \mathrm{trace}(SM). \tag{4.1.10}
$$

We seek to compute the critical points of ℓ_S restricted to a smooth subvariety of $\mathbb{S}^n$. Here, by a *critical point* we mean a nonsingular matrix M in the subvariety whose normal space contains the gradient vector of ℓ_S at M. This is an algebraic problem because the $\binom{n+1}{2}$ partial derivatives of ℓ_S are rational functions.

The determinant and the trace of a square matrix are invariant under conjugation. This implies the following identity for all invertible $n \times n$ matrices g:

$$
\ell_{g^{-1} S (g^{-1})^T}(g^T M g) = \log(\det(g^T M g)) - \mathrm{trace}(g^{-1} S M g) = \ell_S(M) + \mathrm{const}. \tag{4.1.11}
$$

Let $\mathcal{L}$ be a linear subspace of $\mathbb{S}^n$, and fix a generic matrix $S \in \mathbb{S}^n$. The *ML degree* $\mathrm{mld}(\mathcal{L})$ is the number of complex critical points of ℓ_S on $\mathcal{L}$. The *reciprocal ML degree* $\mathrm{rmld}(\mathcal{L})$ of $\mathcal{L}$ is the number of complex critical points of ℓ_S on $\mathcal{L}^{-1}$. Both ML degrees do not depend on the choice of S, as long as S is generic. The ML degrees are invariant under the action of $\mathrm{GL}(n)$ by congruence on $\mathbb{S}^n$:

Lemma 4.1.12. *The ML degree and the reciprocal ML degree of a subspace $\mathcal{L} \subset \mathbb{S}^n$ are determined by its congruence class. In particular, this holds for two-dimensional subspaces $\mathcal{L}$, i.e. for pencils of quadrics.*

Proof. Fix g and $\mathcal{L}$. If the matrix S is generic in $\mathbb{S}^n$ then so is $g^{-1} S (g^{-1})^T$. The image of $\mathcal{L}$ under congruence by g^T consists of all matrices $g^T M g$ where $M \in \mathcal{L}$. By (4.1.11), the likelihood function of S on $\mathcal{L}$ agrees with that of $g^{-1} S (g^{-1})^T$ on $g^T \mathcal{L} g$, up to an additive constant. The two functions have the same number of critical points, so the subspaces $\mathcal{L}$ and $g^T \mathcal{L} g$ have the same ML degree. The same argument works if $\mathcal{L}$ is replaced by any nonlinear variety, such as $\mathcal{L}^{-1}$. ∎

We now focus on pencils ($m = 2$), and we state our main result in Subsection 4.1.2 which provides explicit formulas for the number of critical points of the log-likelihood function when restricting to a pencil of quadrics in terms of Segre symbols.

Theorem 4.1.13. *Let $\mathcal{L}$ be a pencil with Segre symbol $\sigma = [\sigma_1, \ldots, \sigma_r]$. Then*

$$
\mathrm{mld}(\mathcal{L}) = r - 1 \quad \text{and} \quad \mathrm{rmld}(\mathcal{L}) = \sum_{i=1}^r \sigma_{i1} + r - 3 = \deg(\mathcal{L}^{-1}) + \mathrm{mld}(\mathcal{L}) - 1. \tag{4.1.12}
$$

For generic subspaces $\mathcal{L}$, with Segre symbol $\sigma = [1, \ldots, 1]$, this implies

$$\mathrm{mld}(\mathcal{L}) = \deg(\mathcal{L}^{-1}) = n - 1 \qquad \text{and} \qquad \mathrm{rmld}(\mathcal{L}) = 2n - 3. \qquad (4.1.13)$$

The left formula in (4.1.13) appears in [SU10, Section 2.2]. The right formula in (4.1.13) is due to Coons, Marigliano and Ruddy [CMR20]. We here generalize these results to arbitrary pencils $\mathcal{L}$. The proof of Theorem 4.1.13 appears at the end of this subsection.

The log-likelihood function (4.1.10), which appeared already in Chapter 3, is of fundamental importance in statistics. The sample covariance matrix S encodes data points in $\mathbb{R}^n$. The matrix M is the concentration matrix. Its inverse M^{-1} is the covariance matrix. These represent Gaussian distributions on $\mathbb{R}^n$. The subspace $\mathcal{L}$ encodes linear constraints, either on M or on M^{-1}. For the former, we get the ML degree. For the latter, we get the reciprocal ML degree. These degrees measure the algebraic complexity of maximum likelihood estimation. In the language in [CMR20, STZ20], $\mathrm{mld}(\mathcal{L})$ refers to the *linear concentration model,* while $\mathrm{rmld}(\mathcal{L})$ refers to the *linear covariance model.*

If $\mathcal{L}$ is a statistical model, then it contains a positive definite matrix. In symbols, $\mathcal{L} \cap \mathbb{S}_{>0}^n \neq \varnothing$. If this holds and $\dim(\mathcal{L}) = 2$ then $\mathcal{L}$ is called a *d-pencil* [Uhl79]. Thus, our numbers $\mathrm{mld}(\mathcal{L})$ and $\mathrm{rmld}(\mathcal{L})$ are interesting for statistics when $\mathcal{L}$ is a d-pencil. Here, we can take advantage of the following linear algebra fact.

Lemma 4.1.14. *Every d-pencil $\mathcal{L}$ can be simultaneously diagonalized over $\mathbb{R}$. After a change of coordinates, $\mathcal{L}$ is spanned by the quadrics $\sum_{i=1}^n a_i x_i^2$ and $\sum_{i=1}^n x_i^2$.*

Proof. We assume $n \geq 3$. A pencil is a d-pencil if and only if it has no zeros in the real projective space $\mathbb{P}^{n-1}$. This is the Main Theorem in [Uhl79]. It was also proved by Calabi in [Cal64]. The fact that pencils without real zeros in $\mathbb{P}^{n-1}$ can be diagonalized is [Uhl79, page 221, (PM)]. It is also Remark 2 in [Cal64, page 846]. $\blacksquare$

Suppose there are r distinct elements in $\{a_1, \ldots, a_n\}$. Theorem 4.1.13 implies:

Corollary 4.1.15. *If $\mathcal{L}$ is a d-pencil then $\mathrm{mld}(\mathcal{L}) = \deg(\mathcal{L}^{-1}) = r - 1$ and $\mathrm{rmld}(\mathcal{L}) = 2r - 3$, where $\mathcal{L}$ has r distinct eigenvalues. This holds for all subspaces $\mathcal{L}$ that represent statistical models, since such an $\mathcal{L}$ contains positive definite matrices.*

The log-likelihood function for our d-pencil $\mathcal{L}$ can be written as follows:

$$\ell_S(x, y) = \sum_{i=1}^n \big(\log(a_i x + y) - s_i(a_i x + y) \big).$$

Here $s_1, \ldots, s_n \in \mathbb{R}$ represent data. The MLE is the maximizer of $\ell_S(x, y)$ over the cone $\{(x, y) \in \mathbb{R}^2 : a_i x + y > 0 \text{ for } i = 1, \ldots, n\}$. Corollary 4.1.15 says that $\ell_S(x, y)$ has $r - 1$ critical points. One of them is the MLE. The reciprocal log-likelihood is

$$\tilde{\ell}_S(x, y) = \sum_{i=1}^n \Big(-\log(a_i x + y) - \frac{s_i}{a_i x + y} \Big). \qquad (4.1.14)$$

The invariant $\mathrm{rmld}(\mathcal{L})$ is the number of critical points (x^*, y^*) of this function with $\prod_{i=1}^n (a_i x^* + y^*) \neq 0$, provided $s = (s_1, \ldots, s_n)$ is generic in $\mathbb{R}^n$. Corollary 4.1.15 states that $\tilde{\ell}_S(x, y)$ has $2r - 3$ complex critical points. One of them is the MLE.

The following is an extension of a conjecture stated by Coons et al. [CMR20, §6].

Conjecture 4.1.16. *Let $\mathcal{L}$ be a d-pencil with r distinct eigenvalues. There exists $s = (s_1, \ldots, s_n) \in \mathbb{R}^n$ such that the function (4.1.14) has $2r - 3$ distinct real critical points.*

We can prove this conjecture for small values of n by explicit computation.

Example 4.1.17. Fix the pencil $\mathcal{L}$ with $n = r$ and $(a_1, \ldots, a_n) = (1, \ldots, n)$. For $n \leq 7$ we found $s \in \mathbb{R}^n$ such that the reciprocal log-likelihood function $\tilde{\ell}_s$ has $2n - 3$ distinct real critical points. For $n = 7$ we can take $s = \left(-\frac{74}{39}, \frac{13}{47}, \frac{61}{40}, \frac{1}{7}, \frac{23}{18}, -73, -\frac{27}{43}\right)$.

We now return to arbitrary Segre symbols σ. While non-diagonalizable pencils $\mathcal{L}$ do not arise in applied statistics, their likelihood geometry is interesting.

Proof of Theorem 4.1.13. By Lemma 4.1.12, we may assume that $\mathcal{L}$ is parametrized by $(x, y) \mapsto xP - yQ$ with P and Q as in (4.1.4). For generic $S \in \mathbb{S}^n$, we seek the number $\mathrm{mld}(\mathcal{L})$ of critical points in $\mathbb{C}^2$ of the following function in two variables:

$$\ell_S(x, y) \;=\; \log(\det(xP - yQ)) \,-\, \mathrm{trace}(S(xP - yQ)). \tag{4.1.15}$$

After multiplying by $d = \prod_{i=1}^r (\alpha_i x - y)$, the two partial derivatives of $\ell_S(x, y)$ have the form $f(x, y) = \lambda_S d + C$ and $g(x, y) = \mu_S d + D$. Here $\lambda_S = -\mathrm{trace}(SP)$ and $\mu_S = \mathrm{trace}(SQ)$ are constants, and the following are binary forms of degree $r - 1$:

$$C \;=\; \sum_{i=1}^r \sum_{j=1}^n \sigma_{ij}\, \alpha_i \prod_{k=1, k \neq i}^r (\alpha_k x - y) \quad \text{and} \quad D \;=\; -\sum_{i=1}^r \sum_{j=1}^n \sigma_{ij} \prod_{k=1, k \neq i}^r (\alpha_k x - y). \tag{4.1.16}$$

The variety of critical points of ℓ_S in $\mathbb{C}^2$ is $V(f, g) \backslash V(d)$. We adapt the method introduced in [CMR20] to enumerate this set. Let $F(x, y, z)$ and $G(x, y, z)$ denote the homogenizations of f and g with respect to z. Both F and G define curves of degree r in $\mathbb{P}^2$. Since F and G do not share a common component, we can apply Bézout's Theorem to count their intersection points. This tells us that

$$\mathrm{mld}(\mathcal{L}) \;=\; r^2 \,-\, I_{[0:0:1]}(F, G) \,-\, \sum_{q \in V(F, G, z)} I_q(F, G). \tag{4.1.17}$$

The negated expressions are the intersection multiplicities of F and G at the origin and on the line at infinity. By computing these two quantities, we obtain

$$\mathrm{mld}(\mathcal{L}) \;=\; r^2 - (r-1)^2 - r \;=\; r - 1.$$

The proof of the second formula in (4.1.12) is analogous but the details are more delicate. We present an outline. The log-likelihood function for $\mathcal{L}^{-1}$ equals

$$\tilde{\ell}_S(x, y) \;=\; -\log\left(\prod_{i=1}^r (\alpha_i x - y)^{\sigma_{i1} + \cdots + \sigma_{in}}\right) \,-\, \sum_{i=1}^r \sum_{j=1}^{\sigma_{i1}} \tilde{s}_{ij} \frac{x^{j-1}}{(\alpha_i x - y)^j},$$

where the $\tilde{s}_{ij}$ are linear combinations of the entries in the matrix S. This is obtained by replacing the matrix $xP - yQ$ in (4.1.15) with its inverse. We find

$$\begin{aligned}
\tilde{\ell}_{S_x} &= -\sum_{i=1}^r \sum_{j=1}^n \frac{\sigma_{ij}\alpha_i}{\alpha_i x - y} \,+\, \sum_{i=1}^r \sum_{j=1}^{\sigma_{i1}} \tilde{s}_{ij} \frac{(j-1)x^{j-2}(\alpha_i x - y) - j\, x^{j-1}\alpha_i}{(\alpha_i x - y)^{j+1}}, \\
\tilde{\ell}_{S_y} &= \sum_{i=1}^r \sum_{j=1}^n \frac{\sigma_{ij}}{\alpha_i x - y} \,+\, \sum_{i=1}^r \sum_{j=1}^{\sigma_{i1}} \tilde{s}_{ij} \frac{j\, x^{j-1}}{(\alpha_i x - y)^{j+1}}.
\end{aligned} \tag{4.1.18}$$

We claim that the number of common zeros of the two partial derivatives $\tilde{\ell}_{S_x}$ and $\tilde{\ell}_{S_y}$ in $\mathbb{C}^2 \backslash V(d)$ is equal to $\varphi + r - 3$ where $\varphi = \sum_{i=1}^r \sigma_{i1} = \deg(\mathcal{L}^{-1}) + 1$,

Clearing denominators in (4.1.18) yields polynomials $-d'C + U$ and $-d'D + V$, where $d' = \prod_{i=1}^{r}(\alpha_i x - y)^{\sigma_{i1}}$, the binary forms U, V have degree $\varphi + r - 2$, and C, D are precisely as in (4.1.16). Hence $\deg(d') = \varphi$ and $\deg(C) = \deg(D) = r - 1$. As before, these are sums of binary forms in consecutive degrees. We use (4.1.17) to count their zeros in $\mathbb{P}^2$. We find $(\varphi + r - 1)^2 - (\varphi + r - 2)^2 - (\varphi + r) = \varphi + r - 3$ ∎

Example 4.1.18 ($n = 5$). Let $\sigma = [(2,1),2]$ as in Example 4.1.5. The ML degrees are $\mathrm{mld}(\mathcal{L}) = 1$ and $\mathrm{rmld}(\mathcal{L}) = 3$. Restricting the log-likelihood function to $\mathcal{L}$ gives

$$\ell_S = \log\big((ax - y)^3(bx - y)^2\big) + 2s_{12}(ax - y) + s_{22}x + s_{33}(ax - y) + 2s_{45}(bx - y) + s_{55}x.$$

Its two partial derivatives are rational functions in x and y. Equating these to zero, we find that ℓ_S has a unique critical point (x^*, y^*) in $\mathcal{L}$. Its coordinates are

$$
\begin{aligned}
x^* &= \big(4(a - b)s_{12} + 5s_{22} + 2(a - b)s_{33} - 6(b - a)s_{45} + 5s_{55}\big)/\Delta, \\
y^* &= \big(4a(a - b)s_{12} + (2a + 3b)s_{22} + 2a(a - b)s_{33} + 6b(b - a)s_{45} + (2a + 3b)s_{55}\big)/\Delta, \\
\Delta &= \big(-s_{22} + 2(a - b)s_{45} - s_{55}\big) \cdot \big(2(a - b)s_{12} + s_{22} + (a - b)s_{33} + s_{55}\big).
\end{aligned}
$$

The restriction of the log-likelihood function to the reciprocal variety $\mathcal{L}^{-1}$ is

$$\tilde{\ell}_S(x, y) = -\log\big((ax - y)^3(bx - y)^2\big) - \frac{s_{11}\,x}{(ax - y)^2} + \frac{2\,s_{12}}{ax - y} + \frac{s_{33}}{ax - y} - \frac{s_{44}\,x}{(bx - y)^2} + \frac{2\,s_{45}}{bx - y}.$$

The two partial derivatives have 3 zeros, expressible in radicals in $a, b, s_{11}, \ldots, s_{45}$.

4.1.3. Strata in the Grassmannian

In this subsection we study the constructible set defined by a fixed Segre symbol:

$$\mathrm{Gr}_\sigma = \big\{ \mathcal{L} \in \mathrm{Gr}(2, \mathbb{S}^n)^{\mathrm{reg}} : \sigma(\mathcal{L}) = \sigma \big\}. \tag{4.1.19}$$

Its closure $\overline{\mathrm{Gr}}_\sigma$ is a variety. We study these varieties and their poset of inclusions, seen in Figure 4.1. This extends the stratification of $\mathrm{Gr}(2, \mathbb{R}^n)$ by matroids, see [GGMS87]. Indeed, if $\mathcal{L}$ consists of diagonal matrices then the Segre symbol $\sigma(\mathcal{L})$ specifies the rank 2 matroid of $\mathcal{L}$, up to permuting the ground set $\{1, 2, \ldots, n\}$.

Example 4.1.19 ($n = 3$). five strata Gr_σ in the Grassmannian $\mathrm{Gr}(2, \mathbb{S}^3)$:

symbol	codim	degrees	P	Q	variety in $\mathbb{P}^2$
$[1,1,1]$	0	$(2,2,3)$	$ax^2+by^2+cz^2$	$x^2+y^2+z^2$	*four reduced points*
$[2,1]$	1	$(2,1,2)$	$2axy+y^2+bz^2$	$2xy + z^2$	*one double point, two others*
$[3]$	2	$(2,0,1)$	$2axz+ay^2+2yz$	$2xz + y^2$	*one triple point, one other*
$[(1,1),1]$	2	$(1,1,1)$	$ax^2+ay^2+bz^2$	$x^2+y^2+z^2$	*two double points*
$[(2,1)]$	3	$(1,0,0)$	$2axy+y^2+az^2$	$2xy + z^2$	*quadruple point*

For each Segre symbol σ, we display $\mathrm{codim}(\mathrm{Gr}_\sigma)$, the triple of degrees $\deg(\mathcal{L}^{-1})$, $\mathrm{mld}(\mathcal{L})$, and $\mathrm{rmld}(\mathcal{L})$, the basis $\{P, Q\}$ from Section 4.1, and its variety in $\mathbb{P}^2$. Here, x, y, z are coordinates on $\mathbb{P}^2$, and a, b, c are distinct nonzero reals. This accounts for all regular pencils. A pencil is singular if P and Q share a linear factor or if they are generated by two quadrics that are both unions of two lines from the same pencil of lines, see [Kle97] for more details.

We now define a partial order on the set Segre_n of all Segre symbols for fixed n. If σ and τ are in Segre_n then we say that σ *is above* τ if one of the following conditions hold:

    i. $|\sigma| > |\tau|$ and τ is obtained from σ by replacing two partitions σ_i, σ_j by their sum; or

    ii. $|\sigma| = |\tau|$ and σ and τ differ in precisely one partition, with index i, and $\tau_i \lhd \sigma_i$ in the dominance order on partitions.

The partial order on Segre_n is the transitive closure of the relation "is above". The top element of our poset is $[1, 1, \ldots, 1]$, and the bottom element is $[(2, 1, \ldots, 1)]$. The Hasse diagrams for $n = 3, 4$ are shown in Figure 4.1.
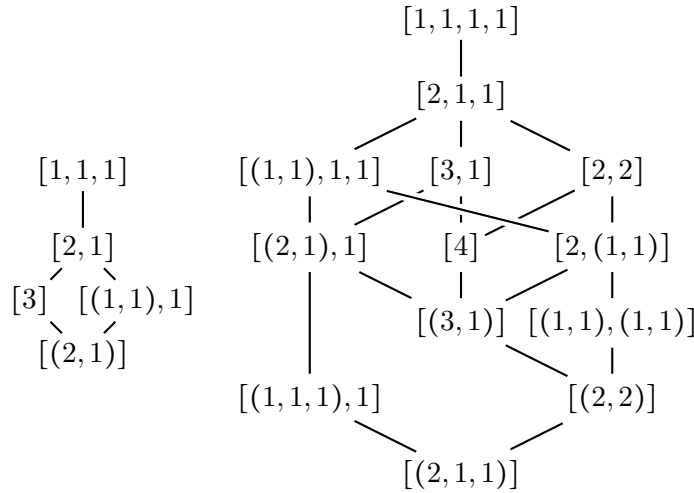

Figure 4.1. The posets of all Segre symbols for $n = 3$ (left) and $n = 4$ (right).

    We wish to study the strata Gr_σ in (4.1.19). Recall that Gr_σ is the constructible subset of $\mathrm{Gr}(2, \mathbb{S}^n)$ whose points are the pencils $\mathcal{L}$ with $\sigma(\mathcal{L}) = \sigma$. Its closure $\overline{\mathrm{Gr}}_\sigma$ is a subvariety of the Grassmannian $\mathrm{Gr}(2, \mathbb{S}^n)$. Its defining equations can be written either in the $\frac{1}{8}(n+2)(n+1)n(n-1)$ Plücker coordinates, or in the $(n+1)n$ Stiefel coordinates which are the matrix entries in a basis $\{A, B\}$ of $\mathcal{L}$. Depending on the choice on the coordinates, we may refer to the strata Gr_σ as Plücker or Stiefel strata, respectively.

    Consider the related *Jordan stratification.* For each $\sigma \in \mathrm{Segre}_n$, the Jordan stratum Jo_σ is the set of $n \times n$ matrices whose Jordan canonical form has pattern σ. Its closure $\overline{\mathrm{Jo}}_\sigma$ is an affine variety in $\mathbb{C}^{n \times n}$. Its defining prime ideal consists of homogeneous polynomials in the entries of an $n \times n$ matrix $X = (x_{ij})$.

Theorem 4.1.20. *Our poset models inclusions of both Grassmann strata and Jordan strata. That is, $\sigma \geq \tau$ in Segre_n if and only if $\overline{\mathrm{Gr}}_\sigma \supseteq \overline{\mathrm{Gr}}_\tau$ if and only if $\overline{\mathrm{Jo}}_\sigma \supseteq \overline{\mathrm{Jo}}_\tau$.*

    The codimensions of the Jordan strata generally differ from those of the Grassmann strata. While the $\overline{\mathrm{Jo}}_\sigma$ are familiar from linear algebra [DE18], the $\overline{\mathrm{Gr}}_\sigma$ capture the geometry of the varieties listed on the right in Examples 4.1.19 and 4.1.8. The codimensions are ≥ 1, unless $\sigma = [1, \ldots, 1]$ where both strata are dense.

Example 4.1.21 ($n = 3$)**.** We computed the prime ideals for the Jordan strata in $\mathbb{C}^{3 \times 3}$, for the Plücker strata in $\mathrm{Gr}(2, \mathbb{S}^3) \subset \mathbb{P}^{14}$, and for the Stiefel strata in $\mathbb{P}^5 \times \mathbb{P}^5$:

symbol	Jordan	Plücker	Stiefel	codims	degrees
$[2, 1]$	6_1	6_1	$(6, 6)_1$	$1, 1, 1$	$6, 6, [6, 6]$
$[3]$	$2_1, 3_1$	4_{21}	$(2, 4)_1, (3, 3)_1, (4, 2)_1$	$2, 2, 2$	$6, 99, [6, 15, 6]$
$[(1,1), 1]$	3_{20}	3_{20}	$(3, 3)_{20}$	$3, 2, 2$	$6, 36, [4, 4, 4]$
$[(2, 1)]$	2_9	2_6	$(2, 2)_6$	$4, 3, 3$	$6, 56, [4, 12, 12, 4]$

The sextic in the first row is the discriminant of the characteristic polynomial of X. We shall explain the last row, indexed by $\sigma = [(2,1)]$. The Jordan stratum Jo_σ has codimension 4 and degree 6. Its ideal is generated by nine quadrics, like $x_{11}x_{31} - 2x_{22}x_{31} + 3x_{21}x_{32} + x_{31}x_{33}$. Under the substitution $X = AB^{-1}$, these transform into six quadrics in Plücker coordinates, like $p_{04}p_{14} + p_{12}p_{14} - p_{03}p_{15} - p_{12}p_{23} - 3p_{02}p_{34} + 2p_{01}p_{35}$. Here $p_{01}, p_{02}, \ldots, p_{45}$ denote the 2×2 minors of

$$\begin{pmatrix} a_{11} & a_{12} & a_{13} & a_{22} & a_{23} & a_{33} \\ b_{11} & b_{12} & b_{13} & b_{22} & b_{23} & b_{33} \end{pmatrix}.$$

The stratum Gr_σ has codimension 3 in $\mathrm{Gr}(2, \mathbb{S}^3)$ and degree 56 in the ambient $\mathbb{P}^{14}$. The six Plücker quadrics give six polynomials of bidegree $(2,2)$ in (A, B). These define a variety of multidegree $4a^3 + 12a^2b + 12ab^2 + 4b^3 \in H^*(\mathbb{P}^5 \times \mathbb{P}^5)$.

Example 4.1.22 $(n = 4)$**.** The column "codims" in Example 4.1.8 gives the codimensions of Jordan strata, Plücker strata and Stiefel strata. The last two agree; they quantify the moduli of quartic curves in $\mathbb{P}^3$ listed on the right. We found equations of low degree for the 13 strata. For instance, $\mathrm{Jo}_{[4]}$ lies on a unique quadric:

$$3x_{11}^2 - 2x_{11}x_{22} - 2x_{11}x_{33} - 2x_{11}x_{44} + 8x_{12}x_{21} + 8x_{13}x_{31} + 8x_{14}x_{41} + 3x_{22}^2$$
$$-2x_{22}x_{33} - 2x_{22}x_{44} + 8x_{23}x_{32} + 8x_{24}x_{42} + 3x_{33}^2 - 2x_{33}x_{44} + 8x_{34}x_{43} + 3x_{44}^2.$$

Proof of Theorem 4.1.20. For Segre symbols σ with one partition σ_1, the Jordan strata Jo_σ are the *nilpotent orbits* of Lie type A_{n-1}. Gerstenhaber's Theorem [Ger61] states that inclusion of nilpotent orbit closures corresponds to the dominance order $\lhd$ among the partitions σ_1. This explains the second condition in our definition of "is above" for the poset Segre_n. The other condition captures the degeneration that occurs when two eigenvalues come together. Generally, this leads to a fusion of Jordan blocks, made manifest by adding partitions σ_i and σ_j. For a precise algebraic version of this argument we refer to [Ger61, Theorem 4].

The inclusions of orbit closures are preserved under the map $X \mapsto AB^{-1}$ that links Stiefel strata to Jordan strata. Furthermore, the Plücker stratification is obtained from the Stiefel stratification by taking the quotient modulo $\mathrm{GL}(2)$. This operation also preserves the combinatorics of orbit closure inclusions. ∎

We close with formulas for the dimensions of our strata. For each partition σ_i occurring in a Segre symbol $\sigma = [\sigma_1, \ldots, \sigma_r]$, we write $\sigma_i^* = (\sigma_{i1}^*, \ldots, \sigma_{in}^*)$ for the conjugate partition. For instance, if $n = 5$ and $\sigma_i = (4, 1)$ then $\sigma_i^* = (2, 1, 1, 1)$.

Proposition 4.1.23. *The codimension of the Jordan strata (in $\mathbb{C}^{n \times n}$) and Grassmann strata (in $\mathrm{Gr}(2, \mathbb{S}^n)$) are:*

$$\mathrm{codim}(\mathrm{Jo}_\sigma) = \sum_{i=1}^r \sum_{j=1}^n (\sigma_{ij}^*)^2 - r \quad \text{and} \quad \mathrm{codim}(\mathrm{Gr}_\sigma) = \sum_{i=1}^r \sum_{j=1}^n \binom{\sigma_{ij}^* + 1}{2} - r.$$

Proof. The dimension is the number r of distinct eigenvalues plus the dimension of the $\mathrm{GL}(n)$-orbit of the general matrix or pencil in the stratum of interest. Thus, the codimension is the dimension of its stabilizer subgroup minus r. The codimension for Grassmann strata agrees with the codimension for Stiefel strata, so we may consider pairs of matrices (A, B) when determining $\mathrm{codim}(\mathrm{Gr}_\sigma)$.

The stabilizer on the left is found in [DE18, Theorem 2.1] or [Ger61, Proposition 8], using the identity $\sum_{k=1}^s (2k - 1) = s^2$. The stabilizer dimension on the right is calculated in [DKgS14, Corollary 2.2] for general symmetric matrix pencils. For regular pencils, the case studied here, the Kronecker canonical form in [DKgS14, eqn. (2.4)] only has H-components.

Thus the dimension formula in [DKgS14] becomes $d_{A,B} = d_H + d_{HH}$, where $d_H = 0$ and $d_{HH} = \sum_{i \leq i', \lambda_i = \lambda_{i'}} \min(h_i, h_{i'})$. In our notation, this is

$$\sum_{i \leq k, \alpha_i = \alpha_k} \min(e_i, e_k) \;=\; \sum_{i=1}^{r} \sum_{k=1}^{n} k\sigma_{ik} \;=\; \sum_{i=1}^{r} \sum_{k=1}^{n} \sum_{j=1}^{\sigma_{ik}} k \;=\; \sum_{i=1}^{r} \sum_{j=1}^{n} \sum_{k=1}^{\sigma^*_{ij}} k \;=\; \sum_{i=1}^{r} \sum_{j=1}^{n} \binom{\sigma^*_{ij} + 1}{2}.$$

In conclusion, our proof consists of specific pointers to the articles [DE18, DKgS14, Ger61]. ∎

4.2. Real tangent quadrics

A classical problem in enumerative geometry is the study of characteristic numbers for families of curves or higher dimensional varieties in a projective space. Such numbers are the solutions to questions of type:

How many smooth degree d hypersurfaces in $\mathbb{P}^n$ are tangent to $\binom{n+d}{d} - 1$ general linear spaces of various dimensions?

For instance, characteristic numbers for plane curves count the number of curves in a family passing through α points and tangent to β lines where $\alpha + \beta$ equals the dimension of the family. There are 3264 conics tangent to five given conics in the projective plane $\mathbb{P}^2$ and it is possible to choose a configuration such that all of them are real, [BST20, RTV97].

In this section, we study the analogous tangency question for one dimension higher. The numbers of tangent quadrics (i.e., quadratic surfaces) were determined by Hermann Schubert in 1879 [Sch79]. This problem was later translated into a problem about the Chow ring of the space of complete quadrics. More recently, the space of complete quadrics has proved useful for studying some classical problems in algebraic statistics related to maximum likelihood estimation [MMM+20]. Schubert found that the number of quadrics in $\mathbb{P}^3$ that are tangent to nine given quadrics is 666841088. We present a first step toward the problem of deciding whether there exist nine real quadrics such that all complex solutions are real.

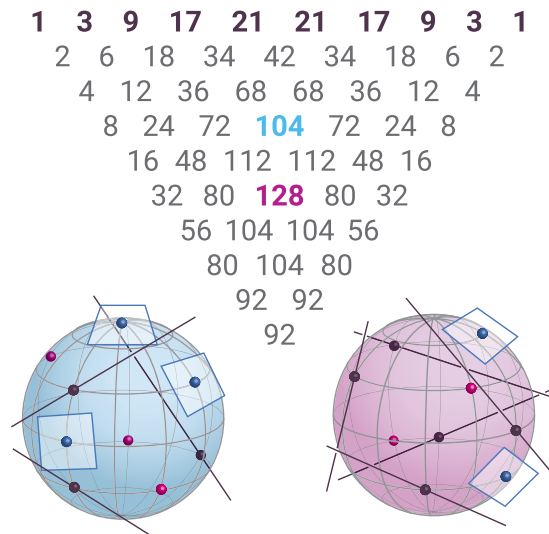**Figure 4.2.** Schubert's triangle for tangency of quadrics in 3-space.

Regarding characteristic numbers for surfaces in projective space, much less is known when it comes to higher degree. The only case where all characteristic numbers were found

is cubic surfaces. This case is worked out in my article [BDFK23], which is not part of this dissertation.

Our study centers around *Schubert's triangle* which is displayed in Figure 4.2. For each triple $(\alpha, \beta, \gamma) \in \mathbb{N}^3$ with $\alpha + \beta + \gamma = 9$, the triangle shows the number $p^\alpha \ell^\beta h^\gamma$ of quadrics that pass through α given points, are tangent to β given lines, and are tangent to γ given planes. The two pictures, in blue and red, illustrate the geometric meaning of the entries $p^3 \ell^3 h^3 = 104$ and $p^2 \ell^5 h^2 = 128$.

Schubert derives these numbers in [Sch79, §22]. In [Sch79, page 106] he argues as follows. Quadrics degenerate into complete flags, consisting of a point on a line in a plane in $\mathbb{P}^3$. Such a flag counts with multiplicity two, since $q = 2(p + \ell + h)$, by Proposition 4.2.3. We seek quadrics that satisfy one of the three tangency conditions, for each of the nine given flags. The number of such quadrics equals

$$q^9 = 2^9 \sum_{\alpha + \beta + \gamma = 9} \frac{9!}{\alpha! \beta! \gamma!} \cdot p^\alpha \ell^\beta h^\gamma = 2^9 \left(\cdots + 1680 \cdot 104 + \cdots + 756 \cdot 128 + \cdots \right). \qquad (4.2.1)$$

The second equation is in the cohomology ring of the space of complete quadrics. In (4.2.1) we multiply each entry in Schubert's triangle with the corresponding trinomial coefficient $\frac{9!}{\alpha! \beta! \gamma!}$, we add up the products, we multiply the sum by $2^9 = 512$, and we obtain $q^9 = 666841088$. This derivation is the analogue in $\mathbb{P}^3$ of the pentagon count for the $2^5 (p + \ell)^5 = 3264$ conics in [BST20, Figure 3].

Schubert's calculus predicts the number of complex solutions to a system of polynomial equations that depend on geometric figures like lines and planes in $\mathbb{P}^3$. In what follows, we study these polynomial equations and present practical tools for solving them. Our main interest is in solutions over the real numbers $\mathbb{R}$.

4.2.1. Coordinates and equations

We begin with the coordinates that describe our geometric figures. A point P in $\mathbb{P}^3$ is represented by a vector $p = (p_1, p_2, p_3, p_4)$. A line can be given by a 2×4 matrix L, and a plane by a 3×4 matrix H. We often use Plücker coordinates

$$\ell = (\ell_{12}, \ell_{13}, \ell_{14}, \ell_{23}, \ell_{24}, \ell_{34}) \quad \text{and} \quad h = (h_{234}, -h_{134}, h_{124}, -h_{123}).$$

Here ℓ_{ij} is the 2×2 minor of L with column indices i and j. Note the *Plücker relation* $\ell_{12} \ell_{34} - \ell_{13} \ell_{24} + \ell_{14} \ell_{23} = 0$. Likewise, h_{ijk} denote the 3×3 minors of H.

Remark 4.2.1. Inclusion relations are written in Plücker coordinates as follows:

$$
\begin{array}{ll}
P \subset H: & p_1 h_{234} - p_2 h_{134} + p_3 h_{124} - p_4 h_{123}, \\[4pt]
P \subset L: & p_1 \ell_{23} - p_2 \ell_{13} + p_3 \ell_{12}, \ \ p_1 \ell_{24} - p_2 \ell_{14} + p_4 \ell_{12}, \\
& p_1 \ell_{34} - p_3 \ell_{14} + p_4 \ell_{13}, \ \ p_2 \ell_{34} - p_3 \ell_{24} + p_4 \ell_{23}, \\[4pt]
L \subset H: & \ell_{12} h_{134} - \ell_{13} h_{124} + \ell_{14} h_{123}, \ \ \ell_{12} h_{234} - \ell_{23} h_{124} + \ell_{24} h_{123}, \\
& \ell_{13} h_{234} - \ell_{23} h_{134} + \ell_{34} h_{123}, \ \ \ell_{14} h_{234} - \ell_{24} h_{134} + \ell_{34} h_{124}.
\end{array}
$$

A triple (P, L, H) satisfying $P \subset L \subset H$ is called a *complete flag*. The variety of complete flags is irreducible of dimension six in $\mathbb{P}^3 \times \mathbb{P}^5 \times \mathbb{P}^3$. The prime ideal of this *flag variety* is generated by the nine quadrics above, together with the Plücker relation. These ten generators form a Gröbner basis [MS04, Theorem 14.6].

Each quadric in $\mathbb{P}^3$ is represented by a symmetric 4×4 matrix $X = (x_{ij})$. The point P lies on the quadric X if $PXP^T = 0$. Similarly, the condition for X to be tangent to a line L or to a plane H is given by the vanishing of the polynomial

$$\det(LXL^T) = \ell(\wedge_2 X)\ell^T \quad \text{or} \quad \det(HXH^T) = h(\wedge_3 X)h^T. \qquad (4.2.2)$$

Here $\wedge_i X$ denotes the i-th exterior power of the 4×4 matrix X. The entries of $\wedge_i X$ are the $i \times i$ minors of X. The rows and columns are labeled so that (4.2.2) holds.

Suppose we are given α points P_i, β lines L_j, and γ planes H_k, all generic, where $\alpha + \beta + \gamma = 9$. We wish to solve these nine homogeneous equations for X:

$$P_i X P_i^T = \det(L_j X L_j^T) = \det(H_k X H_k^T) = 0 \text{ for } 1 \le i \le \alpha, \, 1 \le j \le \beta, \, 1 \le k \le \gamma. \qquad (4.2.3)$$

Here X is an unknown symmetric 4×4 matrix, viewed as a point in $\mathbb{P}^9$, that satisfies $\det(X) \ne 0$. Bézout's Theorem suggests that the number of complex solutions to (4.2.3) equals $1^\alpha 2^\beta 3^\gamma$. This number is correct when $\alpha \ge 4$ and $\gamma \le 2$. In all other cases, the equations (4.2.3) have extraneous solutions that are removed by saturation with respect to the ideal $\langle \det(X) \rangle$. This saturation step can be carried out in `Macaulay2` [GS]. For each choice of (α, β, γ), we obtain a Gröbner basis that reveals the number of solutions in $\mathbb{P}^9$. This computation proves the correctness of Schubert's triangle. For solving (4.2.3) numerically, see Subsection 4.2.4.

We next discuss the condition for X to be tangent to a fixed quadric $U = (u_{ij})$.

Lemma 4.2.2. *The condition for two quadrics U and X to be tangent in $\mathbb{P}^3$ is given by the discriminant of the quartic $f(t) = \det(U + tX)$. This is an irreducible polynomial with 67753552 terms of degree $(12, 12)$ in the 20 unknowns u_{ij}, x_{ij}.*

Proof. The tangency condition means that the intersection curve of the quadrics U and X is singular in $\mathbb{P}^3$. By the Cayley trick of elimination theory [GKZ94a, §3.2.D], this is singular if and only if the line spanned by U and X in $\mathbb{P}^9$ is tangent to the hypersurface $\{\det(X) = 0\}$. That condition is given by the discriminant of $f(t)$, which is known as the *Hurwitz form* of $\{\det(X) = 0\}$. We found its expansion into 67753552 monomials with the computer algebra system `Maple`. ∎

We denote the above discriminant by $\Sigma(U, X)$. If U is a symmetric matrix with random entries in $\mathbb{R}$ or $\mathbb{C}$ then $\Sigma(U, X)$ is a polynomial of degree 12 in ten unknowns x_{ij} with 241592 terms. Given nine quadrics $U_1, \ldots, U_9$ in $\mathbb{P}^3$, the quadrics tangent to these solve the following equations in $\mathbb{P}^9$:

$$\Sigma(U_1, X) = \Sigma(U_2, X) = \cdots = \Sigma(U_9, X) = 0 \quad \text{and} \quad \det(X) \ne 0. \qquad (4.2.4)$$

Bézout's Theorem suggests that the nine equations have 12^9 complex solutions, but the inequation decreases that number to $q^9 = 666841088$. We derived this number in Equation (4.2.1). A key ingredient was the identity $q = 2(p + \ell + h)$.

We next prove this identity by an explicit geometric degeneration. Let V be an invertible real 4×4 matrix, and let $P \subset L \subset H$ be the flag given by its first three rows. We introduce a parameter $\epsilon > 0$, and we consider the quadric defined by

$$U_\epsilon = V^{-1} \cdot \text{diag}(\epsilon^3, \epsilon^2, \epsilon, 1) \cdot (V^{-1})^T. \qquad (4.2.5)$$

We investigate the behavior of the tangency condition for U_ϵ and X, as $\epsilon \to 0$.

Proposition 4.2.3. *The leading form in ϵ of the specialized Hurwitz form equals*

$$\Sigma(U_\epsilon, X) \;=\; (PXP^T)^2 \cdot \det(LXL^T)^2 \cdot \det(HXH^T)^2 \cdot \epsilon^8 \;+\; \text{higher terms in } \epsilon. \qquad (4.2.6)$$

This implies the identity $q = 2(p + \ell + h)$ in the appropriate cohomology ring.

Proof. The factorization in (4.2.6) can be seen directly from the discriminant of

$$f(t) \;=\; \det(U_\epsilon + tX) \;=\; c_0 + c_1 t + c_2 t^2 + c_3 t^3 + c_4 t^4.$$

The coefficients c_i are polynomials in ϵ with orders of vanishing $6, 3, 1, 0, 0$ at $\epsilon = 0$. The discriminant has vanishing order 8 at $\epsilon = 0$, and this order is uniquely attained by its monomial $c_1^2 c_2^2 c_3^2$. The factors c_1, c_2, c_3 map to those in (4.2.6). ∎

4.2.2. Complete quadrics

A geometric setting for our tangency problems is the *space of complete quadrics.* By definition, this is the variety obtained as the closure of the image of the map

$$\mathbb{P}^9 \;\dashrightarrow\; \mathbb{P}^9 \times \mathbb{P}^{20} \times \mathbb{P}^9, \qquad X \;\mapsto\; (X, \wedge_2 X, \wedge_3 X) \;=:\; (X, Y, Z). \qquad (4.2.7)$$

Here $X = (x_{ij})$ and $Z = (z_{ijk,lmn})$ are symmetric 4×4 matrices and $Y = (y_{ij,kl})$ is a symmetric 6×6 matrix. The rows and columns of Y and Z are indexed just like the entries of ℓ and h. The $\mathbb{N}^3$-homogeneous ideal $\mathcal{I}_4$ of that 9-dimensional variety lives in the polynomial ring $\mathbb{Q}[X, Y, Z]$ in $10 + 21 + 10 = 41$ unknowns.

Theorem 4.2.4. *The space of complete quadrics is a smooth variety of dimension nine. Its prime ideal $\mathcal{I}_4$ is minimally generated by 164 polynomials, namely*
- *one linear form of degree (010), i.e. $y_{12,34} - y_{13,24} + y_{14,23}$,*
- *20 quadrics of degree (020), e.g. $y_{12,24}y_{24,34} - y_{13,24}y_{24,24} + y_{14,24}y_{23,24}$,*
- *15 quadrics of degree (101), e.g. $x_{11}z_{123,234} - x_{12}z_{123,134} + x_{13}z_{123,124} - x_{14}z_{123,123}$,*
- *64 quadrics of degree (011), e.g. $y_{12,13}z_{123,134} - y_{13,13}z_{123,124} + y_{13,14}z_{123,123}$,*
- *64 quadrics of degree (110), e.g. $x_{11}y_{12,23} - x_{12}y_{12,13} + x_{13}y_{12,12}$.*

Schubert's triangle in Figure 4.2 equals the multidegree *of $\mathcal{I}_4$ in the $\mathbb{N}^3$-grading.*

Proof. The closure of the image of (4.2.7) is irreducible of dimension nine since X appears in the first coordinate. The smoothness of this variety is well-known in the theory of spherical varieties. For a new perspective and proof see [MMW21, §3.C].

The 164 polynomials were found by computation using `Macaulay2` [GS]. To show that they generate the prime ideal $\mathcal{I}_4$, we use [GSS05, Proposition 23] inductively. We eliminate one variable that occurs linearly in some equation and is not a zero-divisor modulo the current ideal. After checking these hypotheses, we replace the ideal by the elimination ideal, which is prime by induction. This process was found to work for various natural orderings of the entries in X, Y, Z.

The multidegree is a standard construction for multigraded commutative rings [MS04, Section 8.5]. For a variety in a product of projective spaces, it is the class of that variety in the cohomology ring of the ambient space. The built-in command `multidegree` in `Macaulay2` takes only a few seconds to find the multidegree from our 164 polynomials. The output of this `Macaulay2` computation is a ternary form in the unknowns T_0, T_1, T_2. It has 55 terms of degree $\mathrm{codim}(\mathcal{I}_4) = 29$. The coefficient of $T_0^{9-\alpha} T_1^{20-\beta} T_2^{9-\gamma}$ is the number $p^\alpha \ell^\beta h^\gamma$ in Figure 4.2. This computation is an *ab initio* derivation of Schubert's triangle. ∎

The variety $V(\mathcal{I}_4)$ captures degenerations of quadrics that matter in intersection theory [MMW21]. We saw this in Proposition 4.2.3 where the quadric becomes a flag $P \subset L \subset H$. The relationship to the flag variety is made precise as follows:

Corollary 4.2.5. *The variety of complete flags in $\mathbb{P}^3$ is the inverse image of $V(\mathcal{I}_4)$ under the componentwise Veronese embedding $\mathbb{P}^3 \times \mathbb{P}^5 \times \mathbb{P}^3 \hookrightarrow \mathbb{P}^9 \times \mathbb{P}^{20} \times \mathbb{P}^9$.*

Proof. The Veronese map takes (p, ℓ, h) to the rank one matrices $(X, Y, Z) = (p^T p, \ell^T \ell, h^T h)$. Substituting this into $\mathcal{I}_4$ and saturating by the irrelevant ideal of $\mathbb{P}^3 \times \mathbb{P}^5 \times \mathbb{P}^3$ yields the Gröbner basis for the flag variety in Remark 4.2.1. ∎

We next lift our tangency conditions from the space $\mathbb{P}^9$ of symmetric matrices X to the space of complete quadrics in $\mathbb{P}^9 \times \mathbb{P}^{20} \times \mathbb{P}^9$. We write $\mathcal{B} = \langle X \rangle \cap \langle Y \rangle \cap \langle Z \rangle$ for the irrelevant ideal of that product of projective spaces.

The condition that a quadric contains a point p is the linear form pXp^T in the unknown X. Similarly, tangency to a line ℓ is the linear form $\ell Y \ell^T$ in the unknown Y, and tangency to a plane h is the linear form hZh^T in the unknown Z. Without loss of generality, we can assume that one given figure is a coordinate subspace in $\mathbb{P}^3$. Then the three linear forms are variables x_{11}, $y_{12,12}$ or $z_{123,123}$.

However, if we augment $\mathcal{I}_4$ by one such variable then the resulting ideal is not prime. To get the correct prime ideal we must saturate by the irrelevant ideal $\mathcal{B}$. We first summarize what happens when we add the constraint for a point. The result is the same for the plane constraint if we swap the roles of X and Z.

Proposition 4.2.6. *The saturation $\big((\mathcal{I}_4 + \langle x_{11} \rangle) : \mathcal{B}^\infty\big)$ is the prime ideal of the variety of complete quadrics that contain a given point. It has 13 minimal generators in addition to the 164 generators of $\mathcal{I}_4$, namely ten of degree (020) and one each of degree (100), (003) and (011). The multidegree of this ideal is the triangle of size eight that is obtained by deleting the lower right edge in Figure 4.2.*

Proof. This is proved by a `Macaulay2` computation. The new equation of degree (100) is x_{11}. The new equation of degree (003) is the complementary 3×3 minor of Z. Generators of degree (020) arise from Bareiss formula which says that x_{11} times any 3×3 minor of X containing x_{11} equals a 2×2 minor of Y. ∎

Proposition 4.2.7. *The saturation $\big((\mathcal{I}_4 + \langle y_{12,12} \rangle) : \mathcal{B}^\infty\big)$ is the prime ideal for the complete quadrics that are tangent to a line. It has three minimal generators, of degrees (010), (200), (002), in addition to the 164 generators of $\mathcal{I}_4$. This is one entry of Y and the corresponding 2×2 minors of X and Z. The multidegree is the triangle of size eight obtained by deleting the top edge in Figure 4.2.*

It would be desirable to extend Theorem 4.2.4 to $n \times n$ matrices for $n \geq 5$, i.e. to identify minimal generators for the multihomogeneous prime ideal of the space of complete quadrics. These are relations among all minors of a symmetric $n \times n$ matrix that respect the fine grading coming from the size of the minors. Results by Bruns et al. [BCV13] indicate that relations of degree ≤ 2 will not suffice.

4.2.3. Schubert's triangle

At present, we have the following result on the reality of Schubert's triangle.

Theorem 4.2.8. *For at least* 46 *of the* 55 *problems in Schubert's triangle, there exists an open set of real instances, consisting of* α *points,* β *lines and* γ *planes, such that all complex solutions in* $\mathbb{P}^9$ *to the polynomial equations in (4.2.3) are real. For the other nine problems, the current status is summarized in Remark 4.2.10.*

Example 4.2.9. Fix $(\alpha, \beta, \gamma) = (3, 3, 3)$. We consider the configuration

$$
\begin{aligned}
p &= & \left(1, \tfrac{439}{922}, -\tfrac{347}{271}, \tfrac{67}{343}\right),\ \left(1, -\tfrac{211}{484}, \tfrac{153}{346}, \tfrac{257}{254}\right),\ \left(1, -\tfrac{575}{404}, \tfrac{131}{320}, -\tfrac{37}{42}\right), \\
\ell &= & \left(-\tfrac{92}{159}, -\tfrac{92}{293}, \tfrac{120}{307}, \tfrac{77}{256}, -\tfrac{76}{391}, \tfrac{96}{311}\right),\ \left(\tfrac{107}{114}, \tfrac{18}{383}, -\tfrac{109}{116}, \tfrac{37}{217}, \tfrac{45}{307}, \tfrac{47}{264}\right), \\
& & \left(-\tfrac{365}{302}, -\tfrac{45}{368}, \tfrac{172}{209}, \tfrac{74}{245}, \tfrac{25}{62}, \tfrac{87}{353}\right), \\
h &= & \left(\tfrac{193}{182}, \tfrac{75}{397}, -\tfrac{244}{631}, \tfrac{195}{272}\right),\ \left(\tfrac{91}{307}, -\tfrac{17}{122}, -\tfrac{553}{837}, \tfrac{70}{309}\right),\ \left(\tfrac{919}{295}, \tfrac{103}{36}, \tfrac{1199}{371}, \tfrac{57}{176}\right).
\end{aligned}
$$

All 104 complex quadrics tangent to these nine figures are found to be real. Thus, this is a fully real instance for the scenario shown in blue in Figure 4.2.

Remark 4.2.10. Up to the natural involution, given by swapping points and planes, there are 30 distinct tangency problems in Schubert's triangle. For five of the problems we have not yet succeeded in verifying reality. They are as follows:

(α, β, γ)	$(3, 4, 2)$	$(3, 5, 1)$	$(2, 6, 1)$	$(1, 7, 1)$	$(1, 8, 0)$
Schubert's count over $\mathbb{C}$	112	80	104	104	92
Our current record over $\mathbb{R}$	110	74	96	84	84

For instance, we know two points, six lines and a plane in $\mathbb{P}^3_{\mathbb{R}}$ such that 96 real quadrics are tangent to these figures. The remaining eight quadrics are complex. This is derived from Example 4.2.11 by replacing point P_3 with a plane. For the (1,8,0) case with 84 real solutions we use eight tangent lines as in Example 4.2.13.

Discussion and proof of Theorem 4.2.8. All our instances of full reality or maximal reality, along with the software that certifies correctness, can be found at

$$\text{https://mathrepo.mis.mpg.de/TangentQuadricsInThreeSpace} \tag{4.2.8}$$

For instance, for $(\alpha, \beta, \gamma) = (3, 3, 3)$, this website contains the configuration in Example 4.2.9, along with the 104 tangent quadrics. Each quadric is determined by its nine points of tangency. The coordinates of these points form a $104 \times 9 \times 4$ tensor of floating point numbers in Julia format. The proof of correctness was carried out with the certification technique in [BRT20], as discussed in Subsection 4.2.4. ∎

We now present some ideas that were helpful in creating fully real instances. Figures given by the standard basis e_1, e_2, e_3, e_4 lead to sparse equations in (4.2.3).

Example 4.2.11. The condition for X to be tangent to the six coordinate lines is

$$I = \left\langle x_{ii}x_{jj} - x_{ij}^2 : 1 \le i < j \le 4 \right\rangle. \tag{4.2.9}$$

This is the complete intersection of eight prime ideals, each isomorphic to the ideal J generated by all 2×2 minors of X. The eight primes are $U_{ijk} \star J$, where $\star$ is the Hadamard product, and U_{ijk} is the 4×4 matrix with entries $(-1)^i$, $(-1)^j$ and $(-1)^k$ in positions $(2, 3)$, $(2, 4)$ and $(3, 4)$, and entries 1 everywhere else. Seven of these *scaled Veronese varieties* contain matrices of rank 3 or 4. Their union is defined by the radical ideal $(I : J)$, which

has degree 56. This is Schubert's number for $\alpha = 3, \beta = 6, \gamma = 0$. We seek three points such that all 56 quadrics containing these and satisfying I are real. One choice that works is

$$P_1 = (1,2,8,7), \quad P_2 = (1,1,9,2), \quad P_3 = (2,5,3,1).$$

Our six given lines meet pairwise, and they are not generic. This leads to 48 of the 56 quadrics being cones. To get 56 smooth quadrics, one perturbs the lines.

We refer to the article [KW18] by Kahle and Wagner for a general study of the ideal of principal 2×2 minors of a symmetric $n \times n$ matrix of unknowns. Their results elucidate the decomposition we found for the special case $n = 4$ in (4.2.9).

Example 4.2.12. The condition for X to be tangent to the four coordinate planes is the ideal generated by the four principal 3×3 minors. Saturating by the ideal of all 3×3 minors yields a prime ideal K of codimension 4 and degree 21. This is Schubert's number for $\alpha = 5, \beta = 0, \gamma = 4$. It is easy to find five points so that all 21 quadrics containing these and satisfying K are real. This instance is generic.

The ideal K is generated by 10 cubics and 12 quartics. The 5-dimensional variety cut out by K in $\mathbb{P}^9$ has the following nice parametric representation:

$$X = \begin{pmatrix} x_{12}x_{13}x_{14} & x_{12} & x_{13} & x_{14} \\ x_{12} & x_{12}x_{23}x_{24} & x_{23} & x_{24} \\ x_{13} & x_{23} & x_{13}x_{23}x_{34} & x_{34} \\ x_{14} & x_{24} & x_{34} & x_{14}x_{24}x_{34} \end{pmatrix} \text{ where } \det \begin{pmatrix} x_{12}x_{34} & 1 & 1 \\ 1 & x_{13}x_{24} & 1 \\ 1 & 1 & x_{14}x_{24} \end{pmatrix} = 0.$$

Our final technique was inspired by the solution to Shapiro's conjecture [Sot10].

Example 4.2.13. Consider the lines $\ell = (1, 2t, 3t^2, t^2, 2t^3, t^4)$ that are tangent to the twisted cubic curve $\{(1 : t : t^2 : t^3)\}$. There is a surface of quadrics tangent to all such lines. We choose nine nearby lines, by slightly perturbing nine tangent lines. Our fully real instance for $(\alpha, \beta, \gamma) = (0, 9, 0)$ was found in this manner.

4.2.4. Numerical methods

We now explain our techniques for solving the equations (4.2.3) and for certifying the correctness of their solutions. Each instance is presented in the Plücker coordinates of Remark 4.2.1. Following (4.2.2) and Subsection 4.2.2, each line specifies a linear equation in $Y = \wedge_2 X$ and each plane gives a linear equation in $Z = \wedge_3 X$.

We now go over our steps in solving the system for the instance in Example 4.2.9. The input is a system of 11 equations in 11 unknowns, namely the ten entries of the matrix X and one more variable D. One equation is $D = \det(X)$, another specifies a random affine chart, $\sum_{1 \leq i < j \leq 4} c_{ij}x_{ij} = 1$, and the others are the tangency conditions. Our equations are entered into `HomotopyContinuation.jl`:

```
Equations=System(vcat(Point_Conditions,
                      Line_Conditions,
                      Plane_Conditions,
                      det(X)-D, Affine_Chart))
```

After entering `S=solve(Equations)`, the following output appears:
This suggests that the program tracked $216 = 1^\alpha 2^\beta 3^\gamma$ paths from a total degree start system and that it found 104 real nonsingular solutions. The variable `S` is a 104-element array of

```
Tracking 216 paths... 100% |||||||||||||||| Time: 0:00:11
# paths tracked:              216
# non-singular solutions (real):  104 (104)
# singular endpoints (real):     84 (83)
# total solutions (real):       188 (187)


quadric=solutions(S)[17]
@var x[1:4]
Quadric=expand(x'*(X(Equations.variables=>real(quadric)))*x)

-2.974732003076*x2*x1-1.289476735251*x2*x3-10.97658863786*x3*x1+
+8.372046844711*x4*x1+8.886907306683*x4*x2+9.704839838537*x4*x3+
-5.810893956281*x1^2+2.645663598009*x2^2-5.046922439351*x3^2+0.6937980589394*x4^2
```

solutions, each of which is an 11-element array of floating point numbers. The first coordinate is D, and the last ten are the coordinates of X.

The following code extracts the 17-th element of S and prints that quadric:

These Julia fragments give a first impression. The details may be found at (4.2.8).

One key question about numerical output is whether it can serve as a mathematical proof. How can we be sure that the 104 solutions are indeed solutions and moreover, that they are distinct, real, and nondegenerate? This is addressed by the process of *a-posteriori* certification, which generates an actual proof.

We carry this out using the *Krawczyk method*, implemented by Breiding, Rose and Timme [BRT20]. It is based on interval arithmetic and is now available as a standard feature in HomotopyContinuation.jl. We note that this implementation represents a significant advance over Smale's α-certification that was used for the 3264 real quadrics in [BST20, Proposition 1]. This advance has two aspects. First, the new method in [BRT20] is much faster. Second, its output gives a bounding box, allowing us to easily certify that the quadrics are nondegenerate.

We now show how certification works for our instance. The input is easy:

```
C=certify(Equations,S)
```

The program creates a certificate C, and it reports on that as follows:

```
CertificationResult
===================
• 104 solutions given
• 104 certified solutions (104 real)
• 104 distinct certified solutions (104 real)
```

The certificate C is a list of 104 lists of 22 intervals $I_1, \ldots, I_{11}, J_1, \ldots, J_{11}$ in $\mathbb{R}$. The product $B = \prod_{i=1}^{11}(I_i + \mathtt{im} \cdot J_i)$ is a box in $\mathbb{C}^{11} \simeq \mathbb{R}^{22}$. That box provably contains a unique solution to Equations, verified by interval arithmetic.

Checking that these boxes are disjoint proves that the 104 solutions are distinct. Checking that B is the only box which intersects the complex conjugate of B itself proves that this solution is real. Checking that 0 is not contained in I_1, the interval for the unknown D proves that the quadric is nondegenerate.

The following command displays the certifying box B for the 17-th quadric:

```
C.certificates[17].certified_solution
```

```
(1.459827495775684e-6 ± 2.2938e-14) + (0.0 ± 2.2938e-14)im
(-0.9684823260468921 ± 1.516e-09) + (0.0 ± 1.516e-09)im
(-0.24789433358973637 ± 2.2975e-11) + (0.0 ± 2.2975e-11)im
(0.44094393300164797 ± 1.1016e-09) + (0.0 ± 1.1016e-09)im
(-0.9147157198219121 ± 1.3088e-09) + (0.0 ± 1.3088e-09)im
(-0.10745639460424983 ± 3.3522e-10) + (0.0 ± 3.3522e-10)im
(-0.8411537398918771 ± 1.0251e-09) + (0.0 ± 1.0251e-09)im
(0.6976705703926359 ± 9.7633e-10) + (0.0 ± 9.7633e-10)im
(0.7405756088903332 ± 1.1508e-09) + (0.0 ± 1.1508e-09)im
(0.8087366532114602 ± 1.202e-09) + (0.0 ± 1.202e-09)im
(0.11563300982325174 ± 7.2217e-10) + (0.0 ± 7.2217e-10)im
```

Remark 4.2.14. Finding the fully real instances for Theorem 4.2.8 was a challenge. We implemented a heuristic hill-climbing algorithm similar to the one in [Die98]. The idea is to begin at some configuration $\mathcal{C}$ of α real points, β real lines, and γ real planes, solve the equations, and sample many nearby instances. If one has more real solutions, then $\mathcal{C}$ is updated to be that instance. Otherwise, the new $\mathcal{C}$ is the instance with the same number of real solutions, but whose complex solutions are closest to becoming real. This is measured by the minimum norm of the complex parts of each nonreal solution. In this fashion, one greedily travels through the parameter space towards instances with more real solutions. A major issue with such methods is that they get stuck in local maxima. Our success came from many iterations beginning at different randomly chosen parameters. A host of numerical tolerances determine the behavior of this algorithm. Once the number of real solutions approaches the maximum, the instances often become so ill-conditioned that serious monitoring of these tolerances is required.

4.2.5. Schubert's pyramid

We now finally come to the analogue in $\mathbb{P}^3$ of the number 3264. The following conjecture motivated this project. We hope that it can be resolved in the future.

Conjecture 4.2.15. There exist nine quadrics in $\mathbb{P}^3_{\mathbb{R}}$ such that all 666841088 complex quadrics that are tangent to these nine are defined over the real numbers $\mathbb{R}$.

We propose a combinatorial gadget for approaching this problem. Schubert's pyramid is a tetrahedron of 220 intersection numbers $p^\alpha \ell^\beta h^\gamma q^\delta$, where $(\alpha, \beta, \gamma, \delta) \in \mathbb{N}^4$ with $\alpha + \beta + \gamma + \delta = 9$. Here $q = 2(p + \ell + h)$ denotes the cohomology class of the complete quadrics tangent to a given quadric in $\mathbb{P}^3$. Thus the pyramid organizes the number of quadrics tangent to nine figures, as in Figure 4.3.

The levels in Schubert's pyramid are the triangles for fixed δ. Each entry in level δ is twice the sum of the three entries in level $\delta - 1$ that lie below it. For instance, for $\delta = 2$ we marked $3712 = 2 \cdot (576 + 576 + 704)$. This counts quadrics through two points that are tangent to three lines, two planes and two quadrics.

Making Schubert's triangle fully real is only a first step towards Conjecture 4.2.15. What we really want is to find one single instance of nine real flags:

$$P_1 \subset L_1 \subset H_1, \ P_2 \subset L_2 \subset H_2, \ldots, \ P_9 \subset L_9 \subset H_9. \tag{4.2.10}$$

$$
\begin{array}{ccccccccc}
12 & 36 & 88 & 144 & 168 & 144 & 88 & 36 & 12 \\
24 & 72 & 176 & 288 & 288 & 176 & 72 & 24 \\
48 & 144 & 352 & 480 & 352 & 144 & 48 \\
116 & 288 & 576 & 576 & 288 & 116 \\
192 & 480 & 704 & 480 & 192 \\
336 & \textbf{312} & 312 & 336 \\
480 & 624 & 480 \\
552 & 552 \\
552
\end{array}
$$

δ=1

$$
\begin{array}{ccccccc}
144 & 392 & 816 & 1200 & 1200 & 816 & 392 & 144 \\
288 & 784 & 1632 & 2112 & 1632 & 784 & 288 \\
576 & 1568 & 2816 & 2816 & 1568 & 576 \\
1152 & 2688 & \textbf{3712} & 2688 & 1152 \\
2016 & 3616 & 3616 & 2016 \\
2880 & 3744 & 2880 \\
3312 & 3312 \\
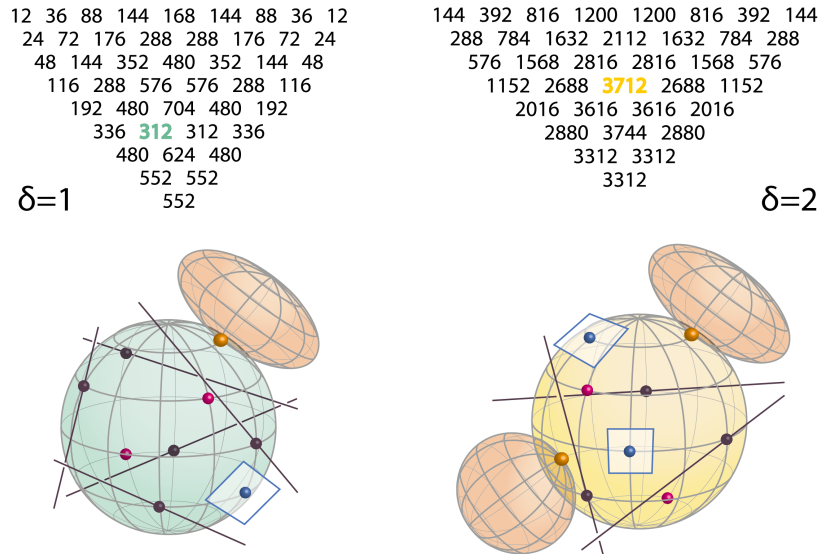3312
\end{array}
$$

δ=2

Figure 4.3. Two consecutive levels in Schubert's pyramid

We want those nine flags to exhibit full reality, simultaneously for all their many tangency problems. Such a configuration (4.2.10) would be the 3-dimensional analogue to the pentagon in [BST20, Figure 3]. To state this precisely, we consider an arbitrary function $\psi : \{1, 2, \ldots, 9\} \to \{P, L, H\}$. This defines a polynomial system

$$\det\big(\psi(i)_i \cdot X \cdot \psi(i)_i^T\big) = 0 \quad \text{for} \quad i = 1, 2, \ldots, 9. \tag{4.2.11}$$

This has the form (4.2.3), where $\alpha = |\psi^{-1}(P)|$, $\beta = |\psi^{-1}(L)|$, and $\gamma = |\psi^{-1}(H)|$. Thus, an instance (4.2.10) of nine flags gives a collection of 3^9 polynomial systems. For each of these, the number of solutions is one entry in Schubert's triangle.

Conjecture 4.2.16. There exist nine real flags (4.2.10) in $\mathbb{P}^3$ such that each complex solution X to any of the 3^9 associated polynomial systems (4.2.11) is a real quadric.

If Conjecture 4.2.16 is true, then we can approach Conjecture 4.2.15 as follows. We are given $(p + \ell + h)^9 = 1302424$ real quadrics X that solve the 3^9 systems. Each solution becomes 2^9 distinct solutions under the deformation in Proposition 4.2.3, where the nine flags for $\epsilon = 0$ become nine smooth quadrics for $\epsilon > 0$. This process can be performed in stages, from the bottom to the top of the pyramid, but its numerical implementation will not be easy. One hope is that reality can be controlled using the results by Ronga, Tognoli and Vust in [RTV97].

4.3. Conclusions

We conclude by emphasizing the crucial role of mathematical software programs in achieving the results presented in Chapters 2–4. Symbolic and numerical computations have in fact provided an effective way to study and manipulate objects we have encountered when producing new results. Sometimes, even to prove theorems, e.g. Theorems 2.2.3, 3.1.24, and 4.2.8. Therefore, we consider the complementary coding material an integral part of this thesis. Findability, accessibility, interoperability, and reusability [WDA+16, FG22] of the research data produced are guaranteed by the online repository MathRepo (https://mathrepo.mis.mpg.de/), for which the author of this thesis operated as a maintainer at the time of writing the thesis.

Appendix A

Feynman integrals for mathematicians

This appendix serves as a gentle and light introduction for non-physicists to the theory of *scattering amplitudes* in *particle physics*. We intend to summarize the role of Feynman integrals in the theory of scattering amplitudes, as well as present various representation of Feynman integrals. Furthermore, we will explain why such integrals are relevant for the purposes of this thesis and how they relate to Section 3.2. We refer to [Wei22, MT22] for additional background on Feynman integrals. See also [Car13, CD13] for a more intuitive introduction to some of these topics.

Imagine a scattering experiment happening in a high energy collider where incoming particles smash into each other and a number of outgoing particles are produced from their collision. A scattering amplitude is a fundamental concept in quantum field theory (QFT) used to calculate the probability of certain particle interactions with the ultimate purpose of predicting the outcome of particle collisions. Particle physics is the study of the properties and interactions of elementary particles, such as bosons, neutrons, protons, and other particles that make up atoms, and it heavily relies on the concepts and techniques of QFT, especially scattering amplitudes. Understanding the behavior of these particles can give insight into the fundamental nature of the universe and help develop new technologies in engineering.

A breakthrough in computing scattering amplitudes was provided by the method developed by physicist Richard Feynman in the 1940s. Feynman introduced some diagrams encoding information on how particle physics collisions unfold. Thus, the Feynman rules give explicit instructions for associating every such diagram with a function, which we can use to calculate the probability that this process actually occurs. For instance, it cannot happen that one boson decays into two bosons of exactly the same type; that would violate energy conservation. But one heavy particle can decay into different, lighter particles.

Assume n is the number of incoming and outgoing particles. More formally, the scattering amplitude is defined as a complex-valued function of the momenta, associated to a scattering process, namely

$$A(p_1, p_2, \ldots, p_n) : (\mathbb{R}^{1,D-1})^n \longrightarrow \mathbb{C}, \tag{A.1}$$

where the $p_i = (p_i^0, p_i^1, \ldots, p_i^{D-1})$ for $i = 1, 2, \ldots, n$ denote the *momenta vectors* one associates to each particle. These are vectors in the D-dimensional *Minkowski momentum space* $\mathbb{R}^{1,D-1}$ endowed with the pairing $p \cdot q = p^0 q^0 - p^1 q^1 - \cdots - p^{D-1} q^{D-1}$. We write p^2 to denote $p \cdot p$, where the product is the pairing in Minkowski space. The most interesting case in physics is when $D = 4$, i.e., one dimension corresponds to time and the other three correspond to space dimensions. The momentum vectors capture important physical information about the particles in the scattering experiment, such as their mass and velocity. This is made

more explicit below. Furthermore, momentum conservation imposes the relation

$$\pm p_1 \pm p_2 + \cdots \pm p_n = 0, \tag{A.2}$$

where the $\pm$ sign of each p_i depends on whether they represent ingoing ($+$) or outgoing ($-$) particles. The modulus squared of the scattering amplitude (A.1) can be interpreted as a joint probability density function describing what to expect for the outcome of the experiment.

In perturbative theory, namely in the Feynman integral approach, the scattering amplitude is represented as a sum over all possible paths that the system could take between the initial and final states. Formally,

$$A(p_1, p_2, \ldots, p_n) = \sum_G a_G \cdot I_G, \tag{A.3}$$

where the sum is over all possible Feynman diagrams G. The contribution I_G denotes the Feynman integral corresponding to a diagram G. The way this integral is defined is determined by the Feynman rules, as explained in the next section. Finally, each factor a_G can be thoughts as a number that depends on the properties of the particles involved. Therefore, each Feynman diagram G is associated with a specific term in the perturbative expansion (A.3), and the scattering amplitude is obtained by summing up the contributions from all the diagrams. A standard strategy to study the analytic properties of the amplitude A is to study those of the summands I_G in (A.3).

Feynman diagrams are graphical representations of the different ways particles can interact: particles are represented by lines, and the lines can be thought of as representing the motion of the particles over time, in fact they can be directed towards or away from each other and can also split or merge, depending on the process being represented; the vertices can be thought of as representing the instant when two or more particles come into contact and interact with each other. Here are some possibilities:
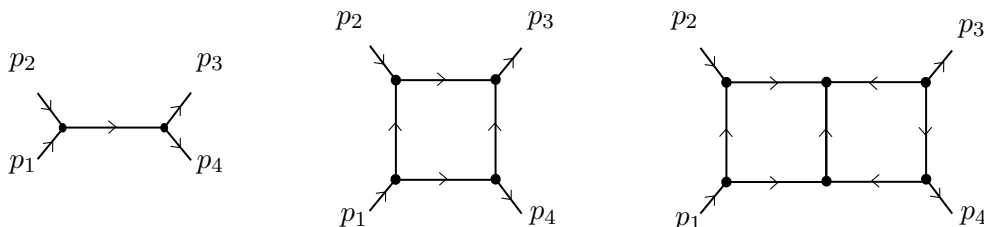

Figure A.1. An example of a tree, a one-loop, and a two-loops Feynman diagram for $n = 4$ particles. For a physical explanation of the tree on the left see [CD13].

The sum in (A.3) is usually infinite. This process is only useful if the contribution corresponding to each diagram decreases with the complexity of the diagrams, which can be the case. Roughly speaking, each vertex in a Feynman diagram carries a number, i.e., the coupling constant for a prescribed theory, which indicates how strongly the particles interact. In more complicated diagrams, with a higher number of vertices, the resulting Feynman integral is proportional to the coupling constant raised to the power of the number of vertices. So, if the coupling constant is less than one, that number gets smaller and smaller as the diagrams become more and more complicated. In practice, one can often get very accurate results from just the simplest Feynman diagrams.

There are several parameterizations of Feynman integrals. In the next sections, we introduce a selection of them in this order: Loop-momentum, Schwinger parameter, Feynman

parameter, and Lee-Pomeransky. The one-loop Feynman diagram in Figure A.1 (center) will serve as running example when illustrating these integral representations. This diagram is also known as the *box diagram* in the physics literature.

Representations of Feynman integrals

A Feynman diagram G is a connected oriented graph with n_G external legs (open edges), E_G internal edges, as well as L_G independent loops and V_G nodes, where

$$L_G = E_G - V_G + 1, \tag{A.4}$$

since G is connected. Recall that the n_G external edges correspond to the incoming and outgoing particles. To each external edge we also associate a momentum vector $p_i \in \mathbb{R}^{1,D-1}$. In the subsequent paragraphs, we will remove the subscript G for the numbers introduced above; however, they need to be understood as varying depending on the Feynman diagram one fixes. A collection of Feynman diagrams can be found in [MT22, Figure 1].

Loop-momentum

Recall that a Feynman diagram G is also oriented, i.e., each edge has an arbitrary orientation. However, the resulting integral I_G is independent of the choice of the orientation. To each internal edge corresponds a momentum vector $q_e \in \mathbb{R}^{1,D-1}$, and the mass $m_e \in \mathbb{R}_{\geq 0}$ of the particle propagating along edge e, for $e = 1, \ldots, E$. Momentum conservation at each node of the diagram imposes that the sum of incoming momenta equals the sum of the outgoing momenta, hence we obtain a linear equation in p_i, q_e for each node of the diagram.

Moreover, these equations allow us to write the internal momenta q_e in terms of the external momenta p_i and L other independent parameters, called the *loop momenta* $\ell_1, \ldots, \ell_L$.

Example A.1. When the Feynman diagram is the box diagram, we write $G = \square$. Thus, we have $n_\square = 4$, $L_\square = 1$, and $E_\square = 4$. We label the internal edges and external legs as illustrated in Figure A.2:
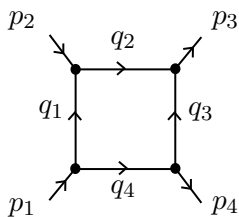
Figure A.2. The one-loop box diagram.

Momentum conservation at each node imposes the relations

$$p_1 = q_1 + q_4, \quad p_2 + q_1 = q_2, \quad p_3 = q_2 + q_3, \quad \text{and} \quad p_4 + q_3 = q_4.$$

Setting $q_1 = \ell$, we obtain $p_1 = \ell + q_4$, $p_2 + \ell = q_2$, $p_3 = q_2 + q_3$, and $p_4 + q_3 = q_4$, which implies the overall momentum conservation (A.2), i.e. $p_1 + p_2 - p_3 - p_4 = 0$.

Hence, momentum conservation fixes the internal momenta q_e up to L degrees of freedom. In the *loop-momenta representation*, the Feynman integral I_G can be expressed as an integral

over all possible loop momenta $\ell_1, \dots, \ell_L$. The integration domain is $(\mathbb{R}^{1,D-1})^L$, where the j-th factor in $\mathbb{R}^{1,D-1}$ has coordinates $\ell_i^0, \dots, \ell_i^{D-1}$. The integrand is defined to be a product over all internal edges of the diagram G, in which the factor corresponding to the e-th edge is $i(q_e^2 - m_e^2)^{-1}$, where $i = \sqrt{-1}$. Here it is understood that q_e is expressed as a linear combination of the external momenta p_j and the loop momenta ℓ_j. The integral reads

$$I_G = \frac{1}{\pi^{D/2}} \int_{(\mathbb{R}^{1,D-1})^L} \prod_{e=1}^{E} \frac{1}{(q_e(\ell_1, \dots, \ell_L, p_1, \dots, p_n)^2 - m_e^2)^{\nu_e}} \, \mathrm{d}^{DL}\ell, \tag{A.5}$$

where $\mathrm{d}^{DL}\ell = \mathrm{d}\ell_1^0 \wedge \cdots \wedge \mathrm{d}\ell_1^{D-1} \wedge \cdots \wedge \mathrm{d}\ell_L^0 \wedge \cdots \wedge \mathrm{d}\ell_L^{D-1}$ and the exponents ν_e are integers. In order to avoid singularities along the integration contour, one can sum $i\epsilon$ to each denominator, where ϵ in an infinitesimal positive parameter. This machinery is known as the *Feynman $i\epsilon$ prescription.*

Example A.2. The momenta vectors appearing in the integral in (A.5) for the box diagram are given by $q_1 = \ell$, $q_2 = p_2 + \ell$, $q_3 = p_3 - p_2 - \ell$, and $q_4 = p_4 + p_3 - p_2 - \ell$.

Schwinger parameters

The Schwinger parameter representation, also known as *wordline formalism*, replaces the loop momenta integration with some auxiliary integration variables. Let G be a Feynman diagram as above. To each internal edge e we associate a *Schwinger parameter* $x_e \in \mathbb{C}^*$. In order to define the desired representation, we first need to introduce some graph-theoretical definitions.

A *spanning tree* in G is a connected subset of $E - L$ internal edges containing all vertices of G. We write $\mathcal{T}_G$ for the set of all spanning tree of the graph G.

Definition A.3. The *first Symanzik polynomial* is

$$\mathcal{U}_G = \mathcal{U} := \sum_{T \in \mathcal{T}_G} \prod_{x_e \notin T} x_e,$$

where the product runs over the L_G internal edges that were removed from G to obtain the spanning tree T.

Given $S \subseteq \{1, 2, \dots, n_G\}$, we write T_S for the subtree of G containing all the vertices attached to the external legs labeled by S. A *spanning 2-tree* $T_S \sqcup T_{\bar{S}}$ in G is a disjoint union (with respect to the set of edges and vertices) of two trees T_S and $T_{\bar{S}}$ in G, containing all of its vertices. We write $\mathcal{T}_{G,S}$ for the set of all spanning 2-trees such that T_S contains the vertices attached to the external legs labeled by S, and no vertices attached to external legs labeled by the complementary set $\bar{S} = \{1, 2, \dots, n_G\} \smallsetminus S$.

Definition A.4. For a set $S \subset \{1, \dots, n_G\}$, define

$$\mathcal{F}_{G,S} := \sum_{T_S \sqcup T_{\bar{S}} \in \mathcal{T}_{G,S}} \prod_{e \notin T_S, T_{\bar{S}}} x_e.$$

The *second Symanzik polynomial* is given as

$$\mathcal{F}_G = \mathcal{F} := \sum_{S, \bar{S} \in \mathcal{P}_G} \left(\sum_{i \in S} p_i \right)^2 \mathcal{F}_{G,S} - \left(\sum_{e=1}^{E_G} m_e^2 x_e \right) \cdot \mathcal{U}_G,$$

where $\mathcal{P}_G$ denotes the set of all partitions of the n external legs into two disjoint non-empty sets S and $\bar{S}$.

In the Schwinger parameters, the first and second Symanzik polynomials are homogeneous of degree, L and $L + 1$, and at most linear and quadratic in each individual x_e, respectively. Moreover, the first Symanzic polynomial $\mathcal{U}$ does not depend on the external parameters p_i, m_e, see [Wei22, Chapter 3].

Example A.5. Consider the diagram $G = \square$ as in Figure A.2, where we replace each internal momentum q_e with an analogously labeled Schwiger parameter x_e. Then, the set of spanning trees $\mathcal{T}_\square$ contains precisely the four trees one attains by deleting a single internal edge. Hence:

$$\mathcal{U}_\square = x_1 + x_2 + x_3 + x_4.$$

The second Symanzik polynomial is instead given by

$$\mathcal{F}_\square = p_1^2 x_1 x_4 + p_2^2 x_1 x_2 + p_3^2 x_2 x_3 + p_4^2 x_3 x_4 + (p_1 + p_4)^2 x_1 x_3 + (p_1 + p_2)^2 x_2 x_4$$
$$- (m_1^2 x_1 + m_2^2 x_2 + m_3^2 x_3 + m_4^2 x_4)\mathcal{U}_\square,$$

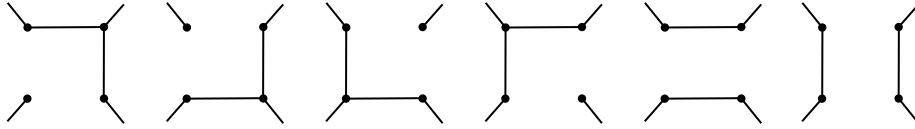where the first six summands correspond to the spanning two trees in Figure A.3.

Figure A.3. The spanning 2-trees for the box diagram. They correspond to the sets S in Definition A.4 being (in this order): $\{1\}, \{2\}, \{3\}, \{4\}, \{1, 4\}, \{1, 2\}$.

A formula for the Symanzik polynomials of an arbitrary one-loop diagram is given in [MT22, Section 2.5].

We can finally introduce the Feynman integral in Schwinger parameterization associated to a diagram G as

$$I_G = \frac{1}{\prod_{e=1}^E \Gamma(\nu_e)} \int_{\mathbb{R}_{\geq 0}^E} \left(\prod_{e=1}^E x_e^{\nu_e - 1}\right) \mathcal{U}^{-D/2} \exp\left[\frac{i}{h}\mathcal{V}\right] \mathrm{d}^E x, \qquad (A.6)$$

where the measure is $\mathrm{d}^E x \coloneqq \prod_{e=1}^E \mathrm{d}x_e$ and $\Gamma(x)$ denotes the Gamma function. The function $\mathcal{V}$ is defined as the ratio

$$\mathcal{V} \coloneqq \mathcal{F}/\mathcal{U}.$$

Remark A.6. Integrals of type (A.6) do not always converge. To deal with singularities in the denominator of (A.6), well-known techniques are *dimensional* and *analytic regularization* which are also relevant for numerical evaluation of the integrals [Wei22].

The equivalence between Feynman integrals in loop-momentum and Schwinger parameter representation is worked out in [MT22, Appendix A].

Feynman parameter representation

The *Feynman parameter representation* is one of the most well-known parametric representations for Feynman integrals. To introduce it, let $a = (a_1, \ldots, a_E)$ be E complex variables (*Feynman parameters*) and $\delta(x)$ denote the Dirac delta distribution, then

$$I_G = \frac{\Gamma(\nu - LD/2)}{\prod_{e=1}^E \Gamma(\nu_e)} \int_0^\infty \delta\left(1 - \sum_{e=1}^E a_e\right) \left(\prod_{e=1}^E a_e^{\nu_e - 1}\right) \frac{\mathcal{U}(a)^{\nu - (L+1)D/2}}{\mathcal{F}(a)^{\nu - LD/2}} \mathrm{d}^E a, \qquad (A.7)$$

where $\mathcal{U}$ and $\mathcal{F}$ are as usual where the x_e get replaces by a_e, and the measure becomes $\mathrm{d}^E a := \prod_{e=1}^{E} \mathrm{d}a_e$. Here, $\nu = \sum_{e=1}^{E} \nu_e$. We now show how recover the integral in (A.7) from the Schwinger parameterization. The first step consists in inserting in the integral in (A.6) one in the form

$$1 = \int_0^\infty \delta\left(t - \sum_{e=1}^n x_e\right) \mathrm{d}t. \tag{A.8}$$

It is enough to integrate on the positive orthant because of the additional assumption that the sum of the Schwinger parameters is non-negative. Hence, we apply the change of variables $x_e = ta_e$ and obtain the following expression

$$\int_0^\infty \int_0^\infty \delta\left(1 - \sum_{e=1}^E a_e\right)\left(\prod_{e=1}^E a_e^{\nu_e-1}\right) t^{\nu-LD/2-1} \mathcal{U}(a)^{-D/2} \exp\left[\frac{t\mathcal{F}(a)}{\mathcal{U}(a)}\right] \mathrm{d}^E x \, \mathrm{d}t.$$

At this point, with the substitution $t \to t\mathcal{U}(a)/\mathcal{F}(a)$ we get

$$\int_0^\infty \delta\left(1 - \sum_{e=1}^E a_e\right)\left(\prod_{e=1}^E a_e^{\nu_e-1}\right) \frac{\mathcal{U}(a)^{\nu-(L+1)D/2}}{\mathcal{F}(a)^{\nu-LD/2}} \mathrm{d}^E a \int_0^\infty t^{\nu-LD/2-1} \exp[-t] \mathrm{d}t$$

where the integral with respect to the variable t equals $\Gamma(\nu - LD/2)$. With this last substitution we attain precisely the integral in Feynman parameter representation.

Lee-Pomeransky

Analogously to the Schwinger representation, the variables that get integrated out in Lee-Pomeranski representation are the Schwinger parameters. Given E complex variables u_e, here is how a Feynman integral looks like in such a parameterization:

$$I_G = \frac{\Gamma(D/2)}{\Gamma((L+1)D/2 - \nu) \prod_{e=1}^n \Gamma(\nu_e)} \int_0^\infty \left(\prod_{e=1}^E u_e^{\nu_e-1}\right) \mathcal{G}^{-D/2} \mathrm{d}^E u, \tag{A.9}$$

where $\mathrm{d}^E u := \prod_{e=1}^E \mathrm{d}u_e$, and $\mathcal{G} = \mathcal{U} + \mathcal{F}$. In what follows, we show that starting with an integral of the form (A.9) it is possible to recover the Feynman parameter representation presented above. For the sake of clarity, we denote N_ν the normalizing factor appearing in (A.9).

We start with the analogous trick involving (A.8) used above. Applying the change of variables $u_j = tx_j$ we obtain

$$I_G = N_\nu \cdot \int_0^\infty \int_0^\infty \delta\left(1 - \sum_{e=1}^E x_e\right) t^\nu \left(\prod_{e=1}^E x_e^{\nu_e-1}\right) \left(t^L \mathcal{U}(x) + t^{L+1} \mathcal{F}(x)\right)^{-D/2} \mathrm{d}^E x \, \mathrm{d}t$$

$$= N_\nu \cdot \int_0^\infty \delta\left(1 - \sum_{e=1}^E x_e\right)\left(\prod_{e=1}^E x_e^{\nu_e-1}\right) \mathrm{d}^E x \int_0^\infty t^{\nu-LD/2-1}(\mathcal{U}(x) + t\mathcal{F}(x))^{-D/2} \mathrm{d}t.$$

Now we substitute $t \to t\mathcal{U}(x)/\mathcal{F}(x)$

$$I_G = N_\nu \int_0^\infty \delta\left(1 - \sum_{e=1}^E x_e\right)\left(\prod_{e=1}^E x_e^{\nu_e-1}\right) \frac{\mathcal{U}(x)^{\nu-(L+1)D/2-1}}{\mathcal{F}(x)^{\nu-LD/2-1}} \mathrm{d}^E x \int_0^\infty t^{\nu-LD/2-1}(1+t)^{-D/2} \mathrm{d}t,$$

where one can recognize that the integral over t is the second integral representation of Euler's beta function:

$$\int_0^\infty t^{\nu-LD/2-1}(1+t)^{-D/2} \mathrm{d}t = \frac{\Gamma(\nu - LD/2)\Gamma((l + 1D/2 - \nu))}{\Gamma(D/2)}.$$

This final substitution concludes the recovery of the parametric representation. The variables u_e appearing in (A.9) are sometimes called *Lee-Pomeransky variables* in the physics literature.

One of the reasons why this representation is relevant for our purposes is that it provides interesting examples of Euler integrals for which we developed the theory in Section 3.2.

Counting master integrals

As explained in Section 3.2, a first step towards evaluating Feynman integrals consists in defining a finite-dimensional vector space of such integrals and establishing linear relationships between them. The basis elements of such a vector space are called master integrals in the physics literature. One of the most popular methods to perform this count and find an integral basis is based on *integration by parts* (IBP). The idea is to generate various identities for integrals of derivatives with respect to loop momenta and use this set of integral relations to solve the reduction problem. This consists in finding out how a general Feynman integral can be expressed linearly in terms of some master integrals. A well-known implemented algorithm used to compute a set of master integrals is the *Laporta algorithm* [Lap00]. However, it requires to generate a high number of integral relations and the result is not totally reliable when it comes to Feynman integrals of diagrams with a high number of vertices and loops. Therefore, it is very useful to a priori compute the number of master integrals, and this is where the various vector spaces introduced in Section 3.2 come in handy.

This final part illustrates in an example how to apply the techniques introduced in Section 3.2 to effectively compute the number of master integrals. As above, we fix the Feynman diagram G to be the box diagram in Figure A.2.

We will consider Feynman integrals in Lee-Pomeransky representation (A.9) since, as mentioned, they are in the form of generalized Euler integrals. One way to compute the number of master integrals for $I_\square$ is to determine the Euler characteristic of the variety

$$X = (\mathbb{C}^*)^4 \smallsetminus V(\mathcal{G}_\square),$$

with $\mathcal{G}_\square = \mathcal{U}_\square + \mathcal{F}_\square$, where the Symanzik polynomials are given in Example A.5. One first effective way of computing the dimension of the vector space is by using the `Julia` package `HomotopyContinuation.jl` as illustrated in Subsection 3.2.4. Here is how to do it in this case:

```
@var x[1:4] s ν[1:4] p[1:4] m[1:4]
L = s*log(U+F) + sum(log(x[i])*ν[i] for i = 1:4)
S = System(differentiate(L,x), parameters = [s;ν;p;m])
monodromy_solve(S)
```

The result is 15 which is known to be the number of master integrals for the box diagram with nonzero masses. We can recover the number 15 also as the normalized volume of the Newton polytope of $\mathcal{G}$. Here is how do do it using the computer algebra system `Oscar` [OSC] available as a `Julia` package:

```
NPexp = exponents_coefficients(U+F,x);
Q = convex_hull(NPexp[1]');
factorial(length(x))*volume(Q)
```

The fact that the number of master integrals coincides with the normalized volume of the Newton polytope of $\mathcal{G}$ is not always true. In this case, the coefficients of the polynomial

$\mathcal{G}_\square$ are generic in the sense of Section 3.2. However, this is not the case for most of Symanzik polynomials.

Bibliography

[ABF⁺23]   Daniele Agostini, Taylor Brysiewicz, Claudia Fevola, Lukas Kühne, Bernd
           Sturmfels, Simon Telen, and Thomas Lam. Likelihood degenerations. *Advances in Mathematics*, 414:108863, 2023.

[ABL⁺10]   Daniel Andres, Michael Brickenstein, Viktor Levandovskyy, Jorge Martín-
           Morales, and Hans Schönemann. Constructive D-module theory with
           `singular`. *Mathematics in Computer Science*, 4(2–3):359–383, 2010.

[AC91]   Mark J. Ablowitz and Peter A. Clarkson. *Solitons, nonlinear evolution equations and inverse scattering*, volume 149. Cambridge university press, 1991.

[AC21]   Daniele Agostini and Lynn Chua. Computing theta functions with Julia.
           Journal of Software for Algebra and Geometry, 11(1):41–51, 2021.

[ACGH85]   Enrico Arbarello, Maurizio Cornalba, Phillip A. Griffiths, and Joe Harris.
           Geometry of Algebraic Curves. Volume I. Springer, 1985.

[AÇL21]   Daniele Agostini, Türkü Özlüm Çelik, and John B. Little. On algebraic theta
           divisors and rational solutions of the KP equation. *arXiv:2112.03147*, 2021.

[AÇS21]   Daniele Agostini, Türkü Özlüm Çelik, and Bernd Sturmfels. The Dubrovin
           threefold of an algebraic curve. *Nonlinearity*, 34(6):3783, 2021.

[AÇSS21]   Daniele Agostini, Türkü Özlüm Çelik, Julia Struwe, and Bernd Sturmfels.
           Theta surfaces. *Vietnam Journal of Mathematics*, 49(2):319–347, 2021.

[ACvM12]   Mark Adler, Mattia Cafasso, and Pierre van Moerbeke. Non-linear PDEs for
           gap probabilities in random matrices and KP theory. *Physica D: Nonlinear
           Phenomena*, 241(23-24):2265–2284, 2012.

[ADC84]   Enrico Arbarello and Corrado De Concini. On a set of equations characterizing
           Riemann matrices. *Annals of Mathematics*, 119:119–140, 1984.

[AFMS23]   Daniele Agostini, Claudia Fevola, Yelena Mandelshtam, and Bernd Sturmfels.
           KP solitons from tropical limits. *Journal of Symbolic Computation*, 114:282–
           301, 2023.

[AFST22]   Daniele Agostini, Claudia Fevola, Anna-Laura Sattelberger, and Simon Telen.
           Vector spaces of generalized Euler integrals. *arXiv:2208.08967*, 2022.

[AG12]   Eugene L. Allgower and Kurt Georg. *Numerical continuation methods: an
           introduction*, volume 13. Springer Science & Business Media, 2012.

[AG18]   Simonetta Abenda and Petr G. Grinevich. Rational degenerations of M-
            curves, totally positive Grassmannians and KP2-solitons. *Communications
            in Mathematical Physics*, 361:1029–1081, 2018.

[AHT14]   Nima Arkani-Hamed and Jaroslav Trnka. The amplituhedron. *Journal of
            High Energy Physics*, 2014(10):1–33, 2014.

[AKKI11]   Kazuhiko Aomoto, Michitake Kita, Toshitake Kohno, and Kenji Iohara. *The-
            ory of hypergeometric functions.* Springer, 2011.

[ALSS20]   Michael F. Adamer, András C Lőrincz, Anna-Laura Sattelberger, and Bernd
            Sturmfels. Algebraic analysis of rotation data. *Algebraic Statistics*, 11(2):189–
            211, 2020.

[AMEP22]   Federico Ardila-Mantilla, Christopher Eur, and Raul Penaguiao. The tropical
            critical points of an affine matroid. *arXiv:2212.08173*, 2022.

[AS97]   Alan Adolphson and Steven Sperber. On twisted de Rham cohomology.
            Nagoya Mathematical Journal, 146:55–81, 1997.

[BB97]   Margaret M. Bayer and Keith A. Brandt. Discriminantal arrangements, fiber
            polytopes and formality. *Journal of Algebraic Combinatorics*, 6(3):229–246,
            1997.

[BBC17]   Barbara Bolognese, Madeline V. Brandt, and Lynn Chua. From curves to
            tropical Jacobians and back. In *Combinatorial algebraic geometry*, pages 21–
            45. Springer, Cham, 2017.

[BBKP19]   Thomas Bitoun, Christian Bogner, Rene Pascal Klausen, and Eric Panzer.
            Feynman integral relations from parametric annihilators. *Letters in Mathe-
            matical Physics*, 109(2), March 2019.

[BÇD⁺21]   Paul Breiding, Türkü Özlüm Çelik, Timothy Duff, Alexander Heaton, Aida
            Maraj, Anna-Laura Sattelberger, Lorenzo Venturello, and Oğuzhan Yürük.
            Nonlinear algebra and applications. *Numerical Algebra, Control and Opti-
            mization*, 2021.

[BCFW05]   Ruth Britto, Freddy Cachazo, Bo Feng, and Edward Witten. Direct proof
            of the tree-level scattering amplitude recursion relation in yang-mills theory.
            Physical review letters, 94(18):181602, 2005.

[BCV13]   Winfried Bruns, Aldo Conca, and Matteo Varbaro. Relations between the
            minors of a generic matrix. *Advances in Mathematics*, 244:171–206, 2013.

[BDFK23]   Mara Belotti, Alessandro Danelon, Claudia Fevola, and Andreas Kretschmer.
            The enumerative geometry of cubic hypersurfaces: point and line conditions.
            Collectanea Mathematica, pages 1–35, 2023.

[BEK21]   Taylor Brysiewicz, Holger Eble, and Lukas Kühne. Enumerating chambers of
            hyperplane arrangements with symmetry. *arXiv:2105.14542*, 2021.

[BFS21]   Taylor Brysiewicz, Claudia Fevola, and Bernd Sturmfels. Tangent quadrics in
            real 3-space. *Le Matematiche*, 76(2):355–367, 2021.

[BGL⁺18]   Janko Böhm, Alessandro Georgoudis, Kasper J. Larsen, Hans Schönemann, and Yang Zhang. Complete integration-by-parts reductions of the non-planar hexagon-box via module intersections. *Journal of High Energy Physics*, 2018(9):1–30, 2018.

[BK21]   Mohamed Barakat and Lukas Kühne. Computing the nonfree locus of the moduli space of arrangements and Terao's freeness conjecture. *arXiv:2112.13065*, 2021.

[BKLH]   Mohamed Barakat, Tom Kuhmichel, and Markus Lange-Hegermann. Zariskiframes–(co) frames/locales of zariski closed/open subsets of affine, projective, or toric varieties, 2018–2019.

[BM96]   Jöel Briançon and Philippe Maisonobe. Caractérisation géométrique de l'existence du polynôme de Bernstein relatif. In *Algebraic Geometry and Singularities*, pages 215–236. Springer, 1996.

[Bob11]   Alexander I. Bobenko. Introduction to compact Riemann surfaces. In *Computational approach to Riemann surfaces*, pages 3–64. Springer, 2011.

[Bra20]   Madeline V. Brandt. *Tropical Geometry of Curves*. University of California, Berkeley, 2020. PhD dissertation.

[BRT20]   Paul Breiding, Kemal Rose, and Sascha Timme. Certifying zeros of polynomial systems using interval arithmetic. *arXiv:2011.05000*, 2020.

[BS06]   Jürgen Bokowski and Bernd Sturmfels. *Computational synthetic geometry*, volume 1355. Springer, 2006.

[BST20]   Paul Breiding, Bernd Sturmfels, and Sascha Timme. 3264 conics in a second. *Notices of the American Mathematical Society*, 67:30–37, 2020.

[BSZ19]   Nils Bruin, Jeroen Sijsling, and Alexandre Zotine. Numerical computation of endomorphism rings of Jacobians. *The Open Book Series*, 2(1):155–171, 2019.

[BT18]   Paul Breiding and Sascha Timme. HomotopyContinuation.jl: A package for homotopy continuation in Julia. In *International Congress on Mathematical Software*, pages 458–465. Springer, 2018.

[BvdVVW21] Nero Budur, Robin van der Veer, and Alexander Van Werde. Estimates for zero loci of Bernstein–Sato ideals. *Inventiones Mathematicae*, 225(1):45–72, July 2021.

[BvdVWZ21] Nero Budur, Robin van der Veer, Lei Wu, and Peng Zhou. Zero loci of Bernstein–Sato ideals-II. *Selecta Mathematica (N.S.)*, 27(32), 2021.

[Cal64]   Eugenio Calabi. Linear systems of real quadratic forms. In *Proceedings of the American Mathematical Society* **15**, pages 844–846, 1964.

[Car13]   Sean Carroll. How quantum field theory becomes "effective", 2013. https://www.preposterousuniverse.com/blog/2013/06/20/how-quantum-field-theory-becomes-effective/, Last accessed on 2022-01-24.

[Cay55]   Arthur Cayley. Récherches sur les matrices dont les termes sont des fonctions linéaires d'une seule indéterminée. *Journal für die reine und angewandte Mathematik*, 50:313–317, 1855.

[CD13]   Sean Carroll and Lance Dixon. Guest post: Lance Dixon on calculating amplitudes, 2013. https://www.preposterousuniverse.com/blog/2013/10/03/guest-post-lance-dixon-on-calculating-amplitudes/, Last accessed on 2022-01-24.

[CEGM19]   Freddy Cachazo, Nick Early, Alfredo Guevara, and Sebastian Mizera. Scattering equations: from projective spaces to tropical Grassmannians. *Journal of High Energy Physics*, 2019(6):1–33, 2019.

[CGM+22]   Vsevolod Chestnov, Federico Gasparotto, Manoj K. Mandal, Pierpaolo Mastrolia, Saiei J. Matsubara-Heo, Henrik J. Munch, and Nobuki Takayama. Macaulay matrix for Feynman integrals: linear relations and intersection numbers. *Journal of High Energy Physics*, 2022(9):1–57, 2022.

[Cha12]   Melody T. Chan. *Tropical curves and metric graphs*. University of California, Berkeley, 2012. PhD dissertation.

[CHKS06]   Fabrizio Catanese, Serkan Hoşten, Amit Khetan, and Bernd Sturmfels. The maximum likelihood degree. *American Journal of Mathematics*, 128(3):671–697, 2006.

[CHY14]   Freddy Cachazo, Song He, and Ellis Ye Yuan. Scattering equations and Kawai-Lewellen-Tye orthogonality. *Physical Review D*, 90(6):065001, 2014.

[CKS19]   Lynn Chua, Mario Kummer, and Bernd Sturmfels. Schottky algorithms: classical meets tropical. *Mathematics of Computation*, 88(319):2541–2558, 2019.

[CMR20]   Jane Coons, Orlando Marigliano, and Michael Ruddy. Maximum likelihood degree of the two-dimensional linear Gaussian covariance model. *Algebraic Statistics*, 1, 2020.

[Cra85]   Henry Crapo. The combinatorial theory of structures. In A. Recski and L. Lovász, editors, *Matroid Theory*, volume 40 of *Colloquia Mathematica Societatis János Bolyai*, pages 107–213, 1985.

[CUZ20]   Freddy Cachazo, Bruno Umbert, and Yong Zhang. Singular solutions in soft limits. *Journal of High Energy Physics*, 2020(5):1–33, 2020.

[DE95]   James W. Demmel and Alan Edelman. The dimension of matrices (matrix pencils) with given Jordan (Kronecker) canonical forms. *Linear Algebra and its Applications*, 230:61–87, 1995.

[DE18]   Jan Draisma and Rob H. Eggermont. Plücker varieties and higher secants of Sato's Grassmannian. *Journal für die reine und angewandte Mathematik (Crelles Journal)*, 2018(737):189–215, 2018.

[Del70]   Pierre Deligne. *Équations différentielles à points singuliers réguliers*, volume 163 of *Lecture Notes in Mathematics*. Springer-Verlag, Berlin-New York, 1970.

[DGPS22]   Wolfram Decker, Gert-Martin Greuel, Gerhard Pfister, and Hans Schöne-mann. SINGULAR 4-3-0 — A computer algebra system for polynomial computations. http://www.singular.uni-kl.de, 2022.

[DHB⁺04]   Bernard Deconinck, Matthias Heil, Alexander Bobenko, Mark van Hoeij, and Marcus Schmies. Computing Riemann theta functions. *Mathematics of Computation*, 73(247):1417–1442, 2004.

[Die98]   Peter Dietmaier. The Stewart-Gough platform of general geometry can have 40 real postures. In *Advances in robot kinematics: Analysis and control*, pages 7–16. Springer, 1998.

[DKgS14]   Andrii Dmytryshyn, Bo Kå gstrom, and Vladimir V. Sergeichuk. Symmetric matrix pencils: Codimension counts and the solution of a pair of matrix equations. *Electronic Journal of Linear Algebra*, 27:1–18, 2014.

[dlC19]   Leonardo de la Cruz. Feynman integrals as A-hypergeometric functions. *Journal of High Energy Physics*, 12(123), 2019.

[Dol12]   Igor Dolgachev. *Classical Algebraic Geometry: A Modern View*. Cambridge University Press, 2012.

[Dou]   Antoine Douai. Notes sur les systèmes de Gauss–Manin algébriques et leurs transformés de Fourier. Prépublication n° 640 de l'Université de Nice, janvier 2002.

[DS03]   Antoine Douai and Claude Sabbah. Gauss–Manin systems and Frobenius structures I. *Annales de l'Institut Fourier*, Tome 53(4):1055–1116, 2003.

[Dub81]   Boris A. Dubrovin. Theta functions and non-linear equations. *Russian mathematical surveys*, 36(2):11–92, 1981.

[Dut04]   Mathieu Dutour. The six-dimensional Delaunay polytopes. *European Journal of Combinatorics*, 25:535–548, 2004.

[ER87]   Robert M. Erdahl and S.S. Ryshkov. The empty sphere. *Canadian Journal of Mathematics*, 39(4):794–824, 1987.

[Eti99]   Pavel I. Etingof. Note on dimensional regularization. In *Quantum fields and strings: a course for mathematicians, Vol. 1*, pages 597–607. Amererican Mathematical Society, Providence, R.I., 1999.

[Fal94]   Michael Falk. A note on discriminantal arrangements. *Proceedings of the American Mathematical Society*, 122(4):1221–1227, 1994.

[FG22]   Claudia Fevola and Christiane Görgen. The mathematical research-data repository MathRepo. *Computeralgebra Rundbrief*, 70:16–20, 2022.

[FGL⁺21]   Hjalte Frellesvig, Federico Gasparotto, Stefano Laporta, Manoj K. Mandal, Pierpaolo Mastrolia, Luca Mattiazzi, and Sebastian Mizera. Decomposition of Feynman integrals by multivariate intersection numbers. *Journal of High Energy Physics*, 2021(3):1–55, 2021.

[FGM⁺19]   Hjalte Frellesvig, Federico Gasparotto, Manoj K. Mandal, Pierpaolo Mastrolia, Luca Mattiazzi, and Sebastian Mizera. Vector space of Feynman integrals and multivariate intersection numbers. *Physical Review Letters*, 123(20):201602, 2019.

[FGSM21]   Hershel M. Farkas, Samuel Grushevsky, and Riccardo Salvati Manni. An explicit solution to the weak Schottky problem. *Algebraic Geometry*, 8:358–373, 2021.

[FJK19]   Jörg Frauendiener, Carine Jaber, and Christian Klein. Efficient computation of multidimensional theta functions. *Journal of Geometry and Physics*, 141:147–158, 2019.

[FM22]   Claudia Fevola and Yelena Mandelshtam. Hirota varieties and rational nodal curves. *arXiv:2203.00203*, 2022.

[FMS21]   Claudia Fevola, Yelena Mandelshtam, and Bernd Sturmfels. Pencils of quadrics: old and new. *Le Matematiche*, 76(2):319–335, 2021.

[Ger61]   Murray Gerstenhaber. On dominance and varieties of commuting matrices. *Annals of Mathematics*, 73:324–348, 1961.

[GGMS87]   Israel M. Gelfand, Robert M. Goresky, Robert D. MacPherson, and Vera V. Serganova. Combinatorial geometries, convex polyhedra, and Schubert cells. *Advances in Mathematics*, 63:301–316, 1987.

[GJ20]   Ewgenij Gawrilow and Michael Joswig. Polymake: a framework for analyzing convex polytopes. *In Polytopes–combinatorics and computation*, pages 43–73, 2020.

[GKZ90]   Israel Gelfand, Mikhail Kapranov, and Andrei Zelevinsky. Generalized Euler integrals and A-hypergeometric functions. *Advances in Mathematics*, 84:255–271, 1990.

[GKZ94a]   Israel Gelfand, Mikhail Kapranov, and Andrei Zelevinsky. *Discriminants, Resultants and Multidimensional Determinants*. Birkhäuser, Boston, 1994.

[GKZ94b]   Israel M. Gelfand, Mikhail M. Kapranov, and Andrei V. Zelevinsky. *Discriminants, resultants, and multidimensional determinants*. Mathematics: Theory & Applications. Birkhäuser Boston, Inc., Boston, MA, 1994.

[GR14]   Elizabeth Gross and Jose Israel Rodriguez. Maximum likelihood geometry in the presence of data zeros. In *Proceedings of the 39th International Symposium on Symbolic and Algebraic Computation*, pages 232–239, 2014.

[Gru12]   Samuel Grushevsky. The Schottky problem. *Current developments in algebraic geometry*, 59:129, 2012.

[GS]   Daniel R. Grayson and Michael E. Stillman. `Macaulay2`, a software system for research in algebraic geometry. Available at http://www.math.uiuc.edu/Macaulay2/.

[GSS05]   Luis D. Garcia, Michael Stillman, and Bernd Sturmfels. Algebraic geometry of Bayesian networks. *Journal of Symbolic Computation*, 39:331–355, 2005.

[Hes02]   Florian Hess. Computing Riemann–Roch spaces in algebraic function fields and related topics. *Journal of Symbolic Computation*, 33(4):425–445, 2002.

[HP52]   William V. D. Hodge and Daniel Pedoe. *Methods of Algebraic Geometry*, volume II. Quadrics and Grassmann Varieties, Cambridge University Press, Book IV, 1952.

[HS14]   June Huh and Bernd Sturmfels. Likelihood geometry. In *Combinatorial algebraic geometry*, pages 63–117. Springer, 2014.

[HTT08]   Ryoshi Hotta, Kiyoshi Takeuchi, and Toshiyuki Tanisaki. *D-Modules, perverse sheaves, and representation theory*, volume 236 of *Progress in Mathematics*. Birkhäuser Boston, 2008.

[Huh13]   June Huh. The maximum likelihood degree of a very affine variety. *Compositio Mathematica*, 149(8):1245–1266, 2013.

[Igu82]   Jun-Ichi Igusa. On the irreducibility of Schottky's divisor. *Journal of the Faculty of Science, the University of Tokyo. Sect. 1 A, Mathematics*, 28(3):531–545, 1982.

[Jel20]   Philipp Jell. Constructing smooth and fully faithful tropicalizations for mumford curves. *Selecta Mathematica*, 26(4):1–23, 2020.

[Kas85]   Masaki Kashiwara. Index theorem for constructible sheaves. *Astérisque*, 130:193–209, 1985.

[Kle97]   Steven L. Kleiman. Bertini and his two fundamental theorems. *Rendiconti del Circolo Matematico di Palermo*, 1997.

[KM19]   Kiumars Kaveh and Christopher Manon. Khovanskii bases, higher rank valuations, and tropical geometry. *SIAM Journal on Applied Algebra and Geometry*, 3(2):292–336, 2019.

[KNT12]   Hiroshi Koizumi, Yasuhide Numata, and Akimichi Takemura. On intersection lattices of hyperplane arrangements generated by generic points. *Annals of Combinatorics*, 16(4):789–813, 2012.

[Kod04]   Yuji Kodama. Young diagrams and N-soliton solutions of the KP equation. *Journal of Physics A: Mathematical and General*, 37: 11169:46, 2004.

[Kod17]   Yuji Kodama. *KP solitons and the Grassmannians: combinatorics and geometry of two-dimensional wave patterns*, volume 22. Springer, 2017.

[KP70]   Boris B. Kadomtsev and Vladimir I. Petviashvili. On the stability of solitary waves in weakly dispersing media. In *Doklady Akademii Nauk*, volume 192, pages 753–756. Russian Academy of Sciences, 1970.

[Kri77]   Igor M. Krichever. Methods of algebraic geometry in the theory of non-linear equations. *Russian Mathematical Surveys*, 32(6):185, 1977.

[KS13]   Igor Krichever and Takahiro Shiota. Soliton equations and the riemann–schottky problem. In *Handbook of Moduli, Vol. II*, volume 25 of *Advanced Lectures in Mathematics*, pages 205–258. International Press, Somerville, 2013.

[KW14]   Yuji Kodama and Lauren Williams. KP solitons and total positivity for the Grassmannian. *Inventiones mathematicae*, 198(3):637–699, 2014.

[KW18]   Thomas Kahle and André Wagner. Veronesean almost binomial almost complete intersections. *Rendiconti dell'Istituto di Matematica dell'Università di Trieste*, 50:75–79, 2018.

[KX21]   Yuji Kodama and Yuancheng Xie. Space curves and solitons of the KP hierarchy. I. the l-th generalized KdV hierarchy. *Symmetry, Integrability and Geometry: Methods and Applications*, 17(0):24–43, 2021.

[Lap00] Stefano Laporta. High-precision calculation of multiloop feynman integrals by difference equations. *International Journal of Modern Physics A*, 15(32):5087–5159, 2000.

[Leu20] Martin Leuner. `alcove` – algebraic combinatorics package for GAP, 2013-2020.

[LP13]   Roman N. Lee and Andrei A. Pomeransky. Critical points and number of master integrals. *Journal of High Energy Physics*, 2013(11):1–17, 2013.

[LS91a] Francois Loeser and Claude Sabbah. Caractérisation des D-modules hypergéométriques irréductibles sur le tore. *Comptes rendus de l'Académie des Sciences I Math.*, 312(10):735—738, 1991.

[LS91b] François Loeser and Claude Sabbah. Equations aux différences finies et déterminants d'intégrales de fonctions multiformes. *Commentarii mathematici Helvetici*, 66(1):458–503, 1991.

[LS92]   Francois Loeser and Claude Sabbah. Caractérisation des D-modules hypergéométriques irréductibles sur le tore, II. *Comptes rendus de l'Académie des Sciences I Math.*, 315:1263–1264, 1992.

[LT]   Anton Leykin and Harrison Tsai. D-modules: functions for computations with D-modules. version 1.4.0.1. A `Macaulay2` package available at https://github.com/Macaulay2/M2/tree/master/M2/Macaulay2/packages.

[MGH+12] Michael B. Monagan, Keith O. Geddes, K. Michael Heal, George Labahn, Stefan M. Vorkoetter, et al. *Maple V Programming Guide: For Release 5.* Springer Science & Business Media, 2012.

[MH20]   Saiei-Jaeyeong Matsubara-Heo. Euler and Laplace integral representations of GKZ hypergeometric functions I. *Proceedings of the Japan Academy, Series A, Mathematical Sciences*, 96(9):75 – 78, 2020.

[MH21]   Saiei-Jaeyeong Matsubara-Heo. Global analysis of GG systems. *International Mathematics Research Notices*, rnab144, 2021.

[MH22]   Saiei-Jaeyeong Matsubara-Heo. Computing cohomology intersection numbers of GKZ hypergeometric systems. *Proceeding of science*, ma2019:013, 2022.

[MHT22] Saiei-Jaeyeong Matsubara-Heo and Nobuki Takayama. An algorithm of computing cohomology intersection number of hypergeometric integrals. *Nagoya Math. J.*, 246:256–272, 2022.

[Mir95]   Rick Miranda. *Algebraic curves and Riemann surfaces*, volume 5. American
              Mathematical Society, 1995.

[Miz18]   Sebastian Mizera. Scattering amplitudes from intersection theory. *Physical
              Review Letters*, 120(14):141602, 2018.

[MM19]   Pierpaolo Mastrolia and Sebastian Mizera. Feynman integrals and intersection
              theory. *Journal of High Energy Physics*, 2019(2):1–25, 2019.

[MMIB12a]   Yoshitake Matsumoto, Sonoko Moriyama, Hiroshi Imai, and David Bremner.
              Database of matroids, 2012.

[MMIB12b]   Yoshitake Matsumoto, Sonoko Moriyama, Hiroshi Imai, and David Bremner.
              Matroid enumeration for incidence geometry. *Discrete & Computational Ge-
              ometry*, 47(1):17–43, 2012.

[MMM+20]   Laurent Manivel, Mateusz Michałek, Leonid Monin, Tim Seynnaeve, and Mar-
              tin Vodička. Complete quadrics: Schubert calculus for Gaussian models and
              semidefinite programming. *arXiv:2011.08791*, 2020.

[MMRS21]   Orlando Marigliano, Mateusz Michaek, Kristian Ranestad, and Tim Seyn-
              naeve, editors. *Special Issue on Linear Spaces of Symmetric Matrices*, volume
              76, Number 2, 2021.

[MMW21]   Mateusz Michałek, Leonid Monin, and Jarosław A Wisniewski. Maximum
              likelihood degree, complete quadrics, and $\mathbb{C}^*$-action. *SIAM Journal on Applied
              Algebra and Geometry*, 5(1):60–85, 2021.

[MS04]   Ezra Miller and Bernd Sturmfels. *Combinatorial Commutative Algebra*. Grad-
              uate Texts in Mathematics, Springer Verlag, New York, 2004.

[MS21a]   Diane Maclagan and Bernd Sturmfels. *Introduction to tropical geometry*, vol-
              ume 161. American Mathematical Society, 2021.

[MS21b]   Mateusz Michałek and Bernd Sturmfels. Invitation to nonlinear algebra. *Vol-
              ume*, 211, 2021.

[MT22]   Sebastian Mizera and Simon Telen. Landau discriminants. *Journal of High
              Energy Physics*, 2022(8):1–57, 2022.

[Nak18]   Atsushi Nakayashiki. Degeneration of trigonal curves and solutions of the
              KP-hierarchy. *Nonlinearity*, 31(8):3567, 2018.

[Nak19]   Atsushi Nakayashiki. On reducible degeneration of hyperelliptic curves and
              soliton solutions. *SIGMA. Symmetry, Integrability and Geometry: Methods
              and Applications*, 15:009, 2019.

[OS16]   Luke Oeding and Steven V. Sam. Equations for the fifth secant variety of
              Segre products of projective spaces. *Experimental Mathematics*, 25(1):94–99,
              2016.

[OSC]   Computer Algebra System OSCAR. https://oscar.computeralgebra.de.

[OT13]   Peter Orlik and Hiroaki Terao. *Arrangements of hyperplanes*, volume 300.
              Springer Science & Business Media, 2013.

[PS05]   Lior Pachter and Bernd Sturmfels. *Algebraic Statistics for Computational Biology.* Cambridge University Press, 2005.

[RTV97]   Felice Ronga, Alberto Tognoli, and Thierry Vust. The number of conics tangent to five given conics: the real case. *Revista Matemática Complutense*, 10:391–421, 1997. Madrid.

[Ryb11]   Grigori L. Rybnikov. On the fundamental group of the complement of a complex hyperplane arrangement. *Functional Analysis and Its Applications*, 45(2):137–148, 2011.

[S+04]   Richard P. Stanley et al. An introduction to hyperplane arrangements. *Geometric combinatorics*, 13(389-496):24, 2004.

[Sab87]   Claude Sabbah. Proximité évanescente. I. La structure polaire d'un D-module. *Compositio Mathematica*, Tome 62(3):283–328, 1987. Proximité évanescente. II. Équations fonctionnelles pour plusieurs fonctions analytiques. Ibid., Tome 64(2):213–214, 1987.

[Sat81]   Mikio Sato. Soliton equations as dynamical systems on an infinite dimensional Grassmann manifolds (Random systems and dynamical systems). *RIMS Kokyuroku*, 439:30–46, 1981.

[Sch79]   Hermann Schubert. *Kalkül der abzählenden Geometrie.* Reprint of the 1879 original, Springer, Berlin, 1979.

[SD16]   Christopher Swierczewski and Bernard Deconinck. Computing Riemann theta functions in Sage with applications. *Mathematics and computers in Simulation*, 127:263–272, 2016.

[Shi86]   Takahiro Shiota. Characterization of Jacobian varieties in terms of soliton equations. *Inventiones mathematicae*, 83(2):333–382, 1986.

[SKK73]   Mikio Sato, Takahiro Kawai, and Masaki Kashiwara. Micro functions and pseudo-differential equations. *Hyperfunctions and Pseudo-Differential Equations*, 6:264–524, 1973.

[Sot10]   Frank Sottile. Frontiers of reality in Schubert calculus. *Bulletin of the American Mathematical Society*, 47:31–71, 2010.

[SS19]   Anna-Laura Sattelberger and Bernd Sturmfels. D-modules and holonomic functions. *arXiv:1910.01395*, 2019.

[SST00]   Mutsumi Saito, Bernd Sturmfels, and Nobuki Takayama. *Gröbner deformations of hypergeometric differential equations*, volume 6 of *Algorithms and Computation in Mathematics.* Springer, 2000.

[ST21]   Bernd Sturmfels and Simon Telen. Likelihood equations and scattering amplitudes. *Algebraic Statistics*, 12(2):167–186, 2021.

[Sta01]   Richard P. Stanley. *Enumerative Combinatorics: Volume 2.* Cambridge University Press, 2001.

[Stu96]   Bernd Sturmfels. *Grobner bases and convex polytopes*, volume 8. American Mathematical Society, 1996.

[STZ20]   Bernd Sturmfels, Sascha Timme, and Piotr Zwiernik. Estimating linear co-
            variance models with numerical nonlinear algebra. *Algebraic Statistics*, 1,
            2020.

[SU10]   Bernd Sturmfels and Caroline Uhler. Multivariate Gaussians, semidefinite
            matrix completion, and convex algebraic geometry. *Annals of the Institute of
            Statistical Mathematics*, 62:603–638, 2010.

[SY22]   Simona Settepanella and So Yamagata. A linear condition for non-very generic
            discriminantal arrangements. *arXiv:2205.04664*, 2022.

[Syl51]   James J. Sylvester. An enumeration of the contacts of lines and surfaces of
            the second order. *Philosophical Magazine*, 1:119–140, 1851.

[Tev07]   Jenia Tevelev. Compactifications of subvarieties of tori. *American Journal of
            Mathematics*, 129(4):1087–1104, 2007.

[The22]   The Sage Developers. SageMath: Open source mathematics software. https:
            //www.sagemath.org, 2022.

[Tho91]   Robert C. Thompson. Pencils of complex and real symmetric and skew ma-
            trices. *Linear Algebra and its Applications*, 147:323–371, 1991.

[Uhl76]   Frank Uhlig. A canonical form for a pair of real symmetric matrices that
            generate a nonsingular pencil. *Linear Algebra and its Applications*, 14:189–
            209, 1976.

[Uhl79]   Frank Uhlig. A recurring theorem about pairs of quadratic forms and exten-
            sions: a survey. *Linear Algebra and its Applications*, 25:219–237, 1979.

[vdVS22]   Robin van der Veer and Anna-Laura Sattelberger. Maximum likelihood esti-
            mation from a tropical and a Bernstein–Sato perspective. *International Math-
            ematics Research Notices*, rnac016, 2022.

[vG98]   Bert van Geemen. The Schottky problem and second order theta functions.
            Workshop on Abelian Varieties and Theta Functions, Morelia, 1996, 1998.

[vG16]   Bert van Geemen. Some equations for the universal Kummer variety. *Trans-
            actions of the American Mathematical Society*, 368(1):209–225, 2016.

[WDA+16]   Mark Wilkinson, Michel Dumontier, IJsbrand J. Aalbersberg, Gaby Apple-
            ton, et al. The FAIR guiding principles for scientific data management and
            stewardship. *Scientific Data*, 3(160018), 2016.

[Wei22]   Stefan Weinzierl. *Feynman Integrals: A Comprehensive Treatment for Stu-
            dents and Researchers*. UNITEXT for Physics. Springer International Pub-
            lishing, 2022.

[Wil21]   Lauren K. Williams. The positive Grassmannian, the amplituhedron, and
            cluster algebras. *arXiv:2110.10856*, 2021.

[Wit88]   Edward Witten. Quantum field theory, Grassmannians, and algebraic curves.
            Communications in Mathematical Physics, 113(4):529–600, 1988.

[Zas97]   Thomas Zaslavsky. Facing up to arrangements: face-count formulas for par-
            titions of space by hyperplanes. *Memoirs of American Mathematical Society*,
            154:1–95, 1997.

Selbstständigkeitserklärung

Hiermit erkläre ich, die vorliegende Dissertation selbständig und ohne unzulässige fremde Hilfe angefertigt zu haben. Ich habe keine anderen als die angeführten Quellen und Hilfsmittel benutzt und sämtliche Textstellen, die wörtlich oder sinngemäß aus veröffentlichten oder unveröffentlichten Schriften entnommen wurden, und alle Angaben, die auf mündlichen Auskünften beruhen, als solche kenntlich gemacht. Ebenfalls sind alle von anderen Personen bereitgestellten Materialien oder erbrachten Dienstleistungen als solche gekennzeichnet.

Leipzig, den July 16, 2023

. . . .
(Claudia Fevola)

Daten zum Autor

Name:	Claudia Fevola
Geburtsdatum:	13.07.1995 in Atripalda (Italien)
09/2013 - 07/2017	B.Sc. in Mathematik
	Universität "Luigi Vanvitelli" Kampanien
09/2017 - 02/2020	M.Sc. in Mathematik
	Universität "Federico II" Neapel
seit 04/2020	Doktorandin der Mathematik